Electromagnetic Radiation and Radon-222 Gas Emissions as Precursors of Seismic Activity

by

Ermioni Petraki

A Thesis submitted for the Degree of Doctor of Philosophy

Department of Electronic and Computer Engineering

Brunel University London

UK

September 2015

Abstract

Earthquakes are amongst the most destructive of natural phenomena and have been the subject of significant research effort over many decades, to predict the onset of seismic events. Electromagnetic emissions detected prior to earthquakes provide a potential data source for seismic predictions and research suggests that specific pre-seismic electromagnetic activity can be directly related to specific earthquakes although it is still an open issue as to the precise links between these electromagnetic emissions and subsequent earthquakes. In this research, findings of the long memory or the self-organization of several pre-earthquake MHz electromagnetic time-series provide significant outcomes regarding the earthquake prediction.

It is also recognised that enhanced radon gas emission has an equally long history as being associated with seismic activity. In general, several anomalous soil radon emissions have been observed prior to earthquakes and this has been recorded all over the world. The abnormal soil radon exhalation from the interior of the earth has been associated with earthquakes and is considered as an important field of research. The research reported in this thesis compared and contrasted the merits of combining electromagnetic emission data and radon exhalation data as precursors of earthquakes with the aim of enhancing earthquake prediction methodology. The findings from the long-memory analysis of radon disturbances in the soil indicated a very significant issue: the radon disturbances in the soil prior to earthquakes exhibit similar behaviour as the MHz RF disturbances of general failure. So, the radon precursors and the MHz electromagnetic correspond to the same pre-earthquake phase. Geological explanations were proposed in view of the asperity model. Persistent and anti-persistent MHz anomalies were due to the micro-cracking of the heterogeneous medium of the earth's crust which may have led the system's evolution towards the global failure.

Fractal methods have been used on historical data, to investigate MHz electromagnetic time-series spectra on emissions preceding major earthquakes over the period 2007 to 2014 and the characteristics of enhanced radon emissions have been studied over the period 2008 to 2015 for seismic events occurring in the Aegean Region. It has been found that both the electromagnetic emissions and the radon exhalation data exhibit similar fractal behaviour and are associated with impending seismic activity. Hence both phenomena are relevant to earthquake predictions and should both be employed in any systematic approach to this problem as the varying geological and geographic conditions under which earthquakes can occur, might preclude one or other data from being measurable. According to the several techniques applied in this thesis, all should be employed in sequential steps, albeit the power-law spectral fractal analysis is the most significant to trace long-memory patterns of 1/f processes as those of the processes of earthquakes.

List of contents

List of Tables & Figures

Acknowledgements

Firstly, I would like to express my sincere gratitude to my supervisor Professor John Stonham for the continuous support of my PhD study and for his patience and motivation. With our discussions, Professor Stonham assisted me to understand what steps I needed to follow to successfully complete my thesis. The insightful comments and the hard questions of Professor Stonham widen my research from various perspectives.

Besides my supervisor, I would also like to thank my advisor Professor Constatinos Nomicos for his guidance which helped me in all the time of research and writing of this thesis. His immense knowledge onto the research topic of my thesis was very important. More than all, I must express my sincere thanks for the confidence he showed me and on the most, I have to thank him for the electromagnetic data that he provided me. Without the electromagnetic data no analysis could have been done. In this manner, Professor Nomicos was the key person for the implementation of my PhD thesis.

I would also like to express the deepest appreciation to my colleagues who read and commented my thesis.

I am grateful to my parents as well, who supported me spiritually and economically for the completion of my PhD.

Last, my sincere thanks goes to my family for the patient, encouragement and supporting. In particular, I want to thank my husband because he believed that I could complete this thesis and supported me when I felt disappointed.

Chapter 1

Introduction and review of electromagnetic precursors

1.1 Introduction to thesis

This thesis reported findings from the long-memory and entropy analysis applied to significant MHz electromagnetic signals and soil radon signals derived between 2007 and 2015 in Greece. Furthermore, this thesis reviewed the electromagnetic precursors and the anomalous radon gas emissions reported prior to earthquakes internationally. In detail, the contents of the chapters are as follows:

Chapter 1 reviewed the electromagnetic precursors of general failure, detected prior to earthquakes internationally.

Chapter 2 reviewed several anomalous radon emissions that have been observed prior to earthquakes all over the world.

Chapter 3 reported the findings from the long-memory analysis based on fractals, regarding several pre-earthquake MHz electromagnetic time-series that were reported in Greece between 2007 and 2014.

Chapter 4 reported the findings from the long-memory analysis applied to significant signals of radon in soil derived in Greece between 2008 and 2015. All these signals lasted several weeks and, importantly, were derived through active methods.

Chapter 5 presented the long-memory analysis of earthquake generation system in terms of Hurst exponent evolution, DFA and the system's self-organisation through block-entropy analysis.

Chapter 6 presents the conclusions of the thesis and outlines the future work.

1.2 Introduction to electromagnetic precursors

This chapter surveys the pre-earthquake electromagnetic precursors. Extensive studies have been carried out during the last decades, to analyse the pre-seismic electromagnetic emissions from 10^{-3}Hz up to MHz. These signals have been analysed through visual, statistical and chaotic techniques. This chapter presents cumulative elements from scientific investigations performed during the last 40 years in this area. Physical models have also been developed for the interpretation of production and propagation of electromagnetic radiation during the fracture process. The ULF (Ultra Low Frequency) fracture-related emissions attempted to be explained via magneto-hydrodynamic, piezomagnetic and electrokinetic effects whereas for the KHz-MHz observations the model of asperities was proposed.

As it is known natural events like earthquakes, tsunamis and volcanic eruptions are inevitable. What makes these events more dangerous and disastrous is not that they are inevitable but that they are still extremely hard to predict. Therefore, it is one of the major challenges for the world scientific community to find a reliable seismic precursor. This has occupied researchers for many decades. However, the problem of earthquake prediction remains unsolved. Precursors recorded for certain earthquakes indicate there is evidence that they can be used for forecasting. In the case of an earthquake rupture, certain precursory activity can be expected, if the observation is made in the near vicinity of causative fracture (Khan et al., 2011). The problem of earthquake prediction consists of consecutive, step-by-step, narrowing of the time interval, space and magnitude ranges, where a strong earthquake should be expected. Five stages of prediction are usually distinguished. The background stage provides maps with the territorial distribution of the maximum possible magnitude and

recurrence time of destructive earthquake of different magnitudes. Four subsequent stages, fuzzily divided, include the time prediction; they differ in the characteristic time interval covered by an alarm. These stages are as follows:

- long-term (10 years)
- intermediate-term (1 year)
- short-term (approximately 36 days to 3.6 days)
- immediate-term (approximately 9 hours or less)

Such division into stages is dictated by the character of the process that leads to a strong earthquake and by the needs of earthquake preparedness; the latter comprises a range of safety measures for each stage of prediction (Keilis-Borok, & Soloviev, 2003). According to Hayakawa and Hobara (2010) the prediction of earthquakes is classified into three categories: long-term (timescale of 10 to 100 years), intermediate-term (timescale of 1 to 10 years) and short-term. Note, that even in short-term prediction there is no one-to-one correspondence between anomalies in the observations and the earthquake events (Eftaxias et al., 2010; Nikolopoulos et al., 2012; Petraki et al., 2015). Although much more difficult than the long-term and intermediate-term predictions, short-term prediction of earthquakes on a timescale of hours, days or weeks, is believed to be of the highest priority for social demands in seismo-active countries.

The short-term earthquake precursors arising from electromagnetic effects are promising tools for earthquake prediction. The subjective study of seismo-electromagnetism refers to electric and magnetic field anomalies (Molchanov, 2011; Molchanov, Hayakawa, Oudoh, & Kawai, 1998) observed during seismicity. Various studies have shown that these pre-seismic electromagnetic emissions occur in wide frequency band ranging from few Hz to MHz. Global efforts to predict earthquakes

were started about a century ago and peaked during 1970s. The first scientifically well documented earthquake prediction was made on the basis of temporal and spatial variation of ts/tp relation in Blue mountain Lake, New York on 3rd August, 1973 (Aggarwal, Sykes, Simpson, & Richards, 1975). Seismologists then successfully predicted the M7.4 Heicheng China earthquake of February 4, 1975 (Cha Chi Yuan), which raised the hopes that it could be possible to make reliable earthquake forecasts. Because of this prediction, an alert was issued within the 24-hour period prior to the main shock, probably preventing a larger number of casualties than the 1328 deaths that actually occurred from this event. However, the failure to predict another devastating earthquake 18 months later, the 1976 M7.8 Tangshan earthquake, possibly due to variable attenuations in the ground conditions, was a major setback to the earthquake prediction effort. Casualties from this earthquake numbered in the hundreds of thousands (Cicerone, Ebel, & Britton, 2009; Petraki et al., 2015). The seismologists have now narrowed down their studies from long term prediction to short term prediction (Khan et al., 2011). The studies carried out in past three decades have given birth to the new field of seismo-electromagnetism. Several research groups all over the world have shown evidences of electromagnetic emissions and anomalies before earthquakes.

Despite the scientific efforts, the preparation and evolution of earthquakes is not delineated yet. A significant reason is that there is restricted knowledge of the fracture mechanisms of the crust (Eftaxias, 2010; Eftaxias et al., 2009, 2010). This is reinforced by the fact that each earthquake is particular and happens in large-scale. Accounting that the fracture of heterogeneous materials is not sufficiently described yet, despite the tremendous up-to-date effort at laboratory, theoretical and numerical level (Eftaxias

2010), it may be understood why the description of the genesis of earthquakes is still limited (Balasis et al., 2009; Balasis, & Mandea, 2007; Contoyiannis, Diakonos, Kapiris, Peratzakis, & Eftaxias, 2004; Contoyiannis, & Eftaxias, 2008; Contoyiannis, Kapiris, & Eftaxias, 2005; Eftaxias, 2010; Eftaxias et al., 2008, 2009, 2010; Eftaxias, Panin, & Deryugin, 2007; Hadjicontis, Mavromatou, & Eftaxias, 2002; Kalimeri, Papadimitriou, Balasis, & Eftaxias, 2008; Kapiris, Eftaxias et al., 2004; Kapiris et al., 2005; Kapiris, Polygiannakis, Peratzakis, Nomicos, & Eftaxias, 2002; Karamanos, & Nicolis, 1999; Karamanos et al., 2005). According to Eftaxias (2010) one should expect that the preparatory processes of earthquakes have various facets, which may be potentially observed before the final catastrophe at geological, geochemical, hydrological and environmental scales (Eftaxias, 2010).

In the following, significant scientific evidence is presented regarding forecasting of earthquakes. The analysis is limited to pre-earthquake electromagnetic disturbances considering these among the most credible precursors of general failure. Focus is mainly on short-term precursors.

1.3 Short-term forecasting of earthquakes-Problems and limitations

The science of short-term earthquake prediction is the study of earthquake precursors. In fact, short-term predictions are typically based on observations of these types of phenomena. The term earthquake precursor is used to describe a wide variety of physical phenomena that reportedly precede at least some earthquakes. These phenomena include induced electric and magnetic fields, ground-water level changes, gas emissions, temperature changes, surface deformations, changes in ionospheric parameters and anomalous seismicity patterns. While each of these phenomena has

been observed prior to certain earthquakes, such observations have been serendipitous in nature (Cicerone et al., 2009; Petraki et al., 2015). It is important however to note that ULF, KHz and MHz EM anomalies have been detected over periods ranging from a few days to a few hours prior to recent destructive earthquakes that occurred in land or were strong and shallow (Balasis et al., 2008, 2009; Balasis, & Mandea, 2007; Contoyiannis et al., 2004, 2005 Contoyiannis, & Eftaxias, 2008; Eftaxias, 2010; Eftaxias et al., 2008, 2009, 2010; Hadjicontis et al., 2002; Kalimeri et al., 2008; Kapiris, Balasis et al., 2004; Kapiris, Eftaxias et al., 2004; Kapiris et al., 2003, 2005; Karamanos, & Nicolis, 1999; Karamanos et al., 2005). Finally, it is the subject of seismo-electromagnetism to study electric and magnetic field anomalies observed during seismicity (Molchanov, 2011; Molchanov et al., 1998). The related studies have reported pre-seismic electromagnetic emissions in wide frequency bands ranging from 0.001 Hz to MHz.

Two major criteria are significant in identifying earthquake precursors. The first criterion is to recognise credible scientific evidence regarding anomalies observed prior to earthquakes (Eftaxias et al. 2010). The successful measurement of some anomalous phenomenon prior to an earthquake usually depends on having a good scientific experiment operating in an area before, during and after an earthquake. The second criterion for the selection of the earthquake precursors is that there are accepted physical models to explain the existence of the precursor (Cicerone et al., 2009; Petraki et al., 2015).

On the other hand, in material science and in geophysics, it is vital to identify precursors of macroscopic defects or shocks (Eftaxias et al., 2010). And this, because

fracture induced physical fields allow real-time monitoring of damage evolution in materials during mechanical loading. A stressed rock behaves like a stress-electromagnetic transformer. The crack propagation is the basic mechanism of the failure of the material (Eftaxias et al., 2008). In many materials emission of photons, electrons, ions and neutral particles is observed during the formation of new surface features after fracturing, deformation, wearing, peeling etc. (Eftaxias, 2010; Eftaxias et al., 2008, 2009, 2010). Collectively, these emissions are referred to as fracto-emissions (Eftaxias, 2010; Eftaxias et al., 2008). The rupture of inter-atomic (ionic) bonds also leads to intense charge separation that is the origin of the electric charge between the micro-crack faces. On the faces of a newly created micro-crack the electric charges constitute an electric dipole or a more complicated system. The motion of a crack has been shown to be governed by a dynamical instability causing oscillations in its velocity and structure on the fracture surface. Experimental evidence indicate that the instability mechanism is that of local branching: a multi-crack state is formed by repetitive, frustrated micro-fracturing events. It is worth mentioning that laboratory experiments show that more intense fracto-emissions are observed during the unstable crack growth (Eftaxias et al. 2008; Petraki, Nikolopoulos, Fotopoulos, Panagiotaras, Koulouras et al., 2013; Petraki, Nikolopoulos, Fotopoulos, Panagiotaras, Nomicos et al., 2013; Nikolopoulos et al., 2014; Petraki et al., 2014, 2015). Due to the strong wall vibration of cracks in the stage of the micro-branching instability, the fractured material behaves as an efficient electromagnetic emitter. Thus, when a material is strained, electromagnetic emissions in a wide frequency spectrum ranging from Hz to MHz are produced by opening cracks, which can be considered as the so-called precursors of general fracture. These electromagnetic precursors are detectable both at laboratory and geological scale (Balasis et al., 2009; Balasis, & Mandea, 2007; Contoyiannis et al.,

2005 Contoyiannis, & Eftaxias, 2005, 2008; Eftaxias, 2010; Eftaxias et al., 2006, 2007, 2008, 2009, 2010; Hadjicontis et al., 2002; Kalimeri et al., 2008; Kapiris, Balasis et al., 2004; Kapiris, Eftaxias et al., 2004; Kapiris et al., 2005 and references therein).

In the above sense, it becomes evident that the main tool of the prediction of earthquakes is the monitoring of the micro-fractures, which possibly occur in the focal area before the final break-up, by recording their electromagnetic emissions (Balasis et al., 2008, 2009; Balasis, & Mandea, 2007; Contoyiannis et al., 2004, 2005 Contoyiannis, & Eftaxias, 2005, 2008; Eftaxias, 2010; Eftaxias et al., 2001, 2002, 2006, 2007, 2008, 2009, 2010; Hadjicontis et al., 2002; Kalimeri et al., 2008; Kapiris, Balasis et al., 2004; Kapiris, Eftaxias et al., 2004; Kapiris et al., 2002, 2003, 2005 and references therein).

Several investigations on earthquake prediction were based on visual observations. Numerous have utilised concepts from the theory of entropy and information (e.g. Kalimeri et al., 2008; Eftaxias et al., 2009). Alternative approximations employed the use of fractal methods, symbolic dynamics, Natural Time, Hurst Exponent and DFA (Detrended Fluctuation Analysis) (Eftaxias et al., 2008, 2010; Petraki, Nikolopoulos, Fotopoulos, Panagiotaras, Koulouras et al., 2013; Petraki, Nikolopoulos, Fotopoulos, Panagiotaras, Nomicos et al., 2013; Varotsos, Sarlis, & Skordas, 2011; Varotsos, Sarlis, Skordas, & Lazaridou, 2007)

Usually employed entropy metrics were (Karamanos, 2001; Karamanos, & Nicolis, 1999; Karamanos et al., 2005): (i) Shannon entropy per letter (ii) Conditional entropy (iii) Entropy of the source (iv) T-entropy (v) Tsallis entropy (vi) Hurst exponent (vii)

Fisher Information (viii) Perturbation entropy (ix) Fractal dimension. Pre-seismic EM precursors were investigated in terms of critical phenomena as well (Contoyiannis et al., 2004, 2005 Contoyiannis, & Eftaxias, 2005, 2008; Eftaxias et al., 2010).

In the above sense, **Table 1** in **Appendix 1** presents a collection of relevant important data including: (1) earthquake details; (2) detected pre-earthquake disturbances; (3) detection techniques employed and analysis methods; (4) references. From **Table 1** (**Appendix 1**) it may be observed that most of the electromagnetic precursors are in ULF, LF (Low Frequency), HF (High Frequency) and VHF (Very High Frequency) range. It may seen that the most disturbances were analysed visually. Analysis based on advanced techniques has been reported in some cases. More significant seem to be the Natural Time and Detrended Fluctuation Analysis, the evolution of fractal dimension and Hurst exponent and the temporal changes of various metrics of entropy. The latter techniques investigated in detail, traces of long-memory hidden in pre-earthquake time-series or features of self-organization of the earthquake generating system (Petraki et al., 2015).

Some characteristic cases of **Table 1** are the following while the full table is in **Appendix 1**:

- An earthquake that occurred in Chile (05/22/1960) and associated with electromagnetic disturbances in the frequency range of 18 MHz. These EM signals were received from a radio-astronomy receiver six days before the event (Warwick, Stoker, & Meyer, 1982).
- An earthquake that occurred in Kyoto, Japan (03/31/1980) and associated with

VLF electric disturbances in the frequency range of 81 KHz. These EM signals were received from electric antennas 1/2 hours before the event (Gokhberg, Morgounov, Yoshino, & Tomizawa, 1982).

- An earthquake that occurred in Watsonville, California (03/23/1991) and associated with ELF (Extremely Low Frequency) magnetic disturbances in the range of 3.0-4.0 Hz. TheseEM signals were received from north-south magnetic sensor 2 days before the event (Dea, Hansen, & Boerner, 1993).
- An earthquake that occurred in Guam, Japan (08/08/1993) and associated with ULF magnetic disturbances in the range of 0.02-0.05 Hz. These EM signals were received from flux-gate-magnetometer 1 month before the event (Hayakawa, Ida, & Gotoh, 2005).
- An earthquake that occurred in Kozani-Grevena, Greece (05/13/1995) and associated with VHF electromagnetic disturbances in the range of 41/54 MHz and 3/10 KHz. These EM signals were received from electric dipole antennas and magnetic loop antennas 20 hours before the event (Contoyiannis et al., 2004).
- An earthquake that occurred in Akita-ken Nairiku-nanbu, Japan (08/11/1996) and associated with VHF electric disturbances in the range of 10 KHz-1 MHz. These EM signals were received from vertical- dipole ground electrodes 6 days before the event (Enomoto, Tsutsumi, Fujinawa, Kasahara, & Hashimoto, 1997).
- An earthquake that occurred in Athens, Greece (09/07/1999) and associated with VLF electromagnetic disturbances in the range of 3 and 10 KHz. These EM signals were received from magnetic loop antennas 12-17 hours before the event (Kapiris et al., 2005).

Following, more specific analysis is presented of pre-seismic electromagnetic disturbances reorganised in the main frequency bands of **Table 1** (**Appendix 1**).

1.4 Preseismic electromagnetic disturbances in frequency bands

1.4.1 ULF emissions

Beginning late in 1980s seismogenic ULF electromagnetic emissions were reported at frequencies lower than 10 Hz (e.g. Hayakawa, & Hobara, 2010; Petraki et al., 2015). Although high frequency components cannot propagate in lithosphere over long distances due to severe attenuation, ULF waves can propagate up to an observation point near the Earth's surface with small attenuation (Hayakawa, & Hobara 2010). ULF electromagnetic noise in the atmosphere, variations of ground electric potential and other known phenomena are found to take place before earthquake occurrences (Varotsos, & Alexopoulos, 1984 a,b; Fraser-Smith et al., 1990; Yu.A., Kopytenko, Matiashviali, Voronov, E.A., Kopytenko, & Molchanov, 1990; Dea et al, 1991; Hayakawa, & Hobara, 2010; Hayakawa, & Ito, 1999; Hayakawa et al., 1996, 2005,2006; Uyeda, 2000; Uyeda, Nagao, & Kamogawa, 2009). ULF precursors are mainly electric, however, several studies have investigated magnetic ULF precursors as well (Cicerone et al., 2009; Petraki et al., 2015).

Regarding the electric ULF precursors, the so-called VAN-method of measuring Seismic Electric Signals (SES) at some days or weeks before earthquake occurrences has been used in Greece (e.g. Varotsos, 2006; Varotsos, & Alexopoulos, 1984 a,b; Varotsos et al., 1986, 1993, 1996, 1999, 2003, 2007, 2011; Varotsos, & Lazaridou, 1991) and Japan (Uyeda, 2000) for earthquake forecasting for more than 20 years (see also Uyeda et al., 2009). SES are ULF (< 1 Hz) signals. Selectivity is one of the most important SES physical properties (e.g. Varotsos et al., 1986, 1993, 1996; Varotsos, &

Lazaridou, 1991), which refers to the experimental fact that a (sensitive) monitoring station is capable to detect SES only from a restricted number of seismic areas. This means that a certain site is sensitive only to SES from some specific focal area(s). These properties can not be explained by a homogeneous medium (e.g. Varotsos, 2006; Varotsos & Alexopoulos, 1984 a,b; Varotsos et al., 1986, 1993, 1996, 1999, 2003; Varotsos & Lazaridou, 1991). A map showing the seismic areas that emit SES detectable (for EQs above a magnitude threshold) at a given station is called "selectivity map of this station" (e.g., Varotsos & Alexopoulos, 1984 a,b; Varotsos et al., 1986, 1993). The remarkable property of SES is that it can be recorded at sensitive sites which are a hundred or more kilometres from the epicentre. Varotsos & Lazaridou (1991) published four criteria according to which true SES can be discriminated from magnetotelluric (MT) variations and from anthropogenic disturbances. The application of these criteria requires the simultaneous operation of short electric dipoles (e.g. with lengths L lying between 50m and 200m) and long dipoles. These allow discrimination of true SES from artificial signals emitted from distances of the order of several kilometres (e.g.Varotsos, 2006 for a correct application of the four VAN criteria).

The empirical dependence of SES amplitude E (mV/m) on earthquake magnitude M looks as (Varotsos et al., 1996):

$$logE=a\cdot M+b, a\sim 0,34-0.37 \qquad (1.1)$$

where a and b are empirical constants. The value of b depends on the azimuth of epicentre reckoned from observation station and the "sensitivity" of station. In other words, the parameter b is not universal. Discussion on the VAN-method has divided the scientific community into two: one supporting it and the other rejecting (e.g. Uyeda,

2000; Petraki et al., 2015).

Either for SES or magnetic pre-seismic ULF signals, three are the mechanisms that have been proposed as potential models:

(a) The first mechanism is the so-called magneto-hydrodynamic (MHD) effect (e.g. Draganov, Inan, & Taranenko, 1991). For this mechanism, the flow of an electrically conducting fluid in the presence of a magnetic field generates a secondary induced field. The MHD equation is derived from Maxwell's equations. The induced magnetic field Bi is given by:

$$B_i = R_m \cdot B \tag{1.2}$$

where R_m is a magnetic Reynolds number analogous to the hydrodynamic Reynolds number and B is the magnetic field that induces B_i . The Reynolds number defines the relative importance of the convective and diffusive terms.

(b) The second mechanism is the so-called piezomagnetic effect (e.g. Sasai, 1991). For this mechanism, a secondary magnetic field is induced due to a change in magnetisation in ferromagnetic rocks in response to an applied stress.

(c) The third mechanism is the electro-kinetic effect (Fitterman, 1978, 1979). The electro-kinetic effect results from the flow of electric currents in the earth, in the presence of an electrified interface at solid–liquid boundaries. These electric currents in turn produce magnetic fields.

More specifically, hypotheses of piezo-stimulated current and current generated by charged dislocations have been proposed by Varotsos & Alexopoulos (1984 a,b). Some theories are based on the electrokinetic hypothesis (Dobrovolsky, Zubkov, & Miachkin, 1989). The electrokinetic currents can be observed in water-saturated media with fluid-

filled channels (Mizutani, & Ishido, 1976; Jouniaux, & Pozzi, 1999). The walls of pores and cracks in a solid body generally adsorb cations from the liquid. Moving along the channel, the liquid carries ions of opposite sign, and thus produces an extrinsic electric current. Surkov, Uyeda, Tanaka, & Hayakawa (2002) in order to model electro-kinetic current parameters, supposed that an earthquake hypo-centre is surrounded by water-saturated porous rocks with fluid-filled pore channels. The pre-earthquake stage is accompanied by appearances of a number of fresh cracks in the vicinity of hypo-centre. Such a zone is called fracture zone. The scale of the fracture zone may be varied from hundreds of metres up to several kilometres. Feder (1988) assumed that the pore space in the fracture zone exhibits fractal structure. Apparently, most of the fresh cracks are closed when formed. Because of the pressure release due to cracking, they are under lower pressure, so that water from uncracked outer region can penetrate into them as soon as a network of connected channels or fractal clusters is formed. The closed fresh cracks may be regarded as the sink of water from surrounding higher pressure areas. Surkov et al. (2002) supposed that the porosity n and permeability of rocks, after the cluster formation, decreases from the centre of the fracture zone towards the periphery by a certain law. The percolation threshold n_c is exceeded in the internal area with typical size L. It means that the permeability tends to zero outside this zone. Actually, there is a finite permeability due to the fact that crustal rocks contain a wide range of small cracks that can be connected. Further there is interest in conductivity of the rock rather than its permeability. The conductivity of the surrounding space is also non-zero due to both the bulk and surface conductivities of the small fluid-filled cracks and conductivity of the rocks itself. Surkov et al. (2002) supposed that these conductivities can be neglected in comparison with that of the fluid-filled cracks, which are formed in the fracture zone, i.e. the conductivity outside the fracture zone is negligible. It means

that the value n_c is rather related to the percolation threshold for conductivity due to the fresh fluid-filled cracks. It should be emphasized that a variety of the crack sizes can be described only in the framework of rather complicated percolation theory. Surkov et al., 2002 restricted the analysis by a simple percolation theory without of account of the crack/channel size distribution. Then the fractal properties near the threshold were determined by the correlation length ξ :

$$\xi \approx \frac{1}{|p-p_c|^{\nu}} \approx \frac{1}{|n-n_c|^{\nu}} \tag{1.3}$$

where *v=0.88* is the correlation length critical exponent, *p* is probability that a channel can conduct the fluid, p_c denotes the critical probability related to percolation threshold, n is the porosity and n_c is the percolation threshold (Feder, 1988).

1.4.2 VHF- emissions

1.4.2.1 KHz band

According to a series of reports (Balasis et al., 2008, 2009; Balasis, & Mandea, 2007; Contoyiannis et al., 2004, 2005 Contoyiannis, & Eftaxias, 2005, 2008; Eftaxias, 2010; Eftaxias et al., 2001, 2002, 2006, 2007, 2008, 2009, 2010; Hadjicontis et al., 2002; Kalimeri et al., 2008; Kapiris, Balasis et al., 2004; Kapiris, Eftaxias et al., 2004; Kapiris et al., 2002, 2003, 2005; Karamanos, 2001; Karamanos, & Nicolis, 1999; Karamanos et al., 2005; Petraki et al., 2015 and references therein), a way to investigate transient phenomena is to analyse a sequence of distinct time windows of short duration into the detected pre-seismic time series. The aim is to discover a clear difference of dynamical characteristics as the catastrophic event is approaching. In order to develop a quantitative identification of KHz EM precursors, the concepts of entropy and tools from information theory are used in order to identify statistical patterns. It is expected

that a significant change of a statistical pattern represents a deviation from normal behaviour, revealing the presence of an anomaly. Symbolic dynamics provide a rigorous way of looking at "real" dynamics. First, a symbolic analysis (Eftaxias et al., 2010; Karamanos, 2001; Karamanos, & Nicolis, 1999; Karamanos et al., 2005; Petraki et al., 2015 and references therein) of experimental data is attempted, in terms of Shannon n-block entropy, Shannon n-block entropy per letter, conditional entropy, entropy of the source and T-entropy. It is well-known that Shannon entropy works best in dealing with systems composed of subsystems, which can access all the available phase space and which are either independent or interact via short-range forces. However, a central property of the earthquake preparation process is the possible occurrence of coherent large-scale collective behaviour with a very rich structure, resulting from repeated non-linear interactions among the constituents of the system. Consequently, non-extensive Tsallis entropy is an appropriate tool for investigating the launch of a KHz EM precursors (Eftaxias, 2010; Eftaxias et al., 2001, 2002, 2006, 2007, 2008, 2009, 2010; Kalimeri et al., 2008). It has been shown (Contoyiannis et al., 2004, 2005 Contoyiannis, & Eftaxias, 2005, 2008; Eftaxias, 2010; Eftaxias et al., 2010; Petraki et al., 2015) that the techniques based on symbolic dynamics discriminate clearly the recorded KHz EM anomalies from the background: they are characterized by a significantly lower complexity (or higher organization). The analysis with Approximate Entropy (ApEn) verified the results of symbolic dynamics. On the other hand, the fractal spectral analysis (Balasis et al., 2008, 2009; Balasis, & Mandea, 2007; Kapiris, Balasis et al., 2004; Kapiris, Eftaxias et al., 2004; Kapiris et al., 2002, 2003, 2005; Eftaxias, 2009; Eftaxias et al., 2010) offers additional information concerning signal/noise discrimination mainly due to two facts. First, it shows that the candidate KHz precursor follows the fractional Brownian motion (fBm)-model while, on the

contrary, the background follows the 1/f-noise model. Second, it implies that the candidate KHz precursor has persistent behaviour (Kapiris, Balasis et al., 2004; Kapiris, Eftaxias, et al., 2004; Kapiris et al., 2003, 2005; Eftaxias et al., 2009; Eftaxias, 2010). The existence of persistency in the candidate precursor is confirmed by R/S analysis, while the conclusion that the anomaly follows the persistent fBm-model is verified by Detrended Fluctuation Analysis.

The abrupt simultaneous appearance of both high organisation and persistency in a launched KHz anomaly implies that the underlying fracto-electromagnetic process is governed by a positive feedback mechanism (Eftaxias et al. 2010). Such a mechanism is consistent with the anomaly's being a candidate precursor. Of course, such an analysis cannot establish, independently, the precursory value of a certain anomaly. Much remains to be done to tackle precursors systematically. It is a difficult task to relate two events separated in time, such as a candidate KHz EM precursor and the ensuing earthquake. It remains to be established whether different approaches could provide additional information that would allow one to accept the seismogenic origin of the recorded KHz EM anomalies and link these to a crucial stage of earthquake generation, i.e., the KHz EM anomalies are associated with the fracture of asperities that are distributed along the fault sustaining the system.

1.4.2.2 MHz band

According to several references (Balasis et al., 2008, 2009; Balasis, & Mandea, 2007; Contoyiannis et al., 2004, 2005 Contoyiannis, & Eftaxias, 2008; Eftaxias et al., 2001, 2002, 2006, 2007, 2008, 2009, 2010; Hadjicontis et al., 2002; Kalimeri et al., 2008; Kapiris, Balasis et al., 2004; Kapiris, Eftaxias et al., 2004; Kapiris et al., 2002, 2003, 2005; Karamanos, 2001; Karamanos et al., 2005; Petraki et al., 2015 and references

therein), the MHz EM precursors present strong anti-persistent behaviour. This behaviour indicates an underlying non-linear feedback of the system that "kicks" the crack-opening rate away from extremes (Eftaxias et al. 2008). This anti-persistent behaviour is similar to the one found in systems which undergo a continuous phase transition at equilibrium (Contoyiannis et al., 2004, 2005 Contoyiannis & Eftaxias, 2005, 2008; Eftaxias et al. 2010; Petraki et al., 2015 and references therein). Heterogeneity could account for the appearance of a stationary-like behaviour in the anti-persistent part of the pre-fracture MHz EM time series. A recently published statistical method of analysis of critical fluctuations has shown that the detected precursory MHz anomalies, could be described in analogy to a continuous thermal phase transition. More specifically, it has been shown (Contoyiannis et al., 2004, 2005 Contoyiannis, & Eftaxias, 2005, 2008; Eftaxias et al., 2010 and references therein) that an underlying strong critical behaviour is consistent to a criterion: the majority of trajectories in the properly defined laminar region carry out information about the underlying criticality. On the contrary, in a recent study (Petraki et al., 2014), it was shown that there might be cases where the MHz EM precursors may exhibit continuous strong persistent behaviour as well. According to Petraki et al., (2014) the candidate MHz precursors are not distinguished a-priory from the KHz precursors. The MHz precursors follow also the fractional Brownian motion (fBm)-model while, the corresponding background follows the 1/f-noise model. The latter finding was also supported by the combined application of fractal methods, rescaled-range analysis and support-vector machines in a very recent study (Cantzos et al., 2015). According to this reference, the background of the MHz EM disturbances follow persistent fGn behaviour, while the corresponding MHz precursors, follow a persistent or anti-persistent fBm-model. Due to the pesistency of the fGn MHz background, it can be

reproduced with accuracy more than 90% through support vector machines. On the other hand, due to the long memory of fBm parts of the MHz EM precursors, they can also be reproduced by support vector machines, either if these are persistent or anti-persistent.

Regarding modelling, according to several references (Contoyiannis et al., 2004, 2005 Contoyiannis, & Eftaxias, 2005, 2008; Eftaxias et al. 2010 and references therein), a thermal second-order phase transition is associated with a "symmetry breaking". To gain insight into the catastrophic character of the fracture phenomena, the evolution of the "symmetry breaking" with time has been elucidated for non-equilibrium-irreversible processes. The analysis showed that the system is gradually driven out of equilibrium. Through this the time was estimated beyond which the process which generates the pre-seismic MHz EM emission could continue only as non-equilibrium instability. More precisely, the analysis revealed the following significant issues: (i) The critical epoch (critical window) during which the short-range correlations evolve to long-range, (ii) The epoch of the "symmetry breaking" occurrence, (iii) The integration of the "symmetry breaking". It is generally accepted that the terminal phase of the earthquake preparation process is accompanied by significant increase in localisation and directionality. It is hence important to distinguish characteristic epochs in the evolution of precursory MHz EM activity and to link these to the equivalent last stages in the earthquake preparation process. Tracing of "symmetry-breaking" may indicate that the micro-fracture propagation has finished in the heterogeneous component of the focal area, which surrounds the backbone of the strong asperities on the fault plane: the rupture has been obstructed at the boundary of the backbone of strong asperities: The "siege" of asperities has already been started (Eftaxias et al., 2008).

According to investigators (Balasis et al., 2008, 2009; Balasis, & Mandea, 2007; Contoyiannis et al., 2004, 2005 Contoyiannis, & Eftaxias, 2005, 2008; Eftaxias, 2010; Eftaxias et al., 2001, 2002, 2006, 2007, 2008, 2009, 2010; Hadjicontis et al., 2002; Kalimeri et al., 2008; Kapiris, Balasis et al., 2004; Kapiris, Eftaxias et al., 2004; Kapiris et al., 2002, 2003, 2005; Karamanos, 2001; Karamanos, & Nicolis, 1999; Karamanos et al., 2005 and references therein), the MHz radiation precedes KHz both at the large (geophysical) and at the small (laboratory) scale . Attention should be given to the fact that the time lags between the pre-earthquake EM anomalies and the impeding earthquakes are different among the MHz and the KHz precursors. According to the above references, the asynchronous emergence of the MHz and the KHz precursors indicates that they refer to different stages of the earthquake preparation process (Eftaxias et al., 2009, 2010; Eftaxias, 2010 and references therein). A significant issue for science is to attempt associations between the numerous detectable EM observations, that appear one after the other, to the consecutive processes within the Earth's crust (Balasis et al., 2008; Contoyiannis et al., 2004, 2005 Contoyiannis, & Eftaxias, 2005, 2008; Eftaxias, 2010; Eftaxias et al., 2001, 2002, 2006, 2007, 2008, 2009, 2010; Hadjicontis et al., 2002; Kapiris, Balasis et al., 2004; Kapiris, Eftaxias et al., 2004; Kapiris et al., 2002, 2003, 2005; Karamanos, 2001; Karamanos, & Nicolis, 1999; Karamanos et al., 2005 and references therein).

According to Eftaxias (2010), the emergence of a MHz EM anomaly is a necessary but not a sufficient condition for the earthquake occurrence (Eftaxias, 2010). Indeed, although numerous MHz EM anomalies have been detected with clear strong, critical and anti-persistent, behaviour, these were not combined with the occurrence of a significant earthquake. Noticeably is that any possible relations of these anomalies

should be excluded if associated to magnetic storm activity, solar flare activity, or, man-made electromagnetic sources.

The above issues are under investigation. Moreover, there is no definite rule to link any kind of pre-earthquake anomaly to a specific forthcoming seismic event, either if this is intense or mild (Eftaxias, 2010; Nikolopoulos et al., 2012, 2014; Petraki et al., 2014; Petraki, Nikolopoulos, Fotopoulos, Panagiotaras, Koulouras et al., 2013; Petraki, Nikolopoulos, Fotopoulos, Panagiotaras, Nomicos et al., 2013; Petraki et al., 2015). So, despite the fairly abundant circumstantial evidence, the scientific community still debates the precursory value of premonitory anomalies detected prior to earthquakes.

1.5 Conclusions

This chapter reviews the electromagnetic precursors focusing on those of the ULF, LF, HF and VHF range. Several investigators have reported pre-seismic electromagnetic disturbances that were claimed to be precursory. The vast majority of the reported electromagnetic disturbances were analysed visually. Advanced techniques based on Natural Time, Detrended Fluctuation Analysis and fractals have been reported for the ULF precursors. Numerous LF and HF pre-earthquake electromagnetic disturbances have been analysed through evolution of fractal dimension, Hurst exponent, DFA and several metrics of entropy. Either the analysis of long memory of the earthquake generating system or the compilation of the system's self-organisation, have provided significant findings regarding the nodal evolution stages of certain earthquakes. Much research needs to be done so as to delineate the process of generation of earthquakes in terms of science.

Chapter 2

Anomalous radon-222 gas emissions and seismic activity

2.1 Introduction

The electromagnetic precursors have been established as seismic phenomena but they can not, however, fully predict the on-set of earthquakes. An additional phenomenon which has been known to exist for many decades is the egress of radon gas. The following chapter will investigate the potential of using radon emission characteristics as earthquake precursors and the research in this thesis will investigate relationships between EM and radon data.

This chapter surveys the published seismic precursors based on the emission of radon gas. A series of papers were searched to collect relevant data, such as the epicentral distance, the extent, time and duration of the radon disturbance and to analyse the precursory value of each observable. In general, enhanced radon emissions have been observed prior to earthquakes and this has been recorded all over the world. The abnormal radon exhalation from the interior of earth has been associated with earthquakes and is considered an important field of research. The proposed physical models attempt to relate the observed radon disturbances with deformations occurring in the earth's crust prior to forthcoming earthquakes. While the models provide some physical explanations, there are many parameters that require further investigation.

Radon is a natural radioactive noble gas. It is generated by the decay of radium. There are thirty nine known isotopes of radon from ^{193}Rn to ^{231}Rn (Nazaroff, & Nero, 1988). The most stable isotope is ^{222}Rn (hereafter radon) with a half-life of 3.823 days. Four isotopes, ^{222}Rn, ^{220}Rn, ^{219}Rn and ^{218}Rn occur in trace quantities in nature as decay products of, respectively, ^{226}Ra, ^{224}Ra, ^{223}Ra and ^{218}At (Nazaroff, & Nero, 1988; UNSCEAR, 2000). ^{222}Rn and ^{218}Rn are intermediate steps in the decay chain of ^{238}U, ^{219}Rn is an intermediate step in the decay chain of ^{235}U and ^{220}Rn occurs in the decay chain of ^{232}Th (Nazaroff, & Nero, 1988; UNSCEAR, 2000; Vogiannis, & Nikolopoulos, 2015). ^{220}Rn is also known as thoron (Nazaroff, & Nero, 1988). The half-life of thoron is 54.5 seconds (Nazaroff, & Nero, 1988). Due to the short half-life, thoron disintegrates very quickly. For this reason, it is usually traced in smaller quantities compared to radon. ^{219}Rn is also called actinon (Nazaroff, & Nero, 1988). It has lesser half-life time than ^{222}Rn and ^{220}Rn (3.92 seconds). It is traced in earth and atmosphere in smaller quantities in respect to radon and thoron (Nikolopoulos, & Louizi, 2008; UNSCEAR, 2008; Vogiannis, & Nikolopoulos, 2015). Most of the radioactivity in the atmosphere at sea level is due to radon (Vogiannis, & Nikolopoulos, 2015). Radon is released primarily from the soil (Nazaroff, & Nero, 1988; Nikolopoulos, & Louizi, 2008; Vogiannis, & Nikolopoulos, 2015). Approximately 10% of the radon in soil is diluted to the atmosphere (Vogiannis, & Nikolopoulos, 2015). Apart from soil, radon is present in fragmented rock, building materials, underground and surface waters (Nikolopoulos, & Louizi, 2008; Vogiannis, & Nikolopoulos, 2015). While in fluids all generated radon atoms are diluted, in porous media and fragmented rock only a percentage of radon emanates, enters the volume of the pores and dissolves into the pore's fluid (Nazaroff, & Nero, 1988; Nikolopoulos, & Louizi, 2008). Once there, a macroscopic transport is possible, either by molecular diffusion, advenction or

convection (Nikolopoulos, & Louizi, 2008). This transport is achieved through interconnected pores and water aquifers (Ghosh, Deb, & Sengupta, 2009; Khayrat et al., 2001; Nikolopoulos, & Louizi, 2008). When the pores are saturated with water, radon is dissolved into water and is transported by it (Nazaroff, & Nero, 1988). The transportation is achieved by means of fluid flow present in soil and fragmented rock (Ghosh et al., 2009; Nazaroff, & Nero, 1988; Nikolopoulos, & Louizi, 2008). Through these processes radon can travel to short, medium or long distances reaching water aquifers and air (Nikolopoulos et al., 2012). Various factors affect the whole process. The most important factors are the permeability of the soil, the temperature gradients and the pressure differences (Nikolopoulos et al., 2012; Vogiannis, & Nikolopoulos, 2015). Radon is very important from radiological point of view, since it accounts for more than half of the natural exposure of the general public (NCRP, 1988; UNSCEAR, 2008; Vogiannis, & Nikolopoulos, 2015). It is well known that among natural radioactivity (not man-made), the most dominant component is radon and, therefore, it is the major contributor to the effective dose equivalent.

2.2 Overview of radon studies with aspects of earthquake prediction

Radon has been used as a trace gas in several studies of Earth, hydrogeology and atmosphere, because of its ability to travel to comparatively long distances from its parent mineral and the efficiency of detecting it at very low levels (Richon et al., 2009). Significant variations of radon and progeny have been observed in geothermal fields (Whitehead et al., 2007), thermal spas (e.g. Vogiannis, & Nikolopoulos, 2008), active faults (e,g. Al-Tamimi, & Abumura, 2001; King, 1980, 1985; Tansi, Tallarico, Iovine, Gallo, & Falcone, 2005; Walia et al., 2009), soil experiments (Zafrir, Steinitz, Malik, Haquin, & Gazit-Yaari, 2009), volcanic processes (e.g. Imme´, Delf, Nigro, Morelli, &

Patane´, 2005; Morelli et al., 2006) and seismotectonic environments (e.g. Chyi, Quick, Yang, & Chen, 2005; Cicerone et al., 2009; Ghosh et al., 2009; Kuo et al., 2009; Majumdar, 2004; Nikolopoulos et al., 2012, 2014; Zafrir et al., 2009; Petraki, Nikolopoulos, Fotopoulos, Panagiotaras, Koulouras et al., 2013; Petraki, Nikolopoulos, Fotopoulos, Panagiotaras, Nomicos et al., 2013; Petraki, Nikolopoulos, Panagiotaras et al., 2015; Singh, Ramola, Singh, Singh, & Virk, 1991; Singh et al., 2010). Due to its importance, radon monitoring has become a continuously growing study area in the search of premonitory signals prior to earthquakes (Ghosh et al., 2009). This falls more or less, in the general area of seismology where one most elusive goals is the short-term earthquake prediction (Cicerone et al., 2009). By the mid 1970s the seismological community was confident that the short-term earthquake prediction would be achieved within a short period of time (Cicerone et al., 2009). One area that may hold promise in advancing the science of short-term earthquake prediction is the study of earthquake precursors (Cicerone et al., 2009). In fact, the short-term predictions are typically based on observations of these types of phenomena (Cicerone et al., 2009). The term earthquake precursor is used to describe a wide variety of physical phenomena that reportedly precede at least some earthquakes (Cicerone et al., 2009). Under this perspective, the real time radon monitoring can be viewed as an interesting possibility for credible earthquake precursors. However, the problem of earthquake prediction still remains unsolved. All the same, positive precursors recorded prior to earthquakes indicate there is evidence that they can be used for forecasting. For example, the strain changes occurring within the earth's surface during an earthquake enhance the radon concentration in soil gas (e.g. Ghosh et al., 2009; Nikolopoulos et al., 2014; Petraki, Nikolopoulos, Fotopoulos, Panagiotaras, Koulouras et al., 2013; Petraki, Nikolopoulos, Fotopoulos, Panagiotaras, Nomicos et al., 2013; Petraki, Nikolopoulos, Panagiotaras, et

al., 2015) and this renders impressive development in the study of the earth's crust which permits the estimate on the probabilities of earthquake risks (Ghosh et al., 2009). In general, during earthquake rupture, certain precursory activity can be expected if the observation is made in the near vicinity of causative fracture (Cicerone et al., 2009). The problem of the earthquake prediction however consists of the consecutive, step-by-step, narrowing of the time interval, space and magnitude ranges, where a strong earthquake should be expected (Keilis-Borok, 2002; Keilis-Borok, & Soloviev, 2003). In this sense, several investigators have attempted connections between earthquake-relating parameters (e.g. magnitude, precursory time, epicentral distance) and time-series characteristics (e.g. range, duration, number of radon anomalies) (e.g. Cicerone et al., 2009; Ghosh et al., 2009; Hashemi, Negarestani, Namvaran, & Nasa, 2013; Mogro-Campero, & Fleischer, 1979; Namvaran, & Negarestani, 2012; Rikitake, 1987; Zoran et al., 2012).

The prediction of earthquakes is usually distinguished in five stages. The background stage provides maps with the territorial distribution of the maximum possible magnitude and recurrence time of destructive earthquake of different magnitudes. The four subsequent stages, fuzzily divided, include the time prediction; they are as follows (Keilis-Borok, 2002): long-term (10 years); intermediate-term (1 year); short-term (approximately 36 days to 3.6 days) and immediate-term (approximately 9 hours or less). Such division into stages is dictated by the character of the process that leads to a strong earthquake and by the needs of earthquake preparedness; the latter comprises an arsenal of safety measures for each stage of prediction (Keilis-Borok, & Soloviev, 2003). According to the classification of Hayakawa and Hobara (2010) the prediction of earthquakes is grouped into three categories: long-term (timescale of 10 to 100 years);

intermediate-term (time-scale of 1 to 10 years); short-term. Note, that even in short-term prediction there is no one-to-one correspondence between anomalies in the observations and the earthquake events (Namvaran, & Negarestani, 2012; Nikolopoulos et al., 2014; Petraki, Nikolopoulos, Fotopoulos, Panagiotaras, Koulouras et al., 2013; Petraki, Nikolopoulos, Fotopoulos, Panagiotaras, Nomicos et al., 2013; Petraki, Nikolopoulos, Panagiotaras et al., 2015). Although much more difficult than the long-term and intermediate-term predictions, the short-term prediction of earthquakes on a time-scale of hours, days or weeks, is believed to be of the highest priority for social demands in seismo-active countries.

Following the classification of Hayakawa and Hobara (2010) and in agreement to the aspects expressed by Hashemi et al. (2013) and several other researchers (e.g references in Ghosh et al., 2009 and Cicerone et al., 2009), radon can be considered as a short-term earthquake precursor. Under this perspective, related research should continue and check further potential associations between radon and earthquakes (Cicerone et al., 2009; Ghosh et al.,2009). Nevertheless, no universal model exists to serve as a pre-earthquake signature (Eftaxias et al., 2008; Petraki, Nikolopoulos, Nomicos et al., 2015; Petraki, Nikolopoulos, Panagiotaras et al., 2015). Moreover, there is no definite rule to link any kind of pre-earthquake anomaly to a specific forthcoming seismic event, either if this is intense or mild (Eftaxias, 2010; Nikolopoulos et al., 2014; Petraki, Nikolopoulos, Fotopoulos, Panagiotaras, Koulouras et al., 2013; Petraki, Nikolopoulos, Fotopoulos, Panagiotaras, Nomicos et al., 2013; Petraki, Nikolopoulos, Nomicos et al., 2015; Petraki, Nikolopoulos, Pangiotaras et al., 2015). In addition, despite the scientific efforts, the preparation and evolution of earthquakes is not delineated yet (Petraki, Nikolopoulos, Nomicos et al., 2015; Petraki, Nikolopoulos, Panagiotaras et al., 2015).

A significant reason is that there is restricted knowledge of the fracture mechanisms of the crust (Contoyiannis, & Eftaxias, 2008; Contoyiannis, Kapiris, & Eftaxias, 2005; Eftaxias, 2010; Eftaxias et al., 2001, 2002, 2006, 2007, 2008, 2009, 2010; Hadjicontis, Mavromatou, & Eftaxias, 2002; Kapiris et al., 2003; Kapiris, Eftaxias, & Chelidze, 2005; Kapiris, Polygiannakis, Peratzakis, Nomicos & Eftaxias, 2002; Nikolopoulos et al., 2014; Petraki, Nikolopoulos, Fotopoulos, Panagiotaras, Koulouras et al., 2013; Petraki, Nikolopoulos, Fotopoulos, Panagiotaras, Nomicos et al., 2013; Petraki, Nikolopoulos, Nomicos et al., 2015; Petraki, Nikolopoulos, Panagiotaras et al., 2015). This is reinforced by the fact that each earthquake is particular and happens in large-scale. Accounting that the fracture of heterogeneous materials is not sufficiently described yet, despite the tremendous up-to-date effort at laboratory, theoretical and numerical level (Eftaxias et al., 2010), it may be understood why the description of the genesis of earthquakes is still limited (Contoyiannis, & Eftaxias, 2008; Contoyiannis, Kapiris, & Eftaxias, 2005; Eftaxias, 2010; Eftaxias et al., 2001, 2002, 2006, 2007, 2008, 2009, 2010; Hadjicontis et al., 2002; Kapiris et al., 2003; Kapiris et al., 2005; Kapiris, Polygiannakis, Peratzakis, Nomicos, & Eftaxias, 2002). According to Eftaxias et al. (2010) one should expect that the preparatory processes of earthquakes have various facets, which may be potentially observed before the final catastrophe at geological, geochemical, hydrological and environmental scales.

In the following, specific scientific evidence is presented regarding the possibilities of forecasting of earthquakes in terms of monitoring of radon gas emissions. The analysis is focused on the short-term precursors of general failure since these are considered of higher prognostic value in terms of societal demands.

2.3 Radon gas emissions and pre-earthquake activity

In the late 1960s and early 1970s reports primarily from Russia and China indicated that concentrations of radon gas in the earth apparently changed prior to the occurrences of nearby earthquakes (Zoran et al., 2012). This stimulated a number of experiments in other parts of the world to monitor underground radon with time and to look for radon changes associated with earthquakes (Cicerone et al., 2009). **Table 2** in **Appendix 2** presents a collection of relevant important data including: (1) the earthquake details; (2) the % (δα) disturbance or detected disturbances in radon concentration; (3) the duration of the detected anomaly or the recorded anomalies; (4) the precursory time; (5) the epicentral distance (6) the related references from 1980 and after.

In general, the anomalous radon variations observed prior to earthquakes have been reported in groundwater, soil gas, atmosphere and thermal spas (Chyi et al., 2005; Cicerone et al., 2009; Petraki, Nikolopoulos, Fotopoulos, Panagiotaras, Koulouras et al., 2013; Petraki, Nikolopoulos, Fotopoulos, Panagiotaras, Nomicos et al., 2013; Petraki, Nikolopoulos, Nomicos et al., 2015; Petraki, Nikolopoulos, Panagiotaras et al., 2015). The seismological data of **Table 2** (**Appendix 2**) are related to radon concentration data of wide fluctuations, peaks and downturns (Petraki, Nikolopoulos, Nomicos et al., 2015; Petraki, Nikolopoulos, Panagiotaras et al., 2015). The earthquake-related connections of **Table 2** (**Appendix 2**), namely the connections between the magnitude, the precursory time and the epicentral distance with the time-series characteristics, viz., the range, the duration and the number of radon anomalies vary significantly (Ghosh et al., 2009, Petraki et al., 2009). For example, the reported precursory times range from 3 months to some days prior to the earthquake event,

whilst the epicentral distances range between 10 and 100 km. It is very important to note here that many precursory signals have been derived only with passive techniques (Nikolopoulos et al., 2014; Petraki, Nikolopoulos, Fotopoulos, Panagiotaras, Koulouras et al., 2013; Petraki, Nikolopoulos, Fotopoulos, Panagiotaras, Nomicos et al., 2013; Petraki et al., 2015) which integrate radon concentrations over long time intervals (at least >1-4 weeks), i.e., they provide coarse time-series estimations. This is a significant disadvantage for the reported estimations. On the other hand, the reported precursory signals with active techniques are limited. Note that the active techniques enable high radon recording rates (between 1 min^{-1} and 1 $hour^{-1}$) and in this manner they provide fine radon signals (Cicerone et al., 2009; Ghosh et al., 2009; Nikolopoulos et al., 2014; Petraki, Nikolopoulos, Fotopoulos, Panagiotaras, Koulouras et al., 2013; Petraki, Nikolopoulos, Fotopoulos, Panagiotaras, Nomicos et al., 2013; Petraki et al., 2015). Important is that there are also other parameters that affect and alter the radon-earthquake estimations. For example, radon concentration levels are influenced by geological and geophysical conditions, the seasonal variations and atmospheric changes such as the rainfall and the barometric pressure alterations (e.g. Nazaroff, & Nero, 1988; Nikolopoulos et al., 2014; Petraki, Nikolopoulos, Fotopoulos, Panagiotaras, Koulouras et al., 2013; Petraki, Nikolopoulos, Fotopoulos, Panagiotaras, Nomicos et al., 2013; Petraki et al., 2015). For this reason the related time-series data are usually presented in parallel to the radon precursory signals (Petraki et al., 2015). As can be observed from **Table 2** (**Appendix 2**), the majority of the associations between radon and earthquakes are based on events of small or intermediate magnitudes. This restricts the estimations more, since, up-to-date there seems not to exist, not only for the mild, but even for the intense earthquakes, a universal model to serve as a signature of a specific forthcoming seismic event (Contoyiannis, & Eftaxias, 2008; Contoyiannis,

Kapiris & Eftaxias, 2005; Eftaxias, 2010; Eftaxias et al., 2001, 2002, 2006, 2007, 2008, 2009, 2010; Hadjicontis et al., 2002; Kapiris et al., 2003; Kapiris et al., 2005; Kapiris, Polygiannakis, Peratzakis, Nomicos, & Eftaxias, 2002 and references therein).

Most of the disturbances of **Table 2** (**Appendix 2**) were determined in terms of visual or simple statistical analysis. The most usual statistical criterion employed is the $\pm 2\sigma$ one. Through this criterion, a radon disturbance is identified as such if it contains parts above the $\pm 2\sigma$ zone. Although simple, this approach was used extensively in many papers of **Table 2** (**Appendix 2**). Only few radon signals have been analysed through advanced techniques (Barman, Chaudhuri, Ghose, Deb, & Sinha, 2014; Ghosh, Deb, Dutta, & Sengupta, 2012; Nikolopoulos et al., 2014; Petraki, Nikolopoulos, Fotopoulos, Panagiotaras, Koulouras et al., 2013; Petraki, Nikolopoulos, Fotopoulos, Panagiotaras, Nomicos et al., 2013; Petraki, Nikolopoulos, Nomicos et al., 2015; Petraki, Nikolopoulos, Panagiotaras et al., 2015; Planinic, Radolic, & Lazanin, 2001; Planinic, Vukovic, & Radolic, 2004; Radolic, Vukovic, Stanic, & Planinic, 2005). Six of these nine reports are recent, viz., published after 2012. Worth to notice is that the analysis was implemented in fine active signals recorded after significant earthquakes of near epicenters (e.g. Nikolopoulos et al., 2014; Petraki, Nikolopoulos, Fotopoulos, Panagiotaras, Koulouras et al., 2013; Petraki, Nikolopoulos, Fotopoulos, Panagiotaras, Nomicos et al., 2013; Petraki, Nikolopoulos, Nomicos et al., 2015; Petraki, Nikolopoulos, Panagiotaras et al., 2015) fact which enhances the estimates of these reports further. A fact that reinforces the estimates of these reports is that the corresponding radon disturbances lasted long, i.e., between five and fifteen days. One of the advanced techniques of these reports (Ghosh et al., 2012; Nikolopoulos et al., 2014; Petraki, Nikolopoulos, Fotopoulos, Panagiotaras, Koulouras et al., 2013; Petraki,

Nikolopoulos, Fotopoulos, Panagiotaras, Nomicos et al., 2013; Petraki, Nikolopoulos, Nomicos et al., 2015; Petraki, Nikolopoulos, Panagiotaras et al., 2015) is the temporal Fractal Analysis based on a windowed version of the short-time wavelet transform of the density of the power spectrum in each window (Nikolopoulos et al., 2014; Petraki, Nikolopoulos, Fotopoulos, Panagiotaras, Koulouras et al., 2013; Petraki, Nikolopoulos, Fotopoulos, Panagiotaras, Nomicos et al., 2013). Note that the method was applied in both mono-fractals (Nikolopoulos et al., 2012; Petraki, Nikolopoulos, Fotopoulos, Panagiotaras, Nomicos et al., 2013) and multifractals (Barman et al., 2014; Ghosh et al., 2012). Another advanced approach is the detrended fluctuation analysis (DFA) (Das et al., 2006; Petraki, Nikolopoulos, Fotopoulos, Panagiotaras, Koulouras et al., 2013; Nikolopoulos et al., 2015). According to reports (Das et al., 2006; Petraki, Nikolopoulos, Fotopoulos, Panagiotaras, Koulouras et al., 2013; Nikolopoulos et al, 2015) and several other related papers (e.g. Eftaxias, 2010; Eftaxias et al., 2009; Varotsos, Sarlis, & Skordas, 2009 and references therein) the detrended fluctuation analysis is the most advantageous technique to trace the long-memory of a system driven to rupture. Significant other techniques are the time-evolution of the fractal dimension (Petraki, Nikolopoulos, Fotopoulos, Panagiotaras, Nomicos et al., 2013) the Hurst exponent (Eftaxias et al., 2009; Nikolopoulos et al., 2014; Petraki, Nikolopoulos, Fotopoulos, Panagiotaras, Koulouras et al., 2013; Petraki, Nikolopoulos, Fotopoulos, Panagiotaras, Nomicos et al., 2013) and the temporal changes of various metrics of entropy (Eftaxias et al, 2010; Kalimeri et al., 2008; Petraki, Nikolopoulos, Fotopoulos, Panagiotaras, Nomicos et al., 2013). Note that the techniques can trace patterns of long-memory that are hidden in the pre-earthquake time-series. They can also identify features related to the self-organisation of the earthquake generating system. It is also important to note that the vast majority of papers of **Table 2** (**Appendix 2**) refer to

measurement of radon in soil. Only some papers refer to radon in underground or thermal water and only one to radon detected in atmosphere prior to earthquakes (Yasuoka, Igarashi, Ishikawa, Tokonami, & Shinogi, 2006). Note that in this paper advanced Fourier based approach was implemented for a significant long-lasting signal retrieved prior to the Kobe earthquake, Japan.

Some characteristic cases of **Table 2** are the following while the full table is in **Appendix 2**:

- An earthquake that occurred in Izu-Oshima, Japan (01/14/1978). The radon signal had 230 days duration and was received 25 km away from the epicentre (Wakita, Nakamura, & Sano, 1988).
- An earthquake that occurred in Kobe, Japan (01/17/1995). The radon signal was received 2 months before the event (Yasuoka et al., 2006).
- An earthquake that occurred in Haicheng, PR China (04/02/1975). The radon signal had 270 days duration (Hauksson, 1981).
- An earthquake that occurred in Tashkent, Ex-USSR (04/26/1966). The radon signal had 400 days duration (Hausson, 1981).
- An earthquake that occurred in Chamoli, India (03/29/1999). The radon signal was received 2 days before the event (Virk, Walia, &Kumar, 2001).
- An earthquake that occurred in Peloponnese, Greece (06/08/2008). The radon signal had 3-5 days duration and was received 2-3 months before the event (Nikolopoulos et al., 2012).

Various physical mechanisms have been reported to relate the sub-surface physical changes with the variation in radon emanations (Nikolopoulos et al., 2014). Regarding

modelling, the available models propose explanations in terms of strain changes within the earth's crust during preparation of earthquakes (Ghosh et al., 2009; Mogro-Campero, & Fleischer, 1979; Namvaran, & Negarestani, 2012; Zoran et al., 2012). It is the displacement of rock mass under tectonic stress that opens up various pathways and exposes new surfaces when cracks open. The stress-strain developed within the earth's crust before earthquakes leads to changes in gas transportation from the deep earth to surface (Dobrovolsky et al., 1979; Ghosh et al., 2009). As a result, unusual quantities of radon emerge out of the pores and fractures of the rocks on the surface. Due to the seismic activity, changes in underground fluid flow may also render anomalous changes in concentration of radon and its decay products (Nikolopoulos et al., 2014). A small change in velocity of gas into or out of the ground causes a significant change in radon concentration at shallow soil depth as changes in gas flow disturb the strong radon concentration gradient that exists between the soil and the atmosphere. A slight compression of pore volume causes gas to flow out of the soil resulting to an increase in radon level. Similarly, when pore volume increases, gas flows into the soil from the atmosphere. Thus, an increased radon concentration occurs in the region of compression and radon concentration decreases in the region of dilation. As small changes in gas flow velocity causes significant change in radon concentration, soil radon monitoring is thus an important way to detect the changes in compression or dilation associated with an earthquake event.

Among the various theoretical models, the dilatancy diffusion model proposed by Martinelli (Ghosh et al., 2009; Martinelli, 1991) is a noteworthy approach. According to this model (Ghosh et al., 2009; Nikolopoulos et al., 2012; Petraki, Nikolopoulos, Fotopoulos, Panagiotaras, Koulouras et al., 2013) the earthquake generating medium is

considered to consist of porous cracked saturated rocks. When a tectonic stress develops, the cracks extend and appear near the pores with the opening of favourably oriented cracks (Ghosh et al., 2009). As a result, the pore pressure decreases in the total preparation zone and water from surrounding medium diffuses into the zone. At the end of the diffusion period the main rupture occurs due to the appearance of pore pressure and increase in cracks (Ghosh et al., 2009). A well-accepted model is the the Crack–Avalanche model (Dobrovolsky et al., 1979; Ghosh et al., 2009; Nikolopoulos et al., 2012; Petraki, Nikolopoulos, Fotopoulos, Panagiotaras, Koulouras et al., 2013). According to the Crack–Avalanche model as tectonic stress increases during the earthquake preparation, a zone of cracked rocks is formed in the region of a future earthquake focal zone under the influence of the tectonic stresses. In the study of the surrounding medium this region may be considered as a solid inclusion with altered moduli. The inclusion appearance causes a redistribution of the stresses accompanied by corresponding deformations. As the tectonic stresses change with time, the shape and size of the zone change as well. According to the theory of stress corrosion, the anomalous behaviour of radon concentration may be associated with this slow crack growth, which is controlled by the stress corrosion in the rock matrix saturated by groundwater.

A very recent model has been proposed (Nikolopoulos et al., 2012, 2015; Petraki, Nikolopoulos, Fotopoulos, Panagiotaras, Koulouras et al., 2013) based on the aspects expressed by Eftaxias (2010), Eftaxias et al., (2008), Minadakis, Potirakis, Nomicos, & Eftaxias, (2012). This model is called the asperity model. According to the asperity model, the focal area consists of a backbone of strong and large asperities that sustain the earthquake-generating system. A strongly heterogeneous medium surrounds the

family of strong asperities. The fracture of the heterogeneous system in the focal area obstructs the backbone of asperities. At this stage, critical anti-persistent MHz electromagnetic anomalies and radon anomalies occur (Eftaxias 2010; Eftaxias et al., 2008; Minadakis et al., 2012 and references therein).

Comparing the aforementioned models, it can be claimed that as an earthquake approaches a region of several cracks is formed. The earthquake is associated with deformations and as a result short or long term precursory phenomena like anomalies in radon concentration may occur. As mentioned already, radon can be considered as a short-term earthquake precursor. Nevertheless, no universal model exists to serve as pre-earthquake signature (Eftaxias 2010; Eftaxias et al., 2008; Minadakis, et al., 2012; Nikolopoulos et al., 2012, 2015; Petraki, Nikolopoulos, Fotopoulos, Panagiotaras, Koulouras et al., 2013 and references therein). Moreover, there is no definite rule to link any kind of pre-earthquake anomaly to a specific forthcoming seismic event, either if this is intense or mild (Eftaxias 2010; Eftaxias et al., 2008; Minadakis et al., 2012; Nikolopoulos et al., 2012, 2015; Petraki, Nikolopoulos, Fotopoulos, Panagiotaras, Koulouras et al., 2013 and references therein). For these reasons, despite the fairly abundant circumstantial evidence, the scientific community still debates the precursory value of premonitory anomalies detected prior to earthquakes (Eftaxias, 2010). On the other hand, well established criteria exist to identify pre-earthquake patterns hidden in time-series, which are based on the concepts of fractality, self-organisation, non-extensivity and entropy (Contoyiannis, & Eftaxias, 2008; Contoyiannis, Kapiris & Eftaxias, 2005; Eftaxias, 2010; Eftaxias et al, 2001, 2002, 2006, 2007, 2008, 2009, 2010; Hadjicontis et al., 2002; Kapiris et al., 2003; Kapiris, et al., 2005; Kapiris, Polygiannakis, Peratzakis, Nomicos & Eftaxias, 2002; Nikolopoulos et al., 2014; Petraki, Nikolo-

poulos, Fotopoulos, Panagiotaras, Koulouras et al., 2013; Petraki, Nikolopoulos, Fotopoulos, Panagiotaras, Nomicos et al., 2013; Petraki, Nikolopoulos, Nomicos et al., 2015; Petraki, Nikolopoulos, Panagiotaras et al., 2015). Especially according to Eftaxias (2010), certain questions still remain: (i) How can a certain observation be recognised as pre-seismic? (ii) How can an individual precursor be linked to a distinctive stage of an earthquake preparation process? (iii) How can certain precursory symptoms in anomalous observations be identified so as to indicate that the occurrence of an earthquake is unavoidable? The above issues clearly indicate that radon monitoring in soil is very important from geological point of view.

2.4 Conclusions

This chapter reviewed the pre-seismic precursors which are based on radon gas emissions. Anomalous pre-seismic radon gas emissions have been addressed in soil, atmosphere and water. The related literature started from the early seventies and still is in progress. According to the presented data the majority of the reported radon pre-earthquake disturbances have been analysed mainly visually. The analysis based on advanced techniques is rare and only nine papers have been published with such data. Four of these papers include the writer in the authors list. The nine latter papers are based on time-evolution analysis of the fractal dimension, the Hurst exponent, the power law beta exponents and several metrics of entropy. Multi-fractal and mono fractal DFA has been employed as well. Either the visual analysis or the analysis of the various metrics of the long memory or the self-organisation of the earthquake generating system, provided significant outcomes regarding the earthquake prediction. More research needs to be done to delineate the process of radon generation during earthquakes.

Chapter 3

Long-term trends in pre-earthquake electromagnetic variations through spectral fractal analysis

3.1 Introduction

In the following, results will be presented from a wavelet-based power spectral analysis of fractals applied in electromagnetic time-series of the MHz range. By tracing pre-earthquake long-memory patterns hidden in the investigated time-series, the analysis attempts to investigate possible associations of the results with thirty seven seismic events. The events occurred in Greece from 2007 to 2015 with local magnitudes $M_L \geqslant 5.0$. The majority of the investigated time-series exhibited numerous parts associated with long-memory of the earthquake generation system. The findings were considered also indicative of the self-organised critical states of the last stages of preparation of the investigated earthquakes. The results showed that spectral fractal analysis achieves to detect successfully if the signal follows the most popular Gaussian $1/f$ processes: fractional Brownian motion (fBm) or fractional Gaussian noise (fGn) models. The precursory value of the signals was also discussed.

3.2 Theoretical aspects

3.2.1 Power Spectral Density (PSD)

Instead of analysing a process in the time domain, it can also be analysed in the frequency or spectral domain (Dieker, 2004; Yannakopoulos, 2012). This technique is called spectral analysis, which has many applications, e.g., in physics and time series analysis. A time-domain series can be transformed into a frequency-domain series without loss of information by the Fourier transform

$$W(f) = \int_{-\infty}^{\infty} w(t) e^{-j2\pi ft} dt \tag{3.1}$$

of a time series w(t). This means that the time-domain series is perfectly recovered from the frequency-domain series by the inverse Fourier transform (Dieker, 2004; Yannakopoulos, 2012)

$$w(t) = \int_{-\infty}^{\infty} W(f) e^{j2\pi ft} df \tag{3.2}$$

Fourier proved that a periodic function can be written as a linear combination of trigonometric functions with different frequencies, making it thus possible to describe this function completely by the amount in which each frequency is present (Dieker, 2004). It is possible and useful to extend this idea to non-periodic functions; a deterministic function can be thought to consist of trigonometric functions with different frequencies. The information to which extend each frequency is present in the signal, is then summarized in the spectral density, also called power spectrum density (PSD) because of its interpretation in physics (Dieker, 2004; Yannakopoulos, 2012):

$$S(f) = \lim_{T \to \infty} \left(\frac{|W(f)|^2}{T} \right) \tag{3.3}$$

3.2.2 Self-Similar Signals and 1/f processes

1/f processes are statistically scale invariant or self- similar random processes which model a wide range of natural signals (Wornell, 1995). They are processes which are defined as having power spectra obeying a power law relationship of the form

$$S(f)=a\cdot f^{-b} \tag{3.4}$$

where α is an amplification constant and b is a spectral parameter related to a parameter H according to the relation:

$$b=2\cdot H+1 \tag{3.5}$$

H is a self-similarity parameter of the process which is broadly known as Hurst exponent (Hurst, 1951; Wornell, 1995). For *1/f* processes, there is a strong relationship between the fractal dimension D and the parameter H of the process. In particular, an increase in the parameter H yields a decrease in the dimension D. This is reasonable: an increase in H corresponds to an increase in b, which in turn reflects a redistribution of power from high to low frequencies and leads to sample functions that are increasingly smooth in appearance (Wornell, 1995).

The most popular mathematical models for *1/f* processes are the fractional Brownian motion (fBm) and the fractional Gaussian noise (fGn). In the work of Mandelbrot and Van Ness (Mandelbrot & Van Ness, 1968), the fBm processes are the ones corresponding to $1<b<3$. The classical Brownian motion is a special case corresponding to $b=2$ (Mandelbrot & Van Ness, 1968; Wornell, 1995). In contrast, processes corresponding to $-1<b<1$ are fractional Gaussian noises and stationary white Gaussian noise is the special case corresponding to $b=0$ (Wornell, 1995) . The theory

does not directly accommodate the cases of *b>3* and *b<-1*, although extensions can be formulated. Furthermore, the models are degenerate for the cases *b=1, b=-1* and *b=3* (Wornell, 1995).

3.2.2.1 Fractional Brownian motion

Fractional Brownian motion is a long-range dependent process which is defined by its stochastic representation:

$$B_H(t) := \frac{1}{\Gamma\left(H+\frac{1}{2}\right)} \cdot \{ \int_{-\infty}^{0} [(t-s)^{H-\frac{1}{2}} - (-s)^{H-\frac{1}{2}}] \cdot dB(s) + \int_{0}^{t} (t-s)^{H-\frac{1}{2}} \cdot dB(s) \} \quad (3.6)$$

In equation (3.6) Γ represents the Gamma function

$$\Gamma(\alpha) := \int_{0}^{\infty} x^{\alpha-1} \exp(-x)\, dx \quad (3.7)$$

and $0<H<1$ the Hurst exponent. The integrator B is a stochastic process, the ordinary Brownian motion. When $H=\frac{1}{2}$ equation (3.6) specializes to the classical Brownian motion (Dieker, 2004; Mandelbrot & Van Ness ,1968; Wornel, 1995).

A normalised fBm process, $B_H=\{B_H(t): 0\leqslant t<\infty\}$ with $0<H<1$, is uniquely characterised by the following properties:

- $B_H(t)$ has stationary increments
- $B_H(0)=0$
- $B_H(t)$ has a Gaussian distribution for $t>0$

It is very important to emphasise here that the Fractional Brownian motions are, in fact,

fractals. More specifically, the Fractional Brownian motions whose self-similarity parameters lie in the range $0<H<1$ (i.e. $1<b<3$) have a fractal dimension of $D=2-H$ which, importantly, is a measure of their roughness (Wornel, 1995).

Figure 3.1 is an example case which consists of simulated sample paths for three different values of *H*. From this figure the negative correlations for *H=0.2* can be observed. The sample is more smooth for *H=0.8* due to the positive correlations (Dieker, 2004).

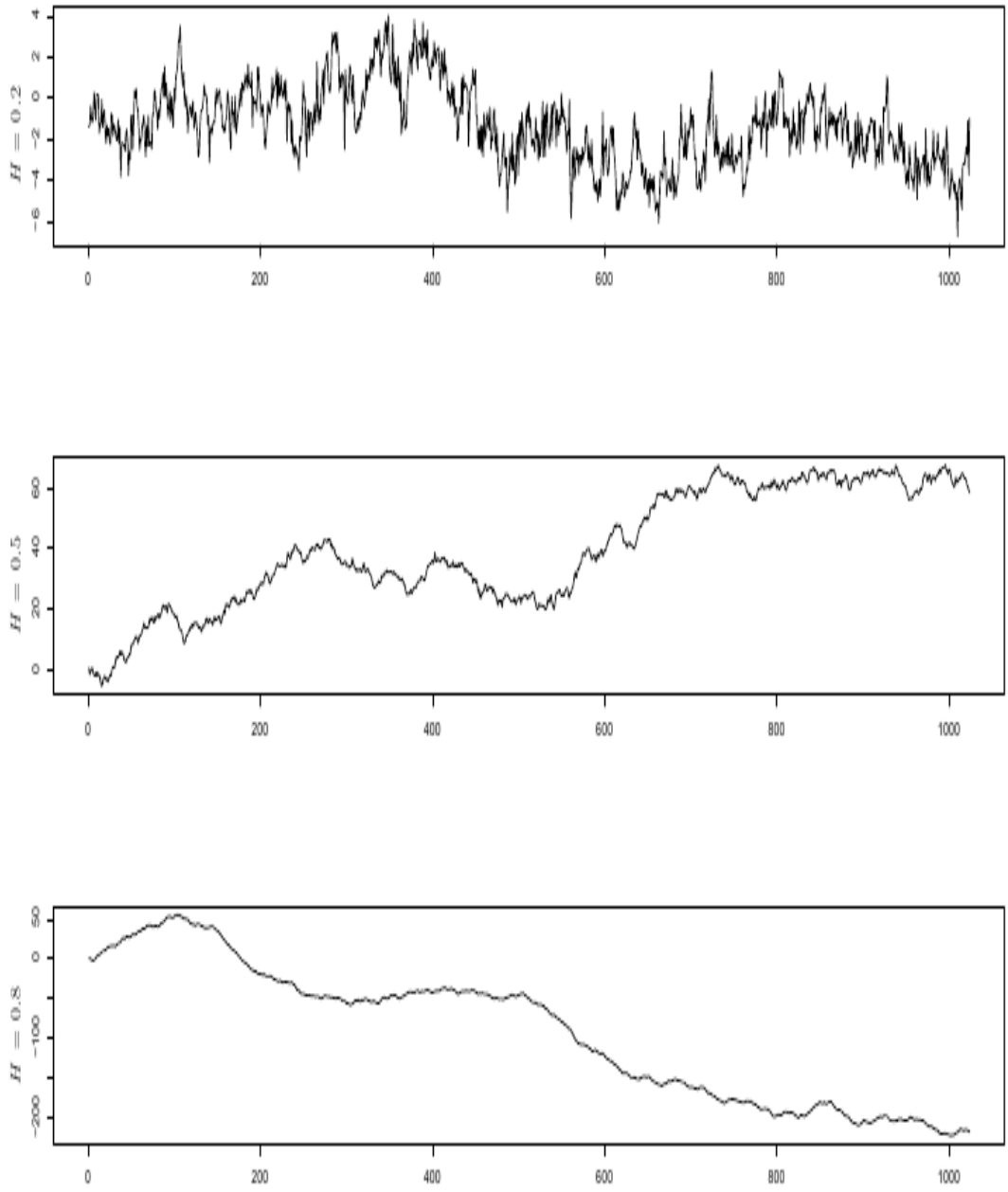

Figure 3.1: Samples of fractional Brownian motion for *H=0.2 , H=0.5, H=0.8.* The horizontal axis is the sample number (Reproduced from Dieker, 2004).

3.2.2.2 Fractional Gaussian noise

The fractional Gaussian noise (fGn) is a long-range dependent process which is defined as the incremental process of the fractional Brownian motion: If X obeys fGn, $X=\{X_k : k=0,1,...\}$ where

$$X_k = B_H(k+1) - B_H(k) \tag{3.8}$$

and X_k has a normal distribution for every k (Dieker, 2004).

For *1/2<H<1* the fGn process exhibits long-term dependence, i.e. persistent correlation structure. For *H=1/2* the process has no correlation (white Gaussian noise), while for *0<H<1/2* it exhibits persistent anti-correlation (Wornel, 1995).

Figure 3.2 presents simulated sample paths for three different values of H .

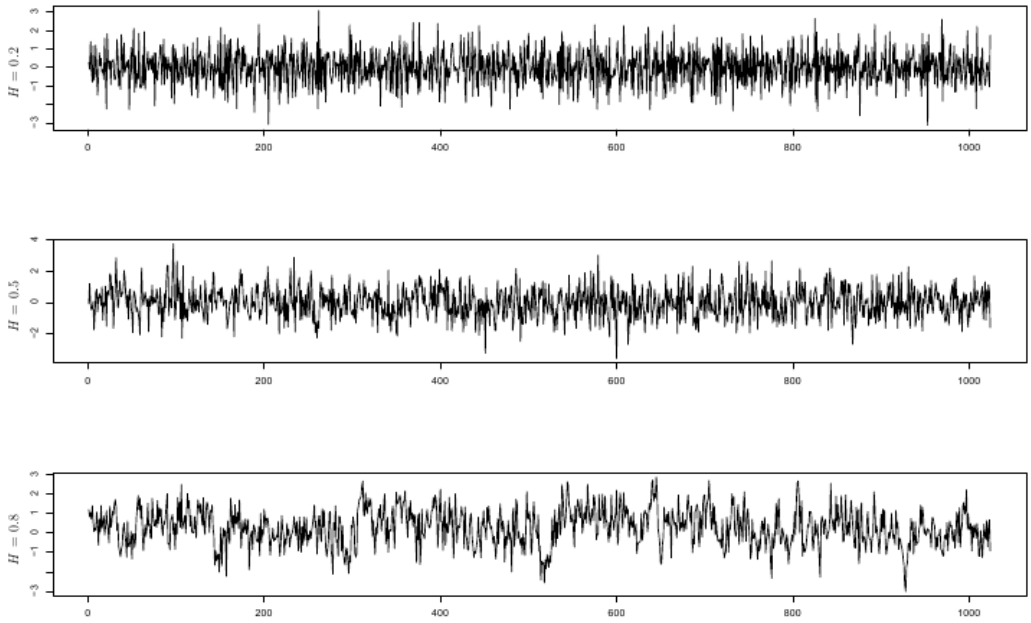

Figure 3.2: Samples of fractional Gaussian noise for *H=0.2 , H=0.5, H=0.8.* The horizontal axis is the sample number (Reproduced from Dieker, 2004).

3.2.3 Fractal analysis from wavelet-based power spectral density

During the complex process of earthquake preparation, linkages between space and time produce characteristic fractal structures (e.g. Eftaxias et al., 2009, 2010; Nikolopoulos et al., 2012, 2014; Petraki, Nikolopoulos, Fotopoulos, Panagiotaras, Koulouras et al., 2013; Petraki, Nikolopoulos, Fotopoulos, Panagiotaras, Nomicos et al., 2013; Smirnova, Hayakawa, & Gotoh, 2004; Smirnova, & Hayakawa, 2007 and references cited in these publications). It is expected that these fractal structures affect signals rooted in the earthquake generation process. The power spectral density, $S(f)$, is probably the most commonly used technique to provide useful information about the inherent memory of the system (Eftaxias et al., 2009; Nikolopoulos et al., 2012, 2014; Petraki, Nikolopoulos, Fotopoulos, Panagiotaras, Koulouras et al., 2013; Petraki, Nikolopoulos, Fotopoulos, Panagiotaras, Nomicos et al., 2013). Although the power spectrum is only the lowest order statistical measure of the deviations of the random density field from homogeneity, it directly reflects the physical scales of the processes that affect structure formation (Eftaxias et al., 2009).

If a recorded time-series, $A(t_i)$, is a temporal fractal, then a power-law spectrum is expected, i.e., $S(f)=a\cdot f^{-b}$, where f is the frequency of the transform. In a $\log(S(f))-\log(f)$ representation, the power spectrum is a straight line, with linear spectral slope b. The spectral amplification quantifies the power of the spectral components following the power spectral density law. The spectral scaling exponent is

a measure of the strength of time correlations. The goodness of the power-law fit to a time-series is represented by the Square of the Spearman's correlation coefficient (Nikolopoulos et al., 2012, 2014; Petraki, Nikolopoulos, Fotopoulos, Panagiotaras, Koulouras et al., 2013). Attention is paid to whether distinct changes in the scaling exponent emerge before or during any detected bursts or anomalies. In this study, the continuous wavelet transform was used with the Morlet wavelet base function.

For the application of the fractal analysis from wavelet-based power spectral density (hereafter abbreviated as spectral fractal analysis) the following steps were followed:

(i) The MHz electromagnetic signals were divided in segments (windows): 1024-2048 samples per segment. These segmentations were expected to reveal the fractal characteristics of the signals (e.g. Eftaxias et al., 2009; Nikolopoulos et al., 2012, 2014; Petraki, Nikolopoulos, Fotopoulos, Panagiotaras, Koulouras et al., 2013; Petraki et al., 2014).

(ii) In each segment the PSD of the signal was calculated. As aforementioned, for the PSD calculation, the DWT using the Morlet wavelet was employed.

(iii) In each segment the existence of a power-law of the form of $S(f)=a\cdot f^{-b}$ was investigated. In DWT PSD calculation, the employed frequency f was the central frequency of the Fourier transform of the Morlet scale.

(iv) The least square method was applied to the $\log(S(f))-\log(f)$ linear representation. Successive representations were considered those that

exhibited squares of the Spearman's correlation coefficient above 0.95, i.e., 95% confidence interval.

3.3 Earthquakes analysed & criteria for selection of earthquakes

Greece is a country prone to earthquakes because it is bounded by the regions of convergence of the Eurasian and African plates and the western termination zone of the North Anatolian Fault (**Figure 3.3**). The country is dominated by extensional seismicity structures and numerous active faults of complex active stress field. The seismicity structures evoked several earthquakes of $M_L \geqslant 5.0$ and $M_W \geqslant 5.0$ during the last century. During the period of the analysis of this research, i.e., between January 2007 and May 2015, several earthquakes occurred in Greece and near with local magnitudes $M_L \geqslant 5.0$ and depths from 2 to 165 km. Thirty seven of these events were analysed in this thesis. The total number of the events with $M_L \geqslant 5.0$ between 2007 and 2015, the number of the analysed events through spectral fractal analysis and the succeeded rate of analysed events are presented in **Table 3.1**.

Table 3.1: Total number of earthquakes with $M_L \geq 5.0$ between 2007 and 2015, number of the analysed events through spectral fractal analysis and the succeeded rates.

Year	Number of events with $M_L \geq 5.0$	Analysed events	Rate of the analysed events
2007	7	4	57.0%
2008	20	12	60.0%
2009	10	9	90.0%
2013	8	3	37.5%
2014	12	6	50.0%
2015	3	3	100%

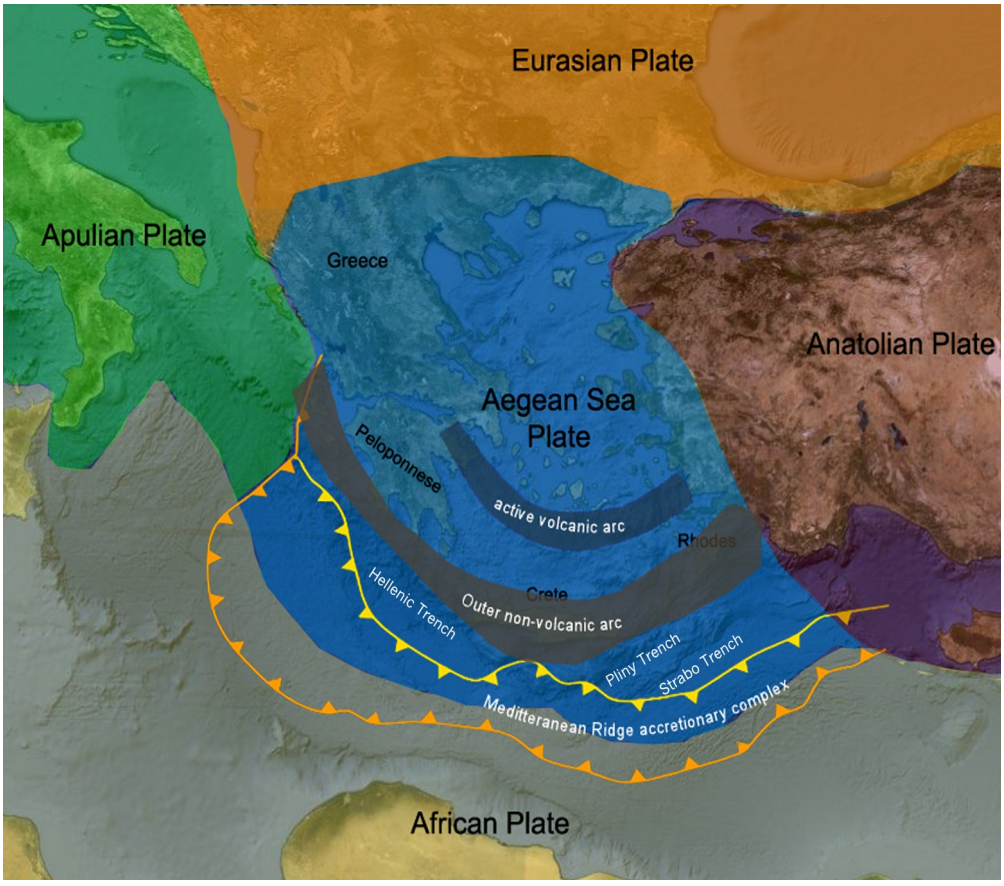

Figure 3.3: Plates bounding Greece.

It can be observed from **Table 3.1** that the selected seismic events analysed with fractal methods, have local magnitudes $M_L \geqslant 5.0$. The criterion for choosing these earthquakes was the national risk that these may cause because of their relatively high magnitudes. A percentage of 67.5% of the studied events with $M_L \geqslant 5.0$ in the years 2007 to 2015, were seismic events that occurred in the Hellenic Trench. As can be observed from **Figure 3.3**, the Hellenic Trench is developed in the western part of the Hellenic Arc and for this reason it is an area of great seismicity and interest. Hence, it is significant that the majority of the studied events corresponded to earthquakes occurred in the Hellenic Trench. Additionally, a percentage of 5.5% of the analysed earthquakes, were seismic events that occurred near the Anatolian Plate. This is also of significance. The remaining 27% of the studied events occurred in scattered areas of the Aegean Sea Plate. From **Table 3.1** it is observed that the percentages of the implemented analysis was above 50% for all years except 2013. This marks up a fairly good proportion for the analysis implemented with PSD based fractals. The overall analysis is significant and towards this point certain facts are outlined below.

It should be emphasised that this is the first study of this range, viz. it is the first study with this amount of analysed events. As will be analysed in detail below in **section 3.4** of this chapter and in conjunction with the data presented in **Chapters 1** and **2**, the majority of research papers of analysis of earthquake events are limited to one event or just few events (of low magnitudes and scattered in space and time in most of the cases). Especially for the case of Greece, the majority of papers (more than 60) referred to three great earthquakes and especially the Pyrgos earthquake (1993), the Kozani-

Grevena earthquake (1995) and the Athens earthquake (1999). This research includes nine great earthquakes with magnitudes $M_L \geqslant 6.0$. Analysis through spectral fractal analysis has been already published to some extend during this research for five of these earthquakes (Nikolopoulos et al., 2012, 2014, 2015; Petraki, Nikolopoulos, Fotopoulos, Panagiotaras, Koulouras et al., 2013; Petraki, Nikolopoulos, Fotopoulos, Panagiotaras, Nomicos et al., 2013). Therefore, either from the view of great earthquakes ($M_L \geqslant 6.0$), either from the perspective of the number of the analysed events (37), this research outlines a significant amount of seismic data.

The extend of the analysis should be emphasised further due to the following argument: there is an enormous need for computation time and computer resources and this just for the part of the spectral fractal analysis. As an example case, the one of electromagnetic data is considered. Assuming that the electromagnetic data from a MHz station are continuously sent from a remote data logger, there is need for the next steps:

(i) Download the signals from the server in which they are stored. The data in the server are stored in hourly basis or continuously. In the first case, the data of each day should be joined to the data of one day. In the second case, the data should be splitted accordingly to daily data.

(ii) Examine daily data visually for bursts or anomalies with custom made software specially designed for that purpose.

(iii) Join multiple daily data in monthly data (as utilised in this research).

(iv) Select and store appropriate one-column channel data for further analysis (channel 9 for the 41 MHz data and channel 10 for the 46 MHz data).

(v) Give the data of step (v) as input for performing spectral fractal analysis with special software designed for that purpose.

(vi) Adjust software parameters of analysis and output and perform the analysis.

(vii) Repeat steps (i)-(vi) in case of loss of power of CPU during run, or incomplete run.

(viii) Store output data in ascii, tif and eps formats (text files and images).

(ix) Perform further calculations from data.

(x) Continuously backup data in removable devices and data cloud emphasising on the adequate naming of the files.

To implement just steps (iv)-(vi) for an one-month one-column single-channel data, there is a need for 15 days of continuous run in a Core Duo PC. Under ideal conditions the time needed for thirty three 41 & 46 MHz monthly time-series data is approximately 33earthquakesX(2*15 days)=33X1month of analysis=33months~3years of continuous non-stop runs in a computer just for the fractal analysis of electromagnetic radiation without data loss. Analytical time-consuming data per earthquake will be presented later in the results section of this chapter. The above argumentation places further emphasis on the work implemented and presented in this chapter.

Table 3.2 presents collectively the data of the earthquakes analysed. The epicentres and the dates of these earthquakes are given. The seismic events which were analysed in this study had depths from 2 to 99 km. Earthquakes 1-33 were analysed through MHz

time-series and earthquakes from 34 to 37 were analysed through radon time-series. The numbering of the earthquakes of this table will be used hereafter as a reference to the analysed earthquakes.

Figures 3.4, 3.5, 3.6, 3.7, 3.8, 3.9 show in maps the corresponding locations of the earthquakes of **Table 3.2**.

Table 3.2: List of earthquake events which were analysed with fractal methods.

Events	Dates	Location	Magnitudes (M_L)
1	2014-05-24	22.9 km SSW of Samothraki	6.3
2	2013-10-12	66.6 km W of Chania	6.2
3	2008-07-15	71.1 km SSW of Rhodes	6.2
4	2008-02-14	35.9 km SSE of Methoni	6.2
5	2015-04-16	56.7 km SSW of Karpathos	6.1
6	2008-02-14	66.5 km S of Methoni	6.1
7	2008-01-06	9.3 km SW of Leonidion	6.1
8	2008-02-20	70.8 km S of Methoni	6.0
9	2014-01-26	6.7 km NE of Argostoli	5.8
10	2013-06-15	109.7 km S of Iraklion	5.8
11	2009-07-01	111.2 km SSE of Iraklion	5.8
12	2014-08-29	69.4 km W of Milos	5.7
13	2013-06-16	116.2 km S of Iraklion	5.6
14	2009-11-03	65.6 km SW of Zakynthos	5.6
15	2009-02-16	74.2 km S of Zakynthos	5.5
16	2008-06-21	88.2 km S of Methoni	5.5
17	2007-03-25	19.3 km NNW of Argostoli	5.5
18	2015-04-17	67.2 km SSW of Karpathos	5.4
19	2009-09-06	124.6 km NW of Florina	5.4
20	2009-06-19	107.8 km ESE of Karpathos	5.4
21	2015-03-27	52.9 km W of Karpathos	5.3
22	2009-11-11	51.8 km SW of Zakynthos	5.3
23	2009-01-13	68.2 km W of Karpathos	5.2
24	2008-02-26	95.3 km S of Methoni	5.2
25	2009-05-24	36.0 km NNW of Kilkis	5.1
26	2008-03-28	39.4 km SSE of Iraklion	5.1
27	2008-02-19	70.0 km S of Methoni	5.1
28	2007-01-28	133.6 km WSW of Chania	5.1
29	2014-08-22	50.6 km S of Poliyiros	5.0
30	2009-01-08	139.9 km NNW of Florina	5.0
31	2008-06-12	99.2 km ESE of Iraklion	5.0

Events	Dates	Location	Magnitudes (M_L)
32	2007-04-16	162.5 km WNW of Florina	5.0
33	2007-02-03	63.8 km SW of Kithira	5.0
34	2008-06-08	23.1 km ENE Andravida	6.5
35	2008-03-19	34.1 km W of Skyros	5.0
36	2014-11-17	25.6 km NW of Chalkida	5.2
37	2014-11-17	26.2 km NW of Chalkida	5.2

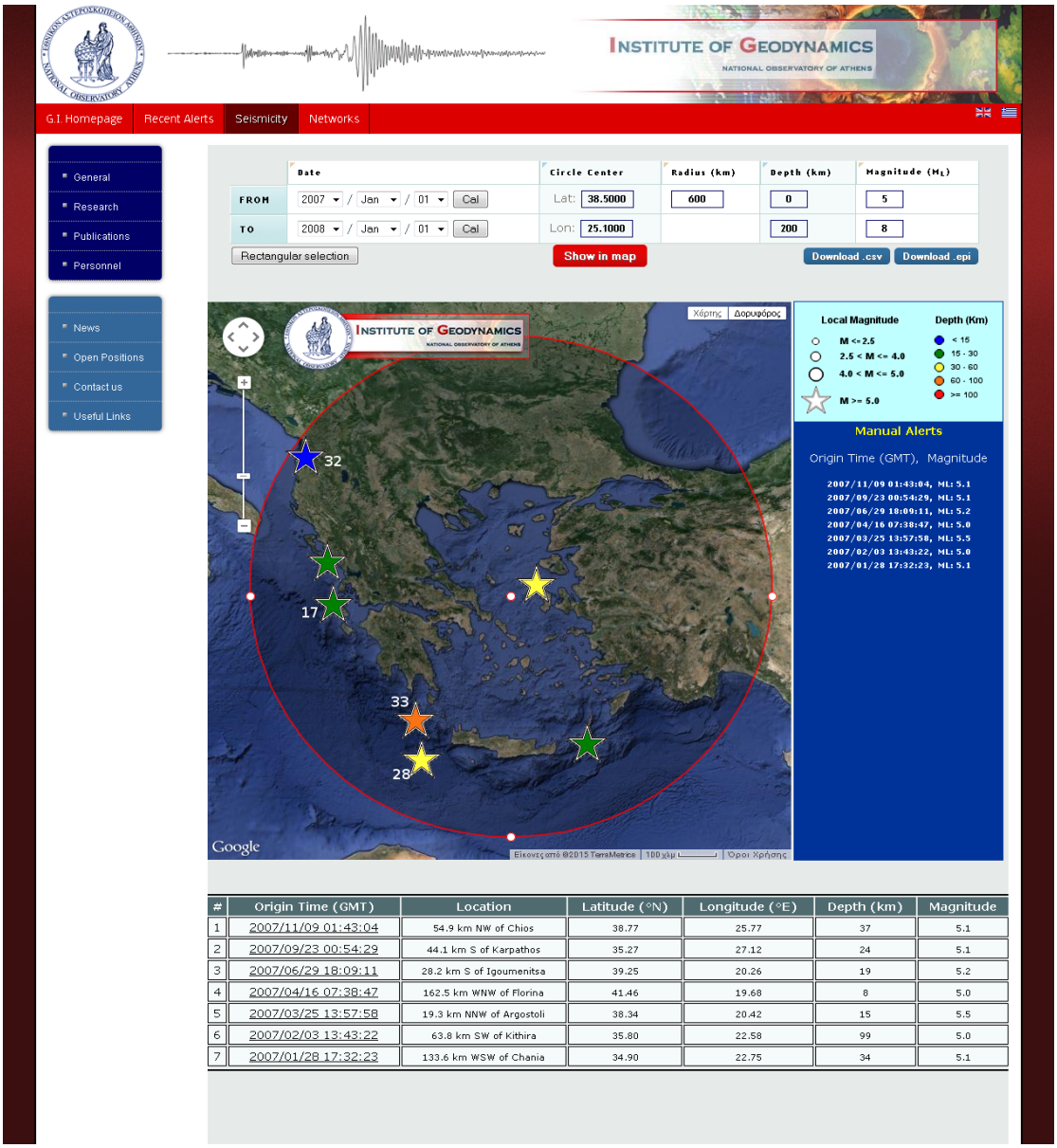

Figure 3.4: Locations of earthquakes of 2007 (Reproduced from National Observatory of Athens, Institute of Geodynamics).

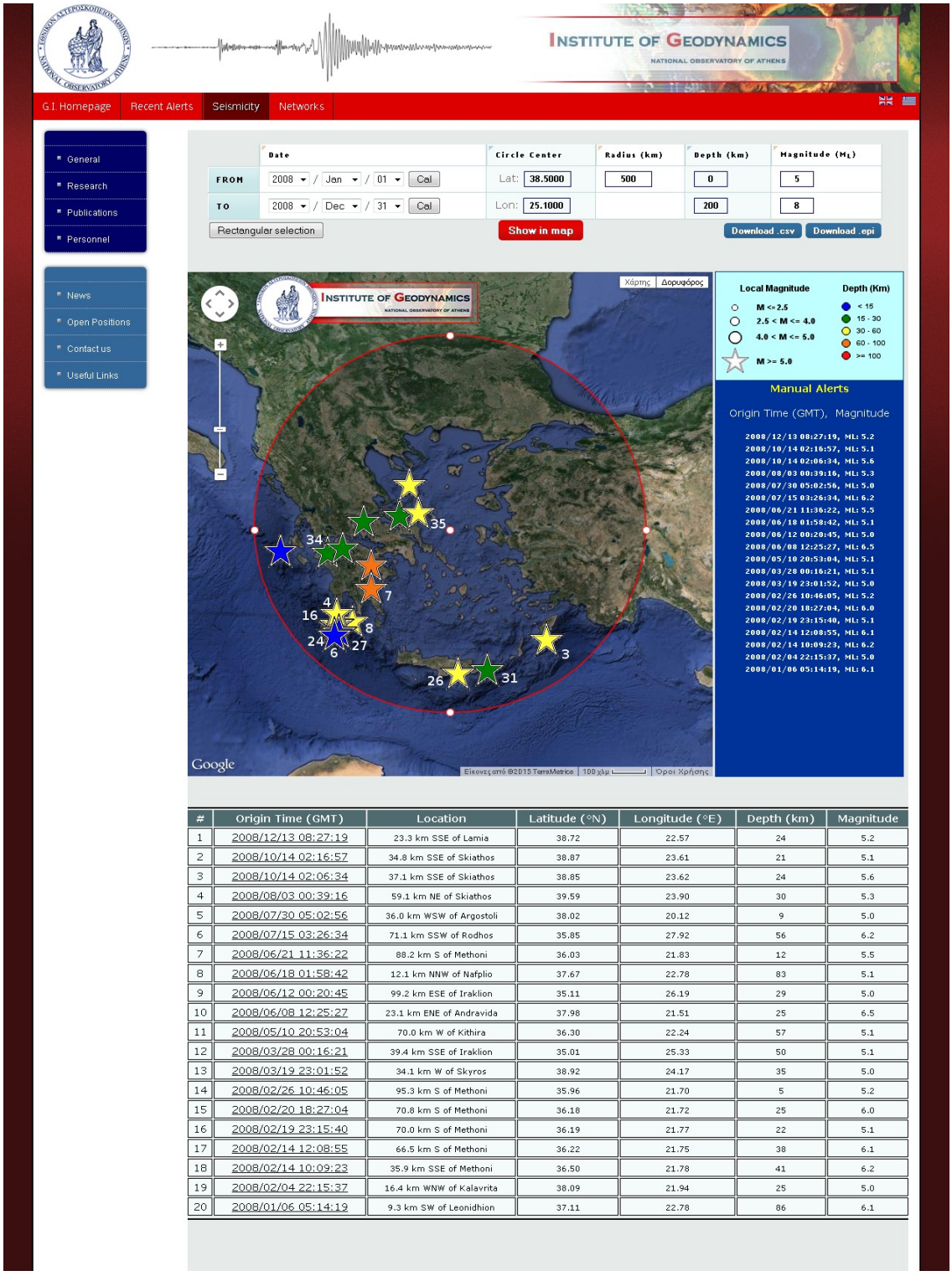

#	Origin Time (GMT)	Location	Latitude (°N)	Longitude (°E)	Depth (km)	Magnitude
1	2008/12/13 08:27:19	23.3 km SSE of Lamia	38.72	22.57	24	5.2
2	2008/10/14 02:16:57	34.8 km SSE of Skiathos	38.87	23.61	21	5.1
3	2008/10/14 02:06:34	37.1 km SSE of Skiathos	38.85	23.62	24	5.6
4	2008/08/03 00:39:16	59.1 km NE of Skiathos	39.59	23.90	30	5.3
5	2008/07/30 05:02:56	36.0 km WSW of Argostoli	38.02	20.12	9	5.0
6	2008/07/15 03:26:34	71.1 km SSW of Rodhos	35.85	27.92	56	6.2
7	2008/06/21 11:36:22	88.2 km S of Methoni	36.03	21.83	12	5.5
8	2008/06/18 01:58:42	12.1 km NNW of Nafplio	37.67	22.78	83	5.1
9	2008/06/12 00:20:45	99.2 km ESE of Iraklion	35.11	26.19	29	5.0
10	2008/06/08 12:25:27	23.1 km ENE of Andravida	37.98	21.51	25	6.5
11	2008/05/10 20:53:04	70.0 km W of Kithira	36.30	22.24	57	5.1
12	2008/03/28 00:16:21	39.4 km SSE of Iraklion	35.01	25.33	50	5.1
13	2008/03/19 23:01:52	34.1 km W of Skyros	38.92	24.17	35	5.0
14	2008/02/26 10:46:05	95.3 km S of Methoni	35.96	21.70	5	5.2
15	2008/02/20 18:27:04	70.8 km S of Methoni	36.18	21.72	25	6.0
16	2008/02/19 23:15:40	70.0 km S of Methoni	36.19	21.77	22	5.1
17	2008/02/14 12:08:55	66.5 km S of Methoni	36.22	21.75	38	6.1
18	2008/02/14 10:09:23	35.9 km SSE of Methoni	36.50	21.78	41	6.2
19	2008/02/04 22:15:37	16.4 km WNW of Kalavrita	38.09	21.94	25	5.0
20	2008/01/06 05:14:19	9.3 km SW of Leonidhion	37.11	22.78	86	6.1

Figure 3.5: Locations of earthquakes of 2008 (Reproduced from National Observatory of Athens, Institute of Geodynamics).

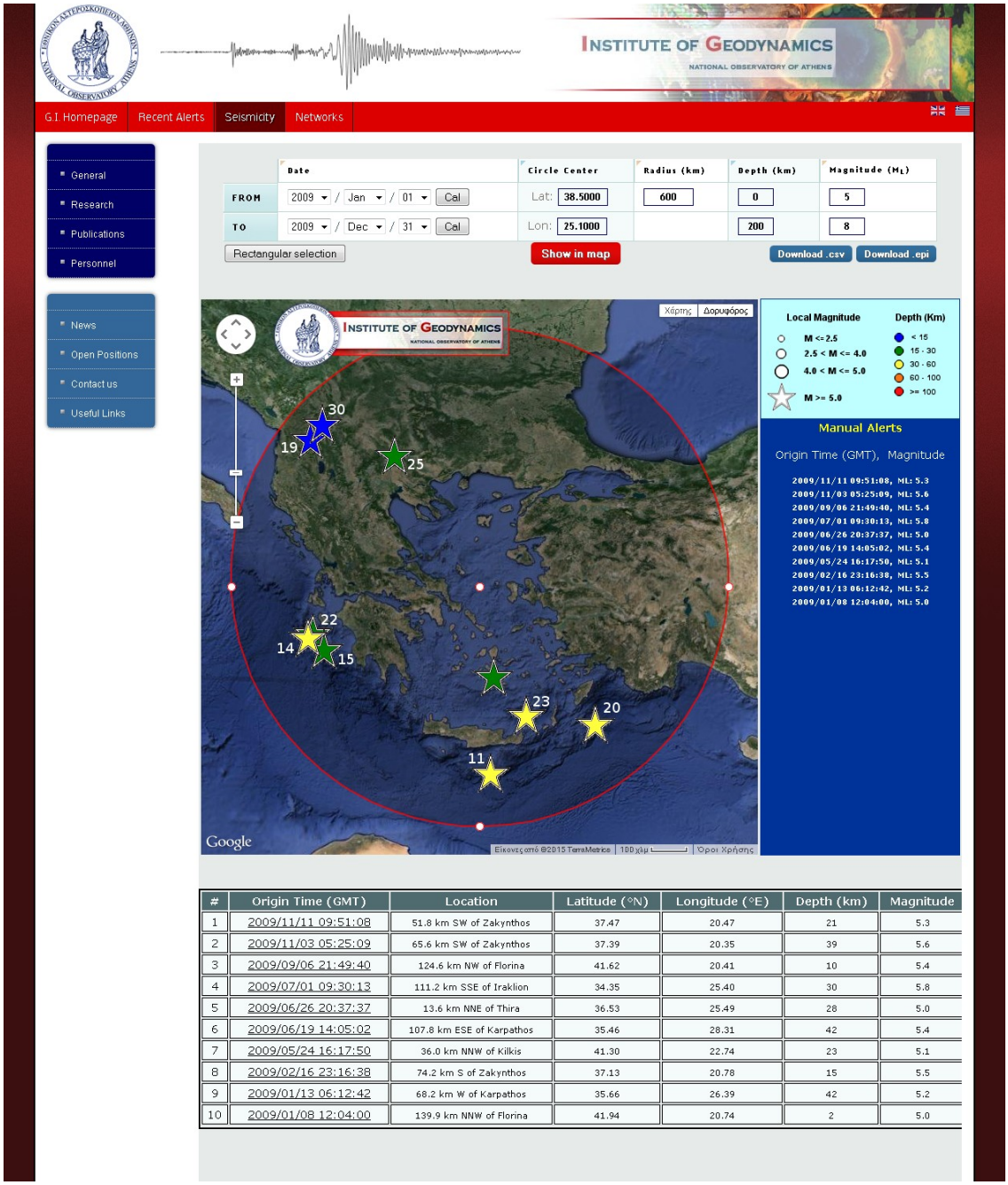

#	Origin Time (GMT)	Location	Latitude (°N)	Longitude (°E)	Depth (km)	Magnitude
1	2009/11/11 09:51:08	51.8 km SW of Zakynthos	37.47	20.47	21	5.3
2	2009/11/03 05:25:09	65.6 km SW of Zakynthos	37.39	20.35	39	5.6
3	2009/09/06 21:49:40	124.6 km NW of Florina	41.62	20.41	10	5.4
4	2009/07/01 09:30:13	111.2 km SSE of Iraklion	34.35	25.40	30	5.8
5	2009/06/26 20:37:37	13.6 km NNE of Thira	36.53	25.49	28	5.0
6	2009/06/19 14:05:02	107.8 km ESE of Karpathos	35.46	28.31	42	5.4
7	2009/05/24 16:17:50	36.0 km NNW of Kilkis	41.30	22.74	23	5.1
8	2009/02/16 23:16:38	74.2 km S of Zakynthos	37.13	20.78	15	5.5
9	2009/01/13 06:12:42	68.2 km W of Karpathos	35.66	26.39	42	5.2
10	2009/01/08 12:04:00	139.9 km NNW of Florina	41.94	20.74	2	5.0

Figure 3.6: Locations of earthquakes of 2009 (Reproduced from National Observatory of Athens, Institute of Geodynamics).

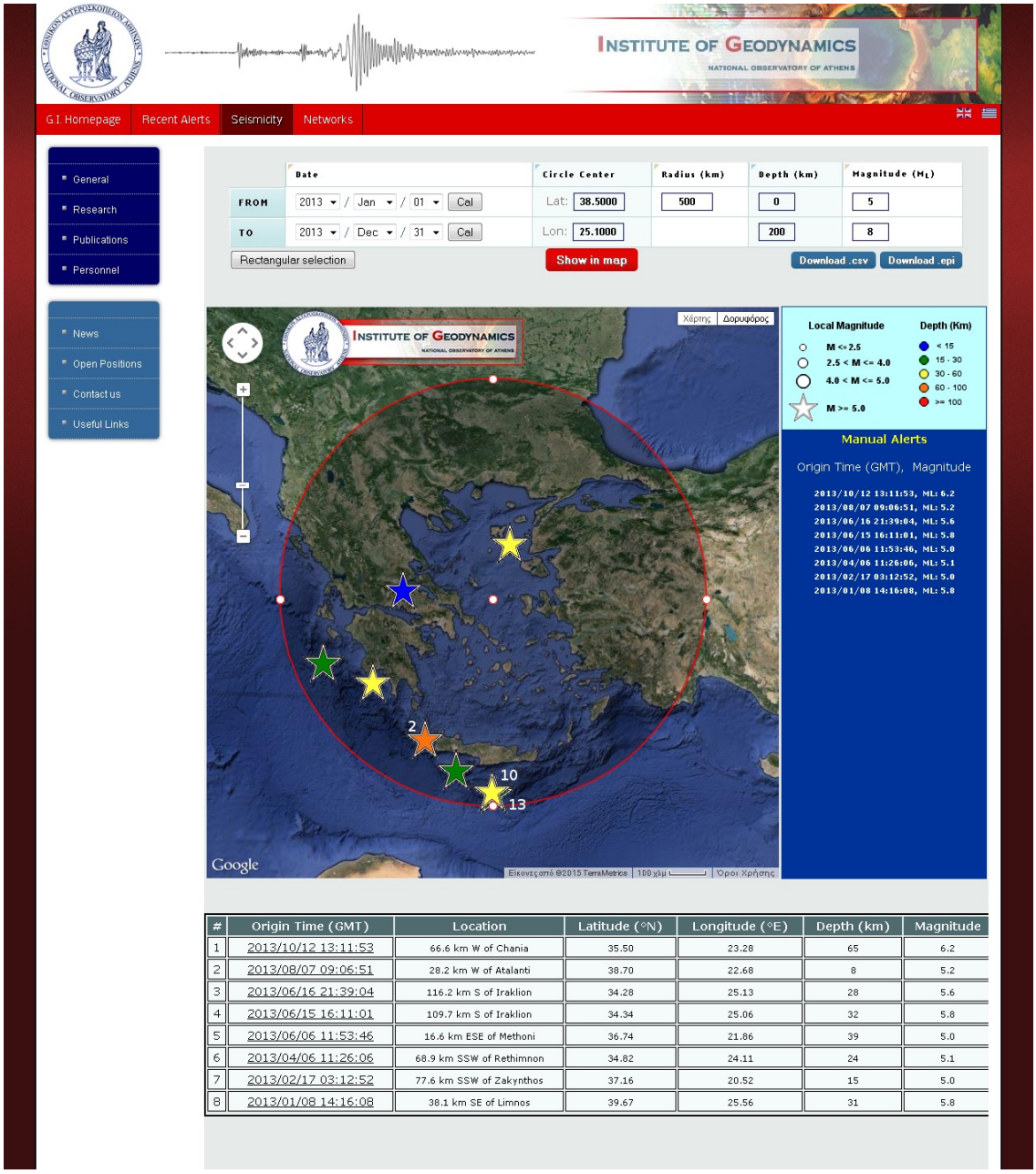

#	Origin Time (GMT)	Location	Latitude (°N)	Longitude (°E)	Depth (km)	Magnitude
1	2013/10/12 13:11:53	66.6 km W of Chania	35.50	23.28	65	6.2
2	2013/08/07 09:06:51	28.2 km W of Atalanti	38.70	22.68	8	5.2
3	2013/06/16 21:39:04	116.2 km S of Iraklion	34.28	25.13	28	5.6
4	2013/06/15 16:11:01	109.7 km S of Iraklion	34.34	25.06	32	5.8
5	2013/06/06 11:53:46	16.6 km ESE of Methoni	36.74	21.86	39	5.0
6	2013/04/06 11:26:06	68.9 km SSW of Rethimnon	34.82	24.11	24	5.1
7	2013/02/17 03:12:52	77.6 km SSW of Zakynthos	37.16	20.52	15	5.0
8	2013/01/08 14:16:08	38.1 km SE of Limnos	39.67	25.56	31	5.8

Figure 3.7: Locations of earthquakes of 2013 (Reproduced from National Observatory of Athens, Institute of Geodynamics).

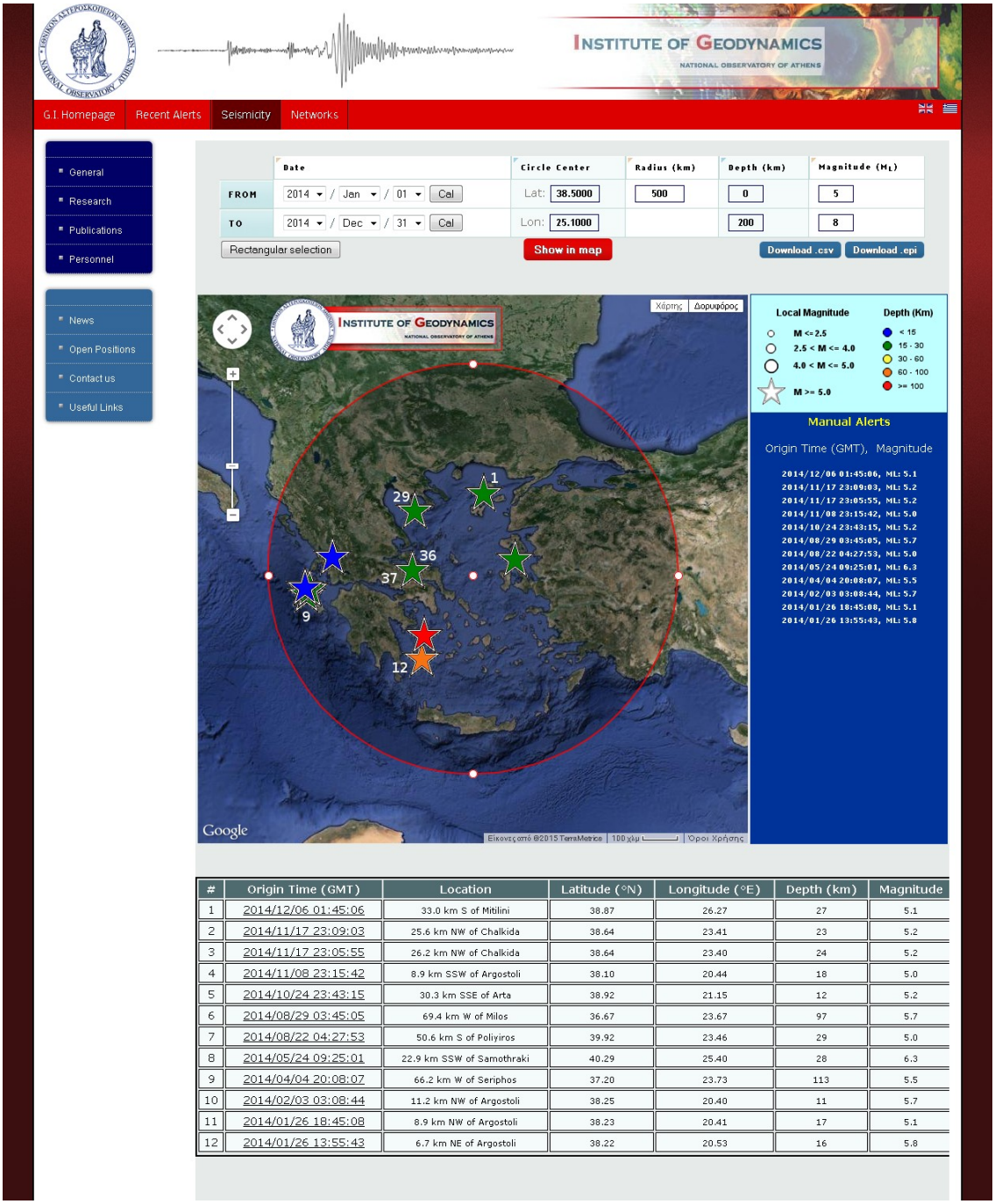

#	Origin Time (GMT)	Location	Latitude (°N)	Longitude (°E)	Depth (km)	Magnitude
1	2014/12/06 01:45:06	33.0 km S of Mitilini	38.87	26.27	27	5.1
2	2014/11/17 23:09:03	25.6 km NW of Chalkida	38.64	23.41	23	5.2
3	2014/11/17 23:05:55	26.2 km NW of Chalkida	38.64	23.40	24	5.2
4	2014/11/08 23:15:42	8.9 km SSW of Argostoli	38.10	20.44	18	5.0
5	2014/10/24 23:43:15	30.3 km SSE of Arta	38.92	21.15	12	5.2
6	2014/08/29 03:45:05	69.4 km W of Milos	36.67	23.67	97	5.7
7	2014/08/22 04:27:53	50.6 km S of Poliyiros	39.92	23.46	29	5.0
8	2014/05/24 09:25:01	22.9 km SSW of Samothraki	40.29	25.40	28	6.3
9	2014/04/04 20:08:07	66.2 km W of Seriphos	37.20	23.73	113	5.5
10	2014/02/03 03:08:44	11.2 km NW of Argostoli	38.25	20.40	11	5.7
11	2014/01/26 18:45:08	8.9 km NW of Argostoli	38.23	20.41	17	5.1
12	2014/01/26 13:55:43	6.7 km NE of Argostoli	38.22	20.53	16	5.8

Figure 3.8: Locations of earthquakes of 2014 (Reproduced from National Observatory of Athens, Institute of Geodynamics).

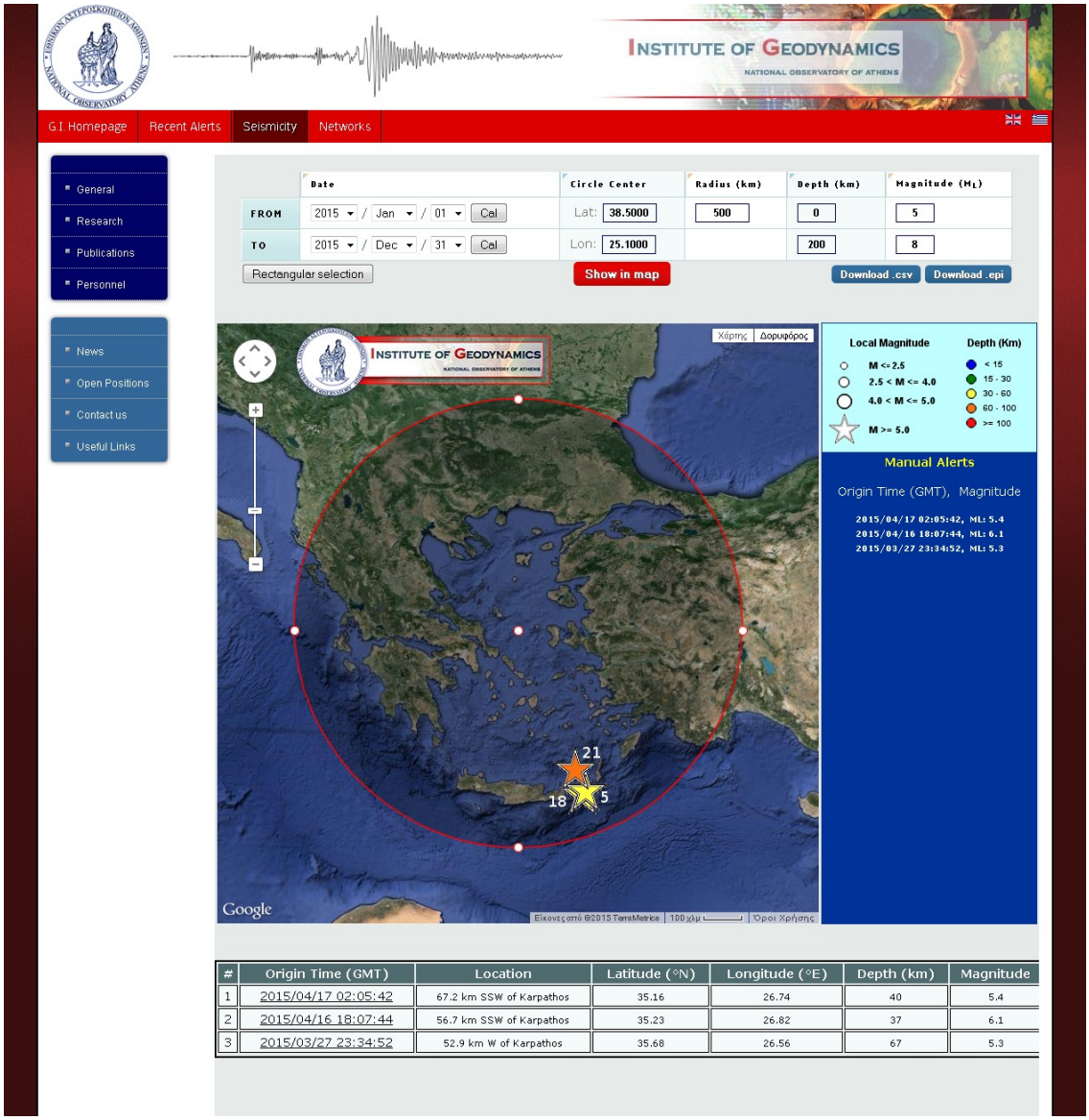

Figure 3.9: Locations of earthquakes until 31th May of 2015 (Reproduced from National Observatory of Athens, Institute of Geodynamics).

3.4 Significance of the analysed earthquakes

Following the literature data that were analysed in **Chapter 1** which refers to electromagnetic radiation and according to reviews of Petraki et al. (2015), Shrivastava (2014), Hayakawa and Hobara (2010), and Uyeda et al. (2009), the short term earthquake precursors related with electromagnetic effects are promising tools for earthquake prediction. Hayakawa and Hobara (2010) reported that several seismogenic phenomena have already been found from direct current (DC), ULF up to VHF. In other words, it is well accepted that electromagnetic precursory phenomena are detected prior to earthquakes in a wide frequency range (e.g. Eftaxias et al., 2009, 2010; Smirnova, & Hayakawa, 2007; Smirnova, Hayakawa, & Gotoh, 2004; Yonaiguchi, Ida, Hayakawa, & Masuda, 2007). In **Table 1** (**Appendix 1**) it may be observed that most of the electromagnetic precursors are in ULF and LF range (e.g. Fraser-Smith et al., 1990; Fujinawa, & Takahashi, 1998; Hayakawa, Ida, & Gotoh, 2005; Kopytenko, Yu A., Matiashviali, Voronov, Kopytenko, E.A., & Molchanov, 1993; Smith, & Johnston, 1976; Smirnova, & Hayakawa, 2007). On the contrary, since 1980, a small number of scientific papers have been published, which use MHz electromagnetic precursors to predict earthquakes (e.g. Eftaxias et al., 2001, 2002; Enomoto et al., 1997; Kapiris et al., 2003, Kapiris et al., 2002; Maeda et al., 1996; Varotsos et al., 1999; Warwick et al., 1982). In this study MHz electromagnetic signals were analysed through chaotic methods (Nikolopoulos et al., 2012, 2015; Petraki, Nikolopoulos, Fotopoulos, Panagiotaras, Koulouras, et al. 2013, Petraki et al. 2014). More specifically, 33 seismic events which happened from 2007 to 2015 in Greece, were analysed using the predictive ability of MHz. This HF (41 & 46 MHz) range has advantages over to ULF and LF emissions. The installation of electric dipoles and magnetic antennas that detect

ULF, perform in shallow depths from the territorial surface so the recordings contains very often electromagnetic noise. It should also be noted that the destruction of these antennas is very often because of their position under surface (Nomicos-VAN, personal communication). Simultaneously, from **Table 1** (**Appendix 1**) it may be observed that LF emissions of the KHz range have been used in only few cases (Kozani-Grevena, Athina and L'Aquila earthquakes) as earthquake precursors. Despite the great research and the divergent related argumentation and analysis (see e.g. the recent publications Eftaxias 2010; Eftaxias et al., 2009, 2010; Minadakis et al., 2012; Potirakis et al, 2011, 2013, 2013 and the references therein), and that the investigators claim that the detected kHz anomalies refer to the inevitable last phase of the earthquake evolution, the few LF detected signals still restrict the predictive ability of kHz radiation. On the other hand, the MHz recordings collected from aboveground-antennas, exhibit low electromagnetic noise and high predicting ability (Kapiris et al., 2002; Petraki, Nikolopoulos, Fotopoulos, Panagiotaras, Koulouras, et al. 2013, Petraki et al., 2014) as proved from more than fifteen MHz signals so far. In the following sections as well as in **Chapter 5**, further analysis and argumentation will be given regarding the enhanced predictability of the MHz electromagnetic precursors especially when assessed in conjunction with continuous recordings of radon in soil.

As far as radon is concerned, according to the review of Thomas (1988), the studies of earthquake precursory phenomena have found that significant geophysical and geochemical changes can occur prior to earthquakes. Among the more intensely investigated geochemical phenomena are the variations of ground gases such as the soil radon. While other gases have also been investigated as possible earthquake precursors,

the bulk of the experiments reported in the scientific literature have focused on radon (Cicerone, Ebel, & Britton, 2009). According to Ghosh, Deb, Dutta, Sengupta, & Samanta (2012), Namvaran, & Negarestami (2012), Nikolopoulos et al. (2012), Nikolopoulos et al. (2013), Nikolopoulos et al. (2015), Petraki, Nikolopoulos, Fotopoulos, Panagiotaras, Koulouras et al. (2013), Petraki, Nikolopoulos, Fotopoulos, Panagiotaras, Nomicos et al., (2013) radon anomaly acts as a precursor to seismic events. Radon emanation before earthquakes have showed increases with amplitudes considerably larger than methodologically induced diurnal variations (King, 1985). In

Chapter 2 it was mentioned that from 1969 to 2014 the earthquakes with $M_L \geqslant 5.0$

which occurred in conjunction with recorded radon emissions are about fifty worldwide. Importantly, three of these were analysed during this research (Nikolopoulos et al., 2012, 2014, 2015; Petraki, Nikolopoulos, Fotopoulos, Panagiotaras, Koulouras et al. 2013), one of which was corresponded to an earthquake

of $M_L = 6.5$. In addition, the magnitude of the reported radon anomalies depend on

the distance of the observation site to the earthquake epicentre and on the magnitude of the event (Cicerone et al., 2009). Additionally, the greatest anomalies were reported closest to the epicentres of the coming earthquakes and the longer the duration of the radon anomaly, the larger the earthquake that might be expected (Cicerone et al., 2009). This was also the case of the Ileia earthquake (Nikolopoulos et al., 2012, 2014; Petraki, Nikolopoulos, Fotopoulos, Panagiotaras, Koulouras et al. 2013), which occurred only 29 km away from the surveillance site. What makes the latter more important is that it is rare to address coincidence or vicinity between the observation site and the epicentre of a large earthquake. For this reason, radon signals with great anomalies and long

duration are very rare in the literature. Further for the Ileia signal, according to Nikolopoulos et al. (2012), Nikolopoulos et al. (2014), Petraki, Nikolopoulos, Fotopoulos, Panagiotaras, Koulouras et al. (2013), Petraki, Nikolopoulos, Fotopoulos, Panagiotaras, Nomicos, et al. (2013), radon anomalies in soil were not only collected actively but also through passive techniques. According to the above publications, the so called Ileia station recorded two extremely-strong radon anomalies with concentration of radon in soil up to $500\,kBq\cdot m^{-3}$. The strong radon anomaly has been linked, with the greater probability, to the strong earthquake of 08/06/2008 of $M_L=6.5$ occurred only 29 km away from the installed instrumentation. This recorded signal is of the few limited in the worldwide literature which had very high and long-lasting radon concentration disturbances and simultaneously short distance from the epicentre of a large earthquake. In **Chapter 4** this very interesting signal will be analysed both with statistical and spectral fractal methods. In **Chapter 5** further entropic methods will be also presented. In addition, in **Chapter 4** the fractal analysis of two other significant radon signals (Nikolopoulos et al., 2014, 2015) will be presented. In overview, **Chapters 3** & **4** address issues of long-range memory of the earthquake generation system through spectral fractal analysis, whereas **Chapter 5** addresses further issues of long memory as issues of self-organisation in variations of radon in soil in Greece. It is significant that in the literature, methods used for processing radon signals are mostly unreliable statistics or rely on the visual observation of the radon disturbances prior to the seismic events (Chyi, Quick, Yang, & Chen, 2010, 2011; Sac, Harmansah, Camgoz, & Sozbilir, 2011; Singh et al., 2010; Zoran et al., 2012; Choubey, Komar, & Arora, 2009).

3.5 Instrumentation

3.5.1 MHz antennas

MHz electromagnetic signals were continuously monitored by a telemetric network, consisting of 12 stations (Nomikos, & Vallianatos, 1998). These stations are located in the following seismic regions: (1) Ithomi (O), Peloponnese, (2) Valsamata (F), Kefalonia Island, (3) Ioannina (J), (4) Kozani (K), (5) Komotini (T), (6) Kalloni (M), Lesvos Island, (7) Rhodes (A), Rhodes Island, (8) Neapolis (E), Crete Island, (9) Vamos (V), Crete Island, (10) Corfu (P), Corfu Island, (11) Ileia (I), Peloponnese and (12) Atalanti (H). Stations 1, 2, 9, 10 and 11 are located along the Hellenic Trench. Stations 5, 6, 7 are located in the vicinity of the Anatolian Plate and stations 3, 4, 8 are located in the wider area of the Aegean Sea Plate (**Figure 3.10**). Each station comprises (1) bipolar antennas synchronized at 41 and 46 MHz; (2) novel acquisition data-loggers (Koulouras, Kontakos, Stavrakas, Stonham, & Nomicos, 2005) and (3) telemetry equipment (e.g. RF modem-wired or cordless internet) (**Figure 3.11**).

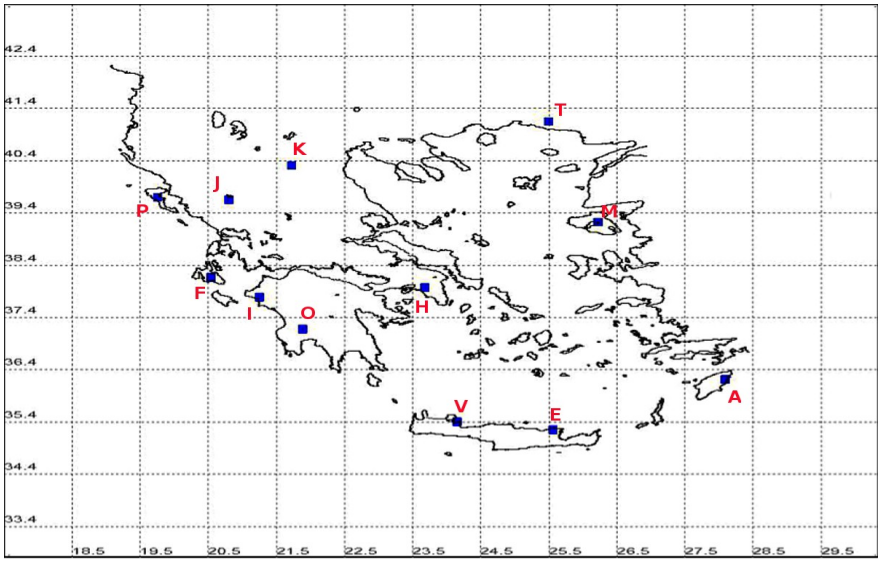

Figure 3.10: Telemetric network of electromagnetic stations.

Figure 3.11: Ileia: a) Bipolar antennas (1,2,3,4) (b) Data-logger (5,6) c) Equipment (7)

3.5.2 Apparatus for radon measurements

3.5.2.1 Alpha Guard

The active techniques utilised Alpha Guard (AG), Genitron Ltd. AG equipped with a soil gas unit (Genitron Ltd.) This unit consists of a 1m probe, a gas tight pump (Alpha Pump, Genitron Instruments) and accompanying equipment (Genitron instruments, 1997). The probe was immersed 1m below the ground to minimise the meteorological influences (Ghosh et al., 2009; Roumelioti, Benetatos, & Kiratzi, 2009). Soil gas was pumped at the maximum available rate of $1\mathrm{L}\cdot min^{-1}$ (Genitron instruments, 1997) for maximising the gas quantity and enhancing the detection efficiency. The gas was driven into the AG through an input flow adapter where it was measured at the rate of 1 measurement per 10 min. The pumped gas escaped the AG through an output flow adapter. Atmospheric pressure (AP), relative humidity (RH) and temperature (T) were continuously monitored as well (Genitron instruments, 1997). The whole set-up was connected to a PC which handled the AG through its licensed software (AVIEW, Genitron Ltd.). The whole operation of the AG (including data manipulation and transfer) was remotely controlled through a secured internet connection. The overall system (AG, host-remote computer, remote control-operation) constituted the radon-telemetry station. The measurements derived from Alpha Guard and analysed in this study, were recorded from two radon-telemetry stations. These two stations were established in Ileia, Peloponnese and in Lesvos Island.

Figure 3.12: Ileia: a) Probe (1,2) b) Alpha Pump and accompanying equipment (3,4,5) c) Alpha Guard (4,5).

3.5.2.2 CR-39 solid state nuclear track detector (SSNTD)

The passive techniques employed a calibrated radon dosimeter (Nikolopoulos, Louizi, Petropoulos, Simopoulos, & Proukakis, 1999) based on the CR-39 solid state nuclear track detector (SSNTD). To measure the radon concentration in soil, two dosimeters were installed and removed every week, near the soil gas unit at approximately 80 cm underground to minimise meteorological influences. Since, soil contains a significant amount of moisture which enters through diffusion into the dosimeter interior and may alter the measurement results, both dosimeters were enclosed in a stainless steel container with holes underneath to allow radon entrance. A silica gel was enclosed, so as together with the container, to disincline the role of moisture. The removed dosimeters were immediately measured with standard techniques (Nikolopoulos et al., 1999, 2002). According to the measurement efficiency the lower limit of detection of radon in soil is equal to approximately $7000\,Bq\cdot m^{-3}\cdot h$. The overall uncertainty of the estimation of the concentration of radon was below 10% at the 95% confidence interval (CI) (Nikolopoulos et al., 1999, 2002). The CR-39 solid state nuclear track detectors (SSNTD) were positioned in Ileia, Peloponnese.

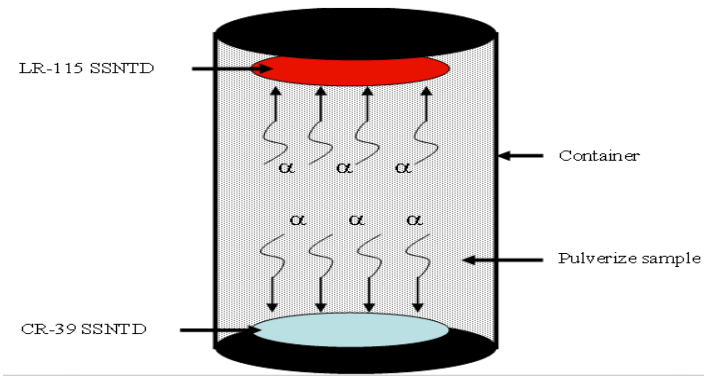

Figure 3.13: CR-39 solid state nuclear track detector.

3.5.2.3 Barasol MC2

Active radon measurements were conducted with VDG Baracol (ALGADE, France) in the Campus of Technological Educational Institution of Athens. Radon in soil was monitored by a telemetric station operating with the radon probe Barasol MC2 (BMC2). The main quantities measured by the BMC2 probe were the concentration of ^{222}Rn, the temperature and the atmospheric pressure. For the measurement, the BMC2 sensor (implanted silicon detector) authorizes counting of atoms of ^{222}Rn and its daughter products by spectrometry. The calibration of the sensor enables the volumetric activity of ^{222}Rn to be calculated. The instrument is designed to be used in difficult environments and to collect passive measurements with no disturbance of the environment. For monitoring purposes, the BMC2 probe was installed in a borehole at 1m depth and data sampling was performed at the rate of 1 measurement per 15 minutes. The Radon telemetric station comprises as well a solar panel, an IEEE box that contains all electronic equipment and the telemetric 3G emitting instrumentation (**Figure 3.14**).

In **Figure 3.15** the network of the radon stations in Greece is depicted. As it is aforementioned it consists from 3 stations: Ileia station with Alpha Guard (active techniques), Lesvos station with Alpha Guard (active techniques) and Athens station with Barasol (active techniques).

Figure 3.14: Barasol MC2.

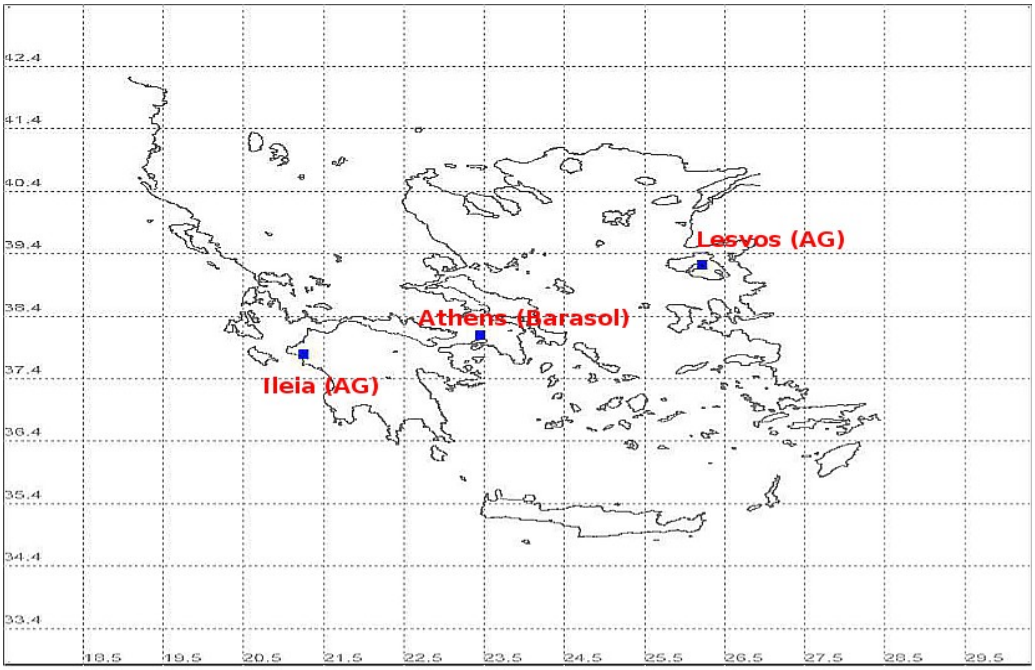

Figure 3.15: Radon telemetry stations.

3.6 Power-law wavelet spectral fractal analysis of MHz-Electromagnetic signals

The complex long-term connections between space and time before earthquakes delineate traces in earthquake hazard systems (Eftaxias, 2010; Nikolopoulos et al., 2014). The pre-seismic traces may unfold with fractal methods (Eftaxias, 2010; Eftaxias et al., 2008, 2009; Gotoh et al., 2004; Kapiris et al., 2002, 2003; Nikolopoulos et al., 2012, 2014; Smirnova, & Hayakawa, 2007; Petraki, Nikolopoulos, Fotopoulos, Panagiotaras, Koulouras et al., 2013; Petraki, Nikolopoulos, Fotopoulos, Panagiotaras, Nomicos et al., 2013; Surkov, Uyeda, Tanaka, & Hayakawa, 2002; Yonaiguchi et al., 2007). These seismic systems evolve naturally to self-organised critical (SOC) states with fractal organisation in space and time (Smirnova, & Hayakawa, 2007). The evolution of fractals can describe different stages of the final catastrophe (Gotoh et al., 2004; Hayakawa, & Hobara, 2010; Kapiris et al., 2002, 2003; Smirnova, & Hayakawa, 2007; Surkov et al., 2002). Attention should be placed on the following: (1) heterogeneous media close to critical points exhibit memory effects (Kapiris et al., 2002) (2) power spectral density (PSD) is the prevailing measure to trace inherent memory of seismic systems (Eftaxias, 2010; Eftaxias et al., 2009; Hayakawa, & Hobara, 2010; Smirnova, & Hayakawa, 2007; Surkov et al., 2002; Yonaiguchi et al., 2007) (3) fractal time series present temporal power laws (Kapiris et al., 2002; Petraki, Nikolopoulos, Fotopoulos, Panagiotaras, Koulouras et al., 2013).

This section presents noteworthy example cases derived through the spectral fractal analysis for certain significant electromagnetic disturbances of the MHz range. These were collected by the continuous telemetric electromagnetic network of **section 3.5.1**.

All data are presented in a collective manner in the next subsection. Special attention is given to the time-series parts recorded up to one month prior to significant earthquakes of Greece and near areas. The results will show that fractal traces exist in segmented portions of the disturbances evaluating these, hence, as candidate precursors of general failure. The underlying concept is what already mentioned; that clear MHz electromagnetic anomalies have been detected over periods ranging from a few days to a few hours prior to recent destructive earthquakes in Greece (e.g. Eftaxias 2010; Kapiris, et al. 2002, 2003). Many data are from the years 2008 and 2009. This was because during 2009 significant earthquakes occurred ($M_L \geq 5.0$) (earthquakes 11, 14, 15, 19, 20, 22, 23 25 & 30 **Table 3.2, Figure 3.6**) some of which were undersea and some other at shallow depths. It is interesting, that both types of earthquakes gave pre-earthquake warnings (Petraki, Nikolopoulos, Fotopoulos, Panagiotaras, Koulouras et al., 2013) and importantly it was the first time where undersea pre-earthquake signs were detected through MHz electromagnetic precursors. In addition during 2008, particular intense seismic activity occurred in the Hellenic Trench or in the vicinity (**Figure 3.5**) with six very destructive earthquakes ($M_L \geq 6.0$) (earthquakes 3,4,6,7,8 & 34 in **Table 3.2**, **Figure 3.5**) and another six earthquakes with $5.0 \leq M_L < 6.0$ (16, 24, 26, 27, 31 & 35 in **Table 3.2**, **Figure 3.5**). What makes the year 2008 even more interesting is that seven of these earthquakes (4, 6, 8, 16, 24, 27 & 34 in **Table 3.2, Figure 3.5**) occurred in the broad vicinity of the telemetric radon station of Ileia. This allowed the collection of different precursors (41 and 46 MHz electromagnetic & radon) simultaneously and from nearby sources. This very rare conjuncture allowed the

direct comparison of the similarities of underlying long-memory dynamics of radon and electromagnetic disturbances (Petraki, Nikolopoulos, Fotopoulos, Panagiotaras, Koulouras et al., 2013). In the following the fractal and long-memory dependencies of the electromagnetic signals is presented. The precursory value of all signals is discussed.

3.6.1 Spectral fractal analysis results

A first set of characteristic results based on the spectral fractal analysis are presented in **Figures 3.16-3.32**. The signals of these figures are electromagnetic of the MHz-range and many extended approximately one month before earthquakes of **Figure 3.6**. For convenience in the reference of the earthquake their identifiers are repeated here (**Year 2009:** 11, 14, 15, 19, 20, 22, 23 25 & 30, **Table 3.2**, **Figure 3.6** and **Year 2008:** 3, 4, 6, 7, 8, 16, 24, 26, 27, 31, 34 & 35, **Table 3.2**, **Figure 3.5**). The top sub-figures of **Figures 3.16-3.32** present the time evolution of the fractal power-law b - values. Each value correspond to the $\log-\log$ power-law fit (**section 3.2.3**) in a window of 1024 samples. To obtain each power-law b - value, the window was slid one sample forward. This technique is more difficult for real time processing, as long-memory analysis methods operate on successive, fixed length segments (e.g. 1024 samples), advancing one sample ahead each time i.e. the sliding window step is one sample (Cantzos et al., 2015). With these parameters, the analysis captures very fine EM variations in time at the expense of high computational cost as any given fractal analysis window almost completely overlaps the preceding one given the same window

length and step size (Cantzos et al., 2015). The middle sub-figures of **Figures 3.16-3.32** present the average (in each window) r^2, as well as the number of successive ($r^2 \geq 0.95$) values. The blue points indicate the successive ($r^2 \geq 0.95$) segments. Note that, as aforementioned, the fBm class is associated with power-law b - values within $1 < b < 3$ and the fGn class with values in the range $-1 < b < 1$. Red points refer to the remaining segments (non-successive fBm & non-successive fGn classes). The bottom sub-figures of **Figures 3.16-3.32** present the detected signal. In the following figures, the term (EQ) refers to earthquake, the term (JD) refers to day of occurrence of each earthquake in the Julian's calendar as well as to the range of days of the fractal analysis. Finally, the term (S) refers to shallow earthquakes (epicentre's depth<10 km) and (U) to undersea earthquakes (depth>30 km, epicentre under the surface of the sea). Since there exist no one to one correspondence between earthquake events and detected disturbances (e.g. Nikolopoulos et al., 2012, 2014, 2015; Eftaxias 2010), the earthquakes in the captions of **Figures 3.16-3.32** are indicated arbitrarily and only for the purpose of referencing. The indicated earthquakes are those spatially closest to the recording station and temporarily nearest to the presented day-range of fractal analysis.

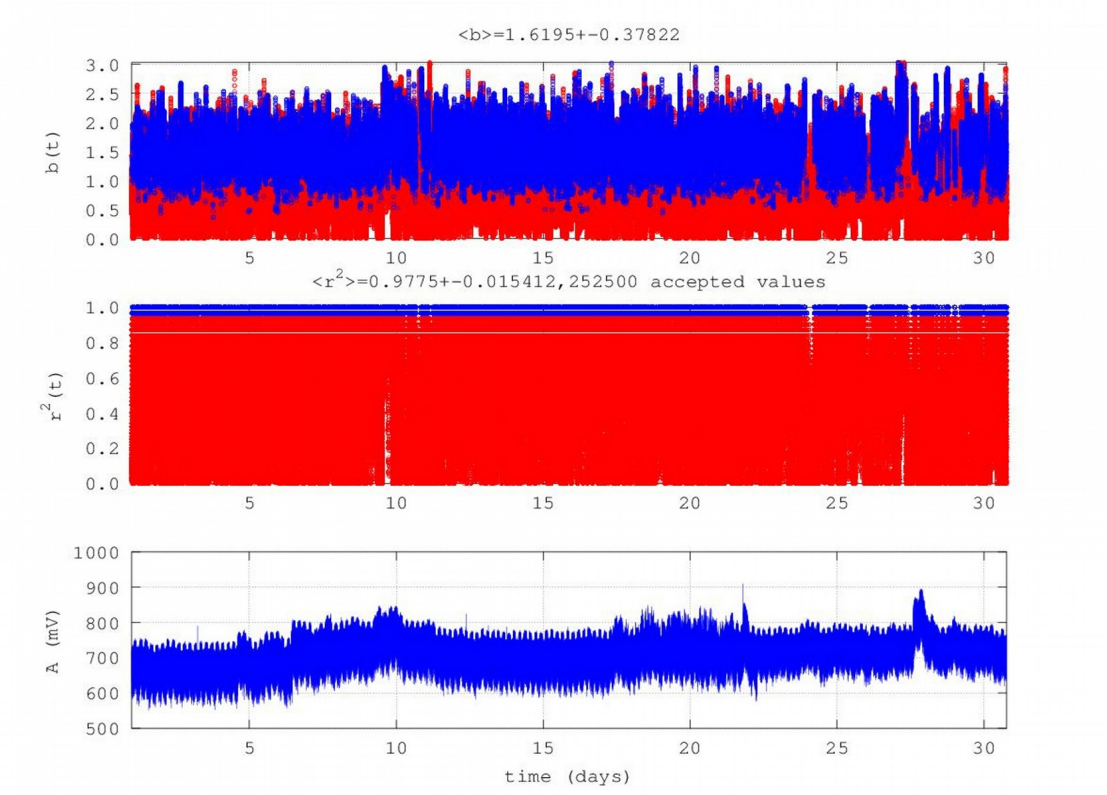

Figure 3.16: EQ:19 (JD 257, 2009). Corfu station, JD 227-257, 2009, 46 MHz (S).

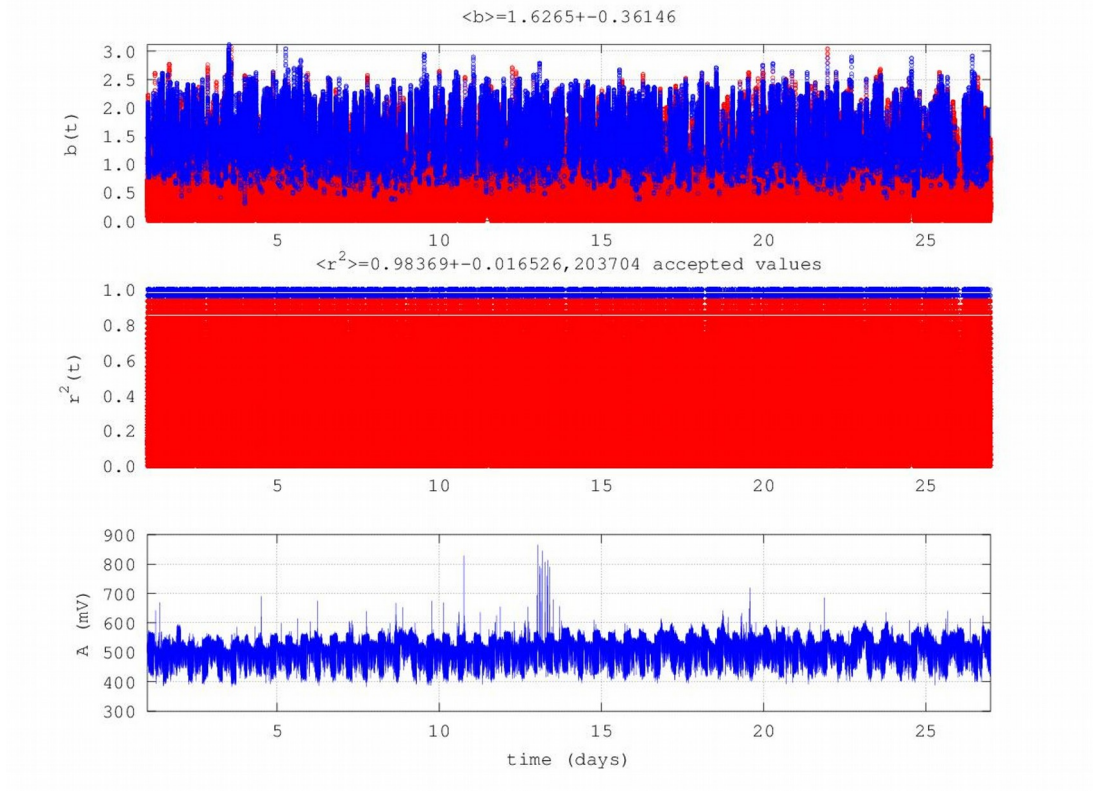

Figure 3.17: EQ:11 (JD 182,2009) Vamos station, JD 152-182, 2009, 41 MHz (U).

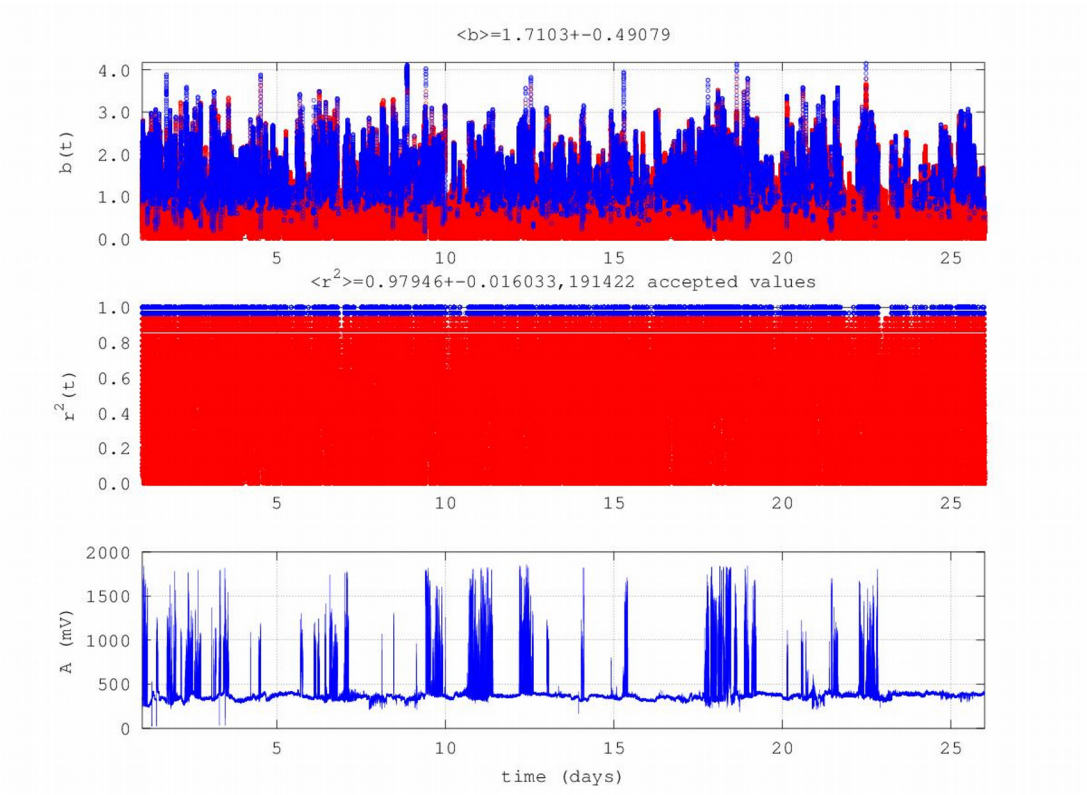

Figure 3.18: EQ:15 (JD 47, 2009), Ileia station, JD 17-47, 46 MHz (U).

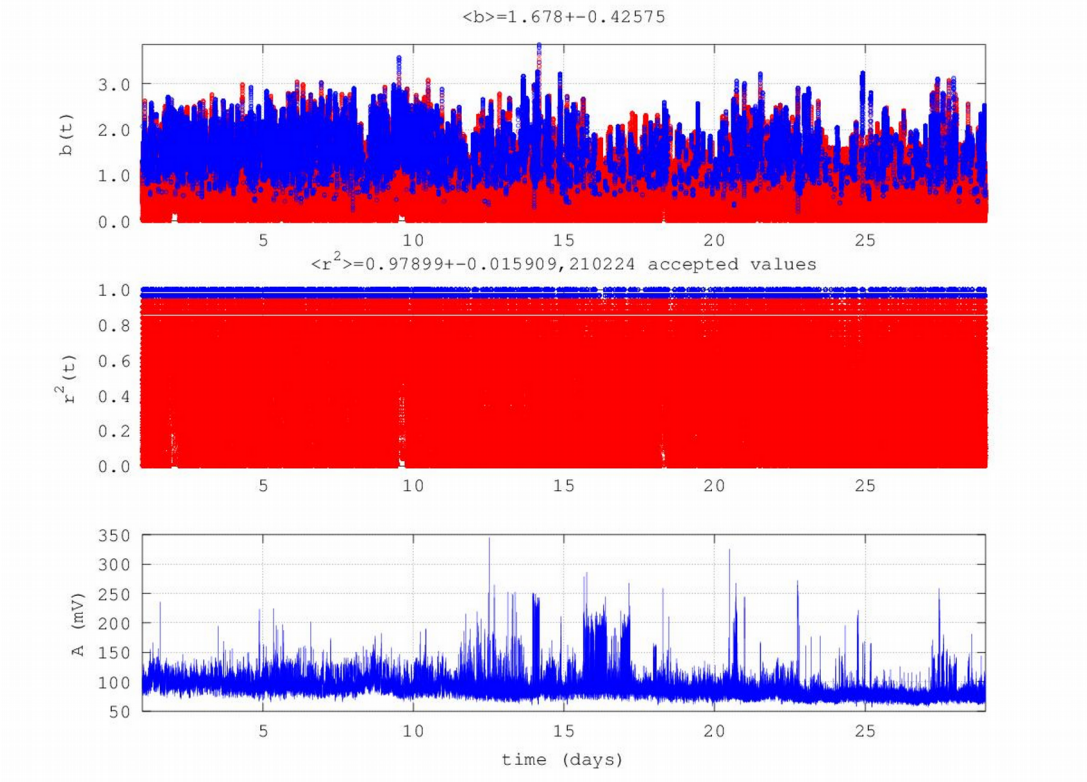

Figure 3.19: EQ:20 (JD 170, 2009), Rhodes station, JD 140-170, 2009 46 MHz (U).

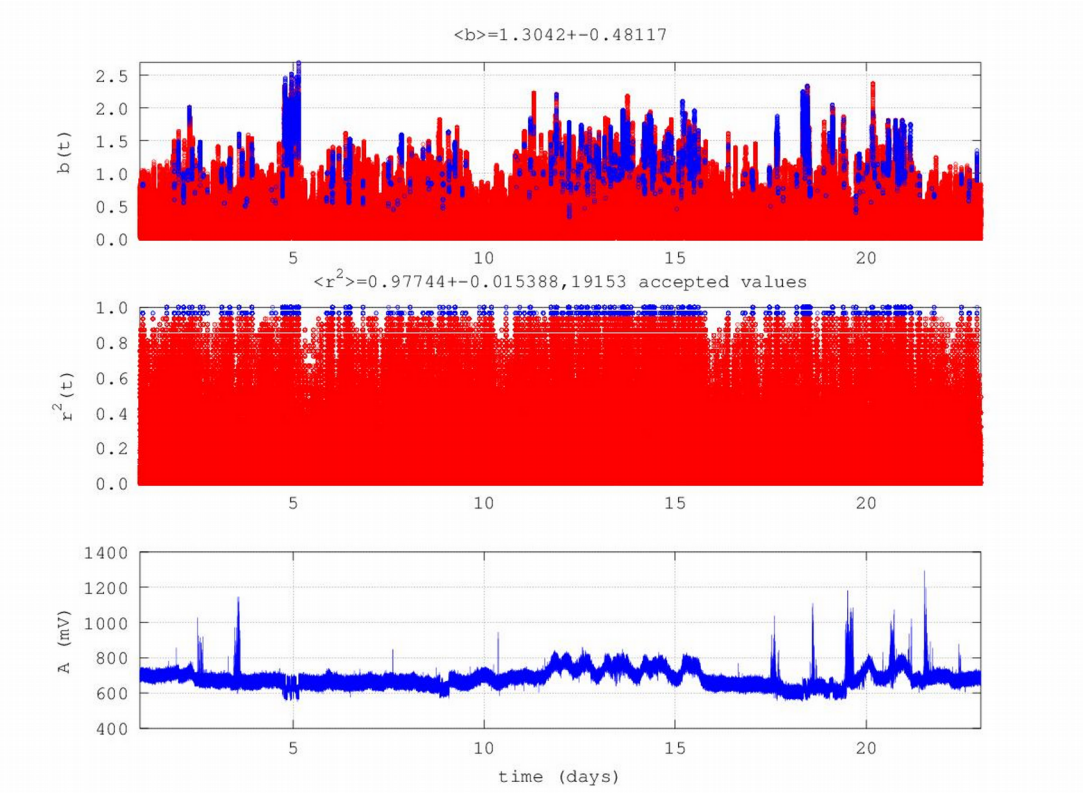

Figure 3.20: EQ:19 (JD 257, 2009), Ioannina station, JD 227-257, 2009, 41 MHz (S).

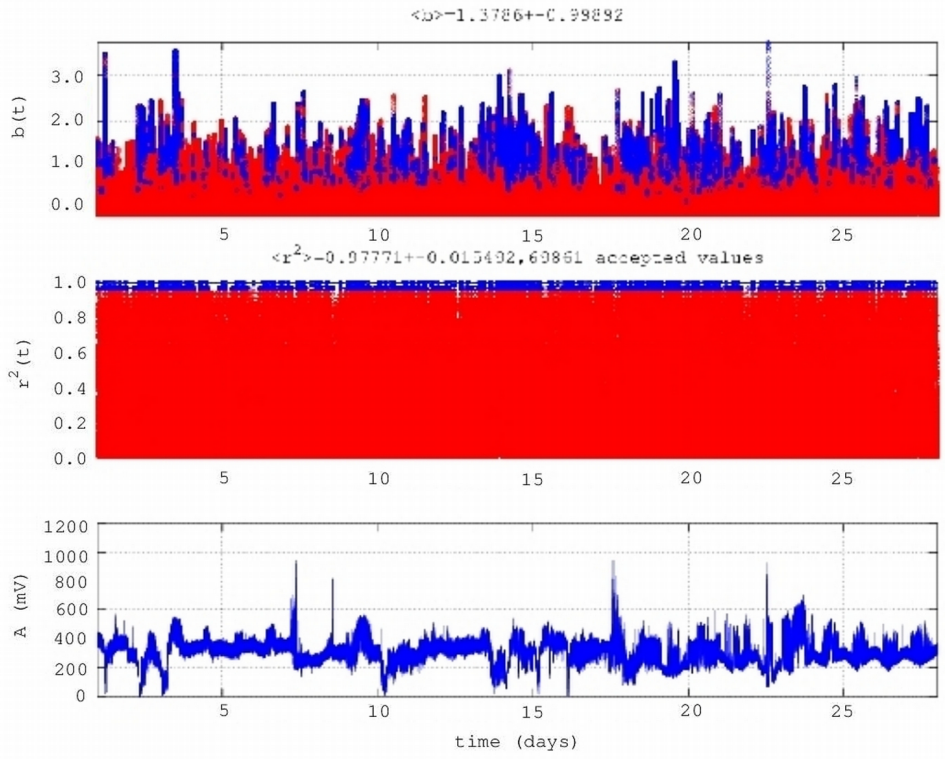

Figure 3.21: EQ:25 (JD 144, 2009), Komotini station, JD 114-144, 2009, 41 MHz.

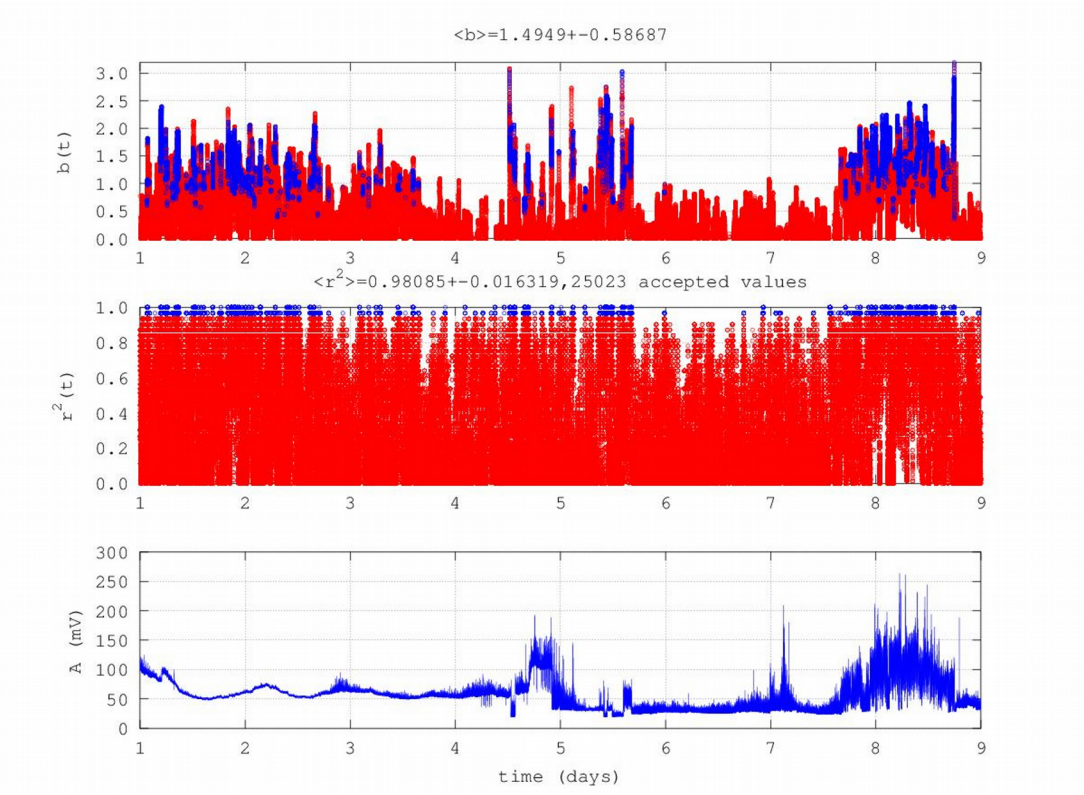

Figure 3.22: EQ:22 (JD 315, 2009), Ileia station, JD 309-315, 2009, 46 MHz (U).

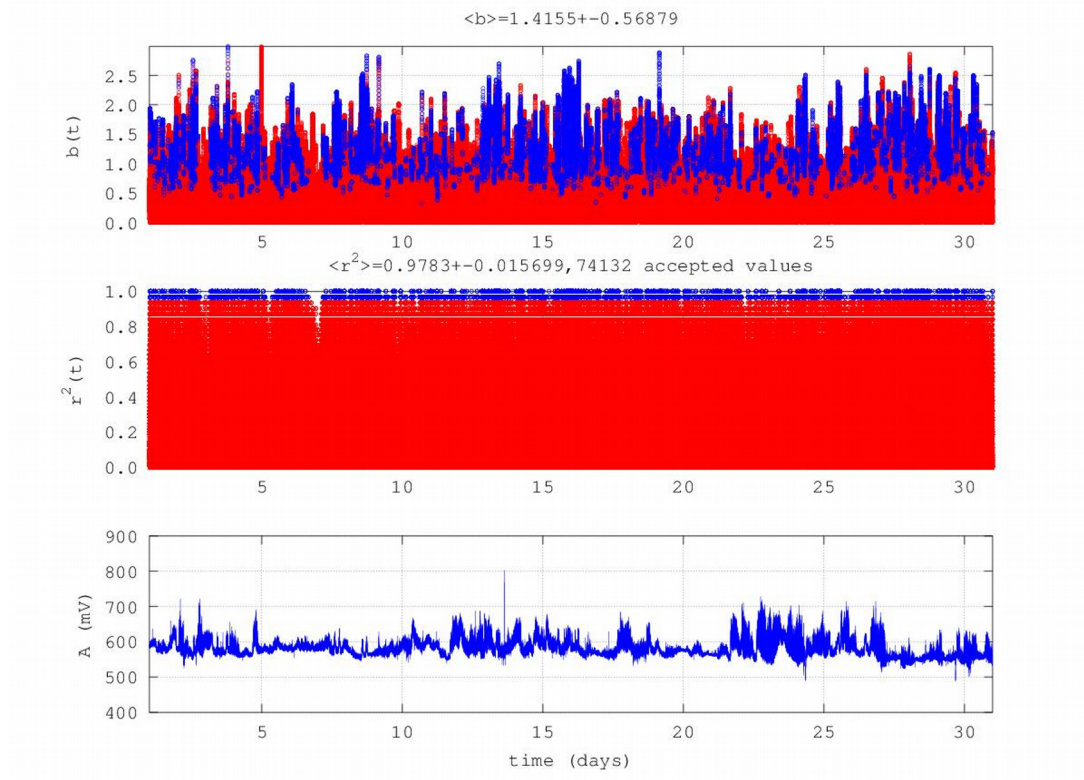

Figure 3.23: EQ:11(JD 182, 2009), Neapoli station, JD 152-182, 2009, 46 MHz (U).

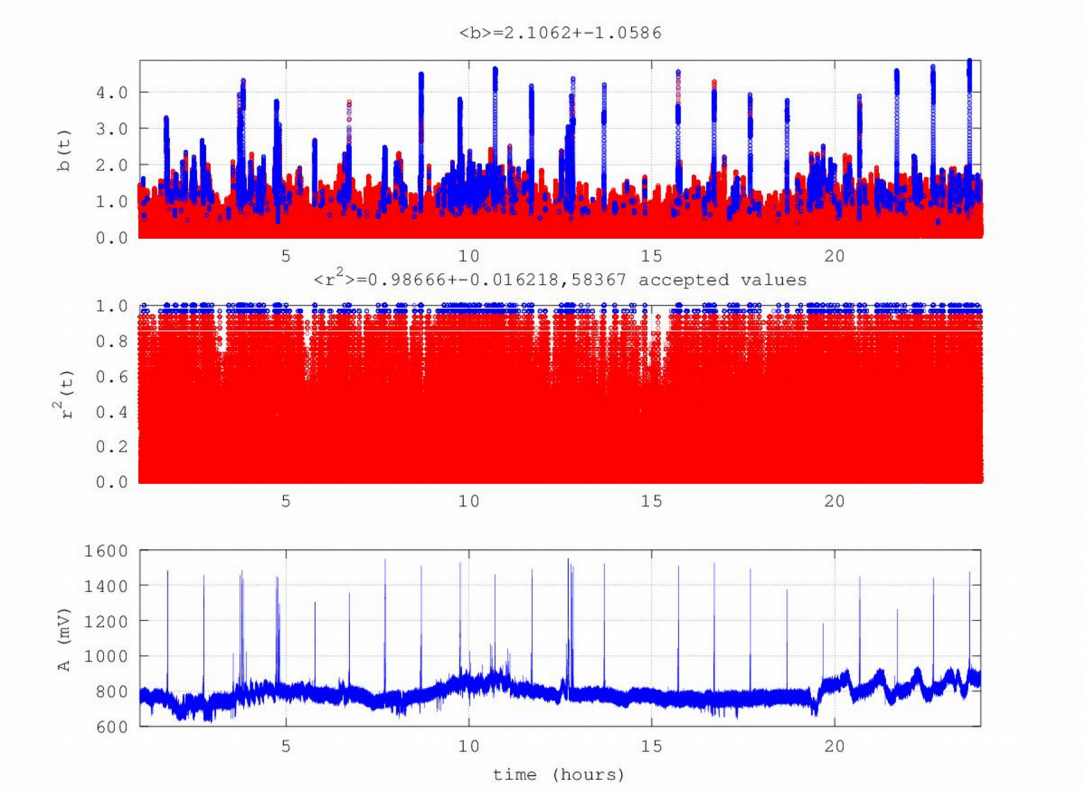

Figure 3.24: EQ:30 (JD 8, 2009) Ioannina station, JD 343-366, 2008, 41 MHz (S).

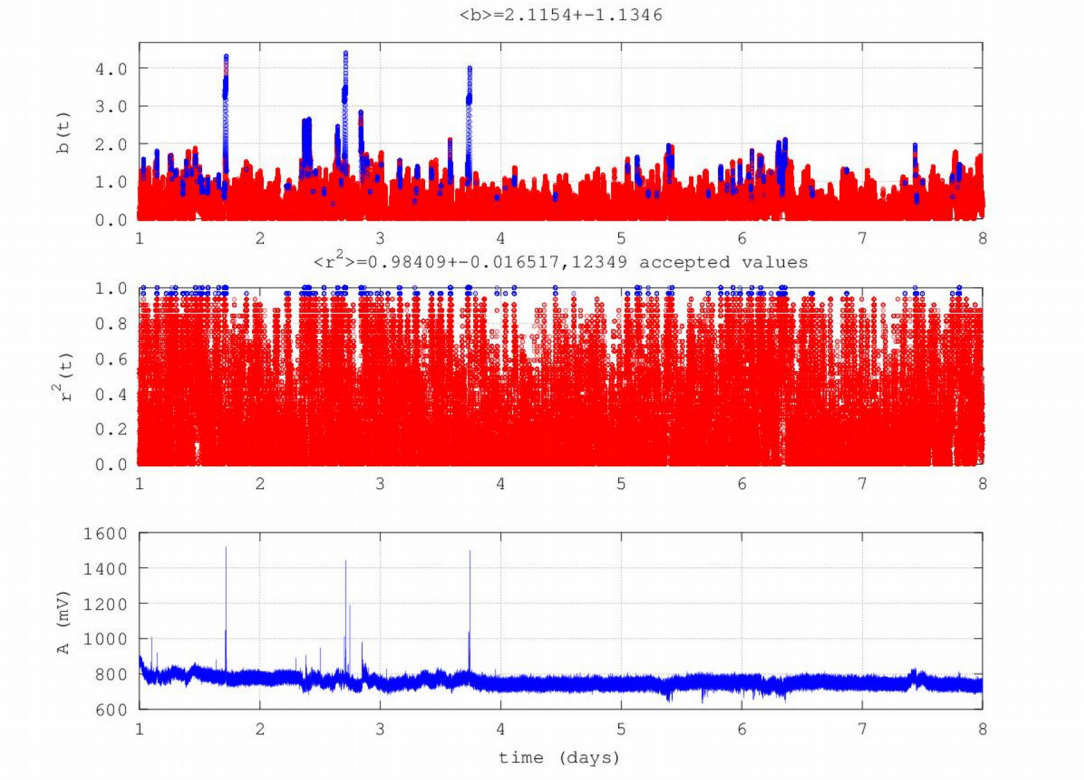

Figure 3.25: EQ:30 (JD 8, 2009) Ioannina station, JD 1-8, 2009, 41 MHz (S).

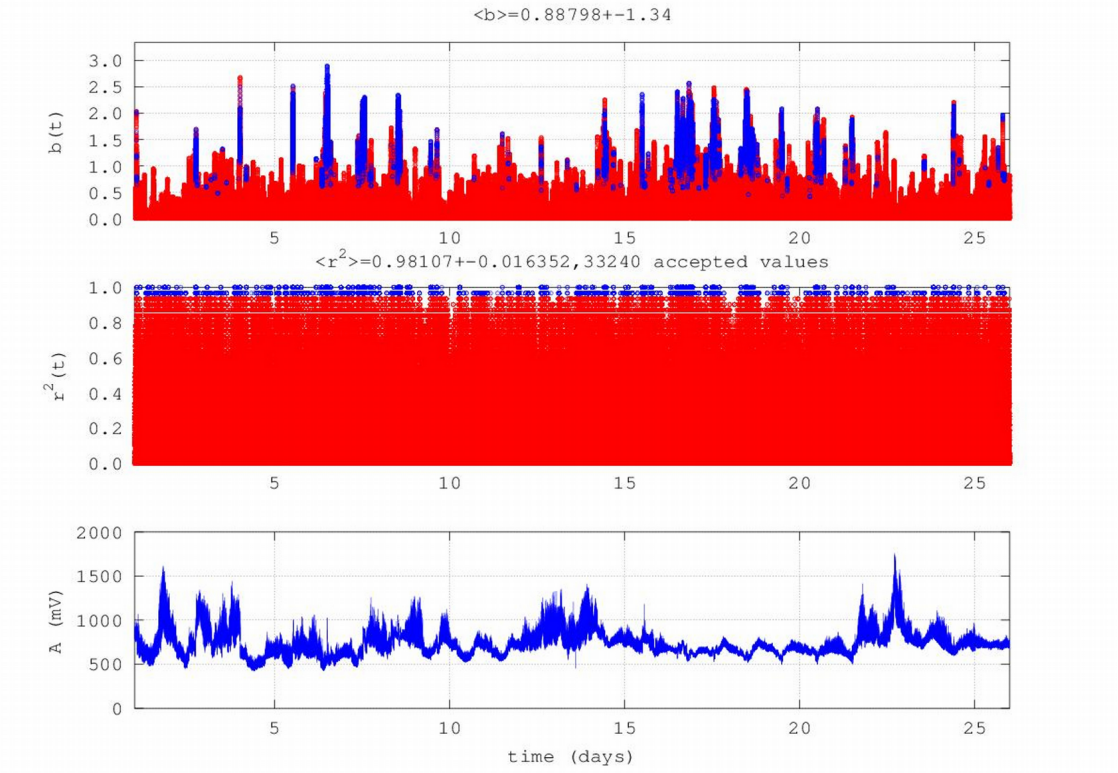

Figure 3.26: EQ:14 (JD 307, 2009), Ileia station (JD 254-306), 2009, 41 MHz (U).

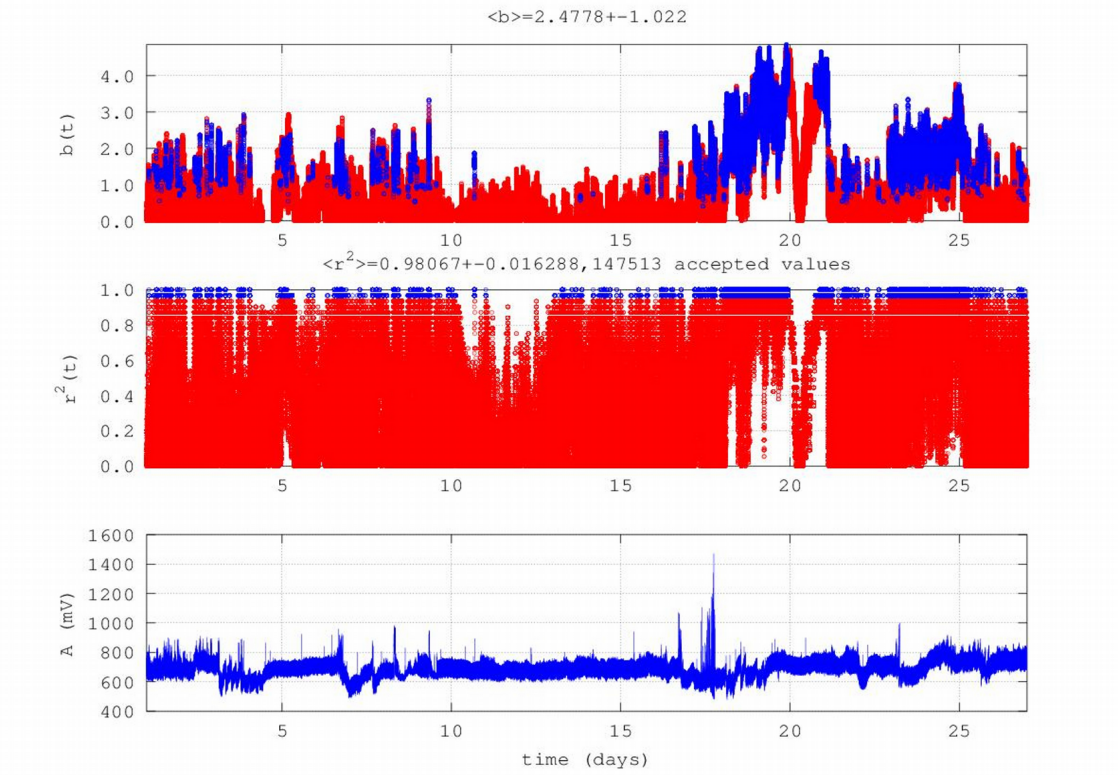

Figure 3.27: EQ:23 (JD 13, 2009), Neapoli station, JD 340-366, 2008, 46 MHz (U).

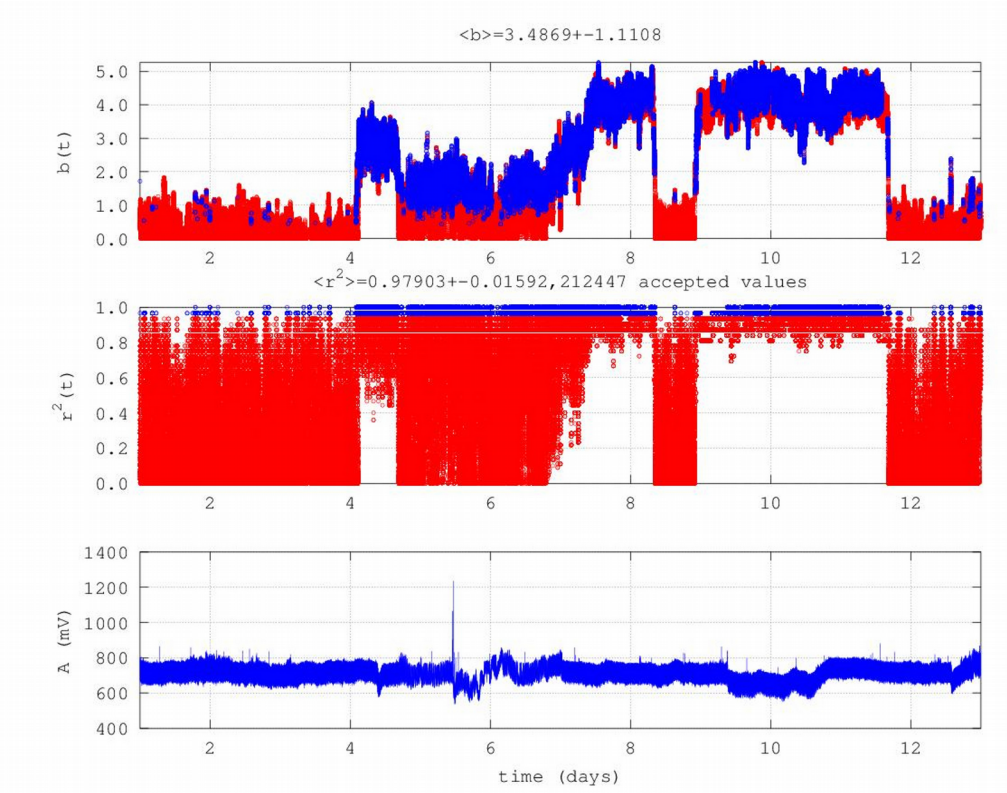

Figure 3.28: EQ:23 (JD 13, 2009), Neapoli station, JD 1-13, 2009, 41 MHz (U).

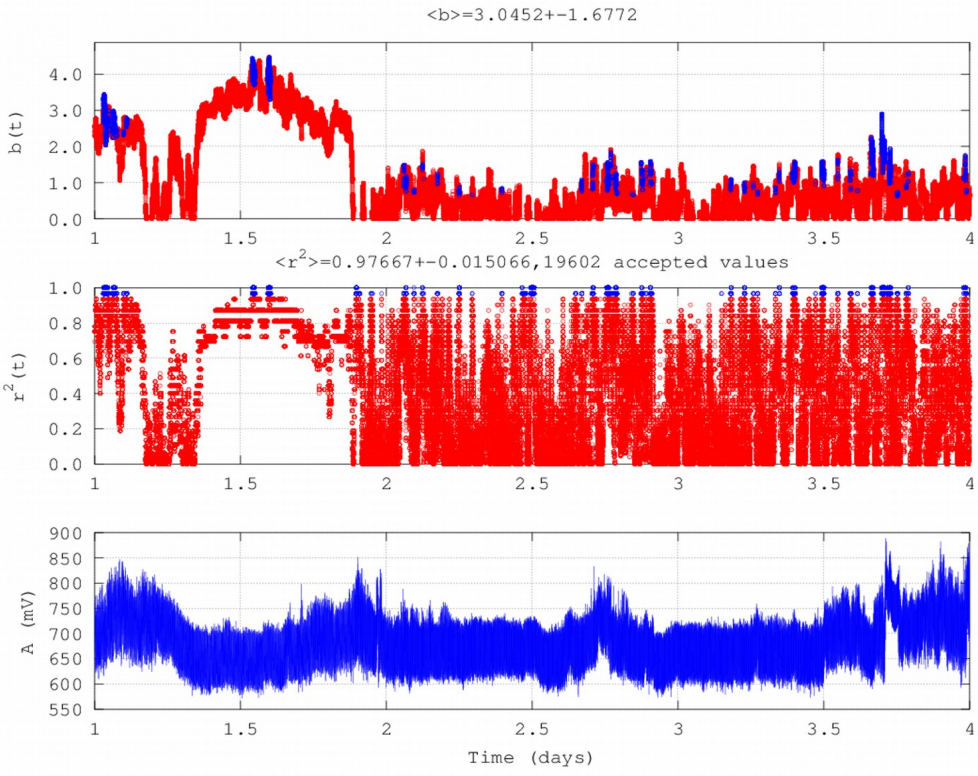

Figure 3.29: EQ:26 (JD 88, 2008), Neapoli station, JD 75-78, 2008, 46 MHz (U).

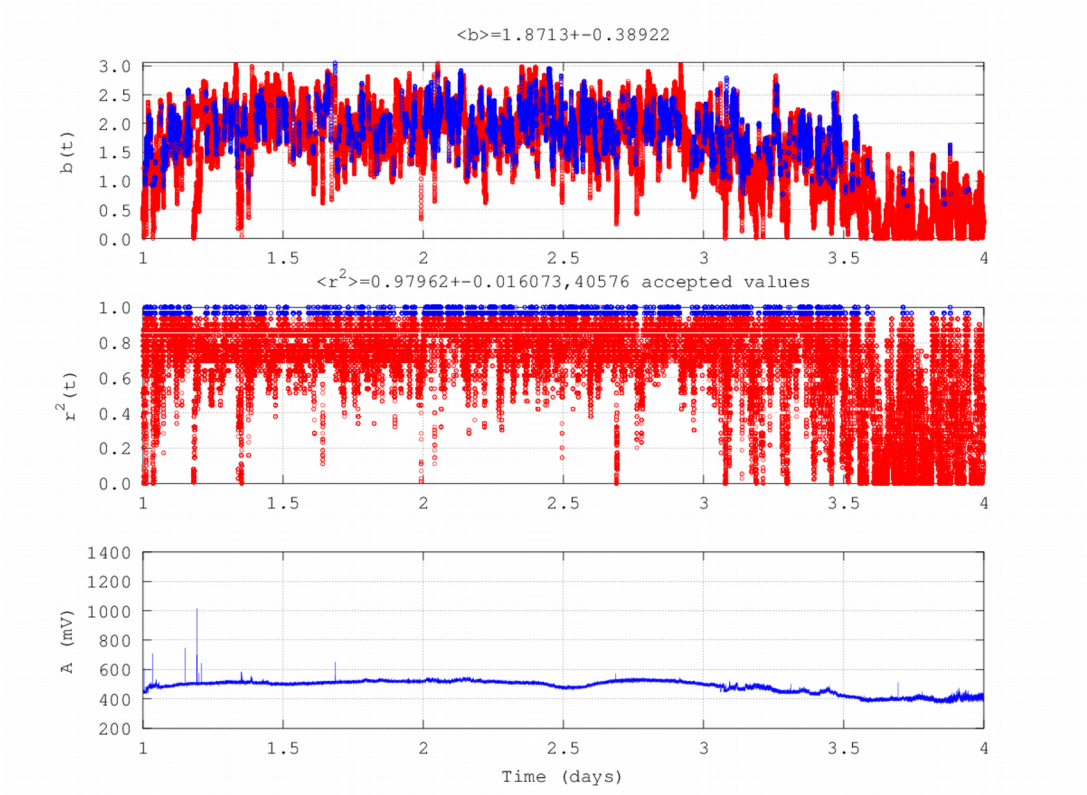

Figure 3.30: EQs:8-24-27 (JDs 50-51-57,2008), Vamos, JD 48-51,2008, 46 MHz (U).

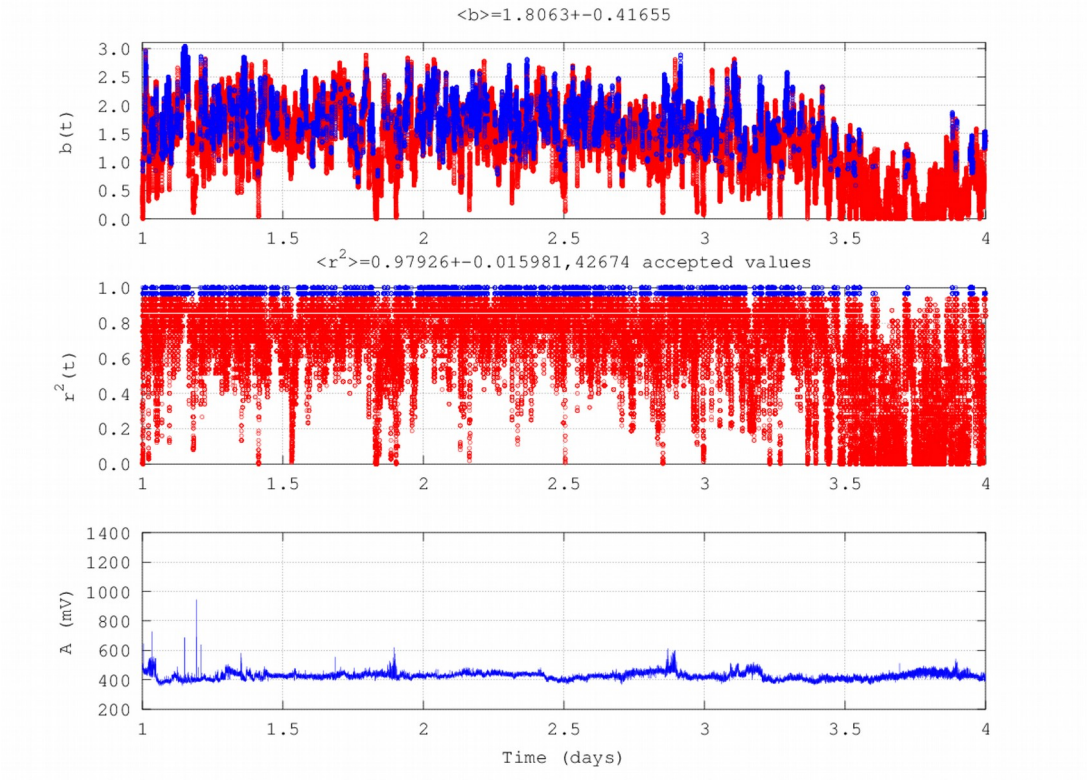

Figure 3.31: EQs:8-24-27 (JDs 50-51-57,2008), Vamos, JD 48-51, 2008, 41 MHz (U).

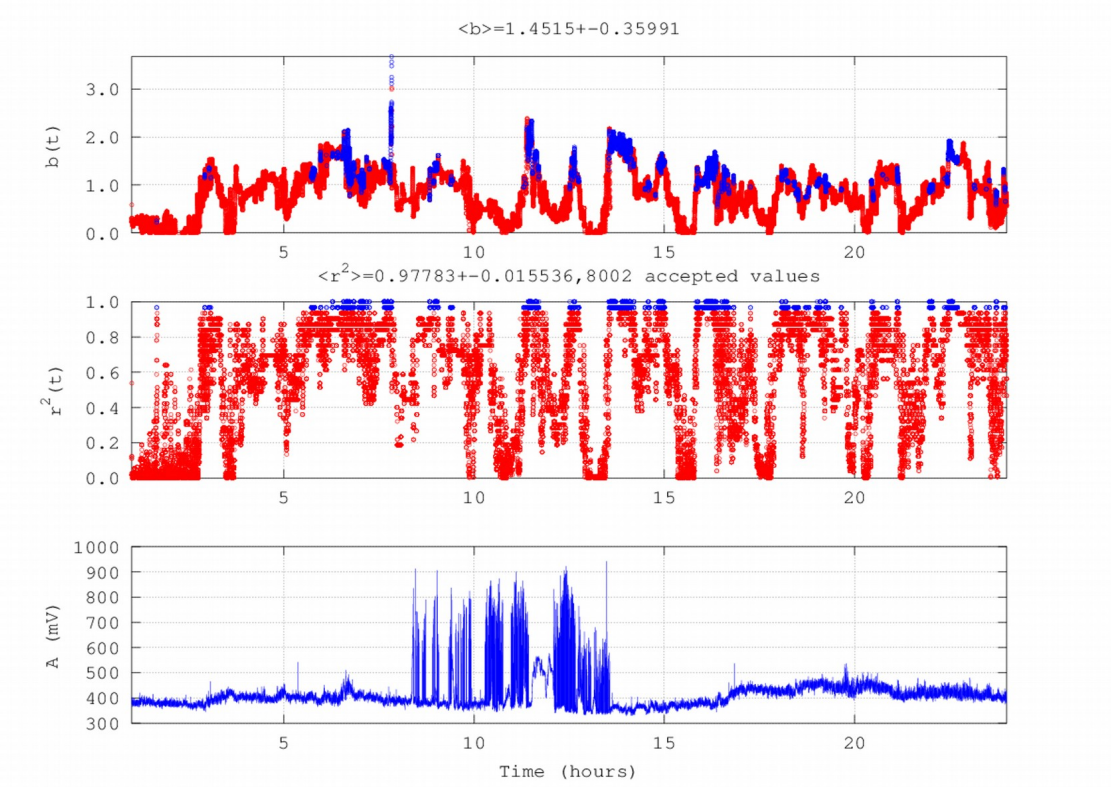

Figure 3.32: EQs:8-24-27 (JDs 50-51-57,2008), Vamos, JD 45, 2008, 41 MHz (U).

The following issues are of importance and should be emphasised in reference to **Figures 3.16-3.32:**

(a) Significant number of time-series parts exhibited successive ($r^2 \geq 0.95$) power-law b - values between 1.5 and 2.0.

(b) Numerous parts presented b - values greater than 2.0. As aforementioned, b - values between 2.0 and 3.0 suggest persistent profiles qualitatively analogous to the fBm model.

(c) Some b - values were above 3.0. This is very peculiar since, according to the theory (**section 3.2.2**), the power-law b - values are normally in the range $-1 < b < 3$. Some aspects on this issue are addressed below.

(d) The *loga* - values associated with (a) and (b) were between 1.0 and 5.0. This finding was also addressed in several publications (e.g. Kapiris et al., 2002, 2003, 2004; Eftaxias et al., 2009 and references therein).

(e) The Morlet scalograms of the great majority of signals presented more power at the low frequencies. Two characteristic cases are shown in **Figure 3.33** and in **Figure 3.34**. In most cases, the signal's epochs with high frequencies were associated with successive *b* - values above 1.5. A characteristic such case is shown in **Figure 3.35**. This case is of importance and is analysed below.

(f) Periods with significant electromagnetic disturbances in the time-series are not associated a-priori or de-facto with observations such as those of (a)-(d).

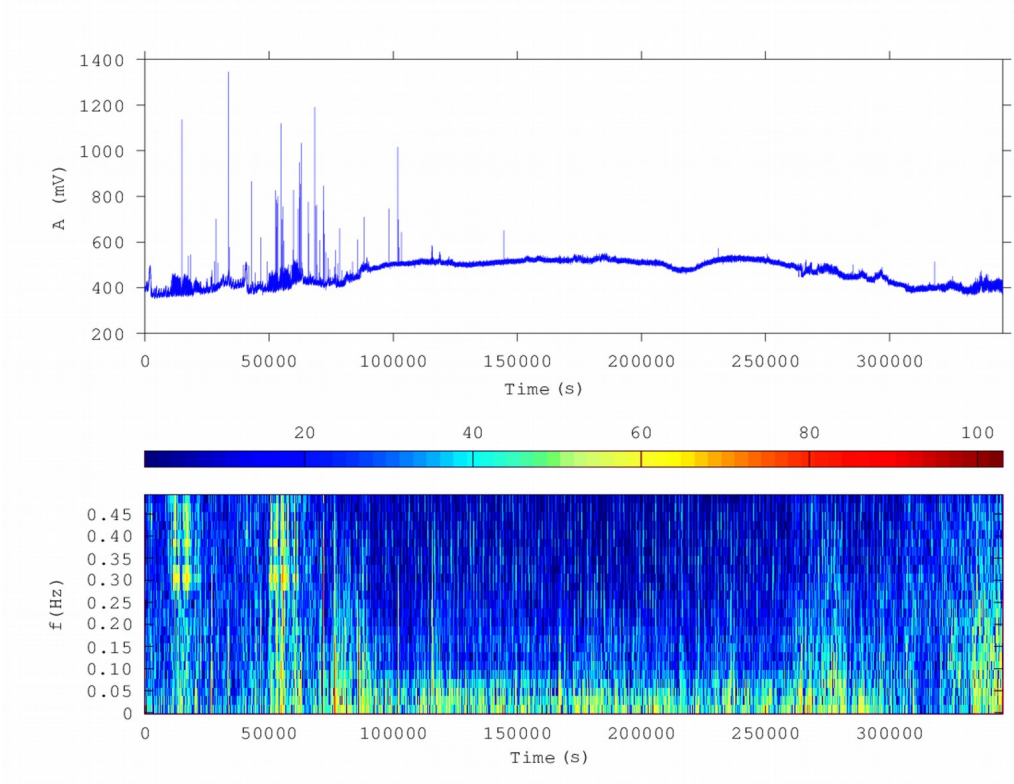

Figure 3.33: Discrete wavelet transform, time-evolution scalogram, Morlet wavelet of the signal of **Figure 3.30**, Vamos, 46 MHz, JD 48-51, 2008, dynamic range 0-100 db.

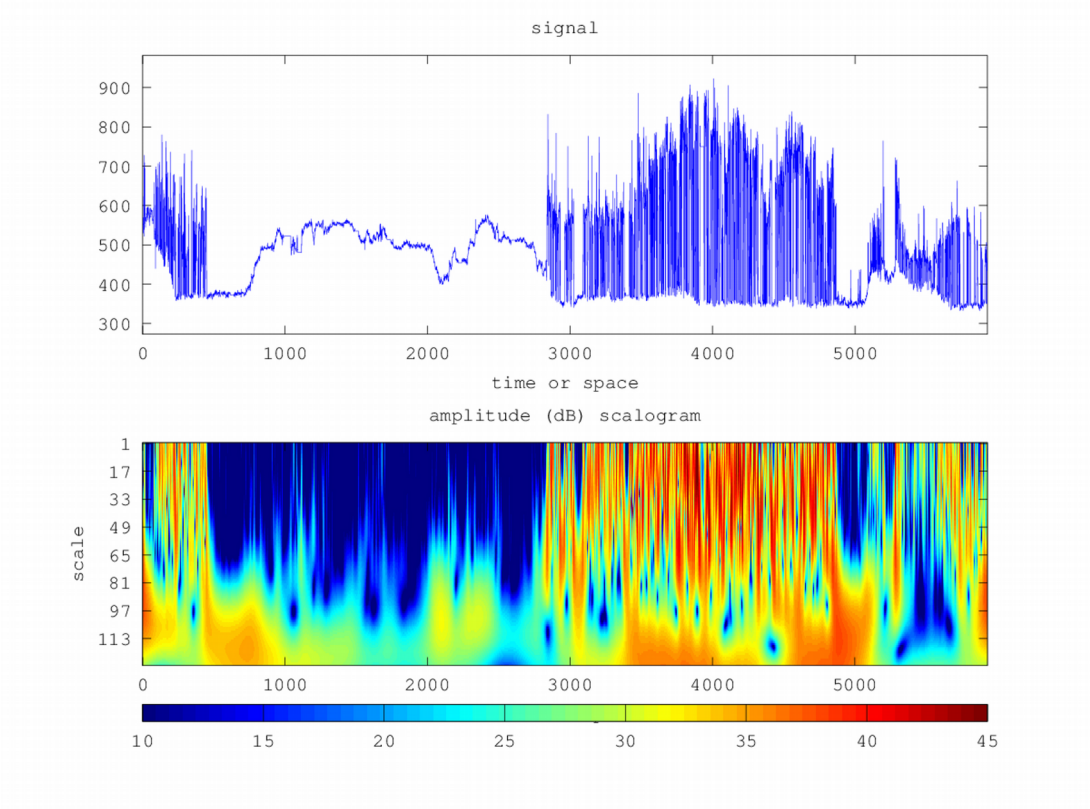

Figure 3.34: Continuous wavelet transform, time-evolution scalogram, Morlet wavelet, electromagnetic signal of **Figure 3.32**,Vamos, 41 MHz, JD 45, 2008, dynamic range 10-45 dB , horizontal axis in seconds.

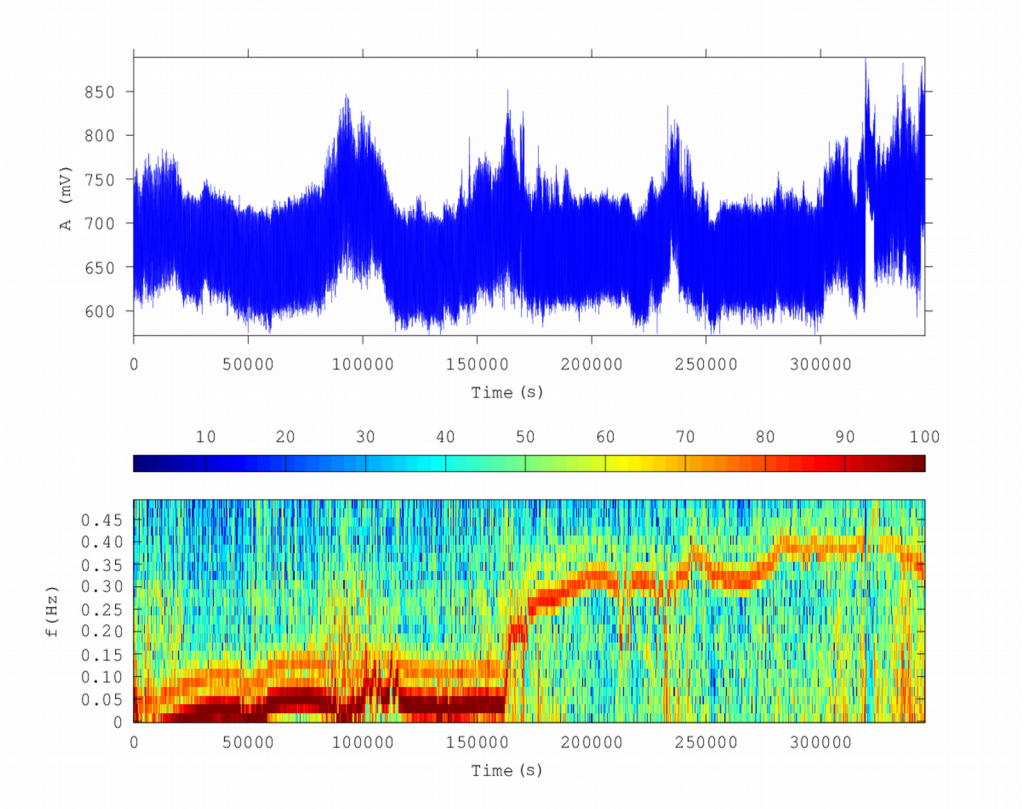

Figure 3.35: Discrete wavelet transform, time-evolution scalogram, Morlet scalogram of the electromagnetic signal of **Figure 3.29**. Neapoli station, 41 MHz, JD 75-78, 2008, dynamic range 0-100 dB.

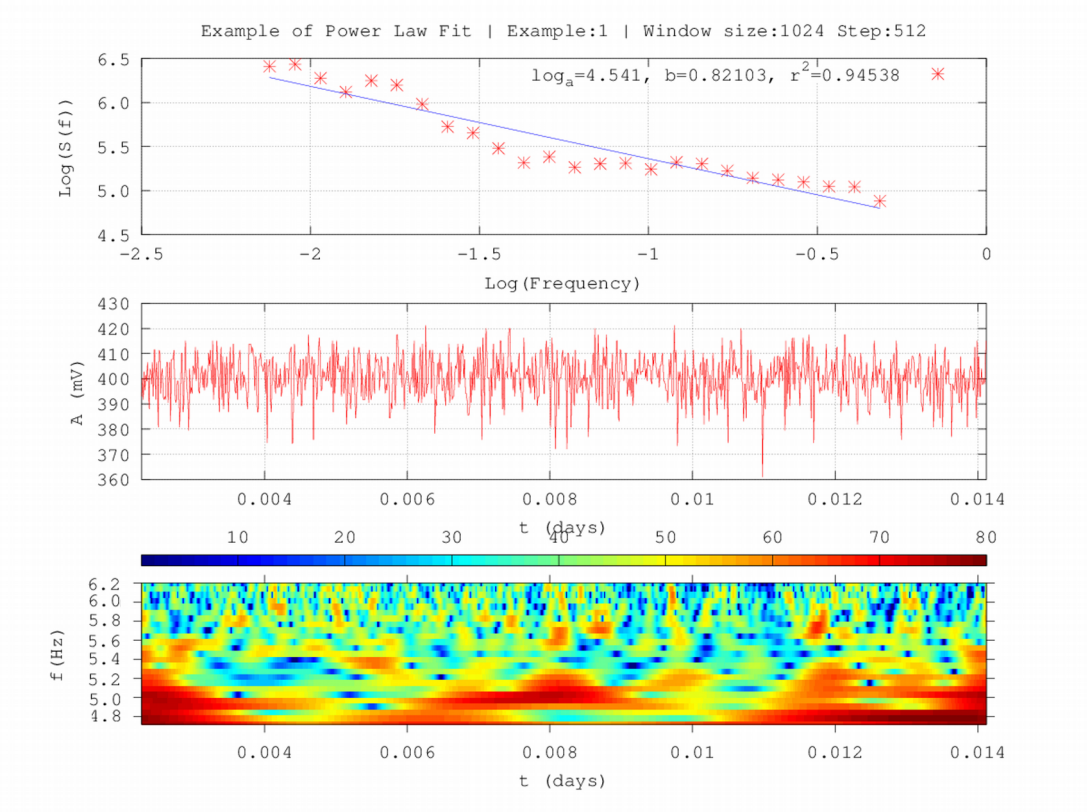

Figure 3.36: Example of a DWT evolution with time, window size 1024, 46 MHz signal from Kefalonia Station, 2008.

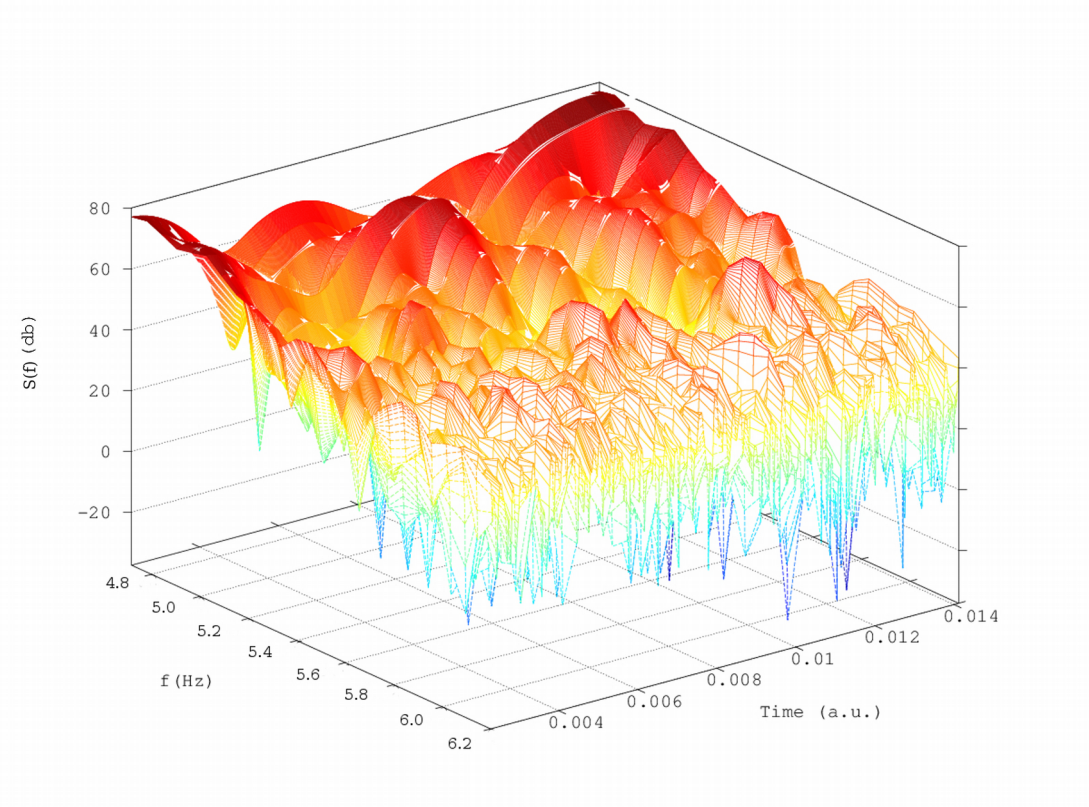

Figure 3.37: Example of a 3D DWT evolution of spectral power, S(f) in db with time and frequency, 46 MHz signal from Kefalonia station, 2008.

In reference to the **Figures 3.33 - 3.35** and the comment (e) of page 99, it is important to note that the low-frequency enhancement has been associated physically by investigators (e.g. Eftaxias, 2010; Eftaxias et al. 2009 and references therein) with the predominance of the larger fracture events and has been considered as a footprint of preparation of earthquakes. To the aspect of the author, an alternative interpretation is that this enhancement is due to the electromagnetic noise that is present in the measurements. This noise is changing frequently and for this reason many Morlet scales are needed for its representation, the majority of which are the larger ones. The centroid frequencies of these larger scales are at the low frequency range and for this

reason an enhancement at the low frequency range is addressed. This can be more characteristically seen in **Figure 3.34** which is associated with **Figure 3.32**. Several bursts can be identified in the signal of both Figures. In the scalogram of **Figure 3.34**, almost all the scales are present during these bursts. On the other hand in the power-law evolution of b in **Figure 3.32**, these bursts do not associate with continuous successive high b - values; on the contrary, the successive high b - values are scattered and addressed rather in other epochs of the signal. The latter finding reinforces the comment (f) of page 99 as well.

The **Figures 3.36** and **3.37** are characteristic in relation to the **Figures 3.33 – 3.35** and their implications. At first the calculation of the power-law b - value can be addressed as the best-fit slope (top sub-figure **Figure 3.36**) of the $\log(f)-\log(S(f))$ diagram (see also **section 3.2.3**). Although the signal does not exhibit any anomalous behaviour (middle sub-figure **Figure 3.36**), the spectral fractal analysis indicates characteristic fractal patterns (bottom sub-figure **Figure 3.36**) which are repeated in all scales (spatial domain) and time (time-domain). This sub-figure (bottom sub-figure **Figure 3.36**) indicates also the low-frequency enhancement mentioned in the above paragraph. Indeed, the low frequencies (high-scales) are enhanced (red) corresponding to the quick-changing background of the signal. This is observed in **Figure 3.37** as well.

In reference to the **Figures 3.16-3.32** and in conjunction to the perspectives expressed

in the **sections 3.2.2** and **3.2.3**, the following facts should be emphasised as well (see also Eftaxias 2010; Eftaxias, et al. 2007, 2008, 2009; Kapiris et al. 2002, 2003; Nikolopoulos et al. 2012, 2014 and references therein):

(1) The value of $b=2$ means that there is no correlation between the process increments. This means that the disturbance generating system follows random paths driven by non-memory dynamics (random-walk).

(2) The value range $2<b<3$ suggests the signal's persistency. This means that the accumulation of the fluctuations of the system is faster than in fBm modelling.

(3) The value range $1<b<2$ implies anti-persistency.

(4) The value of $b=1$ suggests that the fluctuations of the processes do not grow and the electromagnetic signal is stationary.

In the above consensus, certain key periods can be recognised in the disturbances of **Figures 3.16-3.32** with: (A) strong anti-persistency of $b>1.5$, (B) persistency of $2<b<3$ and (C) switching between persistency and anti-persistency. According to the aspects expressed so-far and the view of **sections 3.2.2** and **3.2.3**, the above findings (1-4) imply long-range spatial-temporal correlations, i.e., strong memory of the system which generated the electromagnetic disturbances. This significant implication means that each value of the time-series within the key-periods, correlates not only to its most recent value but also to its long-term history in a scale-invariant, fractal manner (Eftaxias et al. 2008; Eftaxias 2010; Nikolopoulos et al., 2012, 2014; Petraki,

Nikolopoulos, Fotopoulos, Panagiotaras, Koulouras, et al. 2013; Petraki et al., 2014). Hence, the history of the system defines its future (non-Markovian behaviour) (Kapiris et al. 2002; Eftaxias et al. 2008, 2009; Eftaxias 2010; Nikolopoulos et al., 2012, 2014; Petraki, Nikolopoulos, Fotopoulos, Panagiotaras, Koulouras, et al. 2013; Petraki et al., 2014). In specific, (B) suggests that the underlying dynamics are governed by positive feedback mechanisms and, thus, any external influences tend to lead the system out of equilibrium (Telesca & Lasaponara, 2006). The system acquires, hence, a self-regulating character and, to a great extent, the property of irreversibility, one of the important components of prediction reliability (Morgounov, 2001). From another viewpoint, this behaviour suggests that the final output of fracture is affected by many processes that act on different time scales (Smirnova et al., 2004; Smirnova, & Hayakawa, 2007; Eftaxias, 2010). All these results are in good agreement with a hypothesis that the evolution of the earth's crust towards general failure takes place as a SOC phenomenon (Eftaxias 2010; Gotoh et al. 2004; Hayakawa, & Hobara 2010; Nikolopoulos et al., 2012, 2014; Petraki, Nikolopoulos, Fotopoulos, Panagiotaras, Koulouras et al., 2013; Petraki, Nikolopoulos, Fotopoulos, Panagiotaras, Nomicos et al., 2013; Smirnova, & Hayakawa 2007). All these issues are compatible with the last stages of the generation of earthquake.

In connection, it is very important to pay attention on cases like those of **Figures 3.16-3.19, 3.21, 3.23, 3.27** & **3.28**. Indeed, there were several periods with the characteristics (a)-(d) of page 99, yet, with no synchronous significant electromagnetic disturbance. The relevant case of **Figure 3.32**, has been commented already on page 98.

Distinguishing is also the case of **Figure 3.28**. Important high b - values can be

recognised in **Figure 3.28** ranging from 2.0 to 5.0, however, in periods where the electromagnetic fluctuations were slight. Comparable is also the case of **Figure 3.27**. It may be recalled that both signals were derived prior to EQ:23 (**Table 3.2**). In the above-mentioned sense, these results imply strong intrinsic memory of the earthquake generating system. The geological system generated fBm pre-earthquake power-law fractal patterns in periods of strong anti-persistency ($1.5<b<2$) and persistency ($2<b<3$), however, well concealed in the electromagnetic profiles. Indeed, these periods were not visually or statistically recognised and were unfolded only by the fractal methods. As seen in **Figures 3.27**, **3.28**, it is very significant that the system seems to have generated an alarm in the last JD of 2008 (17-26) and in the first days of 2009 (4-12). Since EQ:23 occurred in day 13 of 2009, the system produced a warning between days 21-30 and days 1-9 before the event. The earthquake 23 was an undersea earthquake in the region between Rhodes and Crete. It is worth to note that although the Neapoli station (Crete) generated the above alarms, similar analysis did not reveal any patterns in the electromagnetic time-series data neither of the near station of Rhodes, nor in those from the closer station of Vamos (Crete). Of worthy importance are also the cases of **Figures 3.16-3.19** and **Figure 3.23**. Similarly, the geological system produced long-lasting pre-seismic footprints with power-law b - exponent values ranging between $1.5<b<3$. Several successive periods ($r^2 \geqslant 0.95$) were recognised of anti-persistency, persistency and switching between persistency and anti-persistency. The most important, however, is that the system generated a self-affine

alarm continuously one month prior to each earthquake. It is the first time that such continuous warning was recognised in pre-earthquake electromagnetic signals of the MHz range. From these signals, **Figures 3.17-3.19** and **Figure 3.23** refer to undersea earthquakes. It is worth to mention that, finally, the MHz pre-earthquake signals were recorded with such characteristics, despite that the focal points and depths of the corresponding earthquakes prohibit, in principle, the transferability of the MHz electromagnetic waves. It is, possibly, the complicated transport of micro-cracks (Kapiris et al. 2002, 2003; Eftaxias 2010; Eftaxias et al., 2007, 2008, 2009; Petraki, Nikolopoulos, Fotopoulos, Panagiotaras, Koulouras et al., 2013; Petraki, Nikolopoulos, Fotopoulos, Panagiotaras, Nomicos et al., 2013), and the extent of the heterogeneous medium that obstructs the crack-slip (Eftaxias, 2010; Eftaxias et al., 2008, 2009), which could provide air pathways to earth's surface for the MHz radiation. Very significant is to note that the shallow earthquake EQ:19 (**Table 3.2**, **Figure 3.16**) produced also a continuous one-month fractal pre-seismic warning in the Corfu station. In comparison, the same earthquake (EQ:19, **Table 3.2**) did not give a continuous alarm of such type to the near Ioannina station (**Figure 3.20**) but rather a scattered alarm. Probably, this could be an indication of the sensitivity or the locality of each station regarding the collection of MHz pre-seismic signals. Locality and sensitivity are considered a common issue of the ULF network stations (e.g.Varotsos and Alexopoulos 1984a, 1984b and all the references of the VAN team). The latter claim may provide reasons for not having identified other pre-earthquake fractal patterns, than those already presented in **Figures 3.16-3.26**, despite that other stations were also in the vicinity of the events of **Figure 3.6**. Possibly due to this, the shallow earthquake EQ:30 (**Table 3.2**) produced a continuous warning (**Figure 3.25**), yet, not of the intensity of **Figures 3.16-3.19** and

Figure 3.23. This is reinforced by the electromagnetic time-series data of **Figure 3.26**. The undersea earthquake EQ:14 (**Table 3.2**) generated only scattered fractal alarms. It should be stressed finally that the related analysis was followed in all the MHz signals of 2009 approximately one month prior to the events of **Figure 3.6**, as already mentioned. Important is to mention that there were no systematic observations both in the 41 MHz and the 46 MHz frequencies of the temporal power-law b - profiles of the aforementioned type, even from the data of the same earthquake and from the same station. The systematics of the observations indicate that it is a fortunate conjuncture to recognise: (1) simultaneous visual anomalies in the recordings of a certain station in both the 41 MHz and the 46 MHz frequencies, (2) in parallel with high power-law b - values associated with the analysis of (1), (3) synchronous discovery in the electromagnetic recordings of near stations. Such a conjuncture is hard to find (see e.g. Ciccerone et al., 2009) and if found, it is a very strong sign of the validity of the certain precursors. Nevertheless, emphasis should be stressed on the fact that since no analysis was done on well pre-earthquake (<1 month) signals, the reported tendencies may be biased in the future.

A very significant finding is the following and hence emphasis should be placed on that. The analysis of the post-earthquake signals of the **Figures 3.16-3.28** indicated that only two cases presented noteworthy post-scattered fractal behaviour (Petraki et al., 2014): The first case was (1) for a five-day activity after EQ:15 (**Table 3.2**) recorded in Ileia station (**Figure 3.18**) and the second (2) for a five-day activity after EQ:20 (**Table 3.2**) recorded in the station located Rhodes island (**Figure 3.19**). The signal of the first

case was simultaneous to (i) one earthquake of $M_s = 4.7$ that occurred on 20/2/2009 near Zakynthos island. The signal of the second case was simultaneous to (ii) one earthquake of $M_s = 5.3$ that occurred on 20/6/2009 and (iii) another earthquake of $M_s = 5.2$ that occurred on 23/6/2009, both occurred near Rhodes island.

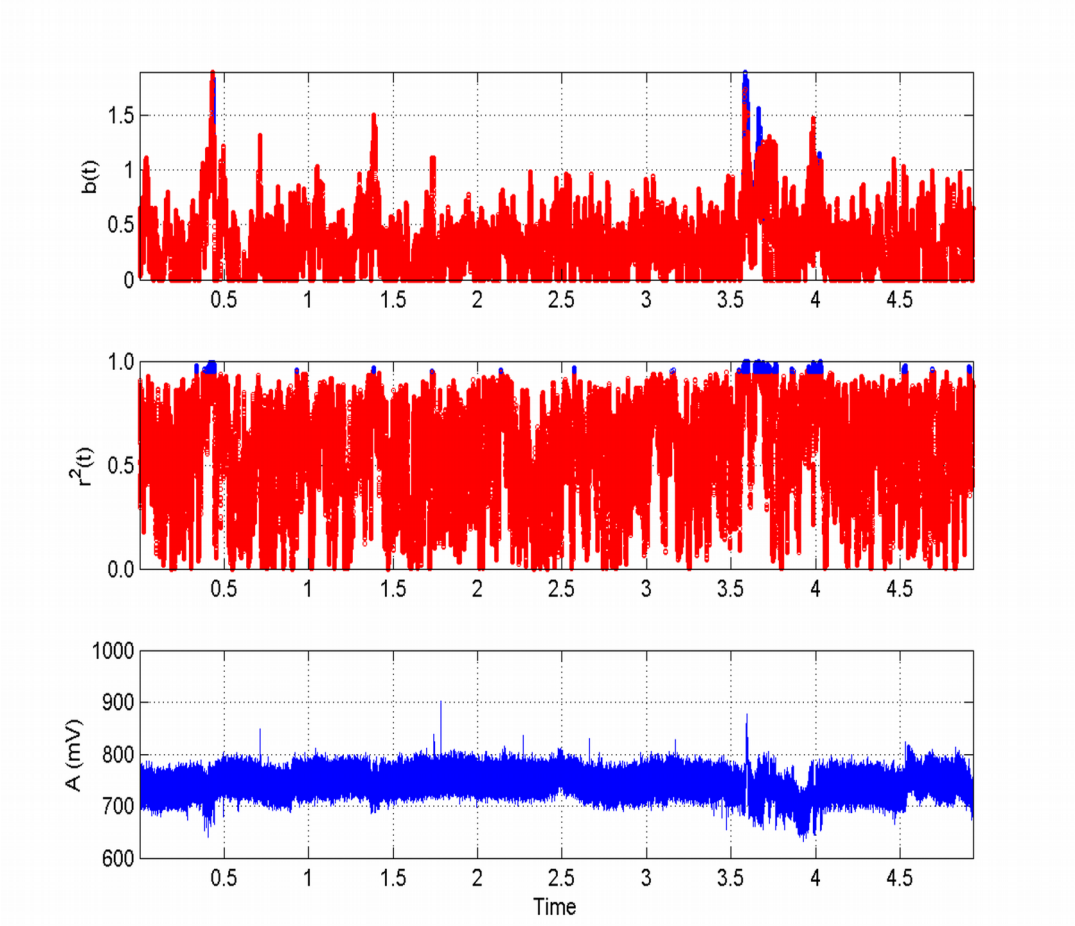

Figure 3.38: EQ:30 (**Table 3.2**), post-activity Ioannina station, 41 MHz, JDs 9-14, 2009.

Non continuous significant variations are addressed.

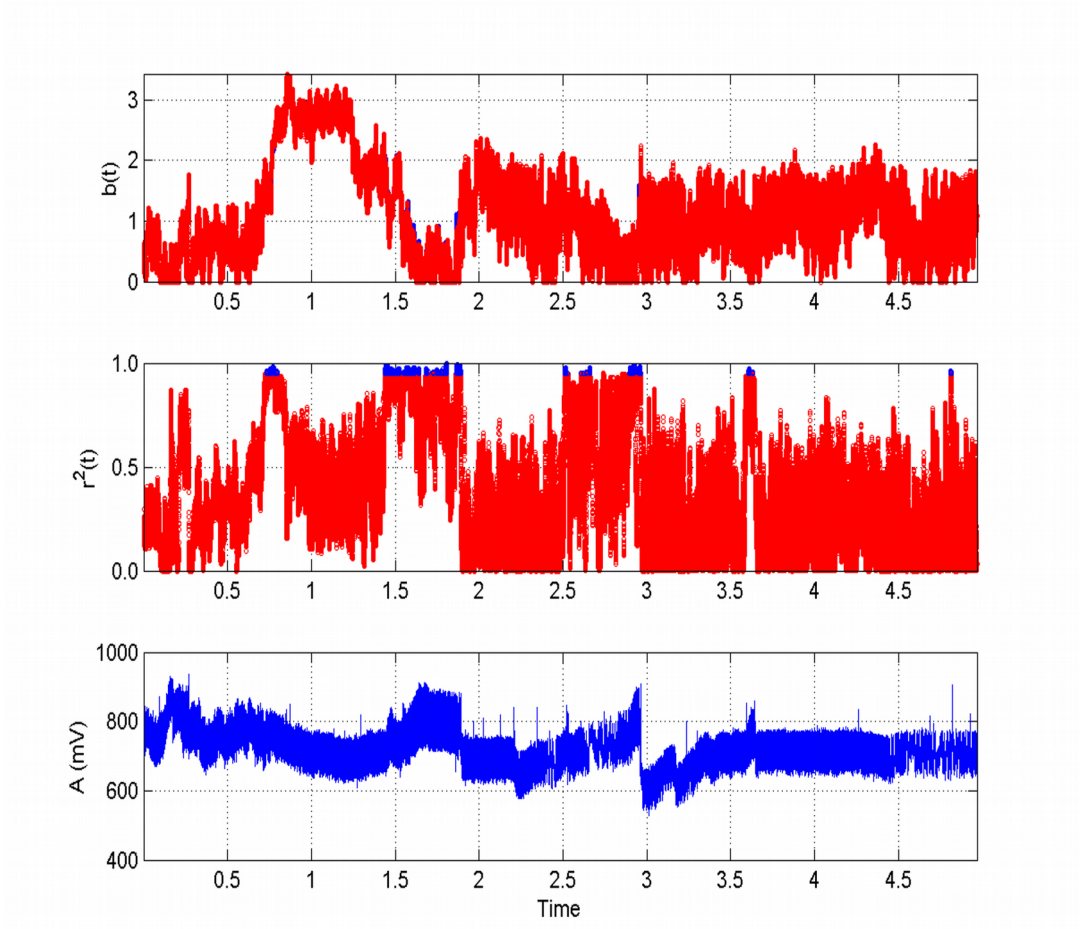

Figure 3.39: EQ:23 (**Table 3.2**), post-activity Neapoli station, 41 MHz, JDs 14-19, 2009.

Non continuous significant variations may be observed. It is important to note that a similar pattern as those of Figure 3.28 is identified. However this does not correspond to successive fractal behaviour. This pattern is to be remarked.

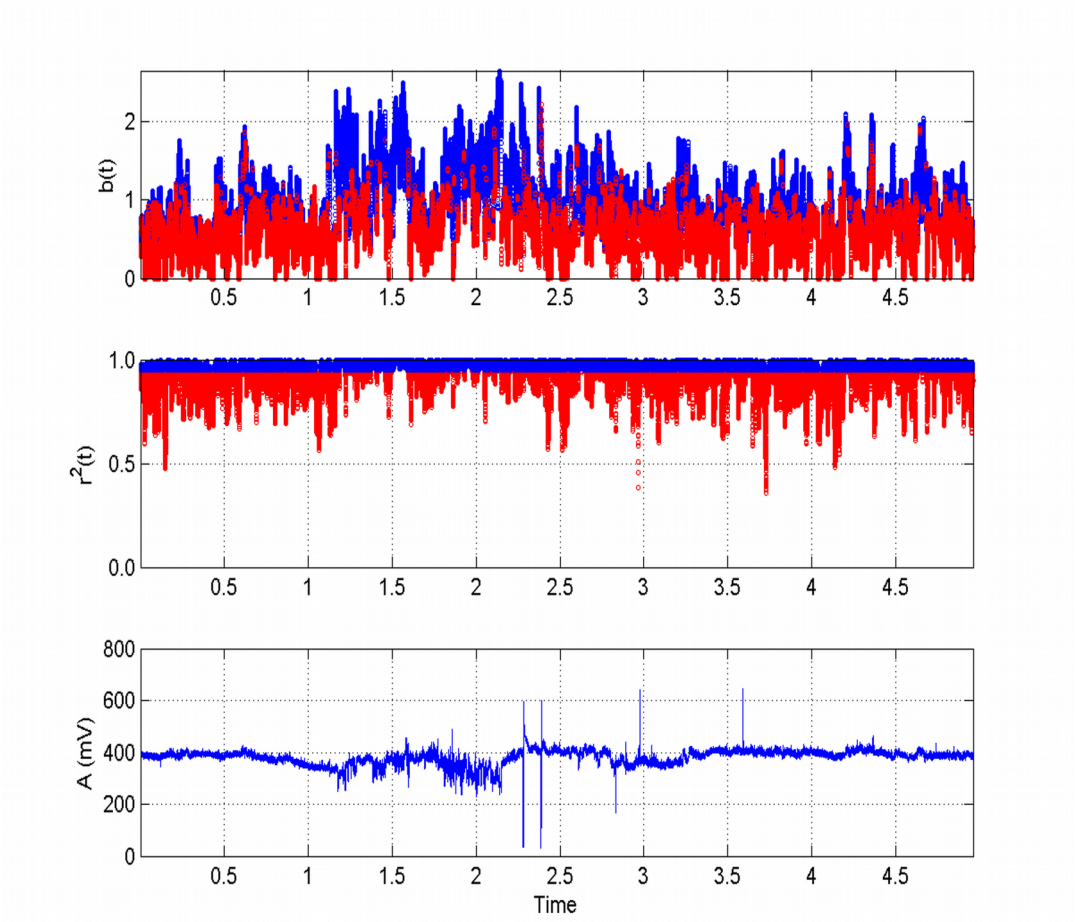

Figure 3.40: EQ:15 (**Table 3.2**), post-activity Ileia station, 46 MHz, JDs 48-53, 2009.

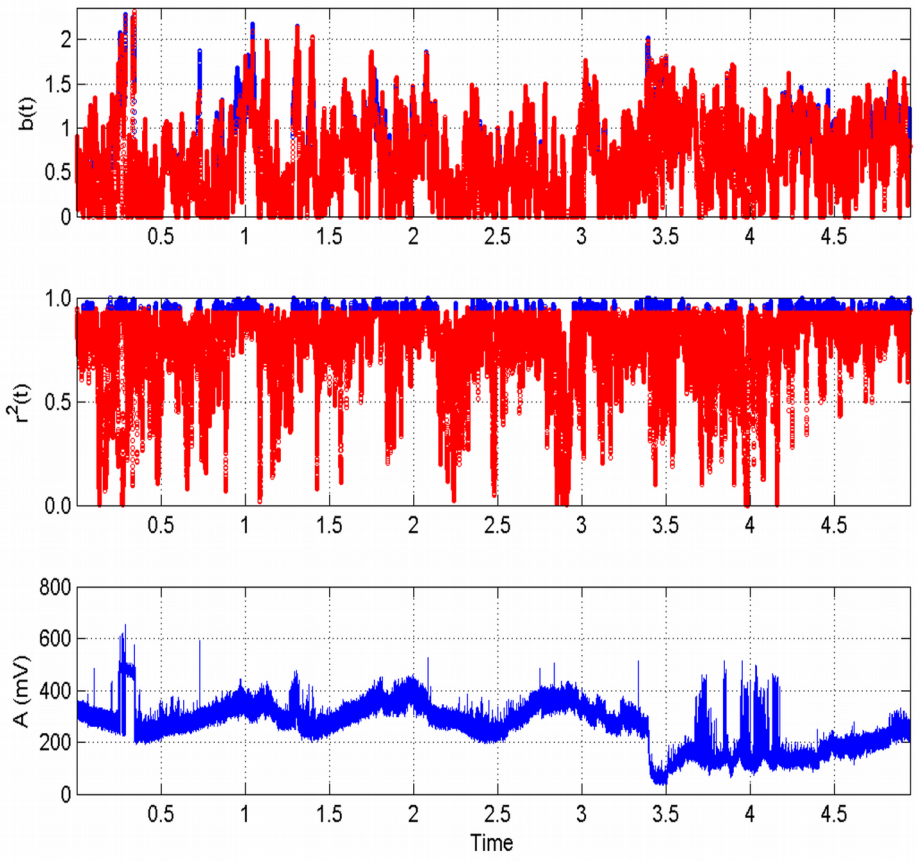

Figure 3.41: EQ:25 (**Table 3.2**), post-activity Komotini station, 41 MHz, JDs 145-150, 2009.

Non continuous significant variations are addressed.

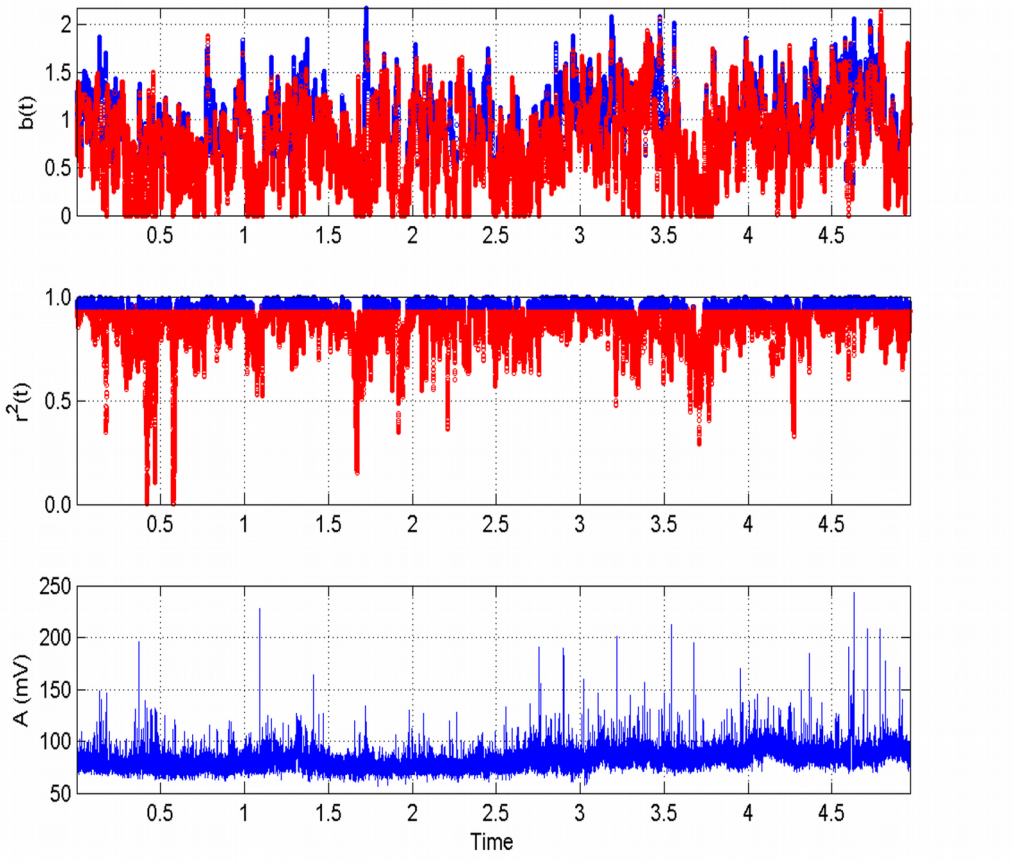

Figure 3.42: EQ:15 (**Table 3.2**), post-activity Rhodes station, 46 MHz, JDs 171-176, 2009.

Some significant variations are addressed. However, observing closely two earthquakes occurred on 20/6/2009 with Ms=5.30 and on 23/6/2009 Ms=5.2 near Rhodes. The observed variations could be due to these EQs.

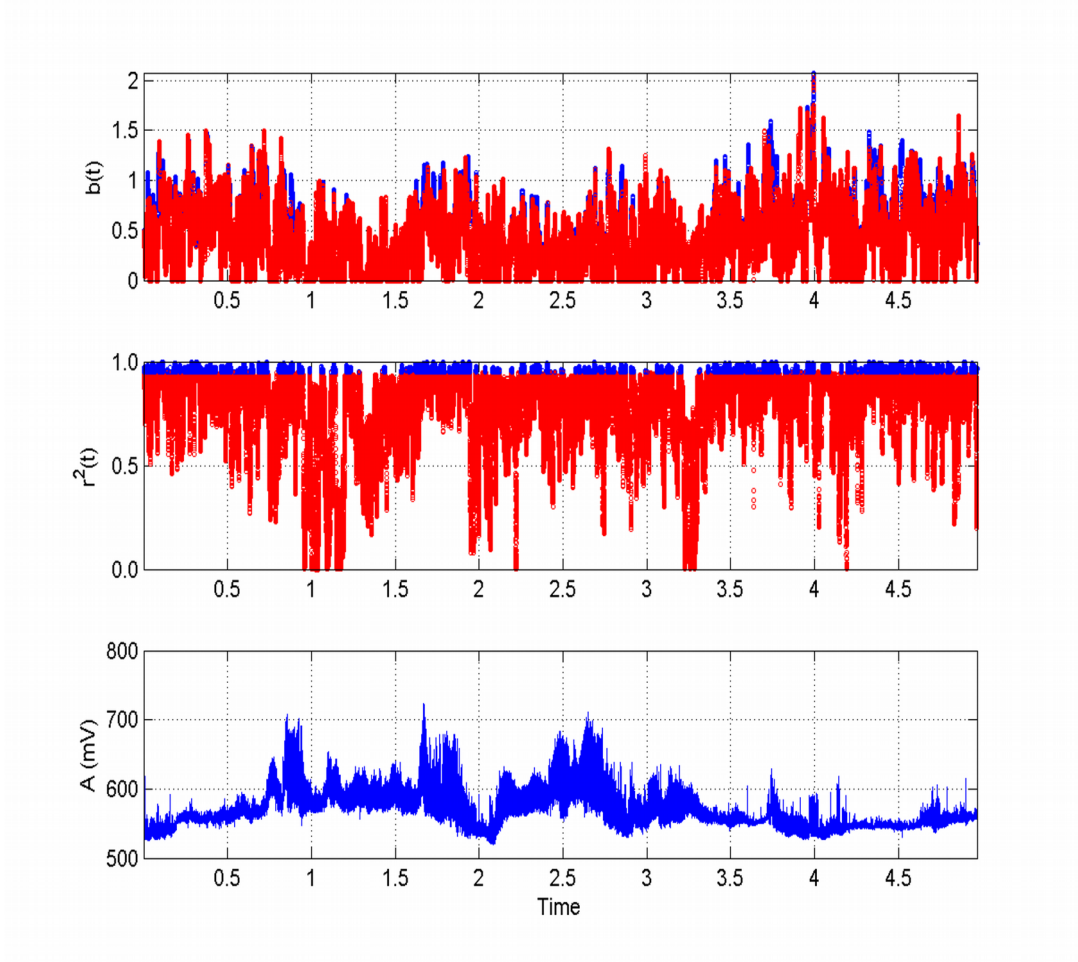

Figure 3.43: EQ:11 (**Table 3.2**), post-activity Neapoli station, 46 MHz, JDs 183-188, 2009.

Non continuous significant variations are addressed.

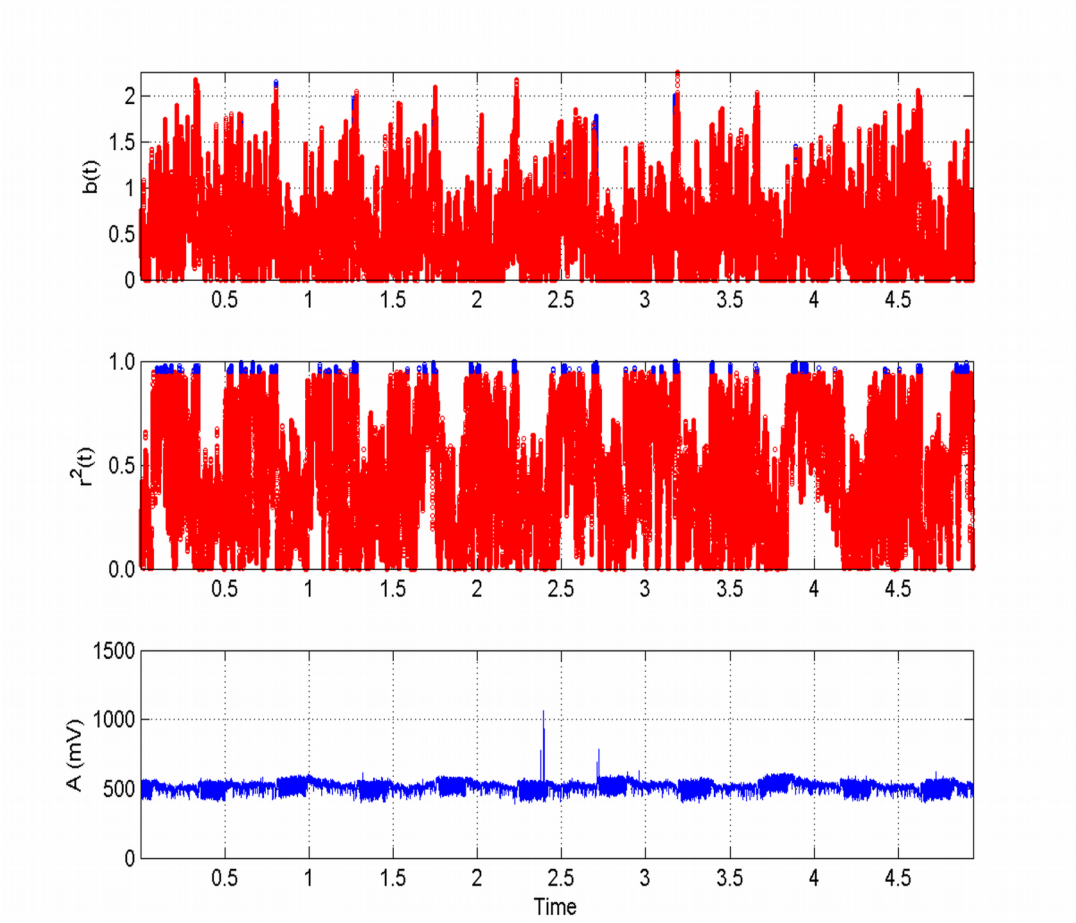

Figure 3.44: EQ:19 (**Table 3.2**), post-activity Vamos station, 41 MHz, JDs 183-188, 2009.

Non continuous significant variations are addressed.

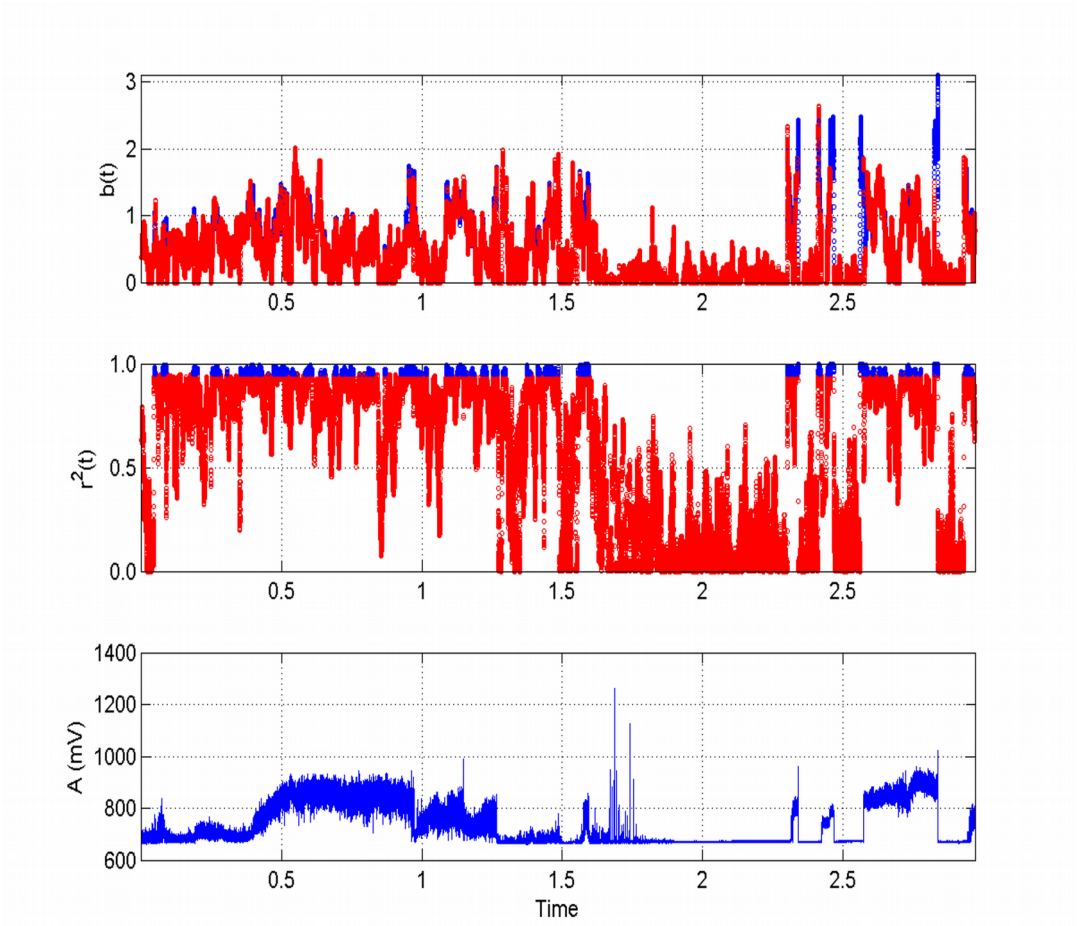

Figure 3.45: EQ:14 (**Table 3.2**), post-activity Ileia station, 41 MHz, JDs 310-313, 2009.

Non continuous significant variations are addressed.

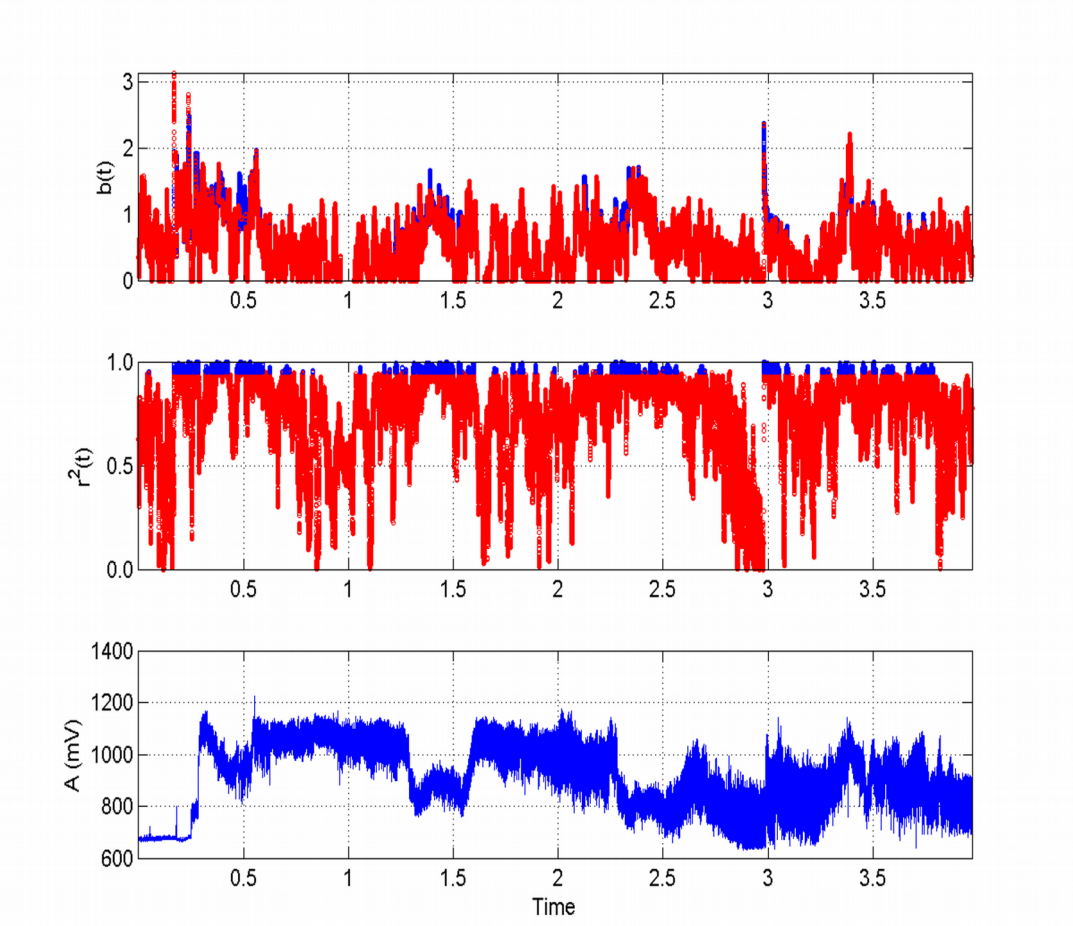

Figure 3.46: EQ:22 (**Table 3.2**), post-activity Ileia station, 46 MHz, JDs 316-320, 2009.

Non continuous significant variations are addressed.

It should be emphasised here that the pre-earthquake and the post-earthquake activity, is a very complicated issue for the following reasons:

(1) Greece is a very seismically active country with many earthquakes of magnitudes above 4 (either M_L or M_s). This fact makes very difficult to attempt any possible link between even well-identified pre-earthquake patterns and certain events.

(2) Up-to-date, there is no universal model to serve as a pre-earthquake signature (Eftaxias et al. 2008; Eftaxias 2010). Hence, there is no certain rule to link some kind of detected anomalies to a specific forthcoming seismic event, either intense or mild. For the above reasons, independent of the fairly abundant circumstantial evidence, the scientific community still debates the precursory value of premonitory anomalies detected prior to earthquakes (Eftaxias 2010).

(3) The variety, as aforementioned, of the several electromagnetic precursors and the wide time lag between events and forthcoming earthquakes (Cicerone et al.2009; Eftaxias et al. 2010) restricts the possibilities of prediction.

For the above reasons, no link of earthquake events and presented signals can be more or less, attempted, despite the fact that the signals of **Figures 3.16-3.26** presented well-identified pre-earthquake patterns. It is worth to note that similar results have been reported for KHz electromagnetic disturbances prior to the great earthquakes of the Kozani-Grevena earthquake (Kapiris et al. 2002, 2003), the Athens earthquake (Eftaxias 2010; Minadakis et al. 2012; Potirakis et al. 2012) and the L' Aquila earthquake (Eftaxias et al. 2009, 2010). Analogous behaviour was identified in radon signals recorded in Ileia (Nikolopoulos et al. 2012; Petraki, Nikolopoulos, Fotopoulos,

Panagiotaras, Koulouras et al., 2013) and Lesvos Island, Greece (Nikolopoulos et al. 2013). Both signals are presented in the following sections together with the similarities that the precursors of radon in soil have with the precursors of the MHz range. Note that fBm modelling of stochastic fractal time series is consistent with the slip of self-affine fractional Brownian surfaces prior, or, during the generation of earthquakes (Eftaxias et al. 2008; Eftaxias 2010). It is also stressed that the addressed persistency-anti-persistency switching has also been reported for the ULF disturbances prior to the Guam earthquake (Smirnova et al. 2004; Smirnova, & Hayakawa 2007).

A very important outcome is the following and it should be remarked separately. In reference to comment (c) of page 98, it was the first time that successive power-law b - values above 3 were observed and reported. At first it should be mentioned that according to the arguments expressed in **section 3.2**, the theory does not a-priory contradicts power-law b - values above 3, despite that most of the literature focuses on the range $-1<b<1$. The interesting issue of the above comment is that there are instances when spectral slope reaches to 5. If the fractal dimension is calculated using the Berry's equation ($D=2-H$), these segments will lead to fractal dimension 0 or below. This peculiar observation can be argued as follows. Regarding the fractal dimension of fBm-modelling of monofractals, Berry's equation is more-or-less accurate and may be employed. However, for power-law spectral b - values above 3, some other aspects have been published (D'Addio, Accardo, Fornasa, Cesarelli, & De Felice, 2013; Kinsley, 2007; Chen, Wang, Chang, Wu, & Lee, 2006 ; Pereda, Gamundi, Rial, & Gonzalez, 1998), namely that fractal dimension saturates to 1. To the opinion of the author, this is probably the case for the high fractal dimensions addressed. What seems even more interesting is that this peculiar behaviour is addressed only in the Neapoli station. To address the behaviour of the recordings of the Neapoli station versus those of the other stations, a specific task was implemented; to produce Fourier spectrograms of a half-month duration for the recordings of the 2009 (**Figures 3.16-3.28**). The case of the Neapoli station is presented in **Figure 3.47** whereas two other cases in **Figures 3.48** and **3.49**. At first very peculiar crossing Fourier iteration-lines are observed in

Figure 3.47. This finding is hard to interpret and is presented here only as an observation. What makes this figure however of great value is that the periods when these lines are diminished are the ones where the signal presented the high power-law b - values, some of which, as aforementioned, were above 3.0 (**Figure 3.27**). It is also important to remark in relation, that the Neapoli station was associated with another very peculiar scalogram (**Figure 3.35**) as presented and discussed already. Nevertheless as can be observed in **Figure 3.47**, this is not a standard behaviour of the Neapoli station, probably because in the second case (**Figure 3.48**), the addressed fractal behaviour was not as the one of **Figure 3.27**. It is interesting that the Fourier spectrograms also indicate a low-frequency enhancement (**Figures 3.48** and **3.49**). It is very important to remark here that it was not possible to generate Fourier spectrograms as those of **Figures 3.47-3.49** in Matlab ® or Octave Forge (GNU), even in four-core machines. Due to this, a special machine was opened in OCEANOS cloud server, and this is very important to allow the generation of the spectrograms.

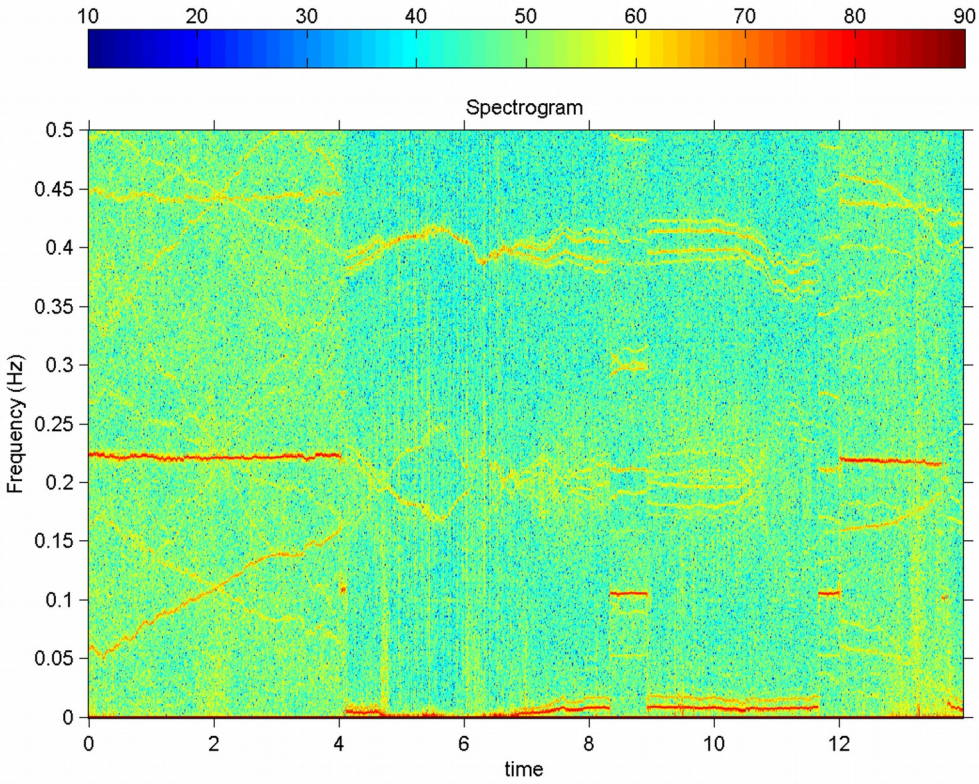

Figure 3.47: EQ:23, Fourier spectrogram of recordings from the Neapoli station, JD 1-14, 2009, 41 MHz, second half of the signal of **Figure 3.27**.

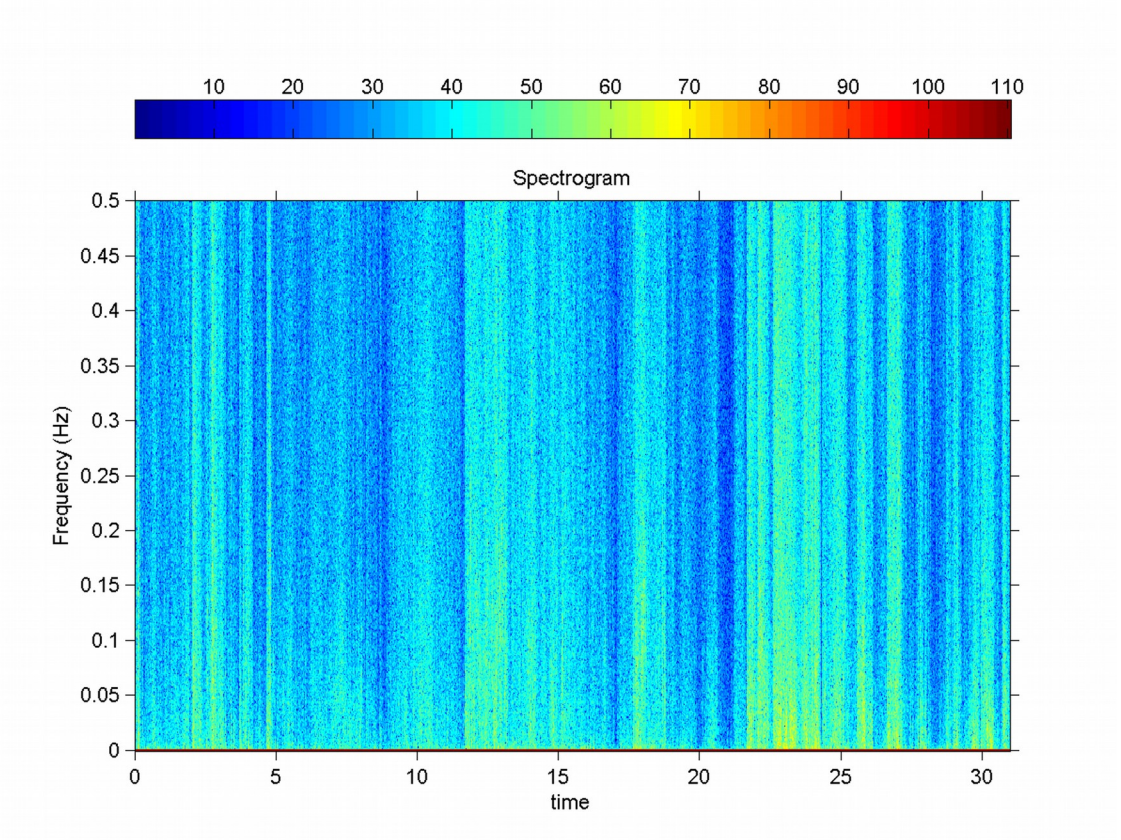

Figure 3.48: EQ:11, Fourier spectrogram of recordings from the Neapoli station, JD 152-182, 2009, 41 MHz, second half of the signal of **Figure 3.23**.

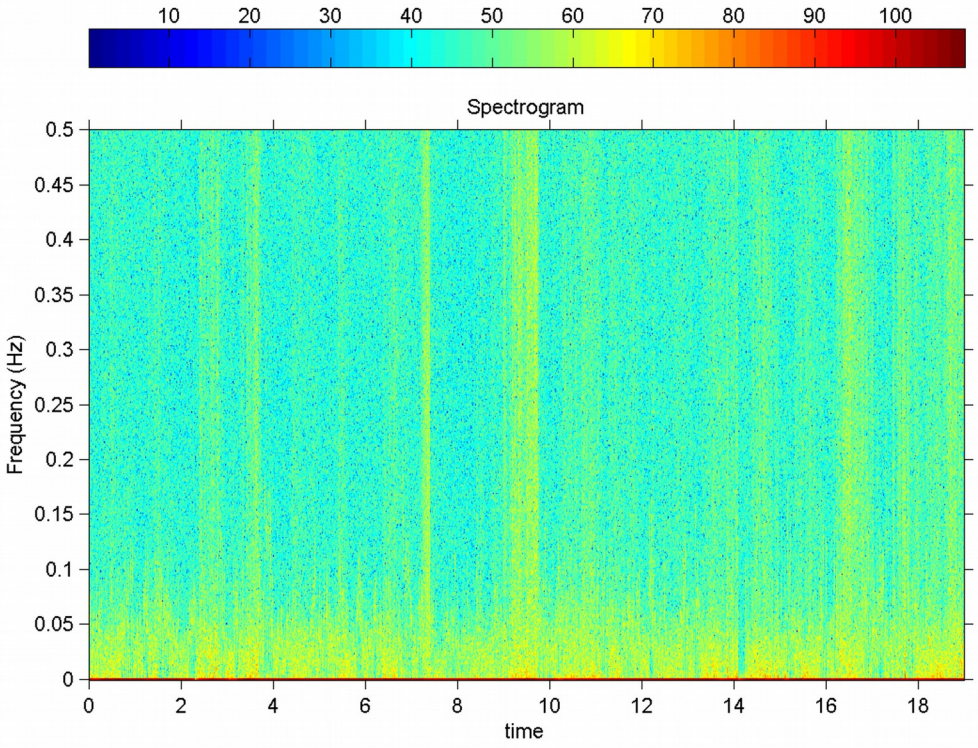

Figure 3.49: EQ:25, Fourier spectrogram of recordings from the Komotini station, JD 114-144, 2009, 41 MHz, signal of **Figure 3.21**.

Regarding the related Hurst exponent the following fact can be supported:

(a) The majority of the successive ($r^2 \geqslant 0.95$) power-law b-values of each signals referred to fBm $0.5 < H < 1$. These values are associated with strong memory and persistent behaviour. This means that if the amplitude of the signal increases in one time interval, it is likely to continue increasing in the period immediately following.

(b) Many successive ($r^2 \geqslant 0.95$) power-law b - values referred to fBm $0 < H < 0.5$. These values suggest that if the fluctuations increase in one period, it is likely to continue decreasing in the period immediately following, and vice versa.

(c) Stationary segments can be identified by Hurst exponent $H = 0$.

(d) Remaining segments referred to fGn modelling.

According to the analysis presented for the example cases presented so far, it could be supported that the recorded MHz disturbances of this research evolved naturally to characteristic epochs of fractal organisation in space and time. All pre-earthquake signals concealed numerous such epochs; in some cases continuously. As aforementioned, such organisation is consistent with the SOC states of the last stage of preparation of earthquakes. These epochs were confronted as pre-earthquake warnings with attributes of locality and sensitivity. Deep undersea earthquakes gave, surprisingly, noteworthy, many fractal epochs. All these issues could be explained under the view of the asperity model (Eftaxias et al. 2008). According to the asperity model (Eftaxias et

al. 2008), focal areas of earthquakes consist of (1) a backbone of strong and large asperities distributed along the fault activated during the earthquake preparation process and (2) a strongly heterogeneous medium, including weaker areas and smaller asperities, that surrounds the family of main asperities (Eftaxias et al. 2008, 2009; Eftaxias 2010). This model is based on aspects rooted in-criticality, spectral fractal analysis by means of wavelets, complexity, non-extensive statistics and meso-mechanics (Contoyiannis et al. 2005; Eftaxias, Panin et al. 2007; Papadimitriou et al. 2008). Importantly, the asperity model is associated with the observation of two discrete epoch stages (Contoyiannis et al. 2005; Eftaxias, Panin et al. 2007). The first epoch stage is combined with emergence of MHz electromagnetic radiation (Eftaxias, Panin et al. 2007; Eftaxias et al. 2008, 2009; Eftaxias 2010) and, possibly, anomalous emissions of radon in soil (Nikolopoulos et al. 2012; Petraki, Nikolopoulos, Fotopoulos, Panagiotaras, Koulouras et al., 2013; Petraki, Nikolopoulos, Fotopoulos, Panagiotaras, Nomicos et al., 2013). This stage originates during cracking in the highly heterogeneous component of the focal area. The results have shown that candidate MHz EM precursors project fracture processes undergoing a generalised continuous phase transition at equilibrium (Contoyiannis et al. 2005; Minadakis et al. 2012; Potirakis et al. 2012). On the other hand and very importantly, the second epoch is associated with unavoidable emergence of strong multi-peaked KHz EM radiation (Eftaxias et al. 2008, 2009; Eftaxias 2010; Minadakis et al. 2012; Potirakis et al. 2012). The latter is due to the fracture of the high-strength large asperities that sustain the system. It should be emphasized, however, that no signature of a generalized continuous phase transition has been observed in KHz EM activity (Contoyiannis et al. 2005; Eftaxias et al. 2008; Potirakis et al. 2012). On the contrary, the related phase-transition occurrence in MHz

electromagnetic precursors has been recognised as a footprint of preparation of earthquakes (Eftaxias 2010). In addition, the asperities follow persistent, or highly anti-persistent, fBm profiles (Eftaxias 2010; Eftaxias et al. 2008). Moreover, at this stage, the fracture of the heterogeneous system obstructs the backbone of fBm asperities and, more importantly, also critical anti-persistent/persistent anomalies occur (Eftaxias et al. 2008). These anomalies signalize the "siege" of the strong asperities (Eftaxias 2010; Eftaxias et al. 2008). Several findings support the view that the fracture of the asperities is accompanied by persistent fBm anomalies which lead the system's evolution processes towards global failure (Eftaxias 2010; Eftaxias et al. 2008, 2009; Papadimitriou et al. 2008). Although the extend of the theory of the kHz radiation has been argued in **Chapter 1 & 3** due to the limited number of signals, the several arguments expressed in the references given in this paragraph, as well as the references within these publications, indicate the asperity model as the most integrated for the time being.

3.7 Conclusions

Summarising the most important findings up to now, the following issues can be supported:

(1) Eleven pre-seismic MHz electromagnetic disturbances of one-month duration prior to nine earthquakes of 2009 with $M_L \geq 5.0$ indicate that the MHz radiation could be of noteworthy pre-seismic precursory value.

(2) All signals exhibited characteristic epochs with fractal organisation in space and time. Continuous epochs were detected in seven one-month signals.

(3) The successive ($r^2 \geq 0.95$) segments exhibited power-law b - values above 1.5. The majority of fractal segments showed anti-persistency ($1.5 < b < 2.0$). Persistent ($2.0 < b < 3.0$) parts were detected. Switching between persistency and anti-persistency was also found. Although several references (e.g the references of Eftaxias, 2010) suggested that the MHz electromagnetic precursors show only anti-persistent behaviour, the systematics of this research supports a different aspect. Significant arguments for the also persistent behaviour of the MHz radiation will be presented in **Chapter 5**.

(4) The Hellenic electromagnetic network showed sensitivity differentiations due to locality. All earthquakes of 2009 with $M_L \geq 5.0$ were pre-signalized through interrupted or continuous fractal segments of long memory. Two earthquakes were detected by two more stations. The remaining stations did not give MHz signals with characteristic pre-earthquake fractal footprints.

(5) Significant pre-signalized earthquakes gave fractal warnings up to one month prior to each event. Some warnings evolved up to some hours prior to the earthquake. The remaining investigated MHz signals gave significant alarms 2-3 weeks and 1 week prior to the event. The latter is the most usual behaviour.

(6) The findings indicated self-organised critical state characteristics of the last stages of the investigated earthquakes.

(7) Geological explanations were proposed in view of the asperity model. Persistent and anti-persistent MHz anomalies were due to micro-cracking of the heterogeneous medium of the earth's crust which may have led the system's

evolution towards global failure.

3.8 Summary

In **Chapter 3** were presented results from the application of wavelet-based power spectral fractal analysis in electromagnetic time-series of the MHz range. The results showed that spectral fractal analysis detected successfully numerous parts of the investigated time-series that follow fBm model. More specifically, it was found that the majority of fractal segments showed fBm anti-persistency behaviour, while persistent parts and switching between persistency and anti- persistency were also detected. The investigated MHz-signals gave alarms from some hours up to one month prior to the seismic event. Fractal footprints indicated self-organised critical state characteristics of the last stages of the investigated earthquakes. Geological explanations were proposed in view of the asperity model.

Chapter 4

Long-term trends in pre-earthquake radon variations through spectral fractal analysis

4.1 Introduction

The following sections present the analysis of the radon in soil recorded signals. Primarily, some sets of experiments were conducted for the examination of the radon profile of the area and for the comparison of active and passive techniques (Nikolopoulos et al., 2012). The effect of the meteorological parameters was investigated and the identification of radon anomalies was searched in terms of statistical analysis focusing on outliers. Finally, power-law wavelet spectral fractal analysis was applied and emerged elements of long-memory were searched in the radon signals.

As already mentioned, to properly select the fractal method, the following issues are significant: (i) A distinguishing feature of the dynamics of a heterogeneous medium close to a critical point is the emergence of memory effects (ii) The power spectral density (PSD) $S(f)$ is the most commonly used technique to provide useful information about the inherent memory of the system (iii) If the recorded time-series is a temporal fractal then a power law spectrum is expected $S(f)=a\cdot f^{-b}$ where f is the frequency of an applied transform. In a $\log S(f)-\log f$ representation the power spectrum is a straight line, with linear spectral slope b . The spectral amplification a quantifies the power of the spectral components following the power

spectral density law .

The spectral fractal method was applied in the same methodological approach as mentioned in **section 3.2.3**, however with the differentiation that the radon signals were divided in segments of 128 samples (windows). Each segment included, hence, radon recordings of 1280 min duration, i.e., of approximately 21h for AG measurements and 30.5h for Barasol measurements. The methodology was applied in three significant radon signals that will be presented, namely the Ileia signal of 2008 (Nikolopoulos et al., 2012; Petraki, Nikolopoulos, Fotopoulos, Panagiotaras, Koulouras, et al. (2013), Lesvos signal of 2008 (Nikolopoulos et al., 2014) & Athens signal of 2014 (Nikolopoulos et al., 2015).

The application of the aforementioned methodology rendered findings which provide significant scientific evidence regarding the pre-seismic behaviour of radon anomalies detected. Two of these were very strong and will be analysed in detail. More specifically, it was found that spectral fractal analysis is the most adequate method for the classification of the segments of the analysed signals, to discriminate the $1/f$ processes in the two most significant (**section 3.2.2**) once, viz., the fBm and fGn processes. As will be shown, the fBm segments exhibit significant pre-earthquake power, where these are identified through the spectral fractal analysis as the successive blue segments with $b>1$. Especially significant are the successive fBm segments if these are associated with importantly distinct changes in the scaling exponent b all of which emerge before or during bursts or anomalies in soil radon. Impressive similar behaviour has been observed between MHz and radon signals before seismic events. More specifically, the similarities were associated to the same pre-earthquake phase of

both MHz and soil radon.

4.2 Results from the analysis & arguments for the precursory value of the Ileia radon signal-2008

4.2.1 Pre-monitoring experiments of the Ileia radon signal-2008

The two sets of the pre-monitoring experiments were conducted during 2007. The first set focused on the active methods and had three targets:

(i) The quantification of the effect of thoron (^{220}Rn) in the time-series collected by AG. This was driven by three facts:

(a) The AG is equally sensitive to radon and thoron if both gases are present (Genitron instruments, 1997).

(b) Soil gas contains both radon and thoron.

(c) The mechanical pumping through Alpha Pump forces the uninterrupted entrance of soil gas into the AG. It is hence evident that the thoron content of the supplied gas biased the recorded AG time-series. This issue was also recognised and investigated in a radon prone area in Greece (Louizi, Nikolopoulos, Koukouliou, & Kehagia, 2003).

(ii) The examination of the radon profile of the measuring site during a seismically quiet period. The study area gives several earthquakes of local magnitudes M_L>3.5 . It is hence difficult to delineate the radon profile of such an area. For this reason, several experiments have been conducted during 2007 for the collection of useful data. From these, ten one week experiments were considered successively, under the restriction, that all earthquakes were of local magnitudes M_L<3.5 during the experiment. The one week duration balanced between measurement accuracy and minimisation of additional deviations due

to the alterations of the atmospheric conditions.

(iii) The comparison of the employed active and passive techniques at the site of measurements, i.e., under non-laboratory conditions. Soil gas was continuously pumped into the AG at a rate of $1\mathrm{L}\cdot min^{-1}$, allowing the escape of the supplied gas to the atmosphere through the output flow adapter. After 2 h, pumping was stopped and the exit of the output flow adapter, was immediately mounted to the input flow adapter through a radon-tight connecting tube. Thereafter, the concentration of the enclosed gas was measured for 6 h. The pumping and measuring intervals balanced between collection of adequate number of measurements, loss through decay and diffusion through the connecting tube. Ten independent experiments were conducted during 2007 to investigate the repetition of the estimations.

Towards (ii) methodology 2 was applied which allowed the net detection of radon in soil. According to methodology 2, the soil gas unit was connected to the AG with an additional 25 m long radon-proof tube. Pursuant to similar work (Mazur, Janik, Loskiewicz, Olko, & Swankon, 1999), this 25 m tube is long enough for the complete disintegration of any thoron present in soil gas. The reproducibility of the results, as well as the correlation of both methodologies, was investigated via the ten successive experiments of (i).

Towards (iii) a methodology similar to the one reported by Mazur et al., 1999 was followed. At first, the probe of the soil gas unit was installed 1 m underground and five pairs of dosimeters were installed around the probe at a depth of 80 cm. The AG monitored, continuously for 5 days, radon in soil according to methodology 2, at the rate of 1 measurement per min. Thereafter, each dosimeter pair was sequentially

uninstalled after an additional 24 h exposure, viz. the first pair after the end of day 1, the second after the end of day 2 and so on. In this manner, five different dosimeter exposures were accomplished. After each exposure, the corresponding paper filters of the SSNTDs were removed and carefully examined for the presence of moisture or dust. Then, the SSNTDs were etched and counted. For the purpose of comparison, the recordings of AG were reorganised in daily exposures, i.e., 24 h, 48 h exposure etc. The measurements were performed during June 2007, i.e., during a non raining season. **Figure 4.1** shows the results of pre-monitoring experiments. In this figure the relative alterations of AP were below 0.5%, of RH below 5%, and of T, below 2%. **Figure 4.1(a)** is indicative to methodology 1. The average radon concentrations ranged between $(29.6 \pm 0.7) \cdot 10^3 \, Bq \cdot m^{-3}$ (95% CI) and $(30.6 \pm 0.8) \cdot 10^3 \, Bq \cdot m^{-3}$ (95% CI), whilst, the corresponding thoron concentrations, between $(70.0 \pm 1.6) \cdot 10^3 \, Bq \cdot m^{-3}$ (95% CI) and $(71.6 \pm 1.5) \cdot 10^3 \, Bq \cdot m^{-3}$ (95% CI). All average concentrations varied slightly. The thoron concentration error bands were higher due to propagation. All relative errors were below 2.5%, despite that non-extensive measurements were collected with methodology 1 (approximately 60 h total for experiment). The average radon concentration for any experiment, did not differ significantly for the one of any other experiment ($p < 0.01$, F-test, one way analysis of variance). These findings indicate, that the contribution of radon and thoron in the soil gas of the measuring site is of a certain level for each isotope. For this reason, the average concentrations of radon and thoron, of all the experiments of methodology 1 were combined and the total average concentration, i.e., the baseline value, was calculated. The total average concentration of radon in soil according to methodology 1 was found equal to $(30.0 \pm 1.0) \cdot 10^3 \, Bq \cdot m^{-3}$ (95% CI) and the corresponding one of thoron, equal to

$(71 \pm 2) \cdot 10^3 \, Bq \cdot m^{-3}$ (95% CI). The uncertainties were calculated according to the equation:

$$\sigma_{\bar{\mu}}^2 = \sum \sigma_{\mu i}^2 + \sigma_{\mu}^2 \tag{4.1}$$

where $\sigma_{\bar{\mu}}$ corresponds to the uncertainty of the total average of the concentration of radon or thoron, $\sigma_{\mu i}$ to the uncertainty of the average concentration of radon or thoron of each experiment of methodology 1, $i = 1...10$ is the consecutive number of each of these experiments and σ_{μ} is the standard error of the total average (Bevington, 1969; Mendenhall, & Sincich, 1995).

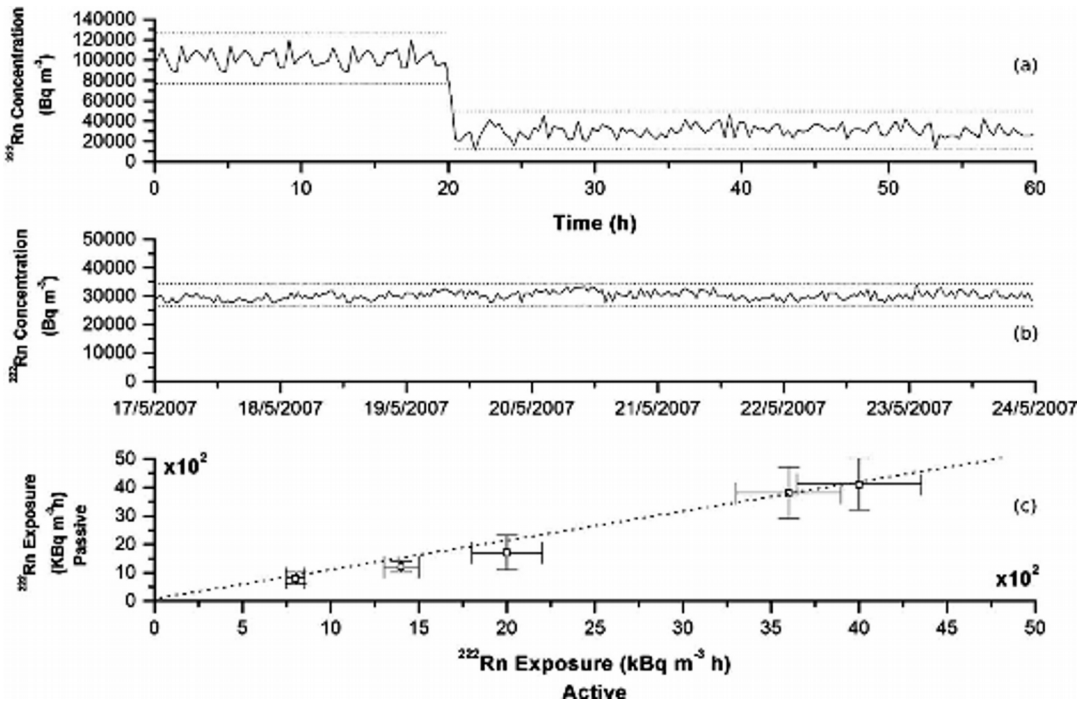

Figure 4.1: (a) A characteristic case of methodology 1 (b) A characteristic case of methodology 2 (c) Comparison results between active and passive techniques.

Figure 4.1(b) is indicative to methodology 2. The average radon concentrations of the ten successive experiments of methodology 1 are between them equal ($p < 0.01$, F-test, one way analysis of variance). The corresponding error bars were narrower in

comparison to those of methodology 1. The total average of radon concentration of methodology 2, was $(30.0 \pm 0.5) \cdot 10^3 Bq \cdot m^{-3}$ (95% CI). The uncertainties were calculated as in methodology 1. Both methodologies produced similar results ($p<0.01$, t-test). It is important to note that the successive experiments of methodology 1 were conducted during sunny and rainy periods, and that not only were the corresponding average radon concentrations between them equal, but also the recorded radon time-series exhibited similar profiles (**Figure 4.1(b)**). Hence, the radon

profile at site of measurements was stable and on average $(30.0 \pm 0.5) \cdot 10^3 Bq \cdot m^{-3}$ during a seismically quiet period. However, methodology 2 was more adequate for telemetry because it is quicker, more accurate and does not necessitate specialised personnel. All the monitoring measurements reported in this paper hereafter, were conducted according to methodology 2. The value $(30.0 \pm 0.5) \cdot 10^3 Bq \cdot m^{-3}$ is considered hence forward, as the radon baseline of the measurement site.

Figure 4.1(c) presents the comparison of active and passive techniques. The exposure errors of the AG were quite lower than those of the passive dosimeters. This finding outlines in another way, the superiority of the active methods in the analysis of signals for seismic surveillance. Even so, the slope of the trend line is almost 1 $((1.0 \pm 0.1), 95\%CI)$ and, hence, both techniques provide similar estimations of the concentration of radon in soil gas. This fact reinforces the use of passive techniques in the study of radon anomalies preceding earthquakes. However, the analysis of the corresponding results should be very cautious, not only due to the wider error bands of the passive techniques (as indicated in **Figure 4.1(c**), but also, due to the significant limitations imposed the integration nature of passive methods, viz. the coarse monitoring that these techniques produce.

For the characteristic case of **Figure 4.1(a)** the average soil gas concentration was

$(101.5\pm1.7)\cdot10^{3}\,Bq\cdot m^{-3}$ (95% CI) and the average radon concentration $(30.9\pm0.8)\cdot10^{3}\,Bq\cdot m^{-3}$ (95% CI). The uncertainty in each average concentration was calculated from the equation (Bevington, 1969) :

$$\sigma_{\mu}^{2}=\frac{1}{\sum\frac{1}{\sigma_{i}^{2}}}+\sigma^{2} \tag{4.2}$$

where σ_{i} was the uncertainty of each measurement of the AG (AG error) (95% CI) and σ the standard error (95% CI). The calculated average thoron concentration was $(70.6\pm1.6)\cdot10^{3}\,Bq\cdot m^{-3}$ (95% CI). For the characteristic case of **Figure 4.1(b)** the average radon concentration for this experiment was $(30.46\pm0.13)\cdot10^{3}\,Bq\cdot m^{-3}$ (95% CI). The uncertainty in the average concentration was calculated as in (a). The dashed lines represent the 95% CI. For the **Figure 4.1(c)** the slope of the linear trend line is (1.0 ± 0.1) (95% CI).

4.2.2 Meteorological influences and statistical analysis of the Ileia radon signal-2008

Figure 4.2 summarises the monitoring results of the AG during 2008. Monitoring started on 15/2/2008, one and a half month after the end of the pre-monitoring experiments. This period was necessary for the concluding operational checks of the instrumentation and the final set-up. Precipitation data are additionally presented. These were obtained from the Hellenic National Meteorological Service and correspond to the two stations closest to the study area (code:16682, distance: 16.2 km, code:16707, distance: 13.2 km). Although these stations are some kilometres away from the measurement site, the provided data are adequate. This is because Ileia is a very flat area which gives similar rainfall between the study area and the stations The

precipitation was measured at 06:00 and 18:00 every day. **Figure 4.2(a)** presents the significant earthquakes (M_L>5.0) that occurred in Greece at the same period.

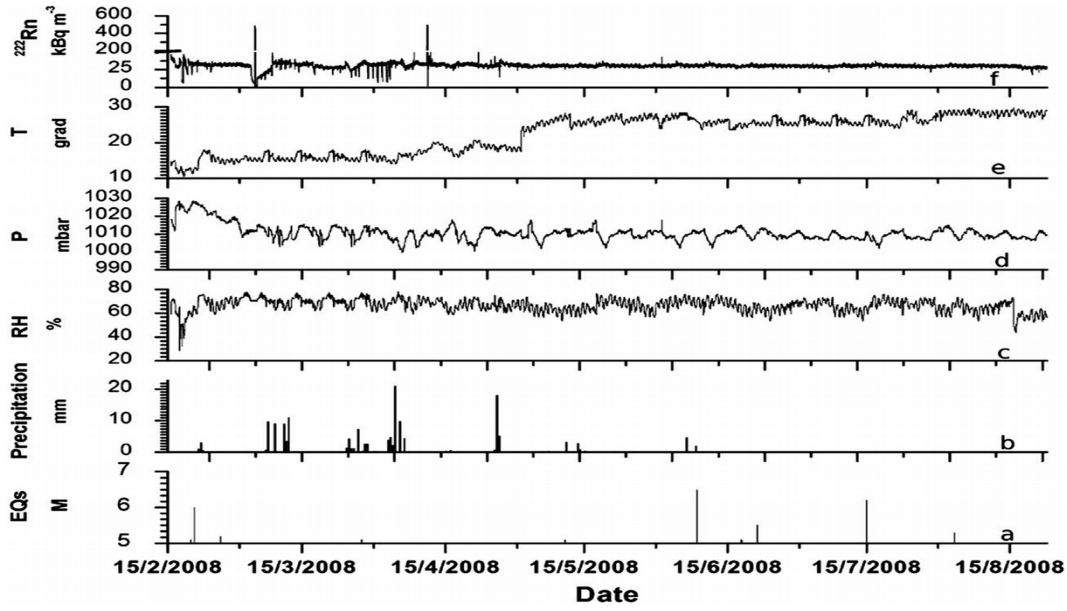

Figure 4.2: During the period of measurements: (a) Significant earthquake activity in Greece (b) Precipitation data. Measurements conducted with the AG: (c) Relative humidity (d) Air pressure (e) Temperature (f) Soil radon.

Numerous radon concentration disturbances were observed. The two very high radon peaks were recorded between 4/3/2008–5/3/2008 and at 11/4/2008. The recorded radon concentrations ranged between $(11\pm6)\,Bq\cdot m^{-3}$ and $(500\pm30)\cdot10^{3}\,Bq\cdot m^{-3}$ (95% CI), whilst the corresponding concentration errors where between $3\,Bq\cdot m^{-3}$ and $13400\,Bq\cdot m^{-3}$. The relative concentration errors ranged between 0.2% and 30%. The errors are not presented in **Figure 4.2(f)** for clarity. The low relative concentration errors (<30%) are indicative of the superiority of the active techniques in radon measurement. **Table 4.1** summarises the descriptive statistics. Highly peaked around the average values were the concentration distributions of both radon and radon error.

Indeed, the kurtosis of both distributions is well above the critical value of 3 (Spiegel, 1975) and the ratio of the standard error over the average value is below 0.2% for both quantities. The majority of the recorded concentrations of the radon in soil were near the average concentration $(30.7 \cdot 10^3 Bq \cdot m^{-3})$ (**Table 4.1**) and the related errors were near the average concentration error $(1.85 \cdot 10^3 Bq \cdot m^{-3})$ (**Table 4.1**). Hence, most of the recorded concentrations were combined with low relative errors. 75% of the measurements were below $32.4 \cdot 10^3 Bq \cdot m^{-3}$ (third quartile, **Table 4.1**) and 25% below $29.4 \cdot 10^3 Bq \cdot m^{-3}$ (first quartile, **Table 4.1**). The mean (S.E.) radon concentration in the soil of the measurement site of the whole data set, was $(30.28 \pm 0.14) \cdot 10^3 Bq \cdot m^{-3}$ (95% CI) (**Table 4.1**). This concentration did not differ significantly (paired t-test, 95% CI) from the total average value of $(30.0 \pm 0.5) \cdot 10^3 Bq \cdot m^{-3}$ of the pre-monitoring experiments. Moreover, if the most stable part of the radon time-series of **Figure 4.2(f)** is considered (i.e., between 1/7/2008 up to the end of the measurement set), then the value of $(29.7 \pm 0.5) \cdot 10^3 Bq \cdot m^{-3}$ is calculated which is statistically equal (paired t-test, 95% CI) to the total average value of the pre-monitoring experiments. These outcomes reinforce in a supplementary way the findings of the pre-monitoring experiments regarding the radon profile of the site of measurements. It is noteworthy that the various radon anomalies act as additional sources of variance, and, hence, increase the standard deviation of the measurements. In this manner, the standard deviation $(11.50 \cdot 10^3 Bq \cdot m^{-3})$ (**Table 4.1**) is approximately 38% of the calculated mean soil radon concentration. The 95% of the recorded radon concentrations were in the $\pm 2\sigma$ range, i.e., between $7.28 \cdot 10^3 Bq \cdot m^{-3}$ and $53.28 \cdot 10^3 Bq \cdot m^{-3}$ (**Table 4.1**). This value range can be used for the identification of radon anomalies in the measuring site, by

employing the commonly accepted $\pm 2\sigma$ approximation. In this consensus, 32 (0.2%) concentration values exceeded the $+2\sigma$ limit and 166 (1%) the -2σ limit. These values may be possibly linked, according to the standard practice, to earthquakes that occurred during the measurement period. However, the $\pm 2\sigma$ range is sensitive, by definition, to the total number of measurements that are used in the σ determination. Accordingly, both the reported $\pm 2\sigma$ range and the number of concentrations that exceed this range, may alter if longer time periods are employed. The aforementioned values can be dramatically altered, if radon anomalies are included in the determination of σ. In this sense, if the detected radon anomalies of **Figure 4.2(f)** are not included in the σ determination, and, only the average baseline value of $(30.0 \pm 0.5) \cdot 10^3 Bq \cdot m^{-3}$ of the pre-monitoring experiments is considered, then the reported $\pm 2\sigma$ range is strongly reduced and becomes comparable to the ± 2S.E range of the whole data set. Under this perspective, as much as 12554 (85%) values can be considered as disturbances possibly related to earthquakes. The whole issue of the role of σ in the identification of the radon precursory abnormalities, has been a subject of interest of other researchers as well (Erees, Aytas, Sac, Yener, & Salk, 2007; Singh, Kumar, Jain, & Chatrath ,1999) nevertheless, only via the investigation of the overall effect of the selection of $\pm\sigma$, $\pm 2\sigma$ or $\pm 3\sigma$ range. However, as mentioned, the interest is stressed on the two detected strong radon disturbances and, in such view, only the high value concentrations have to be taken into consideration. This paper proposes the concept of the outliers in the concentration values of radon in soil as an alternative approach towards identifying radon anomalies on a statistical basis. Under this perspective, and, accounting as outliers (Armitage, & Berry, 1996; Mendenhall, & Sincich, 1995) the concentrations that exceed 1.5 times the interquartile range ($(32.4-29.4) \cdot 10^3 Bq \cdot m^{-3} = 3.0 \cdot 10^3 Bq \cdot m^{-3}$, **Table 4.1**) above or below the

third quartile ($36.8 \cdot 10^3\ Bq \cdot m^{-3}$, **Table 4.1**) , 563 (3.8%) concentrations correspond to outliers of high values and 650 (4.4%) to outliers of low values. The outliers of high values may correspond to earthquakes occurred during the measurement period. The outliers of low values should be taken into account only if these precede or follow the outliers of high values.

Table 4.1: Descriptive statistics of the radon measurements recorded by the AG and the related errors (radon error).

Variable	Mean	S.E.	S.D.	Minimum	Q1
Radon (Bq/m^{-3})	$30.28 \cdot 10^3$	$0.07 \cdot 10^3$	$11.50 \cdot 10^3$	11	$29.4 \cdot 10^3$
Radon error (Bq/m^{-3})	1831	2	353	6	1760

Variable	Median	Q3	Maximum	Skewness	Kurtosis
Radon (Bq/m^{-3})	$30.8 \cdot 10^3$	$32.4 \cdot 10^3$	497664	30	1152
Radon error (Bq/m^{-3})	1848	1928	13376	10	31810

S.E. represents the standard error in the estimation of the mean concentration, and S.D. the standard deviation of the whole measurement set. Q1, Q3 are the first and third quartile, respectively. The significant figures represent the 95% CI.

Figure 4.3 presents the monitoring results of passive techniques. Each point represents the average value calculated from the recordings of independent dosimeters installed near the soil gas unit of AG. The uncertainties were calculated from equation:

$$\sigma_C^2 = \sum \sigma_{Ci}^2 + \sigma^2 \tag{4.3}$$

where σ_C is the uncertainty of the average value, σ_{Ci} is the uncertainty of the recording of each individual dosimeter and σ is the variance of the recordings. The

uncertainty of each dosimeter recording included the Poisson statistical error, the error of the dosimeter efficiency and the estimated error in counting due to overlapping tracks. The presented errors range, relatively, between 7% and 9%. The exposures of the dosimeters employed in **Figure 4.3** were between 7 and 14 days. This period was found adequate to achieve detection of high number of tracks, yet low counting error due to overlapping tracks. A step function connects the individual points of **Figure 4.3**. This regression approach was considered satisfactory as each point represents an integrated average during the period between sequential measurements. A clear disturbance may be observed in **Figure 4.3** between 7/3/2008 and 12/3/2008. This anomaly corresponds to the same period of the first strong radon disturbance of **Figure 4.2(f)** however smoothed. The comparison of **Figure 4.3** and **Figure 4.2(f)** demonstrates in another way the superiority of the active techniques. Nevertheless, the passive techniques give evidence on the alterations of the concentration of radon in soil. This fact has been proven in a manifold manner by several researchers (Cicerone et al., 2009; Gosh et al., 2009) .The signal of the passive techniques is very coarse. The signal roughness should be taken into consideration when analysing detected radon disturbances. On the other hand, the parallel employment of both active and passive methods could be proved particularly useful for soil radon surveillance.

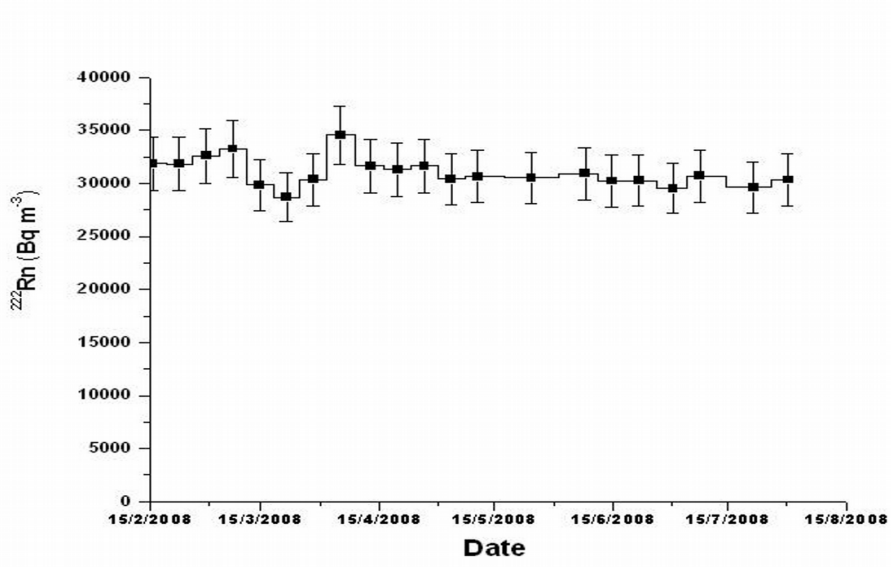

Figure 4.3: Results of monitoring measurements derived with the passive techniques.

Figure 4.4 presents selected parts of **Figure 4.2(f)** in greater detail. The parts (w2) and (w4) correspond to the periods of the two detected strong radon disturbances. The parts (w1) and (w3) match to the periods prior to (w2) and (w4) and illustrate other significant alterations in the recorded radon time-series concentrations. Important is that the first strong radon anomaly (w2) lasted approximatelly 5 days (from 4/3/2008 to 9/3/2008) and the second (w4) approximatelly one day (from 11/4/2008 to 12/4/2008). The first strong radon disturbance (w2) exhibited a progressive decrease down to low values of the order of $3500\,Bq\cdot m^{-3}$, i.e., well below the total average value of $(30.0\pm0.5)\cdot10^{3}\,Bq\cdot m^{-3}$. This progressive decrease lasted approximately one day and was then, immediately, followed by some very intense disturbances. These intense disturbances lasted 1 hour. Thereafter, the radon concentration decreased, even more, down to values of the order of $200\,Bq\cdot m^{-3}$. Then, the radon concentrations increased progressively to the baseline value. The second strong radon anomaly (w4) presented a quite different behaviour. At first, it exhibited an immediate abrupt increase. Then, it was followed by some intense disturbances, a sudden decrease, a progressive increase and some more anomalous disturbances. After 12/4/2008 the concentrations of radon in soil of the measuring site followed the baseline profile.

The two strong radon anomalies are very important for the following reasons:

I. They were detected prior to the very destructive earthquake of 8th June 2008 at the very close distance of 29 km from its epicentre.

II. They are out of the $\pm2\sigma$ range independently from the time-series of **Figure 4.2(f)** that are employed for the σ determination.

III. They are well out of the 30-min time period that is needed by AG in order to respond to sudden sharp radon changes (Genitron, 1997).

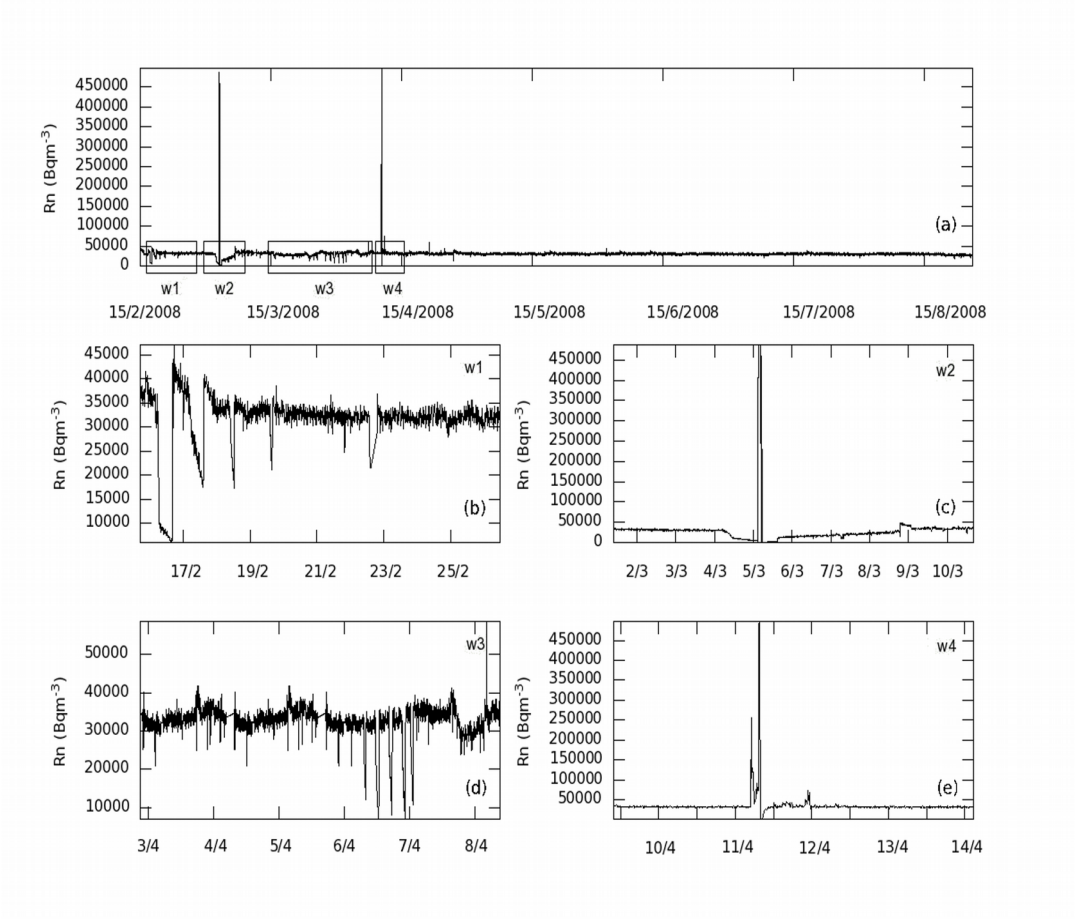

Figure 4.4: Selected parts of **Figure 4.2(f)**. Letter w, followed by a corresponding number, indicates one of the marked windows of the top Figure.

(a) Whole signal (b)Significant disturbances of (w1) (c) The first radon anomaly

(d) Significant disturbances of (w3) (e) The second radon anomaly.

As mentioned, researchers indicate that radon anomalies outside the $\pm 2\sigma$ range are pre-seismic (Cicerone et al., 2009; Gosh et al., 2009; Hauksson, 1981; King, 1978, 1985; Planinic´, Radolic´, & Lazanin, 2001). Under this perspective, the two strong anomalies may be related to seismic activity i.e. the $\pm 2\sigma$ criterion provides only clues about the pre-seismic nature.

This is due to the following facts:

i. The environmental parameters play important role in modulating soil radon emissions and may induce significant anomalies in soil radon concentrations (Nazaroff, & Nero, 1988) .

ii. The study area is a part of graben and is bounded by two major faults. The presence of the two active faults, at short span of distance, creates least-strength zones composed of highly fractured materials. This may provide easy pathway for gas migration towards the surface. If there is rainfall in the catchments region, these faults may act as conduit and, thus, increase the radon concentration for some time.

iii. The crustal fluids may play important role as carriers for radon. In such cases, soil radon spikes may be riven by sudden increases in the efflux of CO_2 or other soil gases (Perez et al., 2007; Toutain, & Baubron, 1999).

iv. The radon concentrations in soil may be significantly affected by the groundwater hydrograph, with an extremely high correlation. Strong annual fluctuation of radon concentrations in shallow groundwater have been reported recently and the variations can reach almost two orders of magnitude (Perez et al., 2007). This variability has been clearly determined to be related to intensification of groundwater circulation, induced by rainfall and aquifer recharge, with maximum values where the hydraulic conductivity is greatest. In this perspective, the hydrological conditions of the area may play a role in the detected radon disturbances.

It is evident that the environmental parameters may affect the radon concentrations in soil, either directly or indirectly. The indirect effects are delivered due to the side effects of the precipitation to the groundwater aquifers and because of the induced changes to the efflux of the radon carrier gases. It is hence important to isolate and evaluate these parameters prior to connecting the anomalies of **Figure 4.2(f)** with the near seismic activity. Towards this, the cross-correlation (Armitage, & Berry, 1996; Devore, 2011; Mendenhall & Sincich, 1995) (**Table 4.2**) was calculated between the radon (**Figure 4.2(f)**) and the environmental time-series (**Figures 4.2(b)-4.2(e)**) because this can reveal the corresponding influences (Choubey, Kumar, & Arora, 2009; Finkelstein, Eppelbaum, & Price, 2006). It can be observed , that there is no influence of the environmental parameters. Accordingly, the application of more complicated models (Pinault, & Baubron, 1996, 1997; Steinitz et al., 2006) would not contribute substantially in altering the validity of the results.

The cross-correlation analysis of the 2008 radon signal did not show dependencies to the measured environmental parameters (Nikolopoulos et al., 2012). Therefore, multivariate statistics were applied to the time-series of **Figure 4.2(f)**. The method of Factor Analysis based on the Principal Component Analysis (see e.g. Armitage, & Berry 1994; Mendenhall, & Sincich, 1995) was employed. The analysis showed that three factors were sufficient to describe the 71% total variance. The communality of radon was 0.703 which is higher than the usually accepted cut-off value of 0.5 (Armitage, & Berry, 1994; Mendenhall, & Sincich, 1995). The communalities of the environmental parameters were also above 0.5 . The first factor was related mainly to the temperature (loading: −0.868) and the air-pressure (loading: 0.795). The second factor was related mainly to the relative humidity (loading: 0.909) and to a

lesser degree to the air-pressure (loading: 0.436). The third factor was related mainly to the radon concentration (loading: -0.791) and the precipitation (loading: -0.871). The latter finding is very important for the time-series of **Figure 4.2(f)**. It indicates that, the decrease in the precipitation was combined with the increase in soil radon concentration. Alternatively, this indicates that the high radon concentrations were combined to the low precipitation values. This latter interpretation is clearly illustrated also in **Figure 4.5b(IV)**. According to this figure, the strong radon anomalies were detected during non-rainy days. According to **Figures 4.5b(I, II, III)**, the high radon values were accompanied with intermediate temperature and air-pressure values and with high values of relative humidity. Due to this behaviour, the first factor, which was related mainly to the temperature and the air pressure, explained only the 28.3% of the total variance and the second, which was related to the relative humidity and the air-pressure, described the 23% of the total variance. The third factor explained the 20% of the total variance. It is important to note relative to the method of Factor Analysis, that the majority of the parameters of **Figure 4.5** followed approximately, Gaussian distributions, viz. radon concentration, corresponding error, air-pressure, relative humidity and precipitation (**Figures 4.5 c,d,f,g,h**). Temperature followed two Gaussian distributions, one for winter - autunm , i.e., February to April and the other one for autumn-summer, i.e., May to August (**Figure 4.5e**).

Table 4.2: Cross-correlation of the recorded time-series of radon in soil with the time-series of the environmental parameters. The cross-correlation coefficient is given together with the probability P of observing the coefficient value by random chance.

	^{222}Rn (Bq m^{-3})	T (^{0}C)	AP (mbar)	RH (%)	H (mm)
^{222}Rn (Bq m^{-3})	1 P=1	*	*	*	*
T (^{0}C)	-0,039 P<0.001	1 P=1	*	*	*
AP (mbar)	-0,014 P=0.024	-0,411 P<0.001	1 P=1	*	*
RH (%)	0,017 P=0.005	-0,210 P<0.001	-0,158 P<0.001	1 *P=1	*
H (mm)	0,029 P=0.210	-0,249 P<0.001	-0,082 P<0.001	0,068 P<0.001	1 P=1

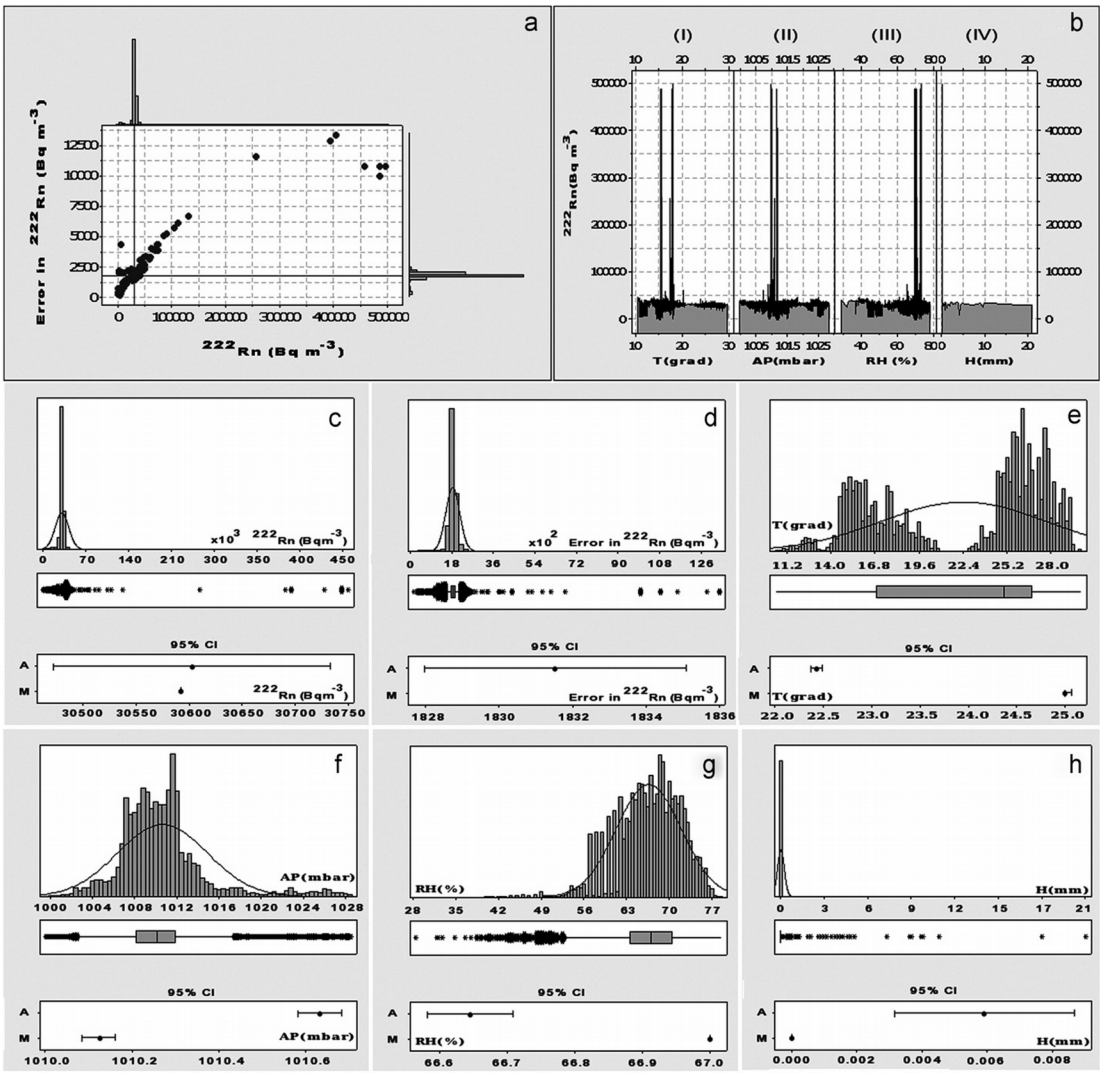

Figure 4.5: Graphical summary of the descriptive statistics of the environmental parameters of **Figure 4.2(f)** (a) Marginal plot of the errors in respect to the corresponding concentrations. The solid lines represent the average values. On the upper and on the left sides, this figure presents additionally the histogram distribution of the errors and the measurements. (b) Radon concentrations with: (I)Temperature, (II)air-pressure, (III)relative humidity, (IV)precipitation. (c)–(h) Histograms, box-plots and 95% confidence intervals for the measured parameters. The curve represents the normal distribution.

All the above findings indicate three important facts. First, radon anomalies presented non-significant cross-correlation with the measured environmental parameters (Nikolopoulos et al., 2012) which means that the variation in the radon time-series of **Figure 4.2(f)** can not be explained by the variation of a single parameter. Secondly, measured environmental parameters can be combined in three factors that affect the radon concentrations in combination and explain almost equivalent parts of the total variance. Thirdly, radon spikes were not combined with extremes in the environmental parameters and cannot be attributed to the variations of these. These findings are also supported by the spectrograms of **Figure 4.6b** and **Figure 4.6c**. Indeed, the high-power frequency range of either spectrograms was observed in other time-periods than the corresponding range of radon. The frequency analysis of the environmental parameters (**Figures 4.6b,c**) reveals a daily (24 h) (constant line at 35-40 dB, **Figures 4.6bi** and **ii**) and a semi-daily (12h) (approximately 25dB constant line, **Figure 4.6bii**) cyclic-variation in the temperature time-series, as well as, daily (24h) (first dashed constant line at 40-45 dB, **Figure 4.6cii**) semi-daily (12h) (second clear constant line at 40-45 dB, **Figure 4.6cii**) and a ter-daily (8h) (dashed constant line at 32 dB, **Figure 4.6cii**) cycle in the atmospheric pressure time-series. No cyclic-variations were observed in the relative humidity or the rainfall time-series. More complicated models (Pinault, & Baubron, 1996, 1997; Steinitz et al., 2006) did not reveal influences not identified already with the applied methods. It should be mentioned however that according to recent scientific data (Francesco, Tommasone, Cuoco, Verrengia, & Tedesco, 2010), radon concentration variations in shallow groundwater can reach almost two orders of magnitude, and this variability is related to intensification of groundwater circulation, induced by rainfall and aquifer recharge, with maximum values where the hydraulic conductivity is greatest. That is, the hydrological conditions of the study area may have

affected the various anomalies of **Figure 4.2(f)**. However, both the environmental analysis and the present analysis, do not support such view.

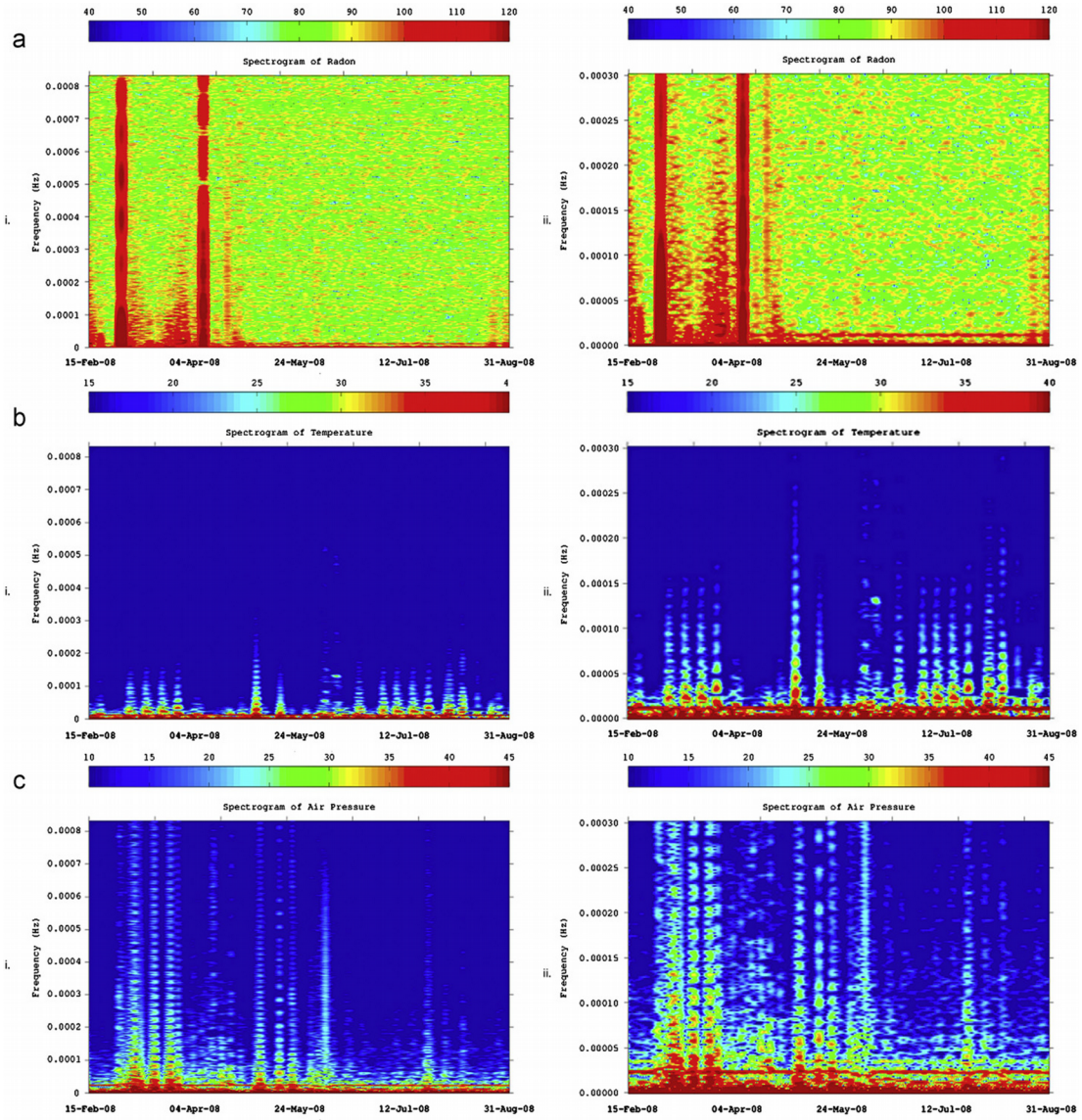

Figure 4.6: Spectrograms of the 2008 radon time-series: (a) Radon ($Bq \cdot m^{-3}$). (b)Temperature (grad) (c) Air-pressure(mbar). Index i refers to the full FFT frequency range and ii to a confined range for resolution enhancement.

4.2.3 Fractal analysis of the Ileia radon signals-2008

It is important to trace pre-seismic information hidden in the radon time-series (**Figure 4.2(f)**). As mentioned already, according to various publications (Devore, 2011; Contoyiannis, Kapiris, & Eftaxias, 2005; Eftaxias et al., 2008, 2009, 2010; Gotoh et al., 2004; Hayakawa et al., 2010; Kapiris et al., 2002, 2003; Smirnova et al., 2004, 2007; Surkov et al., 2002; Yonaiguchi et al., 2007) the fractal methods can reveal such information. Indeed, the earthquake hazard systems evolve naturally to the self-organised critical (SOC) state (Smirnova et al., 2004) a principle of which, is the fractal organisation of the output parameters both in space and in time. Consequently, the fractal methods can investigate the evolutionary processes of the earthquake hazard system regarding the different stages of the catastrophic event preparation (Gotoh et al., 2004; Hayakawa et al., 2010; Smirnova et al., 2004; Surkov et al., 2002). Hence, these methods provide well-accepted criteria for the designation of the pre-seismic texture of the acquired radon signal. As aforementioned, the power spectral density (PSD) $S(f)$ is the best technique to provide useful information about the inherent memory of the system (Eftaxias et al., 2009; Hayakawa et al., 2010; Kapiris et al., 2002, 2003; Surkov et al., 2002; Gotoh et al., 2004; Smirnova et al., 2004; Yonaiguchi et al., 2007) and especially the successive ($r^2 \geq 1$) fractal fBm ($1<b<3$) segments. In the above mentioned consensus, the radon signal of **Figure 4.2(f)** was investigated with power- law fractal methods for tracing pre-seismic fBm behaviour.

The results of the spectral fractal methods for the radon signal of **Figure 4.2(f)** are presented in **Figure 4.7**. **Figure 4.7** reveals the following very important information:

(a) Most of the segments (windows) of the two strong radon anomalies, as well as, many segments of the periods prior to these, exhibited significantly higher values of the b exponent and of the matching squares of the Spearman's correlation coefficient when compared to the corresponding values of the baseline parts. Most importantly, the successive ($r^2 \geqslant 0.95$) b values were between 1.5 and 2.5 and the successive $\log a$ values were between 2 and 3. All these values are in agreement to the corresponding values of the literature (Eftaxias et al., 2009; Hayakawa et al., 2010; Kapiris et al., 2002, 2003; Surkov et al., 2002; Gotoh et al., 2004; Smirnova et al., 2004; Yonaiguchi et al., 2007). It should be emphasised that increase with successive b values of the order of 1.5 was also observed for pre-seismic EM anomalies prior to other destructive earthquakes occurred in Greece for which it was recognised that b values in the range $1<b<2$ characterise the initial phase of pre-ictal (pre-seismic) phase (Eftaxias et al., 2006; Petraki, Nikolopoulos, Fotopoulos, Panagiotaras, Koulouras, et al., 2013; Petraki et al., 2014). It should be additionally stressed that, several parts of the baseline values, also, exhibit power-law behaviour, with b values ranging between 0.9 and 1.0 and with matching squares of the Spearman's correlation coefficient values above 0.75.

(b) The two strong radon disturbances exhibited successive b values of the order of 1.8. The focused analysis of the $b-loga$ values in the areas of the two strong radon disturbances (**Figure 4.4 (w2)** and **Figure 4.4 (w4)**) revealed the following outcomes:

(b1) First anomaly (**Figure 4.4 (w2)**): $b=(1.81\pm0.18)$, $\log a=(2.77\pm0.95)$ (average values within anomaly);

(b2) Second anomaly (**Figure 4.4 (w4)**): $b=(1.78\pm0.31)$,

$\log a = (2.52 \pm 0.14)$ (average values within anomaly).

The above findings indicate the following very significant results:

(I) The time-series of the strong radon anomalies are governed by scaling laws. This is valid as well for other disturbances prior to the strong anomalies. The scaling laws imply that during each anomaly, each value co-varies not only with its most recent value but also with its long-term history in a scale in-variance, fractal manner (Kapiris et al., 2002, 2003).

(II) Both strong radon anomalies may refer to sub-critical or critical phases which represent intermediate stages of a SOC evolution (Smirnova et al., 2004). The power-law behaviour may reflect the fact that the final output of fracture is affected by many processes that act on different time scales (Smirnova et al., 2004).

(III) The increase of the b values of the two strong radon anomalies and of the periods prior to these is consistent with the increase of the fractal dimension (Eftaxias et al., 2009; Hayakawa et al., 2010; Kapiris et al., 2002, 2003; Surkov et al., 2002; Gotoh et al., 2004; Smirnova et al., 2004; Yonaiguchi et al., 2007).

(IV) The average values of both anomalies are also close to 2 which is the critical value for persistent pre-fracture behaviour under a fractional Brownian model (Eftaxias et al., 2009; Hayakawa et al., 2010; Kapiris et al., 2002, 2003; Surkov et al., 2002; Gotoh et al., 2004; Smirnova et al., 2004; Yonaiguchi et al., 2007). Several b values were above this threshold activity ($b value = 2$). For these segments this means that the fluctuations are positively correlated or persistent, which suggests that the underlying dynamics is governed by a positive feedback mechanism. External influences would then tend to lead the

system out of equilibrium (Telesca, & Lasaponara, 2006). The system acquires a self-regulating character and, to a great extent, the property of irreversibility, one of the important components of prediction reliability (Eftaxias et al., 2009, 2010).

The findings of the fractal methods, provide significant scientific evidence regarding the pre-seismic behaviour of the two strong radon anomalies of **Figure 4.2 (f)**. At this point the author would like to emphasise that the predictive value of the 2008-Ileia radon signal is reinforced due to the following facts:

1) The strong radon anomalies were recorded very close to the epicentre of a large earthquake (EQ:34-**Table 3.2**). As aforementioned, this was a fortunate conjecture so the long-memory trends of these signals it is particularly likely to indicate upcoming earthquake.
2) Several successive ($r^2 \geqslant 0.95$) fBm segments (blue segments), i.e., those with $b > 1.5$ appeared during the strong radon anomalies. The threshold of $b = 1.5$ was set as a criterion for the precursory value of the signals in a rather arbitrarily basis. On the contrary, according to Eftaxias et al. (2009), only the persistent ($b > 2$) fBm segments are of precursory value. This is however not a significant differentiation, since the choice of $b > 2$, is also rather arbitrarily. Indeed, the higher b criterion, renders much fewer successive fBm segments, however, well away from the random fGn class. To the opinion of the author, it is the switching between strong anti-persistency ($1.5 < b < 2$) and persistency that is a better potential footprint of a forthcoming earthquake.
3) The criterion 2) is very well adapted to the above-mentioned analysis of the MHz-Electromagnetic signals and reveals similar behaviour between radon and

MHz recordings prior to earthquakes.

4) It is of great significance that the b values of the recorded radon signal from the Ileia station increased sharply.

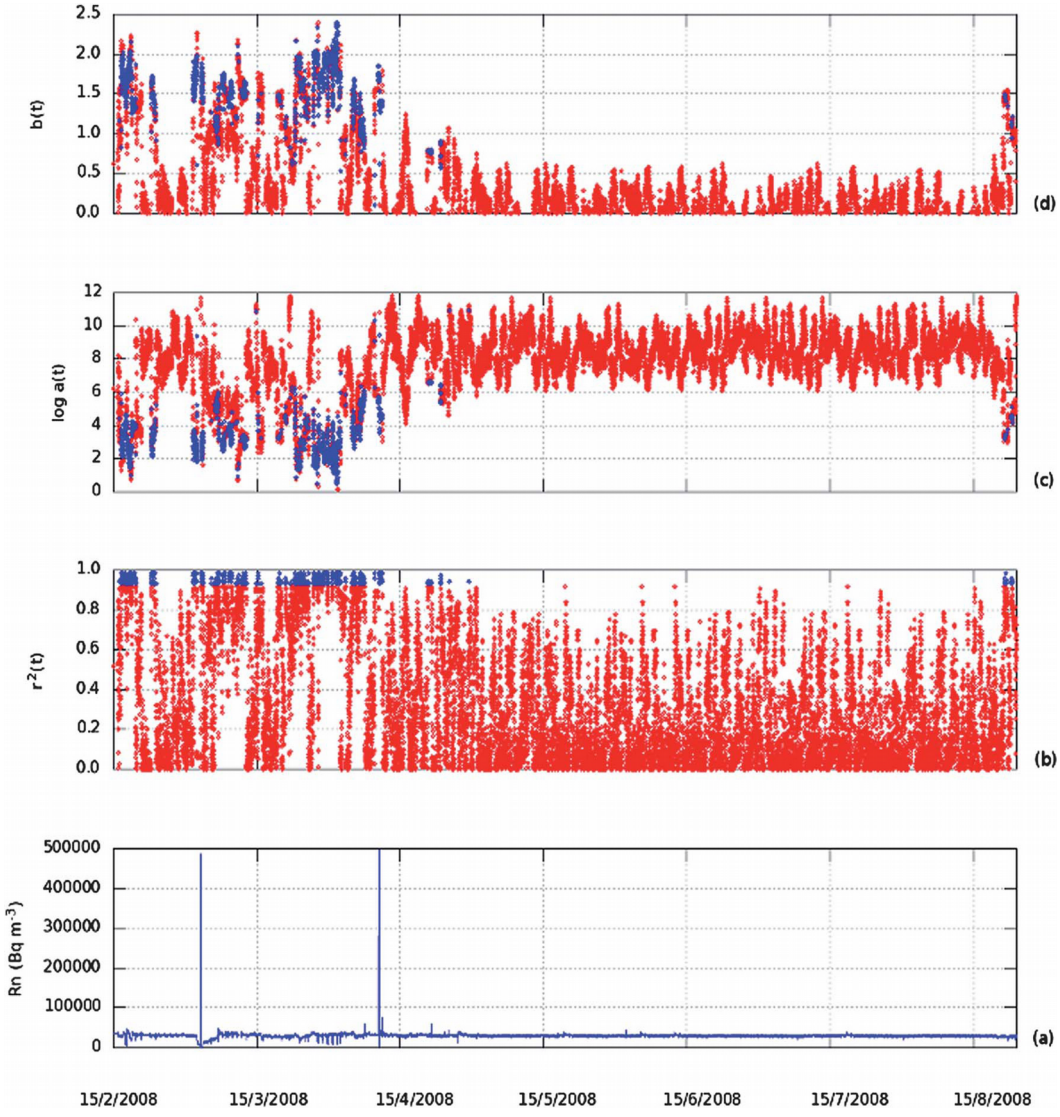

Figure 4.7: Time-evolution of the parameters of the power-law fit: (a) radon time-series (b) square of the correlation coefficient (c) parameter $loga$ (d) parameter b . The blue points correspond to the successive segments, i.e., ($r^2 \geqslant 0.95$). The red points correspond to the remaining segments.

This view is also supported by the scalogram of the DWT of the 2008 radon signal (**Figure 4.8a**). The time-evolution of the power-law beta-values is also presented parallel to the scalogram (**Figure 4.8b**). It may be observed that the high power-law beta-parts, i.e., the parts exhibiting b values above 1.5 (e.g. Eftaxias, 2010; Eftaxias et al., 2010), present more power at the low than at the high frequencies. If one adapts the aspect of Eftaxias (2010) and Eftaxias et al. (2009), this low frequency enhancement reveals, physically, the predominance of the larger fracture events and is considered as a footprint of the preparation of earthquakes.

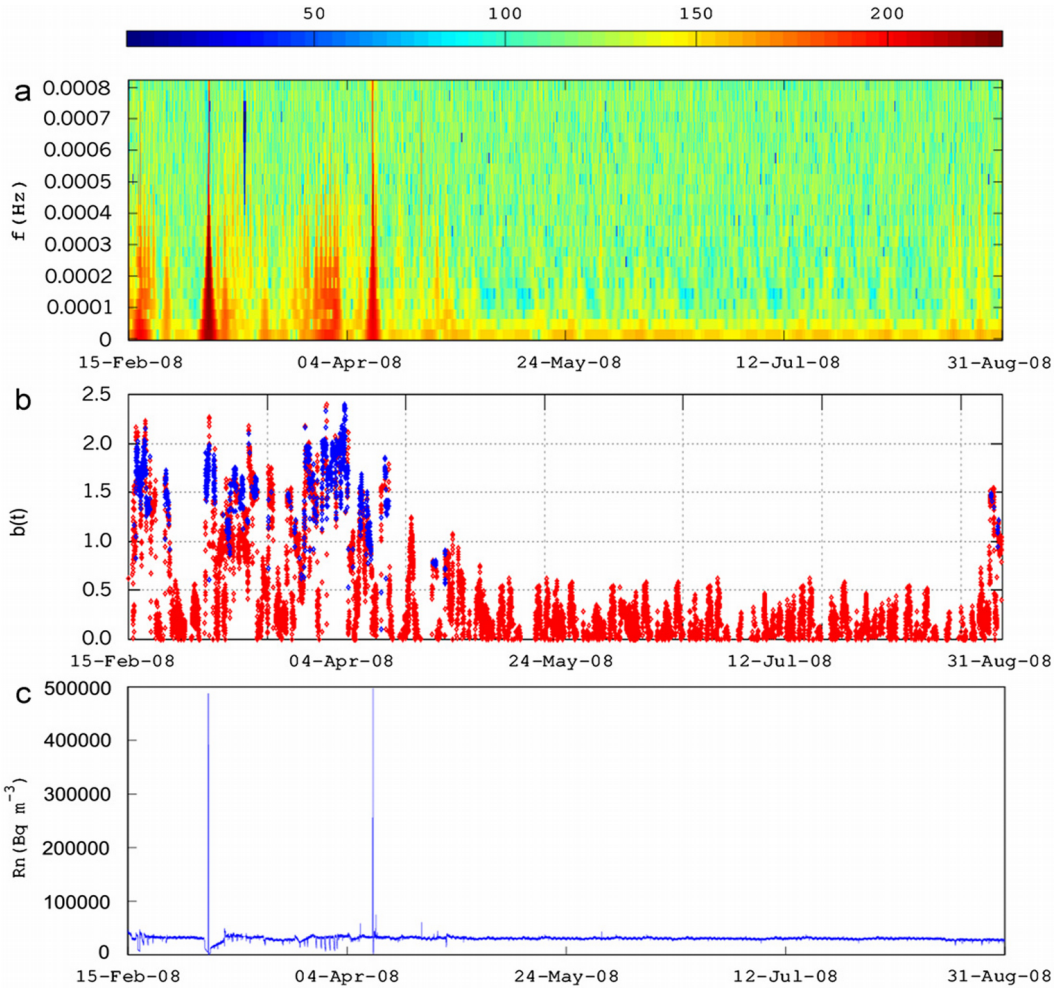

Figure 4.8: Fractal evolution of the 2008 radon signal (a) Scalogram of the DWT of (c).(b) Evolution of the spectral exponent b of (c) . The blue points represent successive parts. (c) Radon ($Bq \cdot m^{-3}$) .

On the contrary, the 2010 and 2011 radon signals (**Figure 4.9 b,c**) did not present such footprint, since both scalograms (**Figures 4.10a-iv**, **4.10b-iv**) did not show favourable high-power parts (in the view of above references of Eftaxias et al.). This perspective is also supported by the time-evolution of the power-law values of the radon signals of 2010 and 2011 (**Figures 4.10a-i**, **4.10b-i**). Both signals presented similar behaviour to the corresponding stable part of the 2008 radon signal (Nikolopoulos et al., 2012). In particular, all power-law beta-values were of the order of 1 and presented Spearman's r-square values of the order of 0.8, i.e., they were not successive. Comparable were also the values of $loga$. It should be noted however that due to the different sampling rates of the 2010 and 2011 signals, the segment size of the 2011 signal was set to 512 values, instead of 128. This was because this value corresponds to the closest power-of-two value which gives analogous time-lags as those of the 2010 and 2008 signals. It is also important to place emphasis on the fact that the simultaneous appearance of the high radon anomalies, high power-law b - values and high-power spectral amplitudes, manifests that the wavelet power spectrum can be used as an alternative method for the recognition and visualisation of candidate precursory anomalies in a radon signal. The spectral Fourier analysis (**Figure 4.6a**) fails to identify such anomalies, since it just recognises the amplitude extremes as high Fourier spectral power parts.

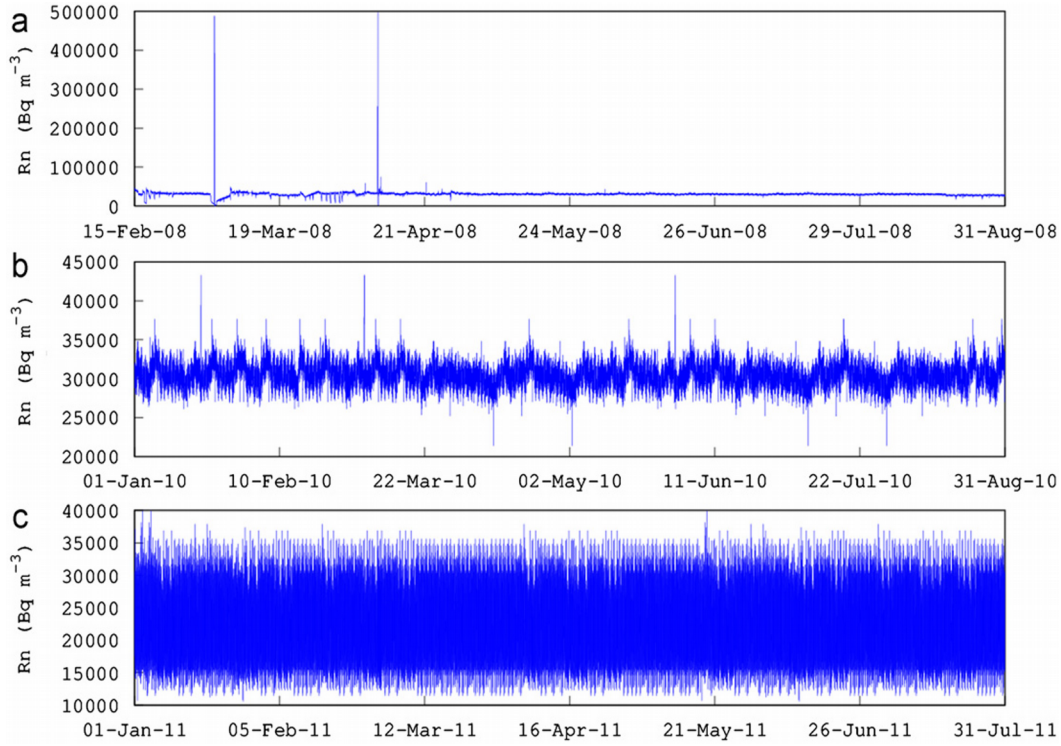

Figure 4.9: Parts of radon time-series measured in Ileia during: (a) 2008, (b) 2010 and (c) 2011.

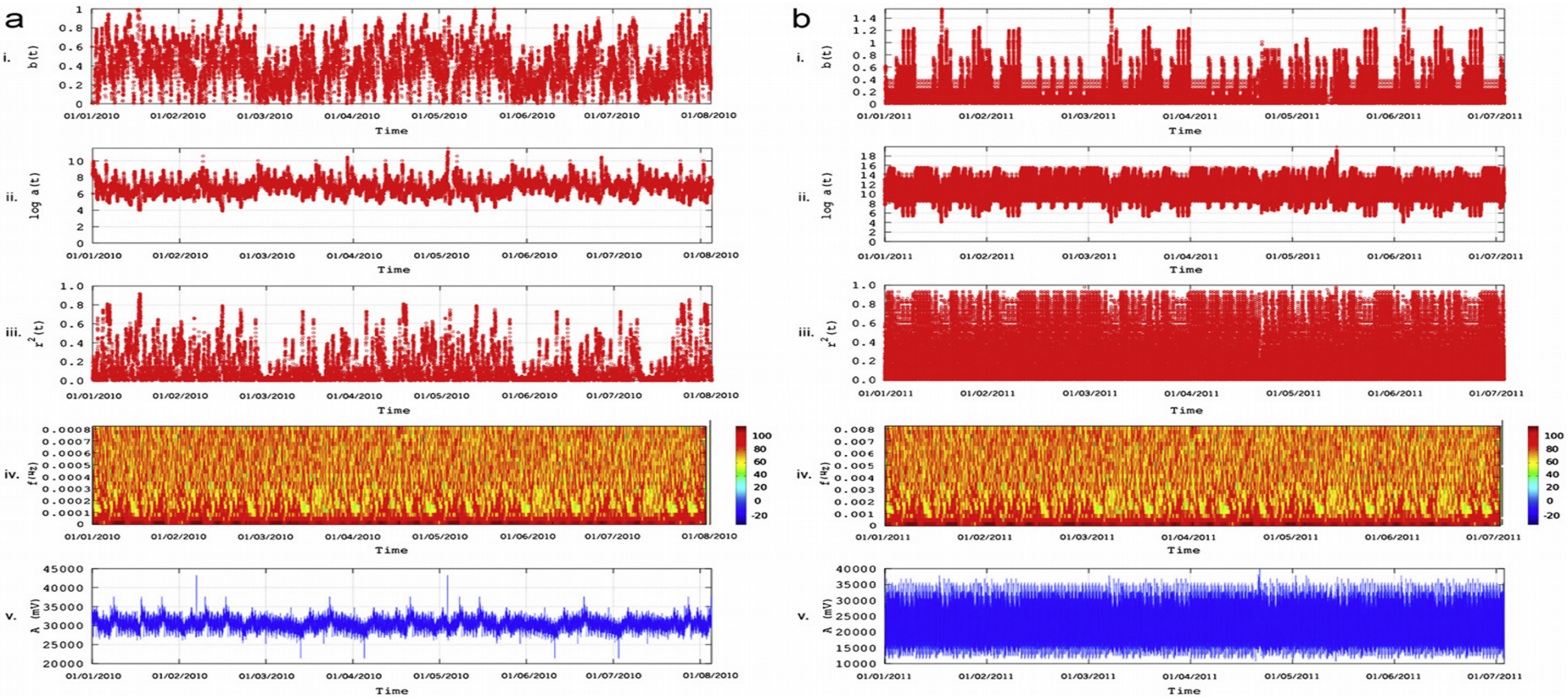

Figure 4.10: Fractal evolution of the 2010 and 2011 radon signals. (a) 2010 signal,(b)2011 signal. Indexes i–iv correspond to the time evolution of the spectral exponent b, the spectral exponent $loga$, the square of the Spearman's correlation coefficient and the scalogram of the DWT, respectively.

Reports of such radon signals prior to very destructive earthquakes are rare in the related literature (Richon et al., 2007; Walia et al., 2009; Perez et al., 2007). The radon signal of the first radon anomaly is of great importance and may has linkage to the strong earthquake of the 8th June of 2008 (EQ:34, **Table 3.2**), for the following reasons: (i) The distance between the site of the detection of this anomaly and the epicentre of the earthquake of the 8th June of 2008 (EQ:34, **Table 3.2**) was only 29 km (ii) The application of fractal methods revealed a pre-seismic behaviour of this anomaly (iii) It lasted approximately 5 days and exhibited a very peculiar time evolution (iv) It involved with very intense radon spikes of 1 hour duration and this anomalous intense behaviour was accompanied by additional long-lasting abnormalities of very low levels (v) The whole time-evolution of the signal was not explained by the simultaneous disturbances of the environmental parameters (vi) A simultaneous anomaly was also detected by the passive methods. If this anomaly is linked to the earthquake of the 8th June of 2008 (EQ:34, **Table 3.2**), then the precursory time window would be approximately 3 months. Such an interpretation is in accordance to the precursory times reported in the literature (please see e.g. reviews (Cicerone et al., 2009; Ghosh et al., 2009). Nevertheless, as already mentioned, even for the strong earthquakes, there exist no universal model to serve as a signature of a specific forthcoming seismic event (Eftaxias, 2010; Eftaxias et al., 2008, 2009, 2010). For this reason further analysis is needed so as to highlight additional evidence on the link of the first anomaly and the earthquake of the 8th June of 2008. On the other hand, similar may be the interpretations for the second strong radon anomaly. In this consensus, the other disturbances shown in **Figure 4.4** (w3 and w4) may be associated to other earthquakes of **Figure 4.2(f)** or even to earthquakes of smaller magnitudes. As aforementioned, It should be emphasised that

during the periods presented in F**igure 4.4(b)** (w1) and **Figure 4.4(d)** (w3) very intense seismic activity was detected in the near area, resulting after the strong earthquakes of Methoni occurred approximately 115 km S of the radon station.

4.2.4 Application of the concept of outliers

Figure 4.11 presents the outcomes of the application of the concept of outliers in the soil radon concentrations of **Figure 4.2(f)**. The top figure presents the whole outlier data set, whilst the other two are two parts of this set, at different starting points. The up-triangles indicate high radon outliers, whilst the down-triangles indicate the corresponding low ones. As aforementioned, 563 (3.8%) outliers correspond to high concentrations and 650 (4.4%) to low ones. For comparison purposes, all sub -figures of **Figure 4.11** present on the right side the significant earthquakes (M_L>6.0) that occurred during the measuring period of **Figure 4.2(f)**. As can be observed, two very strong earthquakes followed the two detected strong radon disturbances. On the top figure, these earthquakes are presented as a function of the time scale of the outlier set. It seems as there exist a corresponding temporal link of these two strong earthquakes with the two strong radon disturbances. According to the corresponding references reported in the review of Ghosh et al., 2009 the two detected strong radon disturbances fall within the temporal precursory window, that may link a radon anomaly and an earthquake. However, this fact may be misleading if the spatial effectiveness of the detection of an earthquake is not taken into account. Towards this direction and for comparison purposes, the middle and down sub-figures, additionally to the radon outliers, present the two very strong earthquakes as a function of the distance of the earthquake (EQ distance, please see upper axes of both sub-figures). For better comparison, the middle sub-figure starts at the detection time of the first radon

anomaly, and the down sub-figure, at the detection time of the second radon anomaly. Additionally, both sub-figures present the relation (earthquake effectiveness) :

$$e = 10^{(1.3 \cdot M - 8.19)} \cdot R^{-3} \tag{4.4}$$

that expresses the potential to detect a seismic event at a measurement site (Dobrovolsky, Zubkov, & Miachkin, 1979; Planinic´ et al., 2001) as a function of the distance from the radon station (please see upper axes of both sub-figures). Both sub-figures clearly indicate that both strong radon disturbances have a potentiality to be linked only to the 8th June 2008 earthquake (EQ:34, **Table 3.2**), since the parameter e has significant values ($> 10^{-4}$) only for this earthquake. This finding clearly suggests that from the two strong earthquakes presented in the top sub-figure, only the first should be taken into account.

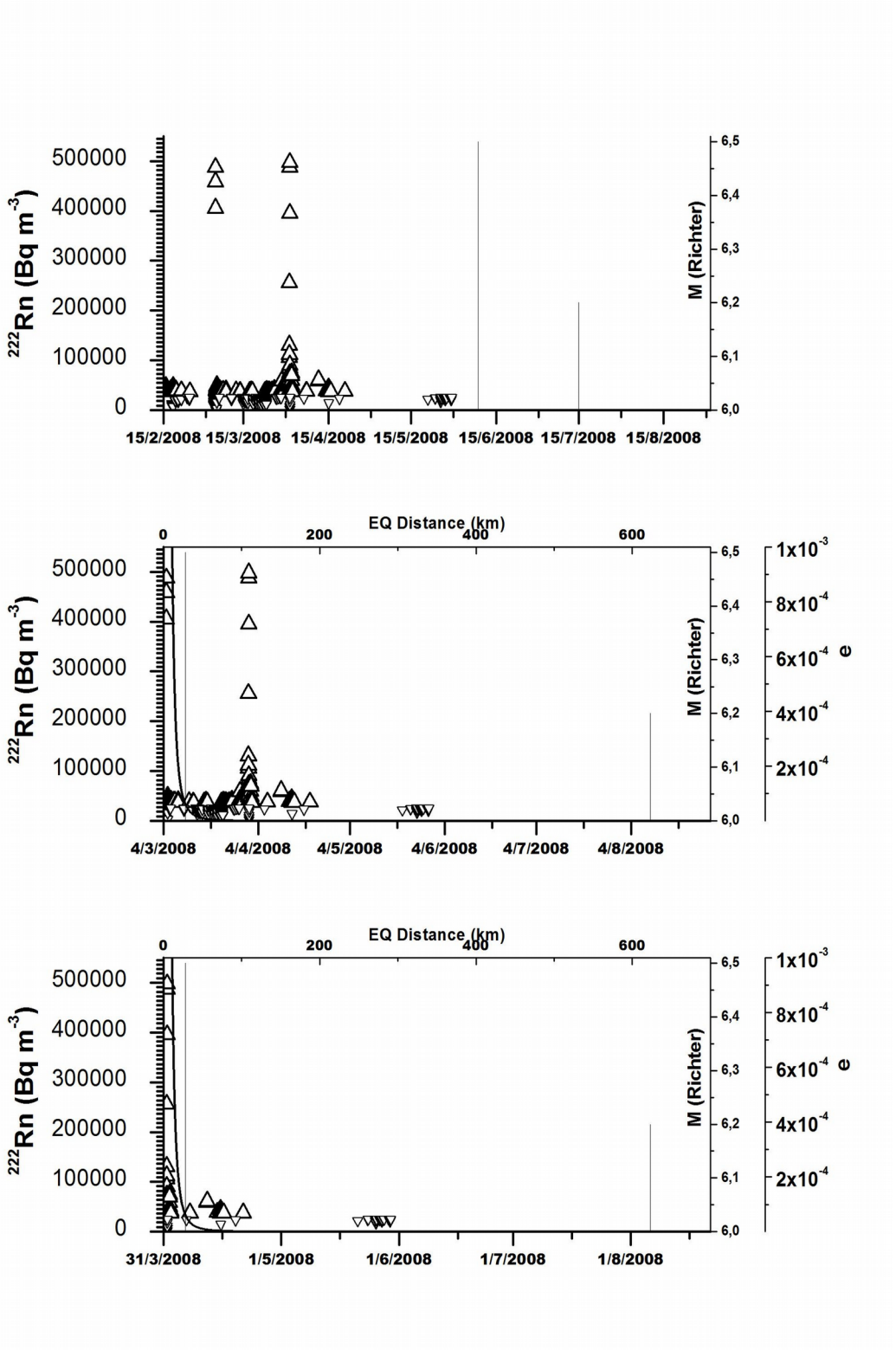

Figure 4.11: Radon outliers together with strong seismic activity of near sources. Middle and bottom sub-Figures also present the effectiveness of earthquake detection.

4.2.5 Physical mechanisms for the interpretation of the emanations of soil radon

Various physical mechanisms have been reported to relate the sub-surface physical changes with the variation in radon emanations. Among the various theoretical models, the well-accepted dilatancy diffusion model (Scholz, Sykes, & Agarwal, 1973) relates the anomalous alterations in radon concentration with the growth rate of mechanical crack in the volume of dilatancy. According to this model, a porous cracked saturated rock constitutes the initial medium. With the increase of the tectonic stresses the cracks extend and disengage near the pores, leading to opening of favourably oriented cracks. This results in a decrease of pore pressure in the total preparation zone, which consequently, results to the flow of water into the zone from the surrounding medium. The return of the pore pressure together with the increase of cracks may yield to abrupt changes of radon emanation. Another accepted theoretical model is the crack-avalance model (Lay, Williams, & Garnero, 1998). According to this model, a cracked focal rock zone is formed by the increasing tectonic stresses. The shape and volume of this focal zone change slowly with time. According to the theory of stress corrosion, the anomalous behaviour of radon concentration may be associated with this slow crack growth, which is controlled by the stress corrosion in the rock matrix saturated by groundwater (Anderson, & Grew, 1977). Another published model is based on the concept of asperities (Eftaxias et al., 2008). According to this model, the focal area consists of a backbone of strong and large asperities that sustain the system. A strongly heterogeneous medium surrounds the family of strong asperities. The fracture of the heterogeneous system in the focal area obstructs the backbone of asperities. At this stage, critical MHz electromagnetic anomalies occur (Eftaxias et al., 2008). Yet,

thereafter, the “siege” of the strong asperities begins. The earthquakes will occur if and when the local stress exceeds the fracture stress of asperities. According to numerous related publications (Eftaxias et al., 2009; Contoyiannis, et al., 2005; Papadimitriou, Kalimeri, & Eftaxias, 2008), this “siege” is combined with the abrupt emergence of KHz and MHz electromagnetic emissions, which indicate the fracture of asperities and, thus, signalise the unavoidable evolution of the process towards the global failure. Adopting the concepts of the aforementioned “asperity” model for the case of radon, the anomalous strong radon emissions reported in this paper prior to the 8th June 2008 earthquake (EQ:34, **Table 3.2**), could be attributed to the first stage of the model, in which the fracture of the strongly heterogeneous medium obstructs the asperities backbone. The findings of this study support such an interpretation because: (a) The two strong radon disturbances exhibited critical behaviour consistent with a SOC phase (b) The b values of both anomalies were of the order of 1.8 and indicated anti-persistent behaviour. More importantly, the average b values were near the critical value of 2, for a persistent behaviour under the fractional Brownian motion model. Moreover, there existed persistent b values, i.e., above 2 (c) Two strong radon anomalies were detected, however, with a possible link only to the 8th June 2008 earthquake (EQ:34, **Table 3.2**). Likewise, the pre-seismic MHz electromagnetic signals are attributed, according to the “asperity” model, to the fracture of the heterogeneous medium that obstructs the backbone of asperities for comparable reasons (Contoyiannis, et al., 2005). According to this publication the pre-seismic MHz electromagnetic radiation exhibits the following characteristics: (i) Emergence of memory effects (ii) Increase of the number of intervals with fractal characteristics with time (iii) Increase of the spatial correlation in the electromagnetic time-series (iv) Decrease with time of the

anti-persistence behaviour of the signal (v) Detection of numerous MHz anomalies which were not accompanied by a significant earthquake. Nevertheless further approaches based on the concepts of complexity and criticality are needed as a future expansion of this work. These approaches will follow in the future, as an extension to the related analysis and as an attempt to investigate the persistent or anti-persistent behaviour of the radon emissions. Supplementary analysis based on the concepts of wavelets and Short-Fourier Transform will provide additional information. It should be emphasised however that in a recent publication for radon (Perez et al., 2007), a single reported $b-value$ of 1.56 was characterised as persistent. According to this publication, this $b-value$ was derived from an FFT-PSD according to obtained radon time-series from the TFE02 geochemical station, Tenerife. The opinion of the authors is, according to the scientific evidence already presented, that $b-values$ below 2 are anti-persistent under a fractional Brownian model.

4.2.6 Relation between radon disturbances and the strain change

According to the arguments already discussed, there exists no universal signature for the arrival of an earthquake. However, these arguments may, and, can not reverse the validity of approximations followed in this study and the related radon literature (Cicerone et al., 2009; Ghosh et al., 2009). Although, according to the aforementioned fact, no definite rule can be practically applied to any earthquake related signal, the proper statistical analysis of critical value may be useful to isolate a precursory signal (Choubey et al., 2009). Following the ideas discussed in this study, if a certain radon anomaly is corresponded to a certain earthquake event, then the ratio of the peak anomaly should be proportional to the magnitude of the

impeding earthquake (Choubey et al., 2009). This implies that $\frac{\Delta C}{C} \propto M$, where ΔC is the change of the soil radon activity concentration from the baseline value, C is the peak value of the anomaly and M is the earthquake magnitude. According to the aforementioned publication (Choubey et al., 2009), this relation is based on the empirical work of Dobrovolsky et. al., (1979) in which it was supposed that the radon concentration is proportional to the strain change when this change is rapid. The relation is reinforced also by other studies (King, 1978; Talwani, Moore, & Chiang, 1980; Virk, 1996; Ramola, Singh, Sandhu, Singh, & Virk, 1990). Even in such an approximation, the effect of the various parameters that affect the radon concentration, i.e. air pressure, relative humidity, temperature, rainfall, should be taken into consideration. According to Choubey et al., 2009, the effect of the various parameters can be assessed by evaluating a relation through the cross-correlation, which may be used to convert the multi-parametric variance of the radon concentration into a single parameter. This publication proposed the parameter β that follows two relations; first that $\frac{\Delta C}{C} \propto \beta$ and that $\beta = \sum A_j$ where A_j represents the correlation coefficient of radon in respect to a certain parameter. Combining the above equations in one then the radon peak value can be expressed as:

$$C = k \cdot \beta \cdot M \cdot \Delta C \tag{4.5}$$

where k is a proportionality constant which can be experimentally determined.

Following the discussion of **Figure 4.5** and **Figure 4.6**, the two detected strong radon disturbances may be corresponded to the nearest earthquake of the 8th June of 2008 of $M=6.5$ (EQ:34, **Table 3.2**). Under this assumption, if accepting $\Delta C=2\sigma=22400\,Bq\cdot m^{-3}$ and $\beta=2.951$ (as calculated from **Table 4.2**) and employing the peak value of the first radon anomaly ($C=487424\,Bq\cdot m^{-3}$), the proportionality constant of the above equation is calculated equal to $k=1.134$. On the other hand, if the peak value of the second radon anomaly is employed ($C=497664\,Bq\cdot m^{-3}$, maximum of **Table 4.1**), then $k=1.158$. As discussed in the aforementioned publication (Choubey et al., 2009) both values are very close to unity. This fact implies that both anomalies are in agreement to the prerequisites of Dobrovolsky et al., 1979 which indicates that the radon concentration is proportional to the strain change.

Independent to the likely interpretation, however, one issue still remains; an earthquake is a sudden mechanical failure in the Earth's crust, which has heterogeneous structures. It is reasonable to expect that its preparatory process has various facets which may be observed before the final catastrophe through seismic, geochemical, hydrological and EM changes (Eftaxias et al., 2010; Uyeda, 2000). Definitely, the mechanical processes of earthquake preparation are always accompanied by deformations, afterwards complex short or long-term precursory phenomena may appear.

4.2.7 Conclusions from the analysis of Ileia radon signals-2008

The analysis so far focused on the investigation of the environmental monitoring of

radon in soil as trace gas in the search of earthquake precursors. As a first stage, the study implemented necessary preparation experiments that included the following:

a. A pre-monitoring phase which included detailed experiments prior to monitoring.
b. Focused experiments on the quality of passive measurements which were performed with already calibrated radon dosimeters.

The pre-monitoring phase validated the employed methods and stabilised the employed techniques. After the report of the outcomes of this pre-monitoring phase, the study focused on a significant radon signal that was actively collected during a very seismically active period in Greece during 2008. This period was combined with the occurrence of two very destructive earthquakes, one just before the beginning of measurements and the other during measurements. Prior to the second earthquake:

i. Two very strong radon disturbances were detected approximately two and three months before the earthquake. The study presented the signals in detail and discussed issues regarding the possible precursory quality of these signals.
ii. One strong disturbance was detected with passive techniques approximately three months before the earthquake.

The analysis presented in detail the inferiority of the passive techniques, both at the pre-monitoring and at the measuring phase. The issues of the use of passive techniques in radon precursory signals were also discussed .

The profile radon time-series for an area in SW Greece was presented, showing very peculiar disorders during 2008. The data verified the previous radon background of

the measurement site which was derived during a pre-monitoring phase before 2008. This corresponded also to the stable part of the 2008 radon signal (Nikolopoulos et al., 2012).

Fourier Analysis, multivariate statistics and cross-correlation analysis were used for the investigation of the role of the environmental parameters on the 2008 radon signal. The results verified, in a supplementary and more integrated way, previous findings and indicated that the 2008 radon disturbances could not be of environmental origin.

The whole signal and both the strong radon anomalies were investigated with fractal methods. These methods employed the application of power spectrum analysis based on wavelets for tracing a power-law behaviour of the collected signal. The analysis indicated that both strong radon anomalies presented a clear power-law behaviour with significantly increased beta values. Numerous successive ($r^2 \geqslant 0.95$) fBm ($1<b<3$) segments were found, where the increased b values were mainly above 1.5 and were associated with a signal anomaly. This is of great significance. To the author the parallel identification of an anomaly (above $\pm 2\sigma$, see **Chapter 2**), with switching of strong anti-persistency ($1.5<b<2$) and persistency ($2<b<3$) and a lot of values with b away from fGn class, makes the signal of enhanced precursory value.

The findings are indicative of a self-organised-critical (SOC) pre-earthquake state. The first anomaly exhibited anti-persistent average value $b=(1.81\pm 0.18)$. Similarly, the second anomaly presented the anti-persistent average value of

$b=(1.78\pm0.31)$. Such values are indicative of the approach of earthquakes. Analysis indicative of self-similarity and self-organisation was applied to the 2008, 2010 and 2011 radon time-series. The results verified previous findings regarding the anti-persistent/persistent behaviour of the 2008 radon disorders. The methods indicated absence of self-organisation in the radon background time-series of 2010 and 2011.

As aforementioned, the MHz electromagnetic signals that were derived concurrently to the 2008 radon signal were analysed with the methods applied to radon. The results indicated analogous behaviour between radon and MHz EM pre-earthquake time-series. Both pre-earthquake time-series were found to be consistent with a fBm-model, while the background values followed the fGn-model. Switching of persistency and anti-persistency is also addressed in the MHz electromagnetic radiation. Note, that according to other investigators (Eftaxias, 2010; Eftaxias et al., 2009; Kapiris et al. 2002, 2003), the MHz radiation exhibits only anti-persistency, however on the basis of few MHz signals compared to those reported in this research.

The research so far discussed, as well, issues regarding the standard application of $\pm2\sigma$ technique in the identification of radon disturbances and proposed the use of outliers as an alternative approach to the above technique. The study presented the outcomes of the application of this latter technique in identifying the linkage of the strong radon anomalies to the strong earthquakes of the near area. According to the related discussion, the two strong radon disturbances could be possibly related only to the 8/6/2008 earthquake (EQ:34, **Table 3.2**). The radon emanation was proposed to be combined to a strongly heterogeneous medium that surrounds a family of

strong asperities according to a very recent model. Arguments are discussed on this issue. Finally, the study applied a recent technique which indicated that both strong radon disturbances were proportional to the strain change.

4.3 Results from the analysis of the Lesvos radon signal-2008

This study addresses issues of self-affinity and long-memory in variations of radon in soil recorded in Lesvos Island (Greece) through power-law wavelet spectral fractal analysis. As will be shown later, long-lasting anti-persistency was identified during a period of anomalous radon variations following fractional Brownian modelling. Remaining variations did not exhibit analogous behaviour and followed fractional Gaussian modelling. It will be shown that anti-persistent power-law-beta-values between 1.5-2.0 were detected during anomalies. Persistent values were also found. Persistency/anti-persistency switching was also observed,. As emphasised already, this is consistent with long-memory dynamics. Due to this, the results will be compared to those of the Ileia signal which were derived under analogous methodology in Greece.

4.3.1 Fractal analysis of the Lesvos radon signal-2008

Figure 3.61 presents the radon signal recorded by the station of Lesvos. The signal was short. However, it was derived prior to significant earthquakes of the Hellenic Trench and the Aegean graben system. As illustrated in **Figure 3.5**, earthquake 35 (19/3/2008, M_L=5.0) occurred in the near area, approximately 45 days after the end of a significantly anomalous part of the signal. Although, as aforementioned, there is no definite rule to link any kind of pre-earthquake anomaly to a specific forthcoming seismic event (Eftaxias, 2010; Eftaxias et al., 2008), the texture of the anomaly in combination with the magnitude , (M_L) and the vicinity of earthquake 35, could

provide some indication for investigating it as pre-earthquake precursor. This was reinforced by the fact that the environmental parameters recorded in Lesvos by AG, viz., atmospheric pressure, relative humidity and temperature, did not present significant alterations. Precipitation data of the area did not present peculiar changes prior to the recorded anomaly, as well.

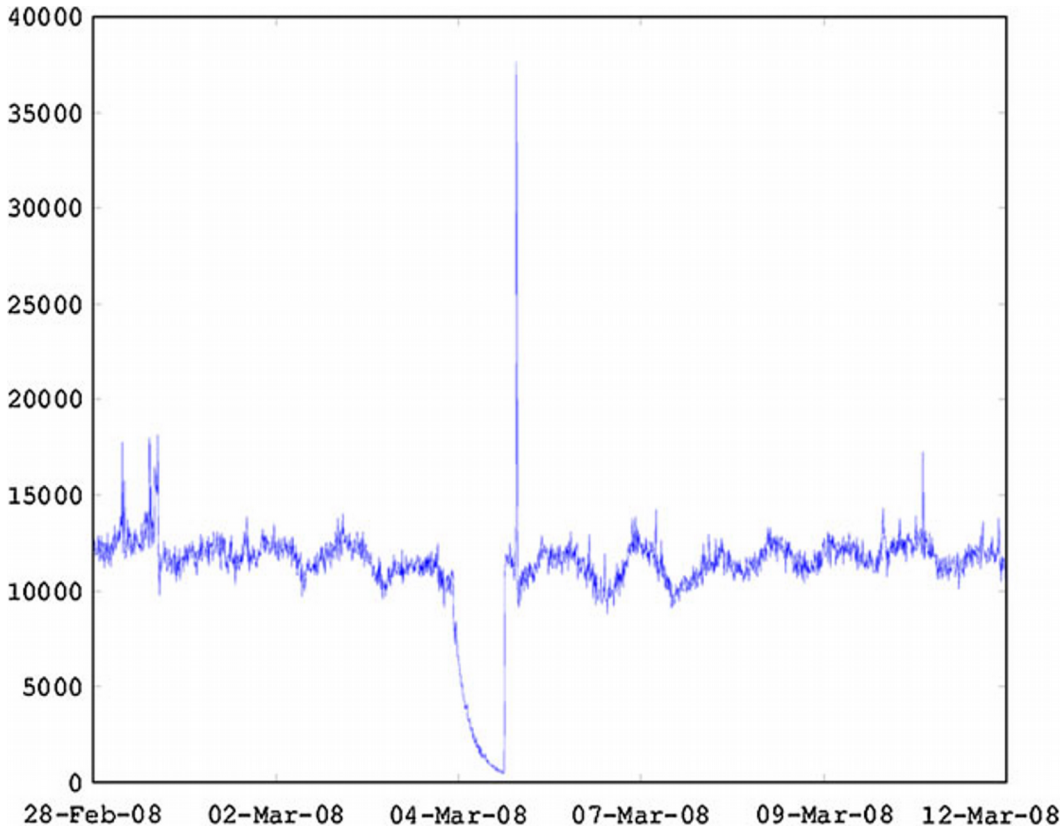

Figure 4.12: Variations of radon in soil recorded in Lesvos between 28-February-2008 and 12-March-2008. The vertical axis is radon concentration in $Bq \cdot m^{-3}$

The texture of this anomalous radon part that was recorded between 4 and 5 of March 2008, exhibited visual similarities with the first extended radon anomaly of the pre-earthquake radon signal of Ileia (SW Greece), derived during 2008 in Ileia (**Figure**

4.2(f)) (Nikolopoulos et al., 2012; Petraki, Nikolopoulos, Fotopoulos, Panagiotaras, Nomicos et al., 2013; Petraki, Nikolopoulos, Fotopoulos, Panagiotaras, Koulouras et al., 2013).

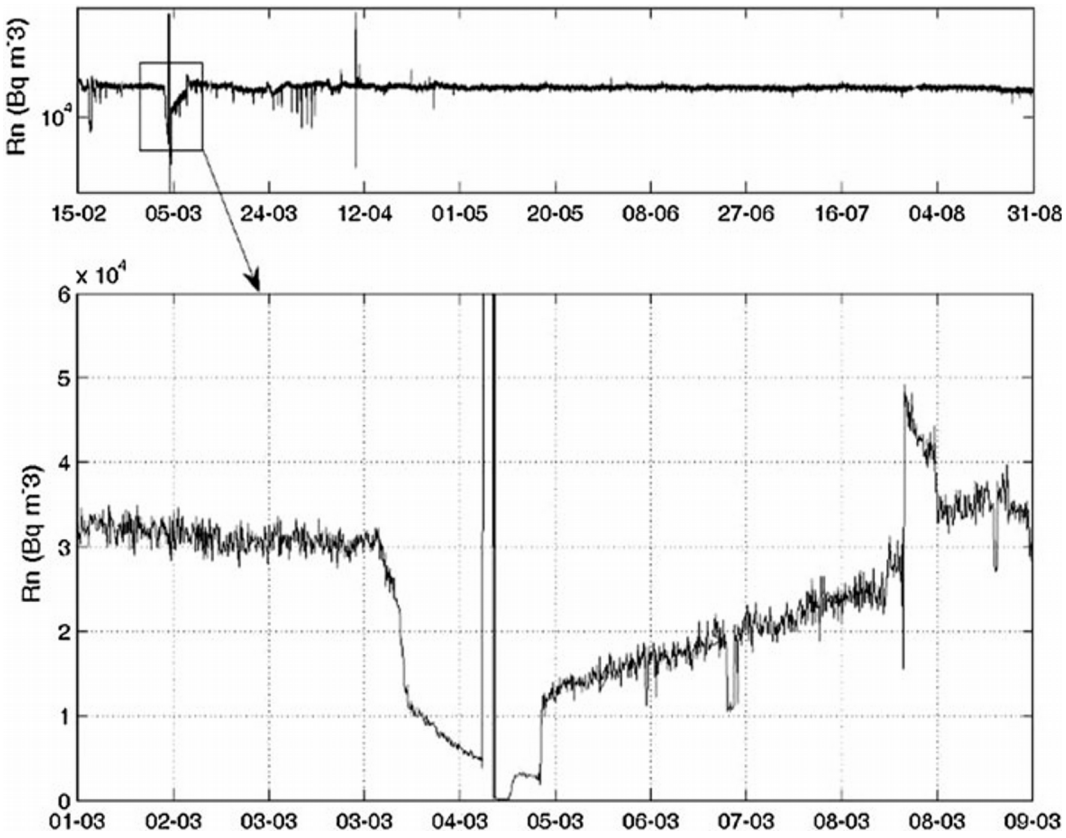

Figure 4.13: The radon signal of the Ileia station (upper figure) between 15-February-2008 and 31-August-2008 (Nikolopoulos et al., 2012) and a zoom of the corresponding variations of the first radon anomaly (down figure) between 1-March-2008 and 9-March-2008.

It is important to note, that this first anomaly was detected between 3/3/2008 and 9/3/2008, i.e., it was concurrent to the radon anomaly of the Lesvos signal. The anomalies of both signals exhibited an intense step fall of approximately one-day duration and were followed by an abrupt radon increase (spike). It is significant, that a very recent paper (Namvaran, & Negarestani, 2012) reported, as well, intense radon decrease prior to earthquakes in the Jooshan hot spring in Iran. The radon spike of the Lesvos signal was at $(37.5 \pm 0.1) \cdot 10^3 \, Bq \cdot m^{-3}$, while the first radon spike of the Ileia signal was quite higher, namely of the order of $(500 \cdot 10^3) \, Bq \cdot m^{-3}$ (Nikolopoulos et al., 2012; Petraki, Nikolopoulos, Fotopoulos, Panagiotaras, Nomicos et al., 2013; Petraki, Nikolopoulos, Fotopoulos, Panagiotaras, Koulouras et al., 2013). The first anomaly of the Ileia signal revealed, among others, self-affine, long-lasting self-organised critical (SOC) characteristics, with switching between anti-persistency and persistency (Nikolopoulos et al., 2012; Petraki, Nikolopoulos, Fotopoulos, Panagiotaras, Nomicos et al., 2013; Petraki, Nikolopoulos, Fotopoulos, Panagiotaras, Koulouras et al., 2013). Most importantly, it exhibited significant similarities with several electromagnetic disturbances of the MHz range, all exhibiting well-established pre-earthquake footprints (Petraki, Nikolopoulos, Fotopoulos, Panagiotaras, Koulouras et al., 2013). In addition, this first extended anomaly showed more self-affine power at low frequencies, i.e., at large scales (Petraki, Nikolopoulos, Fotopoulos, Panagiotaras, Koulouras et al., 2013). This fact is considered as a signature of earthquakes according to several publications (Eftaxias et al., 2010; Eftaxias, Panin, & Deryugin, 2007; Eftaxias et al., 2008, 2009). Simultaneously, the stable parts of 2008 signal of Ileia, as well as, lengthy background radon data, did not show similar behaviour. This perspective, in combination with the results of several publications (e.g. Eftaxias, 2010; Eftaxias et al., 2007, 2008, 2009; Gotoh et al., 2004; Hayakawa, & Hobara, 2010;

Kapiris et al., 2002, 2003; Nikolopoulos et al., 2012; Petraki, Nikolopoulos, Fotopoulos , Panagiotaras, Nomicos et al., 2013; Petraki, Nikolopoulos, Fotopoulos, Panagiotaras, Koulouras et al., 2013; Smirnova et al., 2004, 2007) provide a pathway for evaluating the precursory validity of the premonitory anomaly of the Lesvos signal.

Figure 4.14 a, **c–e** presents the results of the application of the power-law wavelet spectral fractal analysis. This figure reveals the following very important information:

(a) The vast majority of windows during the anomaly of the Lesvos signal, exhibited significantly higher values of the power law b exponent and the matching squares of the Spearman's correlation coefficient when compared to the corresponding values of the baseline parts. Most importantly, the successive ($r^2 \geqslant 0.95$) b -values were between 1.5 and 2.5 (blue segments) and the successive $loga$ -values, between 0 and 5. Completely similar behaviour was identified in the Ileia signal (Nikolopoulos et al., 2012). In addition, these high b -values are in close agreement with published values of electromagnetic anomalies (Petraki, Nikolopoulos, Fotopoulos, Panagiotaras, Koulouras et al., 2013, Eftaxias, 2010; Eftaxias et al., 2007, 2008, 2009; Gotoh et al., 2004; Kapiris et al., 2002, 2003; Smirnova et al., 2004). Noteworthy is that significant increase in successive b -values above 1.5 was also observed in electromagnetic anomalies prior to destructive earthquakes, such as the Kozani–Grevena (Kapiris et al., 2002, 2003) and the Athens earthquake (Eftaxias, 2010; Minadakis, Potirakis, Nomicos, & Eftaxias, 2012; Potirakis, Minadakis, & Eftaxias, 2012) in Greece and the L' Aquila earthquake (Eftaxias et al., 2009, 2010) in Italy.

(b) During the abrupt step downturn of the radon signal of Lesvos, several b -

values were above 2.0 ($b>2.0$). This fact is very important, since b -values between 2.0 and 3.0 ($2.0<b<3.0$), suggest persistent profiles qualitatively analogous to fBm-model.

(c) The Morlet scalogram of the Lesvos signal (**Figure 4.14b**) presented significantly more power at low than at high frequencies during the anomalous parts. It should be emphasised that, according to (a), the low-frequency enhancement is simultaneous with the detection of successive high- b power-law parts, i.e., parts exhibiting b -values above 1.5. This simultaneous low frequency enhancement is consistent, physically, with the predominance of the larger fracture events (Eftaxias et al., 2009) and is considered as a footprint of preparation of earthquakes (Eftaxias, 2010).

In relation, the following very significant facts should be emphasised: (Nikolopoulos et al., 2012, Eftaxias, 2010; Eftaxias et al., 2007, 2008, 2009; Kapiris et al., 2002, 2003; Li, et al. 2005)

(i) Power-law-value of $b=2$ implies that there is no correlation between the process increments. This means that there is a standard diffusing regime and the system follows random paths driven by non-memory dynamics (random-walk).

(ii) Power-law-values of $2.0<b<3.0$ suggest signal's super-diffusion, i.e., persistency. In this b range, the accumulation of fluctuations is faster than in classical Brownian motion, i.e., than in fBm modelling.

(iii) Power-law-values of $1.0<b<2.0$ suggest anti-persistency.

(iv) Power-law-values of $b=1.0$ imply that the fluctuations of the processes do not grow and the signal is stationary.

(v) Successive ($r^2\geqslant 0.95$) power-law-beta-exponent values close or above 1.5 are possibly consistent with pre seismic fBm modelling.

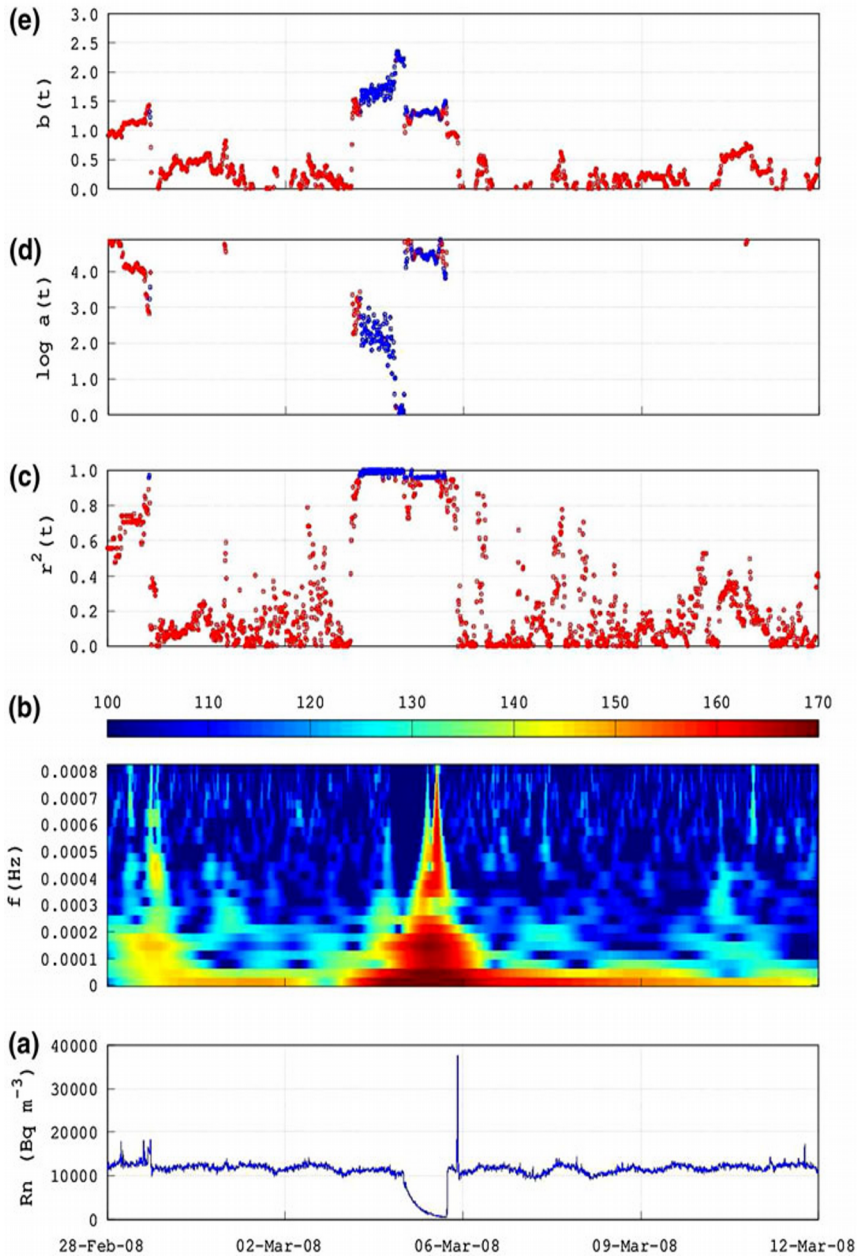

Figure 4.14: (a) The radon signal of the Lesvos station. (b) Morlet wavelet scalogram of (a). (c) evolution of the square of the Spearman's correlation coefficient. (d) evolution of $loga$. (e) evolution of the power-law scaling exponent b. Blue points in c–e correspond to successive ($r^2 \geqslant 0.95$) parts. All other points are marked in red.

4.3.2 Conclusions from the analysis of Lesvos radon signal-2008

In the consensus above, it becomes evident that the anomalous parts of the Lesvos signal presented key periods similar to the Ileia signal, namely periods with

A) Successive ($r^2 \geqslant 0.95$), fBm ($b > 1.5$) segments (blue segments).
B) Strong fBm antipersistent behaviour of $b > 1.5$ and well persistent behaviour of $b > 2.0$,i.e., once again, with long memory pre-earthquake switching between persistency and anti-persistency.
C) Sudden and sharp increase in values of spectral fractal exponent b . The reader may recall, that this has been proposed as an enhanced potential pre-seismic pattern.
D) Low-frequency enhancement of the corresponding Morlet power scalogram.

These issues are very significant since (A), (B) imply long-memory of the underlying geo-generating system. This further implies long-range temporal correlations, i.e., strong system's memory. Furthermore, each value correlates not only to its most recent value but also to its long-term history in a scale-invariant, fractal manner (Eftaxias, 2010; Eftaxias et al., 2008). This further means that the history of the system defines its future (non-Markovian behaviour) (Eftaxias, 2010; Eftaxias et al., 2008, 2009; Kapiris et al., 2002). Moreover, (B) suggests that the underlying dynamics are governed by positive feedback mechanisms and, hence, external influences tend to lead the system out of equilibrium (Telesca, & Lasaponara, 2006). In this manner, the system acquires a self-regulating character and, to a great extent, the property of irreversibility, one of the important components of prediction reliability (Morgounov, 2001). From another viewpoint, this behaviour suggests that the final output of fracture is affected by many

processes that act on different time-scales (Eftaxias, 2010; Smirnova, & Hayakawa, 2007; Smirnova et al., 2004). The aforementioned results are in good agreement with the relevant prediction based on the hypothesis that the evolution of the Earth's crust towards general failure may take place as a SOC phenomenon (Eftaxias, 2010; Hayakawa, & Hobara, 2010). All these issues are compatible with the last stage of earthquake generation (Petraki, Nikolopoulos, Fotopoulos, Panagiotaras, Koulouras et al., 2013; Eftaxias, 2010; Eftaxias et al., 2007, 2008, 2009; Gotoh et al., 2004; Kapiris et al., 2002, 2003; Smirnova et al., 2004). Noteworthy is that fBm modelling of stochastic fractal time-series like those of the anomalies of **Figure 4.14**, is consistent with the slip of self-affine fractional Brownian surfaces prior or during generation of earthquakes (Eftaxias, 2010; Eftaxias et al., 2008). Similar behaviour was also identified in the 2008 significant disorders of the Ileia signal. It is also of importance to note that the non-anomalous part of the Lesvos signal exhibited fractal behaviour of very low statistical significance. This observation was also reported for the stable part of the 2008 Ileia radon time-series and the radon background of 2010 and 2011. It is also stressed that persistency/anti-persistency switching was also reported in detected ULF disturbances prior to the Guam earthquake (Smirnova, & Hayakawa, 2007; Smirnova et al., 2004).

4.4 Results from the analysis of the Athens radon signal-2014

On 17 November 2014, at 23:05 and 23:09 local time, two shallow earthquakes of $M_L = 5.2$ occurred 86 km North-West of Athens, Greece. Prior to the earthquakes a noteworthy radon anomaly was observed by the telemetric radon station operating with the Barasol MC2 probe (Algade France) (**Figure 3.14**) which is installed in the Campus of Technological Educational Institute of Athens. The anomaly lasted approximately

between 24 Oct 2014 and 10 November 2014. Some anomalies can be observed but no association has been attempted to the pre-seismic activity of the near area.

Figure 4.15 presents the radon signal recorded by the monitoring station of radon in Athens (Greece) prior to the earthquakes of 17 November 2014. It also presents radon activity after these twin earthquakes and during 2015 up to the end of the analysis of this research. The signals presented in parallel are the temperature and the air pressure as measured by the BMC2 (Barasol) probe. The measurement data presented in **Figure 4.15** spanned from 10 September 2014 to 17 November 2014, namely they ended approximately one hour after the twin earthquakes. A significant radon anomaly was observed. Other anomalies are also observed. The main anomaly which was associated with the twin earthquakes of 17 November 2014 (Nikolopoulos et al., 2015), started approximately on 24 October 2014 and lasted roughly up to 10 November 2014. During this radon anomaly, significant disturbances were addressed in pressure and temperature in the borehole of the measurements. The environmental conditions in the interim interval did not exhibit any extreme alterations. No external influence was observed as well. Noteworthy is the simultaneous downturn of temperature and pressure in the borehole. Remarkable is also the sudden increase in pressure which may have act as a piston-like procedure for radon emanation. The pressure profile may partially explain the drop of radon concentration, however, it may not explain the gradual increase of it. Most importantly, the source of these alterations could not be attributed to changes of environmental conditions or external influences. On the other hand, a geological long-lasting procedure attributive to the twin earthquakes of 17 November 2014 could justify the noteworthy concentration changes of radon in soil of the borehole between 24 October 2014 and 10 November 2014.

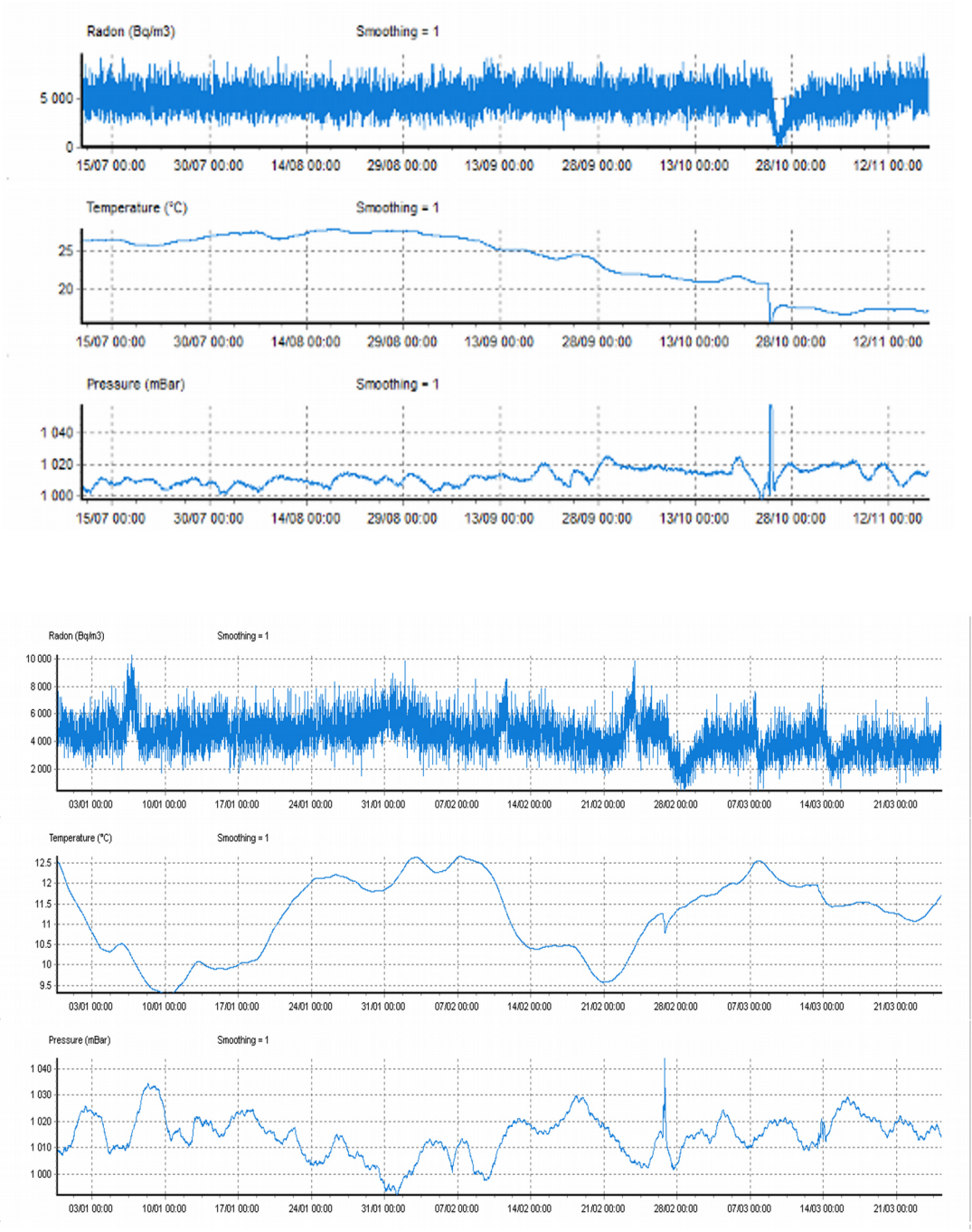

Figure 4.15: The signals recorded by the telemetric station of Barasol from 10/7/2014 until 18/11/2014 and from 1/1/2014 until 25/3/2014 respectively. From the top: evolution of (a) radon (b) temperature and (c) air pressure. The output was produced by the software provided by the manufacturer.

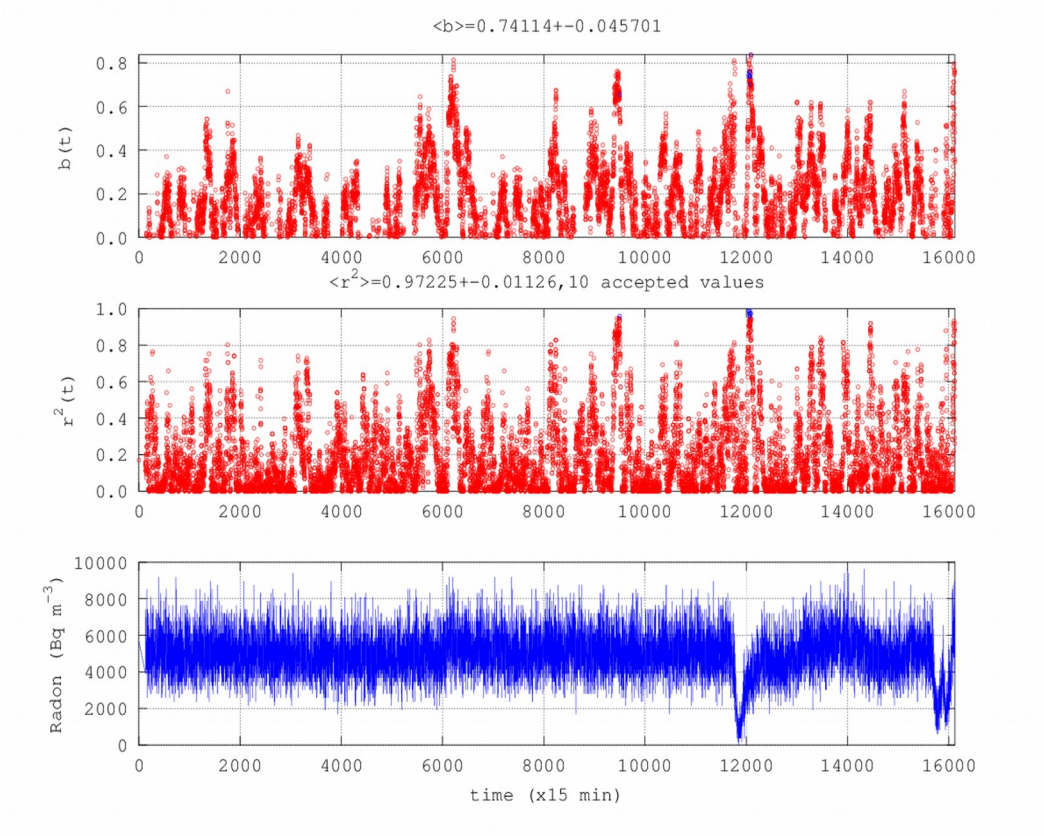

Figure 4.16: The spectral fractal analysis of the signal recorded from Barasol from 10/7/2014 until 18/11/2014. From the top: evolution of (a) spectral fractal exponent b (b) square of the Spearman's correlation coefficient r^2 (c) radon signal.

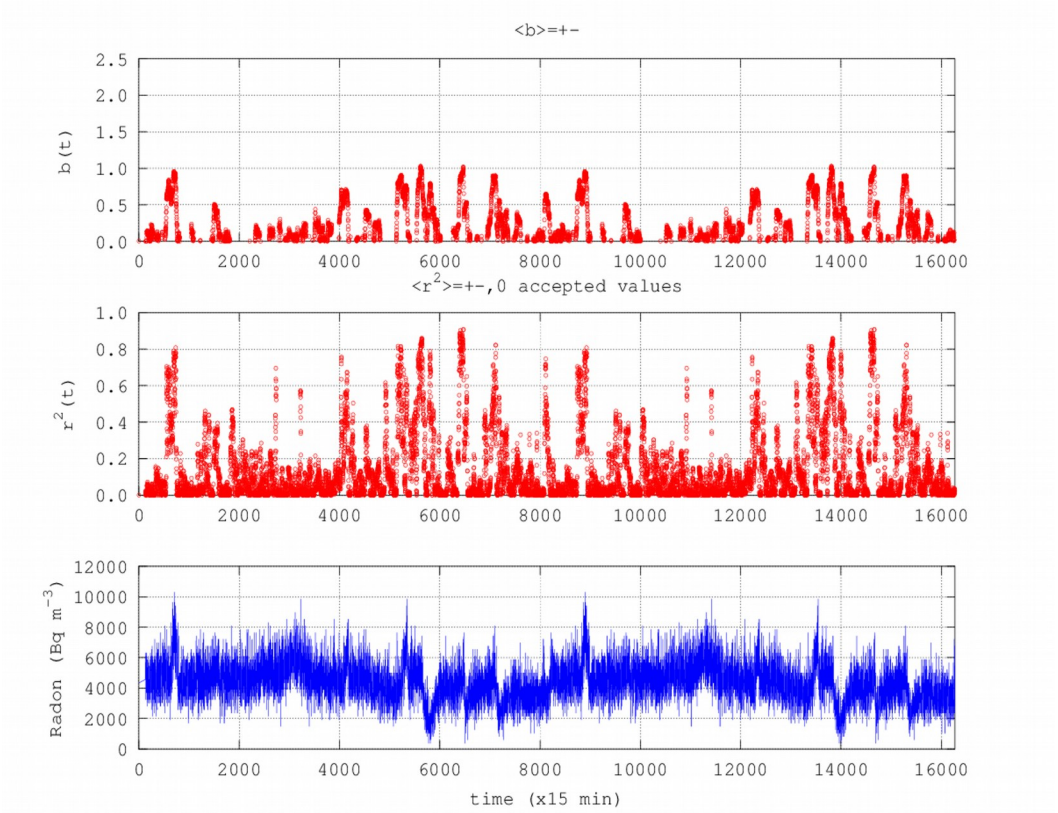

Figure 4.17: The spectral fractal analysis of the signal recorded from Barasol from 1/1/2015 until 25/3/2015. From the top: evolution of (a) spectral fractal exponent b (b) square of the Spearman's correlation coefficient r^2 (c) radon signal.

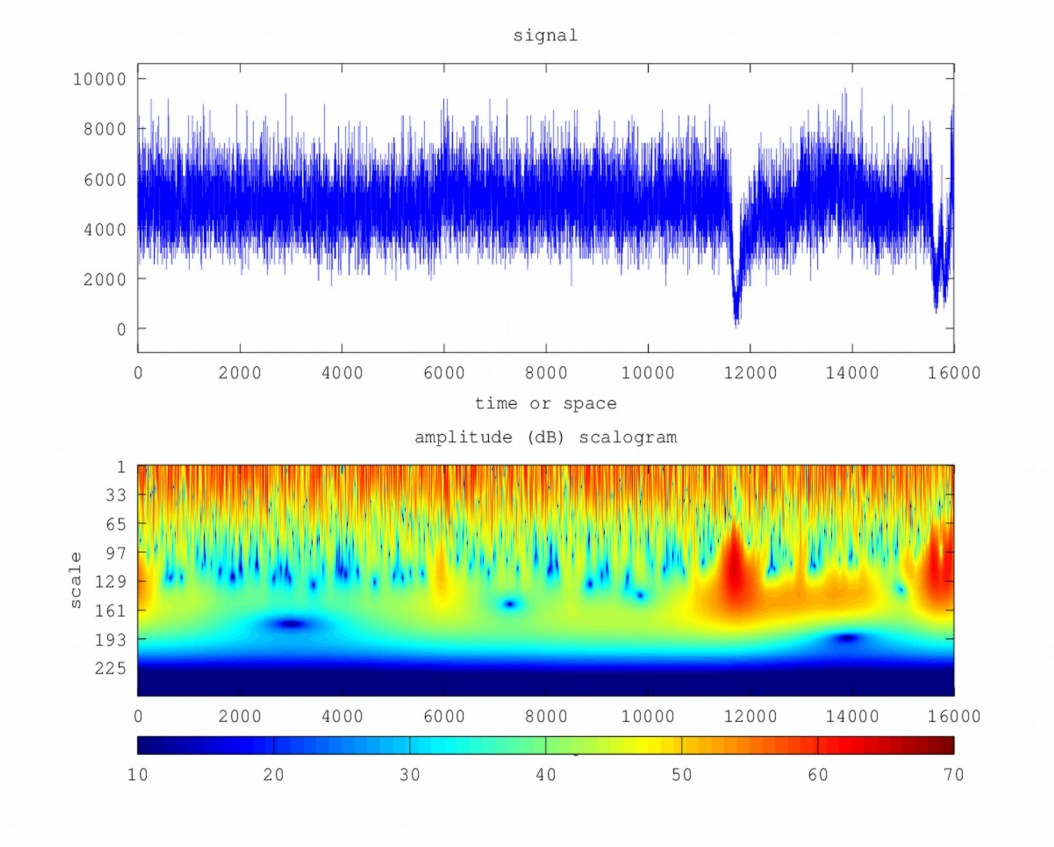

Figure 4.18: 60 db wavelet scalogram of the radon signal of **Figure 4.15**. Signal from 10/7/2014 until 18/11/2014. The term "time or space" is explained in text. The horizontal axis may be corresponded to time intervals (x15 min). Significant high power can be observed approximately between sample 11500 and 13000 and on approximately 16000.

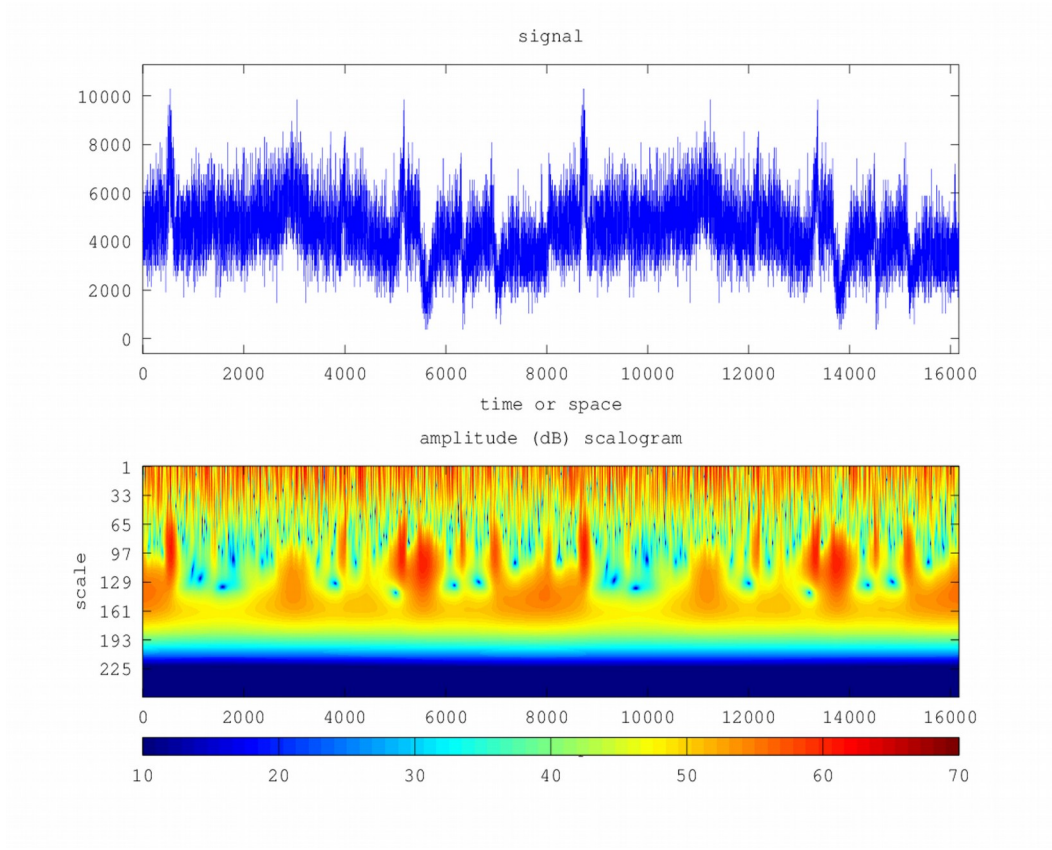

Figure 4.19: 60 db wavelet scalogram of the radon signal of **Figure 4.15**. Signal from 1/1/2015 until 25/3/2015. The term "time or space" is explained in text. The horizontal axis may be corresponded to time intervals (x15 min). Significant high power can be observed approximately between sample 11500 and 13000 and on approximately 16000.

It can be observed from **Figures 4.16** and **4.17** that the behaviour of the Barasol signal corresponds to non-successive fGn modelling. This is very peculiar because as will be shown in the next chapter, this signal presented significant differentiation in the Hurst exponent during the anomalous part (Nikolopoulos et al., 2015), either through the Rescaled Range analysis or the Detrended Fluctuation analysis. This is of significance because in this case the fractal techniques did not operate well as a screening method for fBm segments. Nevertheless, this does not restrict the screening strength of the fractal methods because it corresponds to one earthquake from the 37 studied, 90 km away from the radon station, of medium magnitude. As already mentioned the pre-earthquake value is enhanced when the fractal methods associate with the disturbances and, better if, other long memory techniques provide also similar indications (Cantzos et al., 2015). It is worth to mention however, that more or less, the fractal behaviour is the non successive fGn model, which is the one identified in the majority of the cases of the fractal analysis of the Ileia and Lesvos signals (red areas **Figures 4.7**, **4.10** and **4.14**).

Despite that the fractal analysis did not reveal certain tendencies, the wavelet transform revealed some information. To this direction, **Figure 4.17** and **4.18** show the 60 db wavelet scalograms of the radon signals of **Figure 4.15**. The scalograms were produced with a logarithmic Gabor filter of 256 scales. In reference to the **Figure 4.17** the following issues are valid:

(a) The scalogram of the first 11500 signal's samples did not exhibit alterations;

(b) The useful scale range was approximately from scale 1 to scale 160. Scales above did not contribute in the representation of the signal. Considering that the high scalogram scales (130-160) correspond to the small spatial frequencies,

more power was allocated to the high scales viz. the small spatial frequencies. Investigators (Whitehead, Barry, Ditchburn, Morris, & Stewart, 2007; Eftaxias et al., 2009) have declared this as a footprint of earthquake generation;

(c) The radon anomaly in the scalogram of **Figure 4.18** lasted approximately between samples 11500 and 13000. Each sample corresponded to 15 min of recordings of radon in soil. Hence the radon anomaly in **Figure 4.17**, lasted 1500 samples of fifteen minute duration, viz. approximately 15 days. This finding is in accordance to the data of **Figure 4.15**;

(d) The wavelet transform employed in **Figure 4.17** is superior to the Fourier transform since it involves space and time in a combined way (Choubey et al., 2009; Eftaxias, 2010; Eftaxias et al., 2008, 2009; Erees et al., 2007; Fleischer, & Mogro-Campero, 1985; Hayakawa, & Hobara, 2010; Kapiris, Eftaxias, & Chelidze, 2004; Kapiris et al., 2005; Nikolopoulos et al., 2012, 2014; Petraki, Nikolopoulos, Fotopoulos, Panagiotaras, Koulouras et al., 2013; Petraki, Nikolopoulos, Fotopoulos, Panagiotaras, Nomicos et al., 2013; Whitehead et al., 2007; Zafrir, Steinitz, Malik, Haquin, & Gazit-Yaari, 2009). The temporal variations can be corresponded to spatial frequencies, viz., scale parts in the earth-system that fractured in the crust. Hence, time can be corresponded to space, namely regions in the earth that break. In this sense, a spatially evolving crack-generating procedure (Choubey et al., 2009; Eftaxias, 2010; Eftaxias et al., 2008, 2009; Erees et al., 2007; Fleischer, & Mogro-Campero, 1985; Hayakawa, & Hobara, 2010; Kapiris et al., 2004, 2005; Nikolopoulos et al., 2012, 2014; Petraki, Nikolopoulos, Fotopoulos, Panagiotaras, Koulouras et al., 2013; Petraki, Nikolopoulos, Fotopoulos, Panagiotaras, Nomicos et al., 2013; Whitehead et al., 2007; Zafrir et al., 2009) may be a source of a time evolving

radon-disturbance.

Further to the above it should be mentioned that, as the wavelet spectrogram analysis of **Figure 4.17**, the Fourier spectrogram analysis revealed that the background variations of radon in soil were characteristically different in Fourier space than those of the anomalous parts (Petraki, Nikolopoulos, Fotopoulos, Panagiotaras, Koulouras et al., 2013). In addition, the Fourier spectrograms, presented (Petraki, Nikolopoulos, Fotopoulos, Panagiotaras, Koulouras et al., 2013), as the wavelet scalograms, more power at the high frequencies and, most importantly, similar db profiles of the background parts as those of the scalograms. Hence, it may be supported that the first 11500 samples of **Figure 4.17** referred to background concentrations of radon in soil in the borehole of TEI of Athens. Similar are the interpretations for **Figure 4.18** as well.

4.5 Collection of the results of Chapters 3 & 4

In the following, **Table 4.3**, presents collectively all the data presented in **Chapters 3** & **4** regarding the efficiency of the fractal methods in identifying pre-seismic patterns hidden in MHz and radon time-series. The following abbreviations were used in **Table 4.3**:

1) **(N.D.A.):** Number of Days of Analysis, i.e., the number of continuous signal days that were analysed.

2) **(S):** Station Letter. For reference the reader could see section **3.5.1**.

3) **(L.M.):** Local Magnitude of the earthquake. This was derived from the data of the National Observatory of Athens.

4) **(f):** Frequency of the antennas for the cases of the MHz electromagnetic radiation. Purple was employed for the 46 MHz and grey for the 41 MHz.

5) **(Lat.):** Latitude of the epicentre of the earthquake.

6) **(Long.):** Longitude of the epicentre of the earthquake.

7) **(R.D.A.)**: Required Days for the Analysis, i.e., the number of days (24h working) that were required for a one-core Pentium ® computer from the start up to the end of the analysis with fractal methods.

   This entry, accounts the time needed for: (1a) downloading the data from the server; (1b) uploading the data to the computer employed for the analysis (1c) entering the data required for the analysis; (1d) storing and backing up the analysis data in removable devices and cloud; (1e) Repetition of steps (1a-1d) in the cases of AC power loss or data loss.

   The R.D.A., did not accounted the time needed for the production and debugging of the custom made software that was employed in the analysis.

8) **(D):** Depth of the epicentre of the earthquake.

9) **(T.S.b.V.):** Typification of successful b - values. This refers to a quality quantification of the images of the time evolution of the successive power-law b - values. The quality quantification was arbitrarily characterised as scattered or continuous in the manner used in text.

10) **(Median Vb)**: Median value of the evolution of b - values. This value corresponds to the threshold value, above which the 50% of b - values are. The Median Vb calculated after the end of each run from the ASCII file which contained the full b-data. This was an output of the custom made software.

11) **(IQR):** Interquartile range of b - values. It corresponds to the difference

between the upper (3rd) and lower (1st) quartiles, viz., IQR = $Q_3 - Q_1$. Q1 corresponds to the cut-off value, below of which 25% of the b-values are. Q3 correspond to the threshold value above which the 75% of of the b-values are. IQR contains, more or less, the 50% of b-values. IQR was calculated after the end of each run, as in (9), from the ASCII file which contained the full b-data. This was an output of the custom made software.

12) **(Min/Max V.b):** Minimum/Maximum value of b . This was calculated after the end of each run as in (9-11).

13) **%Vb>=1.5:** The percentage of values above 1.5. This value was arbitrarily selected in this dissertation, as a value adequate to discriminate long-memory dynamics from randomness (please see also text).

14) **%Vb>=2.0:** The percentage of values above 2.0. This value was arbitrarily selected by investigators as another value adequate to discriminate long-memory dynamics from randomness (please see also text).

It can be observed from the above calculations as well as from **Table 4.3**, that, according to the author, what matters is not the identification of some values above a threshold (in the sense employed e.g. in Eftaxias et al., 2009, 2010 and references therein) but rather the following:

1. T.S.b.V. to be continuous, namely the continuous observation of high b -values (above a threshold). This strongly discriminates the long-memory dynamics from randomness.

2. Median Vb to be high, because this indicates that the great majority of b-values are high; and this is a first good sign for a pre-earthquake activity.

3. %Vb>1.5 and %Vb>2 to be high.

In the sense of (a-c) as well as according to the data presented in text, several such cases can be identified in **Table 4.3**. Characteristic examples are the following:

1. EQ:17, 41 and 46 MHz, station F.
2. EQ:3 and EQ: 16, 41 MHz, station V.
3. EQ:24, 41 MHz and 46 MHz, station V.
4. EQ:27, 46 MHz, station V.
5. EQ:4, 46 MHz, station V.
6. EQs: 19, 20, 25, 15.
7. EQ:34 and EQ:35 identified through radon.

It should be emphasised, that this is the first time that such a systematic approach is attempted. Note that **Table 4.3**, includes *1819 days of signal analysis*. However, as can be observed at the end of **Table 4.3**, only the *analysis of fractals required 3.8 years*, not accounting for software production. Although several associations were reported, the available data is still limited, so as to attempt an association of the dependence of the earthquake data with the station that identified a pre-seismic sign, as well as a further investigation of the role of the earthquake parameters, namely depth and position of the epicentre. What complicates the situation is what outlined here and reported next in the **Chapter 5**; the fractal methods are not sufficient to signalise that an earthquake is going to occur in some near area. Such results should be combined with other long-memory methods or methods of self-organisation, in order to provide better estimations (see e.g. Cantzos et al., 2015). Even in such a case, it is still questionable, whether a certain earthquake can, up-to-now, be associated to an anomaly of some kind.

4.6 Conclusions of power-law wavelet spectral fractal analysis of MHz-Electromagnetic signals and radon signals

Summarising the most important findings up to now, the following issues can be supported:

(1) Thirty-three pre-seismic MHz electromagnetic disturbances of some days up to one-month duration prior to earthquakes of 2007, 2008, 2009, 2014, 2015 with $M_L \geq 5.0$ indicate that the MHz electromagnetic, as well as, the radon disturbances can be used as reliable pre-seismic precursors of some scientific value.

(2) Almost all the investigated signals (both MHz and radon) exhibited characteristic epochs with fractal organisation in space and time. Continuous epochs were detected in several one-month signals.

(3) The precursor fractal epochs are those of a successive ($r^2 \geqslant 0.95$) fBm class ($1<b<3$).

(4) Enhanced precursory fractal epochs are the successive fBm ones with *many successive* ($r^2 \geqslant 0.95$) *segments above 1.5* and better, *above 2.0.* These epochs indicate well-established long-memory dynamics well away from fGn randomness.

(5) Several successive ($r^2 \geqslant 0.95$) fractal electromagnetic and radon segments showed anti-persistency ($1.5<b<2.0$). Nevertheless, numerous persistent ($2.0<b<3.0$) parts were detected. Although several references (e.g the references of Eftaxias, 2010) suggested that the MHz electromagnetic precursors show only anti-persistent behaviour, the systematics of this research supports a different aspect. Significant arguments for the also persistent

behaviour of the MHz radiation will be presented also in **Chapter 5**.

(6) Switching between persistency and anti-persistency was identified. According to publications of the author and colleagues, *the switching between persistency and anti-persistency enhances the precursory value* of the electromagnetic and radon precursors.

(7) The Hellenic electromagnetic network showed sensitivity differentiations due to locality. All earthquakes of 2009 with $M_L \geq 5.0$ were pre-signalized through interrupted or continuous fractal segments of long memory. Two earthquakes were detected by two more stations. The remaining stations did not give MHz signals with characteristic pre-earthquake fractal footprints. *Data*, although of great amount, *are still limited to identify the sensitivity dependencies* of the Hellenic network.

(8) Significant pre-signalized earth-quakes gave fractal warnings up to one month prior to some events. Some warnings evolved up to some hours prior to the earthquake. The remaining investigated MHz signals gave significant alarms 2-3 weeks and 1 week prior to the event. The latter is the most usual behaviour (**Table 4.3**). It may be supported hence that *the MHz electromagnetic and the radon precursors correspond to the same pre-earthquake phase.* It may be also supported that *the MHz electromagnetic provide pre-seismic signs ranging from some weeks up to some hours prior to the event. The time lag of the radon precursors can be up to 2-3 months prior to the event.*

(9) A s*udden and sharp increase in values of spectral fractal exponent* b *is as an enhanced potential pre-seismic pattern*, especially when *associated with a visual disturbance.*

(10) The findings indicate *self-organised critical state characteristics of the last*

stages of the investigated earthquakes.

(11) The *fractal analysis* method can be employed as a *first screening method* for the identification of long-memory patterns hidden in pre-seismic time-series. It is also, from the results, a *reliable method for identifying pre-earthquake patterns.*

(12) Geological explanations were proposed in view of the asperity model. Persistent & anti-persistent MHz anomalies were due to micro-cracking of the heterogeneous medium of the earth's crust which may have led the system's evolution towards global failure.

Table 4.3: Collection of the results derived through the spectral fractal analysis (for the abbreviations see text).

			SEISMIC ACTIVITY													Spectral	Fractal	Analysis	
	i/i	EQ:n	Origin Time (GMT)	Location	Lat. (^{0}N)	Long. (^{0}E)	D (km)	L.M.(M_L)	f(MHz)	S	N.D.A.	R.D.A.	T.S.b.V.	Median V.b.	IQR	Min/Max V.b.	%s.V.b.>=1.5	%s.V.b.>2.0
2007	1	32	2007/04/16 07:38:47	162.5 km WNW of Florina	41.46	19.68	8	5.0	41	J	35	25.5	None	~	~	~	~	~
										K	35	25.5	None	~	~	~	~	~
									46	K	35	25.5	Scattered	0.77	0.21	0.75/1.46	0%	0%
	2	17	2007/03/25 13:57:58	19.3 km NNW of Argostoli	38.34	20.42	15	5.5	41	J	31	22.5	None	~	~	~	~	~
										F	31	22.5	Scattered	2.15	0.25	0.80/2.41	80%	73.34%
									46	J	31	22.5	None	~	~	~	~	~
										F	31	22.5	Continuous	2.31	0.20	1.20/2.69	90%	75%
	3	33	2007/02/03 13:43:22	63.8 km SW of Kithira	35.80	22.58	99	5.0	41	E	31	22.5	None	~	~	~	~	~
										O	31	22.5	None	~	~	~	~	~
										V	31	22.5	Scattered	2.03	0.12	1.50/2.16	100%	65%
									46	V	31	22.5	Scattered	1.83	0.23	1.59/2.09	100%	13.34%
	4	28	2007/01/28 17:32:23	133.6 km WSW of Chania	34.90	22.75	34	5.1	41	E	29	21.5	None	~	~	~	~	~
										I	25	18.5	Scattered	1.59	1.42	0.82/2.00	55%	0%
									46	E	29	21.5	None	~	~	~	~	~
										I	25	18.5	Mild	2.03	0.31	0.88/2.21	86.67%	61.54%
										O	29	21.5	None	~	~	~	~	~
										V	29	21.5	Scattered	1.84	0.24	1.21/2.13	86.67%	16.67%
2008	1	3	2008/07/15 03:26:34	71.1 km SSW of Rodhos	35.85	27.92	56	6.2	41	V	7	5.1	Continuous	2.03	0.34	1.11/2.51	96.00%	0.51
	2	16	2008/06/21 11:36:22	88.2 km S of Methoni	36.03	21.83	12	5.5	41	V	1	0.7	Continuous	2.03	0.34	1.11/2.51	96.00%	0.51
									46	V	2	1.4	Mild	1.48	0.51	0.69/2.22	24%	3.00%
	3	31	2008/06/12 00:20:45	99.2 km ESE of Iraklion	35.11	26.19	29	5.0	41	V	2	1.5	Continuous	1.87	0.47	1.13/2.33	85.00%	0.32
	4	34	2008/06/08 12:25:27	23.1 km ENE of Andravida	37.98	21.51	25	6.5										
	5	26	2008/03/28 00:16:21	39.4 km SSE of Iraklion	35.01	25.33	50	5.1	41	E	32	23.5	Mild	2.08	0.82	1.00/3.37	82.59%	53.34%
										V	32	23.5	Continuous	1.38	0.41	0.57/2.63	37.20%	0.80%
									46	E	32	23.5	Mild	1.44	0.55	0.46/2.76	36.40%	11.3%
										V	32	23.5	Continuous	1.24	0.42	0.50/2.50	23.10%	1.40%
	6	35	2008/03/19 23:01:52	34.1 km W of Skyros	38.92	24.17	35	5.0										
	7	24	2008/02/26 10:46:05	95.3 km S of Methoni	35.96	21.70	5	5.2	41	E	57	42.0	None	~	~	~	~	~
										V	57	42.0	Continuous	1.26	0.40	0.25/2.92	29.47%	6.94%
									46	E	57	42.0	Scattered	1.31	0.43	0.46/2.76	30.71%	3.00%
										V	57	42.0	Continuous	1.61	0.37	0.50/2.69	64.92%	7.67%
	8	8	2008/02/20 18:27:04	70.8 km S of Methoni	36.18	21.72	25	6.0	41	E	51	37.5	None	~	~	~	~	~

Table 4.3: Collection of the results derived through the spectral fractal analysis (for the abbreviations see text).

			SEISMIC ACTIVITY													Spectral	Fractal	Analysis	
	i/i	EQ:n	Origin Time (GMT)	Location	Lat. (^{0}N)	Long. (^{0}E)	D (km)	L.M.(M_L)	f(MHz)	S	N.D.A.	R.D.A.	T.S.b.V.	Median V.b.	IQR	Min/Max V.b.	%s.V.b.>=1.5	%s.V.b.>2.0
										V	51	37.5	Continuous	1.33	0.41	0.25/2.92	28.47%	7.93%
									46	E	51	37.5	Scattered	1.32	0.44	0.46/2.76	33.17%	3.50%
										V	51	37.5	Continuous	1.62	0.37	0.50/2.69	66.82%	7.18%
	9	27	2008/02/19 23:15:40	70.0 km S of Methoni	36.19	21.77	22	5.1	41	E	50	36.5	None	~	~	~	~	~
										V	50	36.5	Continuous	1.33	0.41	0.25/2.92	28.47%	7.93%
									46	E	50	36.5	Scattered	1.32	0.44	0.46/2.76	33.17%	3.50%
										V	50	36.5	Continuous	1.62	0.37	0.50/2.69	66.82%	7.18%
	10	6	2008/02/14 12:08:55	66.5 km S of Methoni	36.22	21.75	38	6.1	41	E	45	33.0	None	~	~	~	~	~
										V	45	33.0	Continuous	1.06	0.38	0.25/2.62	23.85%	2.38%
									46	E	45	33.0	Scattered	1.26	0.45	0.46/2.22	27.20%	2.20%
										V	45	33.0	Continuous	1.59	0.37	0.50/2.69	62.22%	6.33%
	11	4	2008/02/14 10:09:23	35.9 km SSE of Methoni	36.50	21.78	41	6.2	41	E	45	33.0	None	~	~	~	~	~
										V	45	33.0	Continuous	1.06	0.38	0.25/2.62	23.85%	2.38%
									46	E	45	33.0	Scattered	1.26	0.45	0.46/2.22	27.20%	2.20%
										V	45	33.0	Continuous	1.59	0.37	0.50/2.69	62.22%	6.33%
	12	7	2008/01/06 05:14:19	9.3 km SW of Leonidhion	37.11	22.78	86	6.1	41	V	5	3.7	Mild	0.90	0.60	0.25/2.56	14%	1.00%
2009	1	22	2009/11/11 09:51:08	51.8 km SW of Zakynthos	37.47	20.47	21	5.3	41	I	9	6.5	Mild	1.66	0.58	0.50/3.00	62.55%	17.06%
									46	I	9	6.5	Mild	1.57	0.54	0.50/3.00	56.96%	11.57%
	2	14	2009/11/03 05:25:09	65.6 km SW of Zakynthos	37.39	20.35	39	5.6	41	I	53	39.0	Mild	1.43	1.10	0.50/3.00	46.50%	14.05%
	3	19	2009/09/06 21:49:40	124.6 km NW of Florina	41.62	20.41	10	5.4	41	J	24	17.5	Mild	1.36	0.50	0.50/2.70	34.88%	2.92%
										P	31	22.5	Continuous	1.60	0.52	0.50/3.00	59,92%	16.57%
									46	J	24	17.5	Continuous	1.57	0.54	0.50/3.00	56.96%	11.57%
										P	31	22.5	Continuous	1.60	0.51	0.50/3.00	60.69%	15.30%
	4	11	2009/07/01 09:30:13	111.2 km SSE of Iraklion	34.35	25.40	30	5.8	41	E	31	22.5	Continuous	1.43	0.49	0.50/3.00	42.31%	5.90%
										V	31	22.5	Continuous	1.43	0.49	0.50/2.95	42.31%	5.90%
									46	E	31	22.5	Continuous	1.48	0.60	0.50/2.99	48.28%	9.48%
										V	31	22.5	Continuous	1.35	0.55	0.50/3.00	37.38%	4.64%
	5	20	2009/06/19 14:05:02	107.8 km ESE of Karpathos	35.46	28.31	42	5.4	41	A	31	22.5	Continuous	1.38	0.61	0.50/3.00	38.41%	9.90%
									46	A	31	22.5	Continuous	1.68	0.50	0.50/3.00	68.20%	19.41%
	6	25	2009/05/24 16:17:50	36.0 km NNW of Kilkis	41.30	22.74	23	5.1	41	T	31	22.5	Continuous	1.53	0.71	1.00/3.00	52.61%	21.72%
									46	T	31	22.5	Continuous	1.68	0.50	0.80/3.00	61.52%	16.71%
	7	15	2009/02/16 23:16:38	74.2 km S of Zakynthos	37.13	20.78	15	5.5	46	I	31	22.5	Continuous	1.69	0.65	0.50/3.00	64.51%	26.48%

Table 4.3: Collection of the results derived through the spectral fractal analysis (for the abbreviations see text).

			SEISMIC ACTIVITY													Spectral	Fractal	Analysis	
	i/i	EQ:n	Origin Time (GMT)	Location	Lat. (^{0}N)	Long. (^{0}E)	D (km)	L.M.(M_L)	f(MHz)	S	N.D.A.	R.D.A.	T.S.b.V.	Median V.b.	IQR	Min/Max V.b.	%s.V.b.>=1.5	%s.V.b.>2.0
	8	23	2009/01/13 06:12:42	68.2 km W of Karpathos	35.66	26.39	42	5.2	41	E	30	22.0	Mild	2.21	1.29	1.00/3.00	84.15%	58.68%
									46	E	30	22.0	Continuous	2.81	1.41	0.50/3.00	87.18%	67.65%
										V	30	22.0	Continuous	1.49	0.53	0.50/3.00	48.62%	8.92%
	9	30	2009/01/08 12:04:00	139.9 km NNW of Florina	41.94	20.74	2	5.0	41	J	32	21.5	Continuous	1.74	1.78	0.50/3.00	62.91%	39.24%
									46	J	32	21.5	Continuous	1.67	0.68	0.50/3.00	57.95%	25.88%
2013	1	2	2013/10/12 13:11:53	66.6 km W of Chania	35.50	23.28	65	6.2	41	A	32	23.5	Mild	0.98	0.60	0.40/2.42	18.00%	10.00%
									41	H	32	23.5	Continuous	1.20	0.64	0.10/2.80	25.03%	3.14%
									41	E	32	23.5	Scattered	2.04	0.74	0.50/2.95	90.00%	5.34%
									41	V	32	23.5	Continuous	0.96	0.54	0.07/3.00	11.36%	1.58%
	2	13	2013/06/16 21:39:04	116.2 km S of Iraklion	34.28	25.13	28	5.6	41	E	10	7.5	Mild	1.32	0.48	0.50/2.52	31.56%	4.07%
										V	10	7.5	Continuous	1.49	0.51	0.59/2.82	48.27%	7.61%
	3	10	2013/06/15 16:11:01	109.7 km S of Iraklion	34.34	25.06	32	5.8	41	E	10	7.5	Mild	1.32	0.48	0.50/2.52	31.56%	4.07%
										V	10	7.5	Continuous	1.49	0.51	0.50/2.82	48.27%	7.61%
2014	1	36	2014/11/17 23:09:03	25.6 km NW of Chalkida	38.64	23.41	23	5.2										
	2	37	2014/11/17 23:05:55	26.2 km NW of Chalkida	38.64	23.40	24	5.2										
	3	12	2014/08/29 03:45:05	69.4 km W of Milos	36.67	23.67	97	5.7	41	E	30	22.0	Scattered	0.72	0.19	038/1.35	0.00%	0.00%
									46	E	28	20.5	Scattered	0.86	0.41	0.25/1.62	1.16%	0.00%
										V	30	22.0	Scattered	0.82	0.20	0.26/1.77	0.70%	0.00%
	4	29	2014/08/22 04:27:53	50.6 km S of Poliyiros	39.92	23.46	29	5.0	41	J	32	23.5	Scattered	0.76	0.20	0.28/1.58	0.10%	0.00%
										K	44	32.5	Continuous			0.8/1.6		
									46	J	32	23.5	Mild			0.8/1.7		
										T	44	32.5	Continuous			0.2/2.2		
	5	1	2014/05/24 09:25:01	22.9 km SSW of Samothraki	40.29	25.40	28	6.3	41	M	36	26.5	Continuous	0.73	0.25	0.30/1.94	4.60%	0.00%
										T	36	26.5	Mild	0.77	0.34	0.03/2.02	1.63%	0.07%
									46	M	36	26.5	Scattered	1.06	0.33	0.89/1.35	0,00%	0.00%
										T	36	26.5	Continuous	1.04	0.60	0.05/2.09	15.07%	0.03%
	6	9	2014/01/26 13:55:42	6.7 km NE of Argostoli	38.22	20.53	21	5.8	41	F	10	7.5	Scattered	2.10	0.20	0.80/2.40	80%	73.34%
2015	1	18	2015/04/17 02:05:42	67.2 km SSW of Karpathos	35.16	26.74	40	5.4	46	E	10	7.5	Continuous			0.3/1.8		
	2	5	2015/04/16 18:07:44	56.7 km SSW of Karpathos	35.23	26.82	37	6.1	46	E	9	6.5	Continuous			0.3/1.8		
	3	21	2015/03/27 23:34:52	52.9 km W of Karpathos	35.68	26.56	67	5.3	46	E	3	2.3	Continuous			0.3/1.8		

Chapter 5

Long-memory analysis of earthquake generation systems in terms of Hurst exponent evolution and DFA & system's self-organisation in terms of block-entropy

5.1 Introduction

In the following, several methods are employed in the signals that were analysed in **Chapters 3** & **4** through the spectral fractal method. The main set of methods presented in this chapter, estimate the Hurst exponent directly or indirectly. The second set of methods refers to the self-organisation of the system of earthquake generation. This is done through several metrics of entropy. At first the mathematical basis is given for both sets of methods. Then, the Hurst exponent analysis is employed through mainly the R/S technique. Detrended fluctuation analysis is reviewed to some extend mainly because it is a very robust method. Finally, the results from the entropic techniques are reviewed. The conclusion is that, more or less, all techniques should be employed in steps, albeit the power-law spectral fractal analysis (**Chapters 3** & **4**) is the first and most significant technique to trace long-memory patterns of $1/f$ processes as those of the processes of earthquakes.

5.2 Mathematical methods

5.2.1 Hurst exponent

As mentioned in **section 3.2.2**, the Hurst exponent (H) is a mathematical quantity, which can categorise the $1/f$ processes and especially the random and those presenting long-range dependencies in time or space (Hurst, 1951; Hurst, Black, & Simaiki,1965), i.e., those exhibiting hidden long-memory patterns. The Hurst exponent is a metric which can distinguish the parts of a time-series (if any) following the fractional Gaussian noise (fGn) class and those following the fractional Brownian motion (fBm) class (please see also **Chapter 3**). H can estimate the temporal smoothness of time-series and can search if the related phenomenon is a temporal fractal (Lopez, Martınez-Gonzalez, Manjarrez, Plascencia, & Balankin, 2009). Hurst exponent was initially conceptualised for hydrology (Hurst, 1951; Hurst, Black, & Simaiki, 1965). It has been employed however in other research topics as well, for example, in traffic traces (Dattatreya, 2005), plasma turbulence (Gilmore et al., 2002), ULF geomagnetic fields (Smirnova et al., 2004; Smirnova, & Hayakawa, 2007), climatic dynamics (Rehman, & Siddiqi, 2009), pre-epileptic seizures (Li et al., 2005; Lopez et al., 2009), astronomy and astrophysics (Kilcik et al., 2009), economy (Granero, Segovia, & Perez, 2008) and pre-seismic activity (e.g. Eftaxias et al., 2009; Nikolopoulos et al., 2014; Petraki, Nikolopoulos, Fotopoulos, Panagiotaras, Koulouras et al., 2013; Petraki, Nikolopoulos, Fotopoulos, Panagiotaras, Nomicos et al., 2013).

H -values between $0.5<H<1$ manifest long-term positive autocorrelation in time-series. This means that a high present value will be possibly followed by a high future

value and this tendency will last for long future time-periods (persistency) (Eftaxias et al., 2007, 2009; Kapiris, Eftaxias, & Chelidze, 2004; Kapiris et al., 2002, 2003, 2004, 2005). H -values between $0<H<0.5$ indicate time-series with long-term switching between high and low values. Namely, a high present value will be, possibly, followed by a low future value, whereas the next future value will be high and this switching will last long, into future (anti-persistency) (Eftaxias et al., 2007, 2009; Kapiris et al., 2002, 2003). $H=0.5$ implies completely uncorrelated time-series.

As will be analysed later, the Hurst exponents of several pre-seismic electromagnetic (EM) and radon disturbances were estimated through the analysis of the Rescaled Range (R/S) (Hurst, 1951; Hurst, Black, & Simaiki, 1965) and through the PSD Fractal analysis (the reader should refer to **Chapters 3** & **4** for the details of the latter method). To compare with the analysis of the R/S , the Hurst exponents of certain disturbances were also calculated, through the Roughness-Length (R-L) method and through Variogram (Lopez et al., 2009; Stratakos, & Sakellariou, 2006; Warwick, Stoker, & Meyer, 2007). For selected disturbances the fractal dimension was also derived from the values of the Hurst exponent.

In overview, the calculations of the R/S analysis were performed through equation

$$R/S=\frac{R(n)}{S(n)} \tag{5.1}$$

through equation

$$S(w)=A\cdot w^{H} \tag{5.2}$$

for the R-L method and through equation

$$2\gamma(x,h)=K\cdot h^{2\mathrm{H}} \tag{5.3}$$

for the Variogram. The symbols and the mathematical derivation of these equations will be given later. The H -values of the successive power-law fBm ($1<b<3$) parts (**Chapters 3 & 4**) of the electromagnetic or radon time-series, were calculated by considering that H and b are related by the formula (Eftaxias et al., 2009; Kapiris et al., 2002, 2003)

$$b=2\cdot H+1 \tag{5.4}$$

for the time-series parts following the fBm class ($1<b<3$) and by the formula (Buldyrev et al., 1995; Contoyiannis et al., 2005; Eftaxias, 2010)

$$b=2\cdot H-1 \tag{5.5}$$

for the time-series parts following the fractional Gaussian (fGn) class ($-1<b<1$) .

As will be presented later, a very robust technique for the investigation of fast-changing time-series signals (even non-stationary) is the Detrended Fluctuation Analysis (abbrv DFA) (e.g. Peng et al., 1992, 1993, 1994, 1995, 1998). This technique was also employed for the calculation of Hurst exponents. As will be shown later, the DFA is associated with an exponent α indicative of the long-memory of the investigated time-series. From this exponent α (the so called DFA exponent), the fractal exponent b of the PSD of the time-series can be calculated by the formula (e.g. Eftaxias et al., 2009;

Nikolopoulos et al., 2015; Petraki, Nikolopoulos, Fotopoulos, Panagiotaras, Koulouras et al., 2013)

$$b = 2 \cdot \alpha - 1 \tag{5.6}$$

both for the fBm and the fGn class. By the time-evolving fractal PSD exponent b of the electromagnetic or radon time-series data, the time-evolution of the Hurst exponent was calculated by utilising the relations $b = 2 \cdot H + 1$ and $b = 2 \cdot H - 1$.

In the following, details are presented regarding the performed calculations for the R/S and R-L analysis, the Variogram and the fractal dimension.

5.2.2 Rescaled Range (R/S) analysis

The R/S analysis was introduced by Hurst (1951) and attempts to find patterns that might repeat in the future. The method employs two variables, the range, R , and the standard deviation, S , of the data. According to the R/S method, a natural record in time, $X(N) = x(1), x(2), \ldots, x(N)$ is transformed into a new variable $y(n, N)$ in a certain time period $n (n = 1,2,\ldots, N)$ from the average

$$\langle x \rangle_N = \frac{1}{N} \sum_{n=1}^{N} x(n) \tag{5.7}$$

over a period of N time units (Hurst, 1951; Nikolopoulos et al., 2015; Petraki,

Nikolopoulos, Fotopoulos, Panagiotaras, Koulouras et al., 2013). $y(n,N)$ is called accumulated departure of the natural record in time (Hurst, 1951; Nikolopoulos et al., 2015; Petraki, Nikolopoulos, Fotopoulos, Panagiotaras, Koulouras et al., 2013). The transformation follows the formula:

$$y(n,N)=\sum_{i=1}^{n}(x(i)-\langle x\rangle_N) \tag{5.8}$$

The rescaled range R/S is calculated from (5.1) (Hurst, 1951; Eftaxias et al., 2009; López et al., 2009; Nikolopoulos et al., 2015; Petraki, Nikolopoulos, Fotopoulos, Panagiotaras, Koulouras et al., 2013; Stratakos, & Sakellariou, 2006; Wawszczak, 2004).

The range $R(n)$ in (5.1) is defined as the distance between the minimum and maximum value of $y(n,N)$ by :

$$R(n)=\max_{1\leq n\leq N} y(n,N)-\min_{1\leq n\leq N} y(n,N) \tag{5.9}$$

The standard deviation $S(n)$ in (5.1) is calculated by :

$$S(n)=\sqrt{\frac{1}{N}\sum_{n=1}^{N}(x(n)-\langle x\rangle_N)^2} \tag{5.10}$$

R/S is expected to show a power-law dependence on the bin size n

$$\frac{R(n)}{S(n)}=C\cdot n^H \tag{5.11}$$

where H is the Hurst exponent and C is a proportionality constant.

The $\log$ transformation of equation (5.11) is a linear relation

$$\log\left(\frac{R(n)}{S(n)}\right)=\log(C)+H\cdot\log(n) \tag{5.12}$$

from which exponent H can be estimated as the slope of the best line fit.

To employ the R/S analysis two different approaches were followed. These approaches were the sliding window technique and the lumping technique. To apply the sliding window technique the following four steps were followed (Nikolopoulos et al., 2015):

i. The signal was divided in segments-windows of certain size (number of samples).
ii. In each segment-window, R/S analysis was applied.
iii. In each segment, the least square fit was applied to the $\log\left(\frac{R(n)}{S(n)}\right)-\log(n)$ linear representation of equation (5.12). Successive representations were considered those exhibiting squares of Spearman's correlation coefficient above 0.95.
iv. The window was slid for one sample and steps (i)-(iii) were repeated until the end of the signal.

To apply the lumping technique, step (iv) was modified. Instead of the continuous sliding of one-sample per segment, the signal was lumped at the whole size of the segment, viz. the sliding step was set equal to the segment size.

It is very important to mention here that the sliding window technique for the R/S analysis, was employed in identical manner as of the one for the PSD fractal analysis

(the reader should refer to **Chapters 3** & **4** for this case). This was done to allow for the direct comparison between the Hurst exponents derived by the R/S analysis and those derived by the PSD fractal analysis method, according to the aforementioned relations $b=2\cdot H+1$ ($1<b<3$) and $b=2\cdot H-1$ ($-1<b<1$).

5.2.3 The Roughness-Length Method (R-L)

The R-L method is based on the Fractal Geometry concept which is used for the accurate calculation of the Hurst Exponent (Petraki, Nikolopoulos, Fotopoulos, Panagiotaras, Nomicos et al., 2013; Stratakos, & Sakellariou, 2006). The calculation of the Hurst exponent through the R-L method is performed by calculating the standard deviation $S(w)$ of the height values of a segment of length (w) of a self-affine profile by the formula (5.2) (López et al., 2009; Petraki, Nikolopoulos, Fotopoulos, Panagiotaras, Nomicos et al., 2013; Stratakos, & Sakellariou, 2006; Wawszczak, 2004).

In (5.2) A is a proportionality constant that describes the profile waviness amplitude and H is the Hurst exponent. $S(w)$ is calculated by

$$S(w)=\frac{1}{n_w}\cdot\sum_{i=1}^{n_w}\sqrt{\frac{1}{m_i-2}\sum_{j\in w_i}(z_j-\bar{z})^2} \tag{5.13}$$

where n_w is the total segment number of width w in which the profile is divided, m_i is the number of points included in each segment, z_j is the aperture of the

profile nodes from the best fitting line and $\bar{z}$ is the mean value of z_j in the segment w_i . Representing the pairs of $\{w, S(w)\}$ in a double logarithmic diagram, the Hurst exponent is calculated through a least square fit (Petraki, Nikolopoulos, Fotopoulos, Panagiotaras, Koulouras et al., 2013; Stratakos, & Sakellariou, 2006).

5.2.4 The Variogram

The Variogram, also known as variance of the increments (López et al., 2009), is the expected value of the squared difference between two Z values in a trace separated by a distance h i.e. the sample variogram $2\gamma(x,h)$ of a series $Z(x)$ is measured by the following equation (Kulatilake et al., 1998; López et al., 2009; Petraki, Nikolopoulos, Fotopoulos, Panagiotaras, Nomicos et al., 2013; Stratakos, & Sakellariou, 2006; Wawszczak, 2005)

$$2\gamma(x,h)=\frac{1}{M}\sum_{i=1}^{M}[Z(x_i)-Z(x_i+h)]^2 \tag{5.14}$$

where M is the total number of pairs of roughness heights of the profile that are spaced at a lag distance h .

The variogram $2\gamma(x,h)$ and the Hurst exponent H are related with the aforementioned equation (5.3) (Petraki, Nikolopoulos, Fotopoulos, Panagiotaras,

Nomicos et al., 2013) where K is a proportionality constant (Kulatilake et al., 1998). The slope of the linear fit of $\log(2\gamma(x,h))$ and $\log(h)$ equals $2\mathrm{H}$.

5.2.5 Detrended Fluctuation Analysis (DFA)

DFA is a very powerful method for detecting long-range power-law correlations in even non-stationary, noisy or randomised signals and sometimes of short data length (Chen, Ivanov, Hu, & Stanley, 2002; Hu, Ivanov, Chen, Carpena, & Stanley, 2001; Nikolopoulos et al., 2015; Peng et al., 1998, 1995, 1994, 1993; Petraki, Nikolopoulos, Fotopoulos, Panagiotaras, Koulouras et al., 2013; Sarlis, Skordas, & Varotsos, 2010; Varotsos, Sarlis, & Skordas, 2009, 2012; Xie, Wan, & Zhu, 2011). It is a modified root-mean-square analysis of a random walk based on the observation that a stationary time-series with long-range correlations can be integrated to form a self-similar process. Therefore, measurement of the self-similarity scaling exponent of the integrated series show the long-range correlation properties of the original time-series (Nikolopoulos et al., 2015; Peng et al., 1998; Petraki, Nikolopoulos, Fotopoulos, Panagiotaras, Koulouras et al., 2013; Xie, Wan, & Zhu, 2011). In short, the original time-series is integrated once; then the fluctuations $F(n)$ of the integrated signal are determined around the best linear fit in a time window of size n . The slope of the line relating $\log(F(n))-\log(n)$ determines the scaling exponent (self-similarity parameter) α . This line may display a deflection (crossover) at a certain time scale where the slope

abruptly changes. The interpretations of power-law scaling exponents and the crossovers are system dependent.

The DFA algorithm (e.g. Nikolopoulos et al., 2015; Petraki, Nikolopoulos, Fotopoulos, Panagiotaras, Koulouras et al., 2013) on an one-dimensional signal y_i ,($i=1,\ldots,N$), involves the following six steps:

(i) In the first step, the integrated profile is determined:

$$y(k)=\sum_{i=1}^{k}\left(y(i)-\langle y\rangle\right) \tag{5.15}$$

where <...> denotes the mean and k is the symbol of the different time scales.

(ii) The integrated signal, $y(k)$, is divided into non-overlapping bins of equal length , n .

(iii) In each bin of length n , $y(k)$ is fitted by using a polynomial function of order l, which represents the trend in that box. A linear fit is usually used. The y coordinate of the fit line in each box is denoted by $y_n(k)$.

(iv) The integrated signal $y(k)$ is detrended by subtracting the local trend, $y_n(k)$,

ineach box of duration n . The detrended signal $y_n^d(k)$ is hence calculated in each box as :

$$y_n^d(k)=y(k)-y_n(k) \tag{5.16}$$

(v) For a given bin size n , the root-mean-square (rms) fluctuations of this integrated and detrended signal is calculated as:

$$F(n)=\sqrt{\frac{1}{N}\sum_{k=1}^{N}\left\{y(k)-y_n(k)\right\}^2} \tag{5.17}$$

Hence, $F(n)$ represents the rms fluctuations of the detrended time-series $y_n^d(k)$.

(vi) The above is repeated for a broad range of scale box sizes (n) to provide a relationship between $F(n)$ and the box size n . In general $F(n)$ increases with the size of segment n . Then a logarithmic graph ($logF(n)$ vs $\log(n)$) is created. The linear dependence between the average root-mean square fluctuation $F(n)$ and the bin size n indicates the presence of long-lasting self-fluctuations:

$$F(n)\sim n^{\alpha} \tag{5.18}$$

the slope of the line, i.e., the scaling exponent α , quantifies the strength of the long-

range correlations in the time-series.

The DFA method was applied both in radon and electromagnetic signals. The DFA was applied by three different approaches: (a) the sliding-window technique; (b) the manual DFA fluctuation-bin plot technique; (c) the DFA scatter plot.

The sliding window technique followed similar steps as those of the sliding window fractal-analysis technique (**Chapters 3 & 4**). In specific, the following steps were followed (Nikolopoulos et al., 2015; Petraki, Nikolopoulos, Fotopoulos, Panagiotaras, Koulouras et al., 2013):

i. The signal was divided in segments-windows of certain size (number of samples).

ii. In each segment, the least square fit was applied to the $logF(n)$ vs $\log(n)$ linear representation of equation (5.18).

Depending on the bin size n cross-overs were automatically searched or not. In specific:

(a) If the segment size n was smaller than 3X1024 samples, no cross-over was searched. This was done because, as investigated thoroughly for such cases, the DFA fluctuation-bin plots do not exhibit cross-overs. Successive representations were considered those exhibiting squares of Spearman's correlation coefficient above 0.95.

(b) If the segment size n was larger than 3X1024 samples, a single cross-over was computationally searched. The cross-over was the one for which the slope exhibited the most abrupt change. Successive representations were

considered those exhibiting squares of Spearman's correlation coefficient above 0.95 in both slopes.

iii. The window was slid for one sample and steps (i)-(ii) were repeated until the end of the signal.

From the single DFA exponent a the spectral fractal exponent b are related with the formula

$$b=2\cdot\alpha-1 \tag{5.19}$$

both for fBm and fGn modelling (Buldyrev et al., 1995; Nikolopoulos et al., 2015; Petraki, Nikolopoulos, Fotopoulos, Panagiotaras, Koulouras et al., 2013). In the cases where two DFA exponents a_1 and a_2 were calculated, the spectral fractal exponent b was calculated from the exponent a_2 which corresponded to the long-range interactions, namely the slope for the large values of $\log(n)$ and $logF(n)$. Note, that due to the sliding window technique, the DFA exponent or exponents were also time evolving and hence the calculated spectral fractal exponents b (Petraki, Nikolopoulos, Fotopoulos, Panagiotaras, Koulouras et al., 2013). Then, from the calculated spectral fractal exponents b, the time evolution of the corresponding Hurst exponent was further calculated from the aforementioned relations $b=2\cdot H+1$ ($1<b<3$) and $b=2\cdot H-1$ ($-1<b<1$). It is very important that the sliding window DFA technique was applied in the identical time-series parts as those of the sliding window

R/S technique and the sliding window PSD fractal analysis (the reader should refer to **Chapters 3** & **4** for the latter case). This was done to allow the direct comparison between the Hurst exponents derived by DFA and those derived by the R/S analysis and the PSD fractal analysis method, according to aforementioned relations.

To apply the manual DFA fluctuation-bin plot technique, at first the time-series signal was subdivided in independent non-overlapping parts. Then in each part, a $\log(n)$ - $logF(n)$ plot was created. Depending on the plot, manually cross-over or cross-overs were identified. The latter is of high significance since there have been identified areas in DFA fluctuation-bin plots in electromagnetic time-series with two crossovers (please see Petraki, Nikolopoulos, Fotopoulos, Panagiotaras, Koulouras et al., 2013). Afterwards, the two slopes were calculated for a single cross-over or the three slopes for a double cross-over. Calculation was done in terms of linear fit under the constraint of exhibiting each slope the Spearman's square correlation coefficient above 0.95. Note that in this form DFA was initially introduced by Peng et al (1992) and utilised by several researchers as well (Chen et al., 2002; Hu et al., 2001; Eftaxias et al., 2009; Nikolopoulos et al., 2015; Petraki, Nikolopoulos, Fotopoulos, Panagiotaras, Koulouras et al., 2013; Sarlis et al., 2010; Varotsos et al., 2009, 2012).

The DFA scatter-plot was applied only to time-series parts which exhibited two cross-overs. To apply the techniques, two DFA exponents a_1 and a_2 were derived either

manually through the manual DFA fluctuation-bin plot technique or computationally from the sliding-window technique. Then these exponents a_1 and a_2 were plotted one against the other. This plot is considered of significance so as to identify differentiations in pre-seismic electromagnetic and radon time-series (please see Eftaxias et al., 2009, 2010; Nikolopoulos et al., 2014; Petraki, Nikolopoulos, Fotopoulos, Panagiotaras, Koulouras et al., 2013 and references therein). Note also that in this form DFA was also introduced by Peng et al (1993) and utilised by several researchers as well (Eftaxias et al., 2009; Petraki, Nikolopoulos, Fotopoulos, Panagiotaras, Koulouras et al., 2013).

5.2.6 Block entropy analysis

5.2.6.1 Symbolic dynamics and analysis blocks

Complex non-linear dynamical systems can be modelled and studied in the context of coarse-graining, i.e., they can viewed as information generators producing messages of discrete sets of symbols (e.g. Karamanos et al., 2006, 2005; Karamanos, 2001; Karamanos, & Nicolis, 1999; Nicolis, G., 1995; Nicolis, J.S., 1991). This process provides a rigorous way of looking at the real dynamics with finite precision by partitioning the full continuous phase space into a finite number of cells (Hao, 1991, 1989; Kitchens, 1998; Karamanos & Nicolis, 1999). This operational procedure is referred as symbolic dynamics (Eftaxias et al., 2009; Kalimeri et al., 2008; Karamanos et al., 2006; Karamanos & Nicolis, 1999; Nicolis, G., 1995; Nicolis, J.S., 1991). One of the merits of symbolic dynamics is that it provides a strong link between dynamical systems and information theory (Karamanos & Nicolis, 1999; Nicolis, G., 1995; Nicolis, J.S., 1991; Voss et al., 1996). Various implementations have been studied in

electromagnetic anomalies (Eftaxias et al., 2009; Karamanos et al., 2005), electrocardiograms (Karamanos et al., 2006) and solar spike events (Schwarz et al., 1993). According to symbolic dynamics (Eftaxias et al., 2009; Kalimeri et al., 2008; Karamanos et al., 2006, 2005; Karamanos, 2001; Karamanos & Nicolis, 1999), a time-series is reinitialised into a new symbolic sequence, where every symbol stands for a partition of the original time-series. Every different symbol is represented by an alphabet letter and the whole procedure is called lettering (Eftaxias et al., 2009; Kalimeri et al., 2008; Karamanos et al., 2006, 2005; Karamanos, 2001). From the generated symbol sequence, new sub-sequences can be constructed by proper grouping (Eftaxias et al., 2009; Kalimeri et al., 2008; Karamanos et al., 2006, 2005; Karamanos, 2001; Karamanos & Nicolis, 1999). These sub-sequences of symbols are called words (Karamanos et al., 2006, 2005; Karamanos, 2001). Reading of symbolic sub-sequences can be derived through the processes of lumping or gliding (Karamanos et al., 2006, 2005; Karamanos, 2001). Lumping is the interpretation of symbolic words through independent sequential discrete portions of certain number of words, as opposed to gliding where the portions are not independent (Karamanos et al., 2006, 2005; Karamanos, 2001). Note that gliding is the standard convention in literature and is often referred also as sliding or moving-frame (Karamanos et al., 2006, 2005; Karamanos, 2001). As an example of a $\lambda=2$ letter symbolisation, a threshold C may be considered for the purpose of lettering. Each value above this threshold may be symbolised by 1 and each below, by 0 (Karamanos et al., 2006, 2005; Karamanos, 2001). For example, initial time-series of length $L=20$ may be transformed through symbolic dynamics to a symbolic series as e.g. 11001010111000101010 for a $\lambda=2$

letter symbolisation. Through lumping the $\lambda=2$ letter symbolic time-series may be organised in sets of $n=2$ blocks, each block consisting of $N=2$ fixed-length words, namely as (11|00|10|10|11|10|00|10|10|10|). The same sequence through sliding for $\lambda=2$, $N=2$ and $n=2$ is transformed to (11|10|00|01|10|01|10|01|11|11|10|00|00|01|10|01|10|01|10|01|10), i.e., the sequence is of greater length. Wording of $N=2$ different letters produces $N_{max}=N_{2,2}=N^{\lambda}=2^2=4$ number of different words, i.e., (00, 01, 10, 11) (Karamanos et al., 2006, 2005; Karamanos, 2001). The sequence may be also organised in sets of $N=3$ words of $\lambda=2$ letters at a maximum of $N_{max}=N_{2,3}=N^{\lambda}=3^2=9$ number of different words, i.e., (000, 001, 010, 100, 110, 011, 010, 001, 111). Other sequences of words may also be generated. Note that rearrangement in blocks of size n , is independent of the word settlement of the fixed size N and $n\geq N$. However, n is frequently chosen equal to N and $N\geq\lambda$ (please see for the above e.g analysis in Eftaxias et al., 2009; Kalimeri et al., 2008; Karamanos et al., 2006, 2005; Karamanos, 2001). In general (Eftaxias et al., 2009; Kalimeri et al., 2008; Karamanos et al., 2006, 2005; Karamanos, 2001 and references therein), through symbolic dynamics a L-length time-series is transformed to a symbolic time-series sequence, $[A_1, A_2 \ldots A_n \ldots A_L]$, composed by λ different

letters, $[A^1, A^2 \ldots A^\lambda]$, from a λ -length alphabet. Symbolic time-series sequences can be organised as words composed by the alphabet $[A^1, A^2 \ldots A^\lambda]$. In linguistics the words contain some of the letters, all letters, or any letter combination. However, in symbolic dynamics fixed word lengths of N , $N \geq \lambda$ are chosen and the number of different fixed-sized words is $N_{max} = N_{\lambda, N} = N^\lambda$ for the alphabet $[A^1, A^2 \ldots A^\lambda]$. Each different word is hence a N fixed-size sub-sequence of the symbolic time-series which is produced by some of the λ different letters $[A^1, A^2 \ldots A^\lambda]$. The symbolic words can be further organised through lumping or sliding in portions of length n , $n \geq N$ called word blocks or blocks, however usually $n = N$ is chosen. This means that depending on the reading process, n discrete blocks of a N fixed-size words are produced, $n \geq N$. In this manner, the symbolic time-series is reorganised as $\ldots \underbrace{A_1 \ldots A_n}_{B_1} \underbrace{A_{n+1} \ldots A_{2n}}_{B_2} \ldots \underbrace{A_{jn+1} \ldots A_{(j+1)n}}_{B_{i+1}} \ldots$ blocks, where i is the consecutive number of the block, i.e., $i = 1 \ldots Total\ number\ of\ blocks$ and j points inside each letter of the symbolic time-series. If lumping is employed the n blocks are sequentially

independent on the contrary to the dependent sequential blocks in the sliding process. The total number of blocks of the symbolic time-series is greater for sliding and hence more computations are needed. The probability of occurrence of a block, $[A_1, A_2 \ldots A_n]$, of size n is calculated by

$$p^{(n)}(A_1, A_2 \ldots A_n) = \frac{Number\ of\ occurences\ of\ block\ [A_1, A_2 \ldots A_n]}{Total\ number\ of\ blocks} \qquad (5.20)$$

Note that if $n = N$, the size of the word blocks coincides with the length of the words, i.e., the organisation in blocks and words renders identical results. Continuing and in text, the rule $n = N$ is followed.

5.2.6.2 Metrics of block entropy

5.2.6.2.1 Shannon block entropy

In the framework of complex signal analysis, specific entropy methodologies based on symbolic dynamics have been developed in the previous decade (Nicolis & Gaspard, 1994; Ebeling & Nicolis, 1991, 1992; Ebeling, 1997; Karamanos, 2001, 2000). All these methodologies are referred as block entropies. Most common techniques rely on the extension of Shannon entropy (Shannon, 1948)

$$H_S = -\sum p_i \ln p_i \qquad (5.21)$$

where p_i is the number of possible microscopic configurations. Note that equation

(5.21) represents the classical Boltzman's entropy for the Gibbs canonical ensemble (B-G entropy) (Kalimeri et al., 2008). Combining equations (5.20) and (5.21), the Shannon block entropy, $H(n)$ of n - sized blocks is derived by:

$$H(n)=-\sum_i p^{(n)}(A_1, A_2, \ldots A_n)\, lnp^{(n)}(A_1, A_2, \ldots A_n) \tag{5.22}$$

Note that the rule $n=N$ is followed in (5.22). Equation (5.22) calculates the entropy due to all possible words since $N=n$. It is a measure of uncertainty or disorder i.e., it measures organisation deficiency of a complex system. It also gives the average amount of information necessary to predict a sub-sequence of words or blocks of length $N=n$.

5.2.6.2.2 Shannon block entropy per letter

From equation (5.22), the Shannon block entropy per letter may be derived by:

$$h^{(n)}=\frac{H(n)}{n}=\frac{-\sum_i p^n(A_1, A_2, \ldots A_n)\, lnp^n(A_1, A_2, \ldots A_n)}{n} \tag{5.23}$$

This entropy may be interpreted as the average uncertainty of a block of size $n=N$ per letter (Eftaxias et al, 2009).

5.2.6.2.3 Conditional block entropy

From the Shannon block entropy the conditional entropy may be derived by equation (5.24):

$$h_{(n)} = H(n+1) - H(n) \tag{5.24}$$

The conditional entropy $h_{(n)}$ measures the uncertainty of predicting a state one step into the future, provided a history of the preceding n states (Eftaxias et al, 2009).

5.2.6.2.4 Tsallis block entropy

For physical phenomena with long-range interactions or long-range memory effects, an important property observed is the violation of Boltzmann-Gibbs (B-G) statistics (Contoyiannis & Eftaxias, 2008). A generalised expression of the B-G statistics has been proposed based on multi-fractal concepts by Tsallis (1988):

$$S_q = k\frac{1}{q-1}\left(1 - \sum_{i=1}^{W} p_i^q\right) \tag{5.25}$$

where p_i are the probabilities of a sequence, W is their total number, k is the Boltzmann's constant and q is a real number which is the measure of non-extensivity of the system (Eftaxias et al, 2009).

Using $p_i^{(q-1)} = e^{(q-1)\ln(p_i)} \sim 1 + (q-1)\ln(p_i)$ in the limit $q \to 1$ the B-G entropy is derived (Eftaxias et al, 2009, Kalimeri et al., 2008). The generalization of B-G expression, suggests the non-extensive statistical mechanics. The entropic index q characterizes the degree of non-additivity in the following pseudo-additivity rule (Eftaxias et al, 2009, Kalimeri et al., 2008):

$$S_q(A,B)=S_q(A)+S_q(B)+(1-q)\,S_q(A)\,S_q(B) \tag{5.26}$$

with $q>1$ refers to sub-additivity and $q<1$ to super-additivity. Systems that called non-extensive, have special probability correlations and extensivity may occur for S_q for specific value of index q (Boon & Tsallis, 2005).

Tsallis entropy has been used in terms of symbolic dynamics for electromagnetic time series for the detection of pre-seismic emissions (Eftaxias et al, 2009, Kalimeri et al., 2008). The Tsallis entropy of a block $[A_1, A_2 \ldots A_n]$ of length L in a λ -letter alphabet is given by (Eftaxias et al, 2009, Kalimeri et al., 2008)

$$S_q(n)=k\frac{1}{q-1}(1-\sum_i [\,p(n)(A_1, A_2 \ldots A_n)]^q) \tag{5.27}$$

where $p(n)(A_1, A_2 \ldots A_L)$ is the probability of occurrence of block $[A_1, A_2 \ldots A_n]$.

As already mentioned, high level of organization is indicated when low values of entropy (Tsallis entropy) are produced.

Tsallis entropy has been explored in the field of earthquake time series analysis (Contoyiannis & Eftaxias, 2008; Eftaxias, 2010; Eftaxias et al., 2009; Kallimeri et al., 2008; Zunino et al., 2008). Recent work has also been published in biomedical imaging, with suggestions in replacing Shannon's theorem (Mohanalin et al., 2010) and in bioinformatics (Lopes, 2011). An interconnection between fractals and Tsallis entropy that has been introduced in previous decade could provide natural frame for studying fractally structured systems (Alemany & Zanette, 1994). Moreover a possible

interconnection could exist between generalized Tsallis statistics and quantum groups (Tsallis, 1994).

5.2.6.2.5 Normalised Tsallis block entropy

The formula for the computation of the normalised Tsallis entropy is the following (Suyari, 2002):

$$\hat{S}_q(p_1,\dots,p_n)=\frac{k\frac{1}{q-1}(1-\sum_{i=1}^{W}p_i^q)}{\sum_{j=1}^{n}p_i^q} \tag{5.28}$$

where $p_i=p(n)(A_1, A_2 \dots A_n)$ is the probability of occurrence of the i - block $[A_1, A_2 \dots A_n]$, W is their total number, k is the Boltzmann's constant and q is the corresponding real number of equation (5.25). As it can be observed it derives directly from Tsallis entropy.

The appropriate choice of the entropic index q has crucial meaning for the Tsallis entropy computation and requires further exploration for its proper use (Balasis, 2008; Naudts, 2002). For every specific use of Tsallis entropy the ranges of the q values will result in significant discrimination (Abe & Okamoto, 2001; Tsallis, 1998). Non-additive Tsallis entropy combined with Gutenberg – Richter law provided excellent fit to seismicities with q -values range from 1.4 to 1.85. The q - values are rooted in a rather solid physical background and describe the non-additivity of a seismic emission in a correct manner (Kalimeri et al., 2008 ; Solotongo et al., 2004; Vilar et al.,

2007). Moreover index q can be consider as bias parameter with $q<1$ refers to rare events and $q>1$ refers to prominent events (Zunino et al., 2008). For pre-earthquake electromagnetic disturbances, the q -values are restricted in the region $1<q<2$, and are consistent with several studies that suggest the upper limit to be equal to 2 (Kalimeri et al., 2008). It is noteworthy that entropic index q is not a measure of complexity but measures the non-extensivity of the system (Eftaxias et al., 2009).

5.3 Results based on the analysis of Hurst exponents

The reliable estimation of the Hurst exponents in segmented portions or in the whole of the electromagnetic or the radon time-series (**Chapters 3** & **4**) should, in principle, include the different views expressed by the different methods of the calculation of H . The combined use of different methods advances the calculation and enables the correct identification of the segments that exhibit long-memory. The identification prerequisites the correct class-labelling of the segments that are used both, through the direct H -calculating techniques (R/S , R-L and Variogram, **section 5.2),** as well as through those that are indirect (spectral fractal analysis-**Chapters 3** & **4**, detrended fluctuation analysis (DFA)-**section 5.2**). The main goal is to find a reliable criterion to label the electromagnetic and radon segments that are afterwards used for the precise

classification of the long-lasting pre-earthquake signs, as well as the correct evaluation of these. For this scenario two classes are needed. Class I (prominent successive fBm class) consists of electromagnetic or radon time-series segments that are deemed as significant or of some earthquake precursory value. Class II (not prominent fBm or non-fBm class) consists of electromagnetic or radon time-series segments that are deemed as insignificant or of no earthquake precursory value. Apparently, Class II electromagnetic or radon time-series segments are the complement of Class I segments. Two of the long-memory analysis methods described previously, have been evaluated as of higher discrimination significance (Cantzos et al., 2015) and for this reason they will be employed here mainly. In the following, the spectral fractal and R/S analysis methods, are combined in terms of their common output, the Hurst exponent, in order to establish a criterion for separating the electromagnetic or radon time-series segments into significant or insignificant entities.

At first, the spectral fractal-analysis method is employed as the standard method for detecting prominent (successive, $r^2 \geq 0.95$) fractal-exhibiting fBm ($1<b<3$) segments in data. For the correct classification the segments are searched to identify those exhibiting strong fractal behaviour (blue segments, fractal analysis plots, **Chapters 3** & **4**), given by Spearman's correlation coefficient *r* with values $r^2 \geq 0.95$.

A second screening is applied on the segments with $r^2 \geq 0.95$ to find the ones with b-exponents in the range $1<b<3$ which indicates fBm behaviour (both indicate

finally the prominent fractal-exhibiting fBm-segments, **Chapters 3** & **4**). The R/S method is then applied on the successive (prominent) fBm segments and on the remaining segments in order to further refine the fBm tracking process, in terms of analysis of Hurst exponents. As it is shown later in the results, the Hurst exponents of the segments with $r^2 \geq 0.95$ and $1<b<3$ (successive-prominent fBm segments) are generally higher as compared to the Hurst exponents of the fBm segments with $r^2<0.95$ and $1<b<3$ (non-successive fBm segments) or the segments with $b \notin (1, 3)$ (non-fBm segments). Under this observation, a minimum threshold operator can also be applied on all the EM segments as a multiple of the mean Hurst exponent value *M* of the total of non-fBm and non-successive fBm segments in order to isolate the successive fractal fBm segments with high Hurst exponents (e.g Cantzos et al., 2015). Hence, the following definitions are employed in terms of application of the R/S analysis after the spectral fractal analysis (further refinement):

(I) Class I segments as the successive fractal fBm segments ($r^2 \geq 0.95$ and $1<b<3$) with H above the threshold (mean H of class II).

(II) Class II segments as the successive fBm segments with H below the threshold and also all the remaining (cases of non-successive fBm segments viz., with $r^2<0.95$ and $1<b<3$ and cases of non-fbm segments, viz. with

$b \notin (1, 3)$).

The overall procedure is presented in the form of a flowchart in **Figure 5.1**.

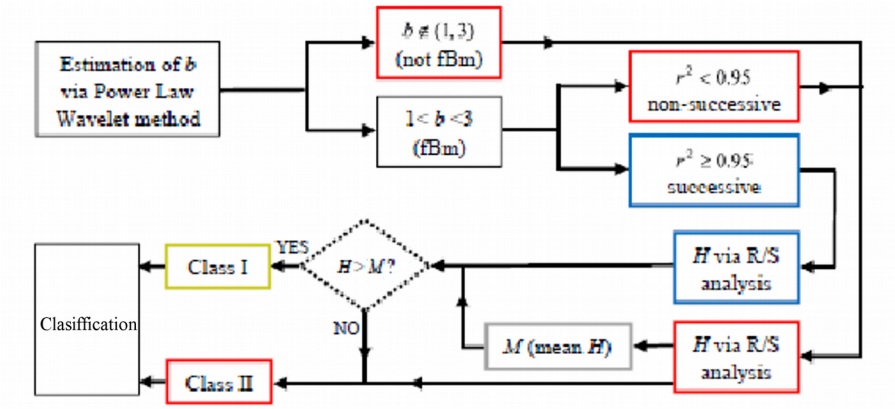

Figure 5.1: Structure of the overall algorithm for the combined use of the spectral fractal method (Power Law Wavelet Method) and the R/S analysis.

The following figures present some characteristic results based on the R/S analysis.

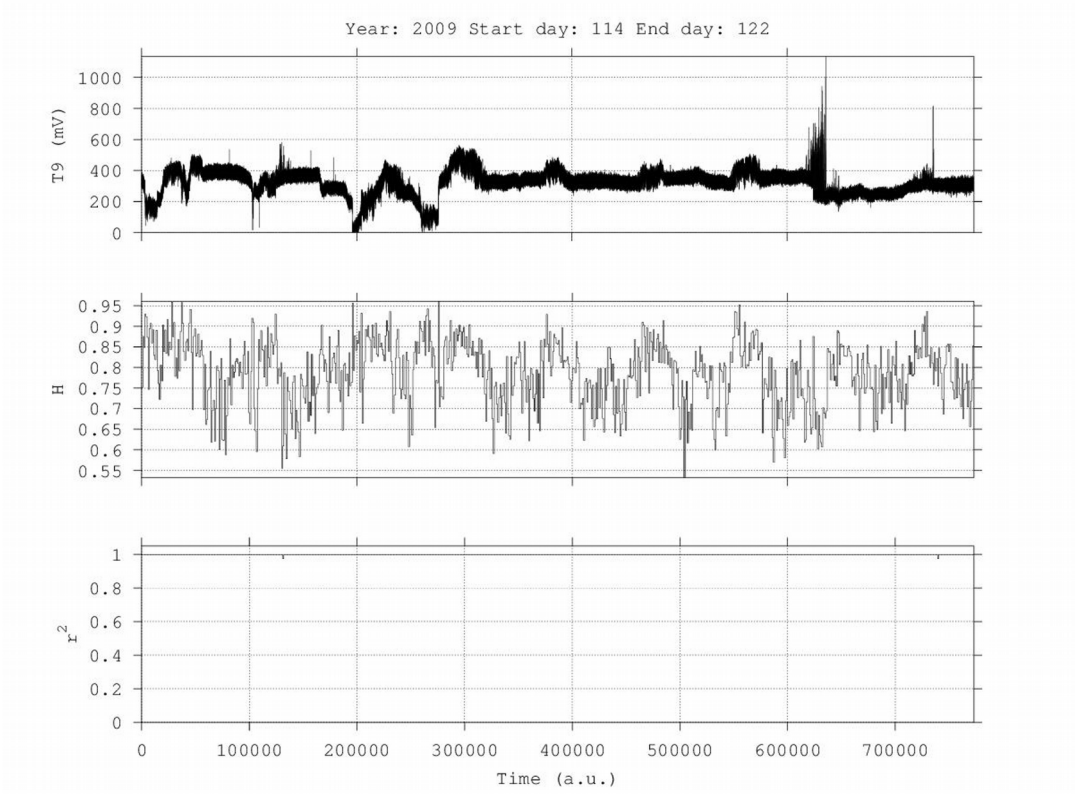

Figure 5.2: Time evolution of Hurst exponent. Calculation through sliding-window R/S analysis. EQ:25, **Table 3.2**, **Chapter 3**, Komotini station, JDs 114-122, 2009, 41 MHz. Time in seconds (a.u.).

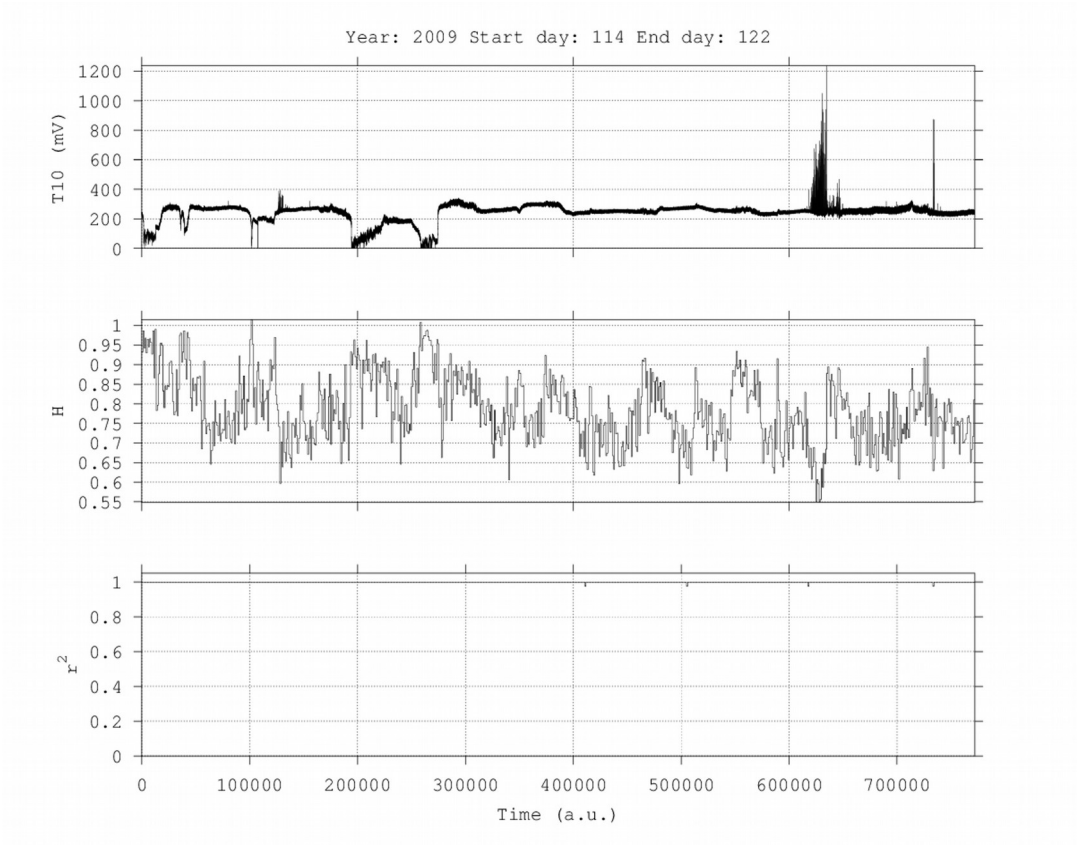

Figure 5.3: Time evolution of Hurst exponent. Calculation through sliding-window R/S analysis. EQ:25, **Table 3.2**, **Chapter 3**, Komotini station, JDs 114-122, 2009, 46 MHz. Time in seconds (a.u.).

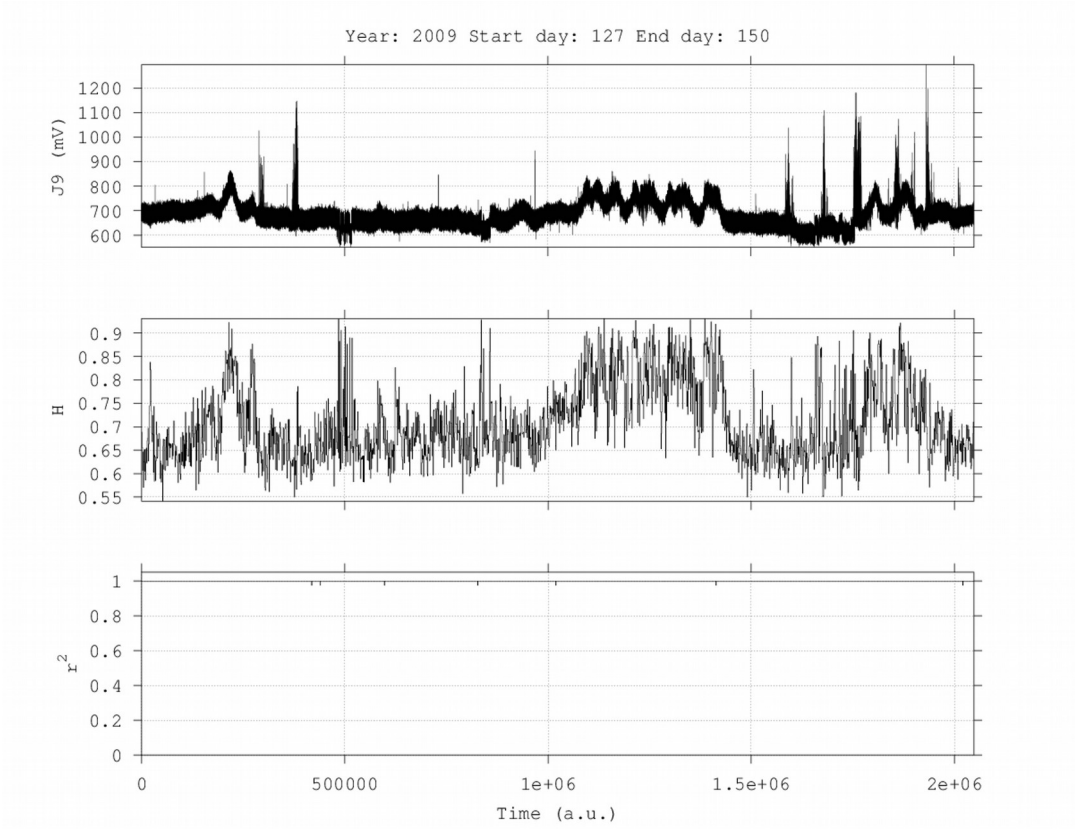

Figure 5.4: Time evolution of Hurst exponent. Calculation through sliding-window R/S analysis. EQ:30, **Table 3.2**, **Chapter 3**, Ioannina station, JDs 127-150, 2009, 41 MHz. Time in seconds (a.u.).

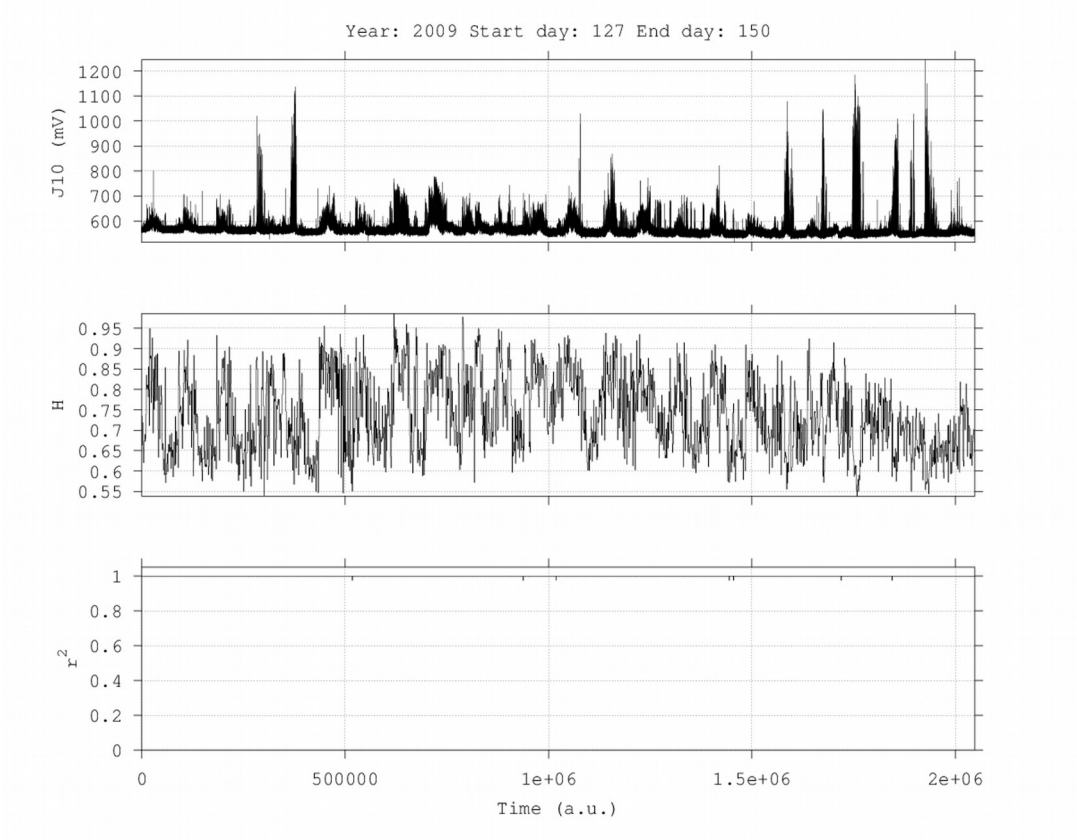

Figure 5.5: Time evolution of Hurst exponent. Calculation through sliding-window R/S analysis. EQ:30, **Table 3.2**, **Chapter 3**, Ioannina station, JDs 127-150, 2009, 46 MHz. Time in seconds (a.u.).

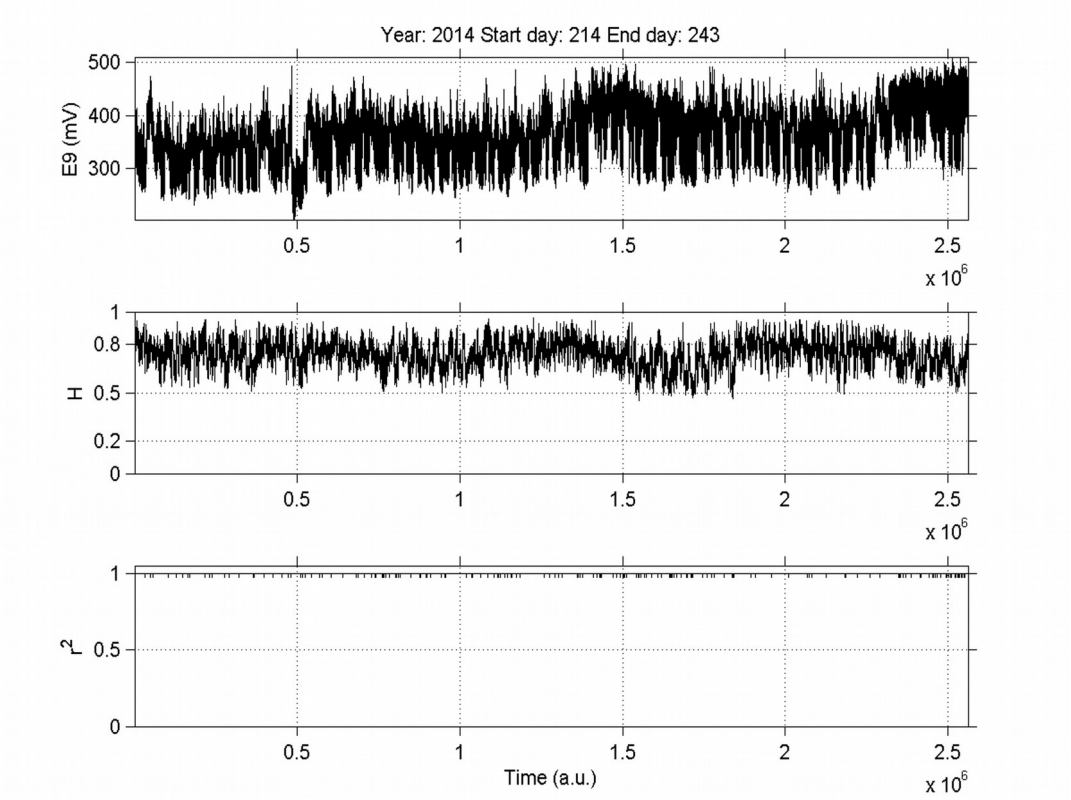

Figure 5.6: Time evolution of Hurst exponent. Calculation through sliding-window R/S analysis. EQ:12, **Table 3.2**, **Chapter 3**, Neapoli station, JDs 214-243, 2014, 41 MHz. Time in seconds (a.u.).

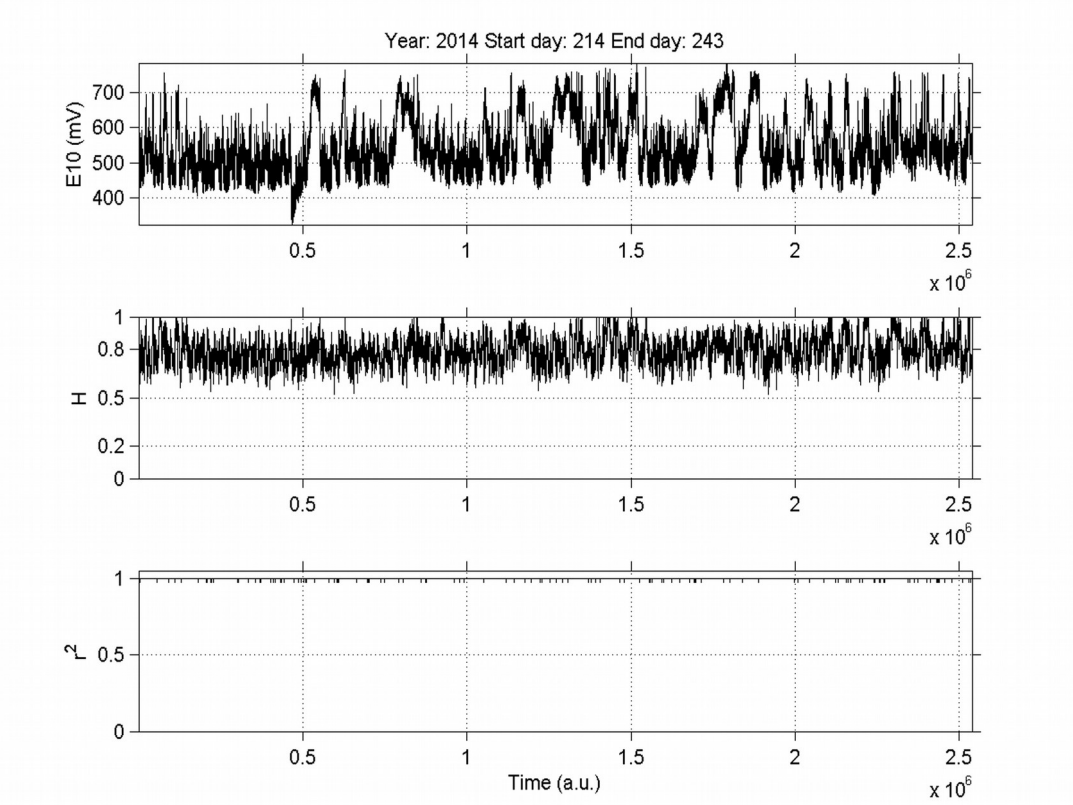

Figure 5.7: Time evolution of Hurst exponent. Calculation through sliding-window R/S analysis. EQ:12, **Table 3.2**, **Chapter 3**, Neapoli station, JDs 214-243, 2014, 46 MHz. Time in seconds (a.u.).

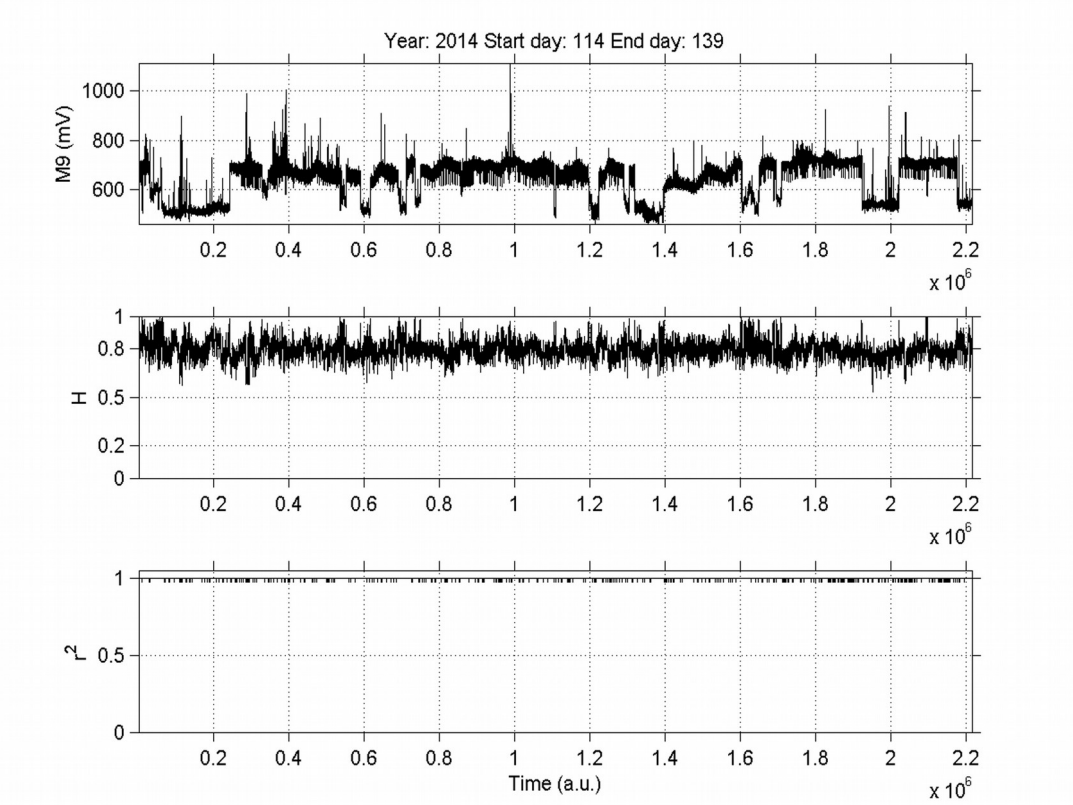

Figure 5.8: Time evolution of Hurst exponent. Calculation through sliding-window R/S analysis. EQ:1, **Table 3.2**, **Chapter 3**, Mytilene station, JDs 114-139, 2014, 41 MHz. Time in seconds (a.u.).

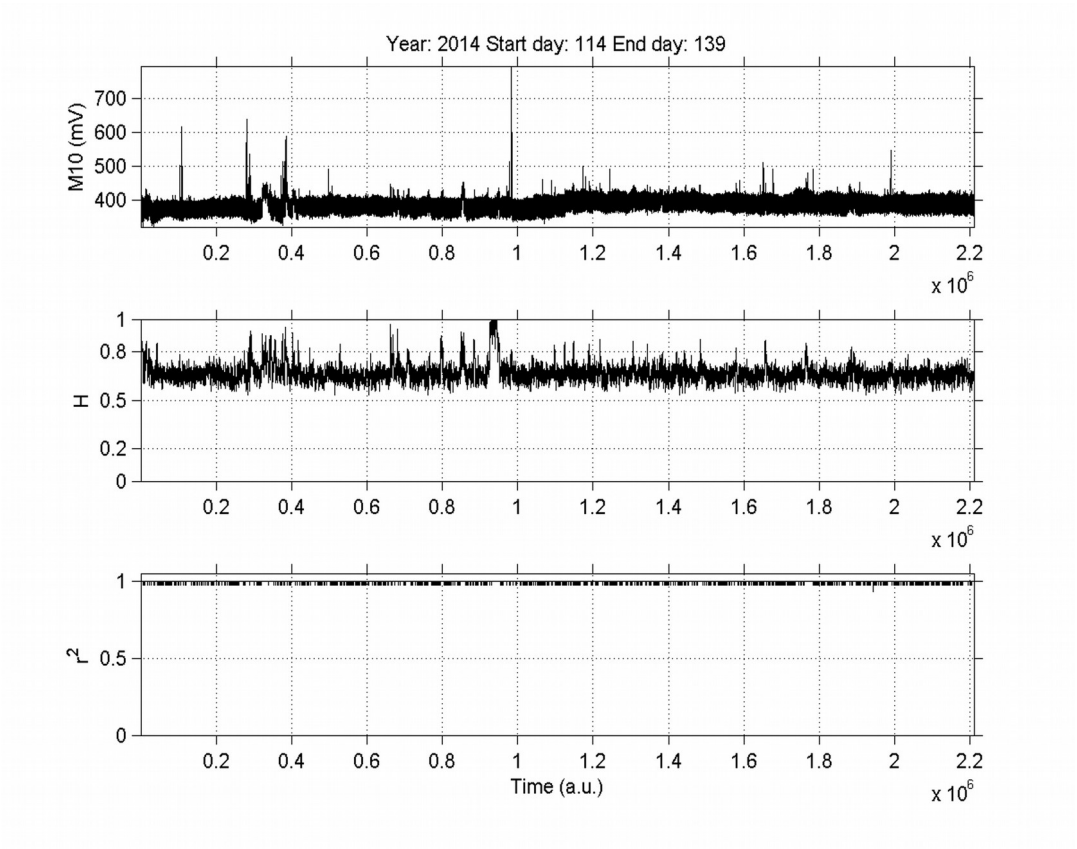

Figure 5.9: Time evolution of Hurst exponent. Calculation through sliding-window R/S analysis. EQ:1, **Table 3.2**, **Chapter 3**, Mytilene station, JDs 114-139, 2014, 46 MHz. Time in seconds (a.u.).

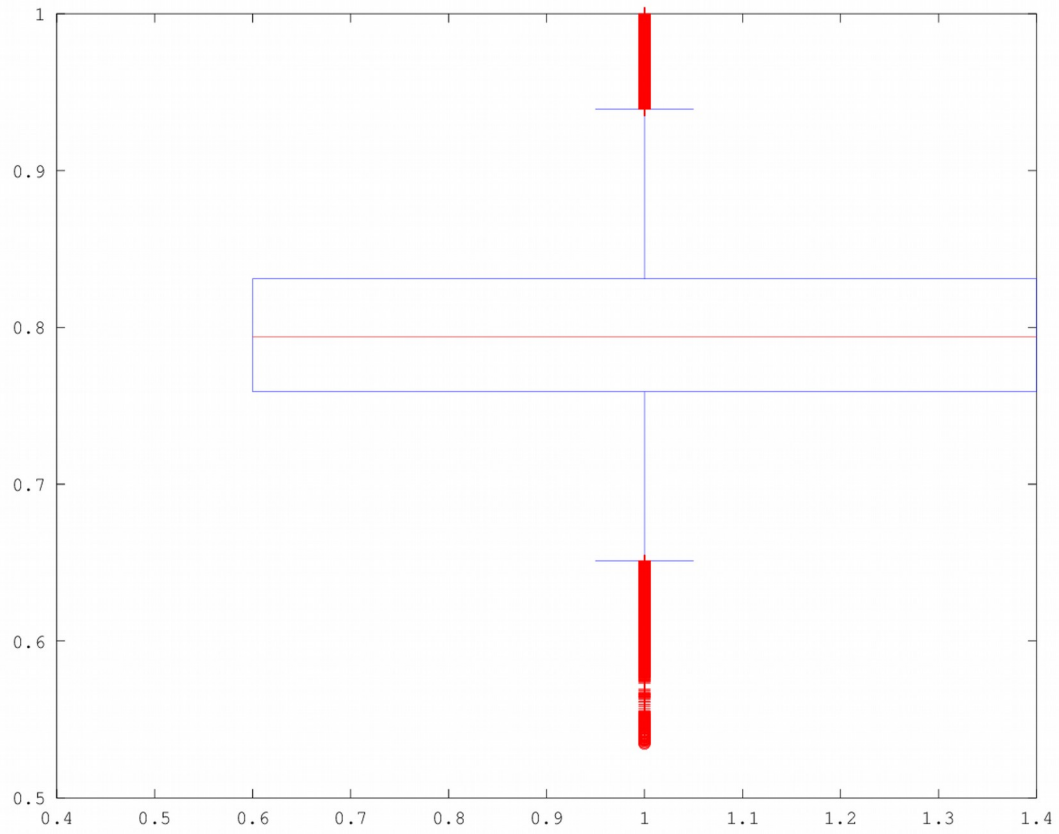

Figure 5.10: Box and whiskers plot of the time evolution of the Hurst exponent. Calculation through R/S analysis. EQ:1, **Table 3.2**, **Chapter 3**, Mytilene station, JDs 114-139, 2014, 41 MHz. Data from **Figure 5.8**.

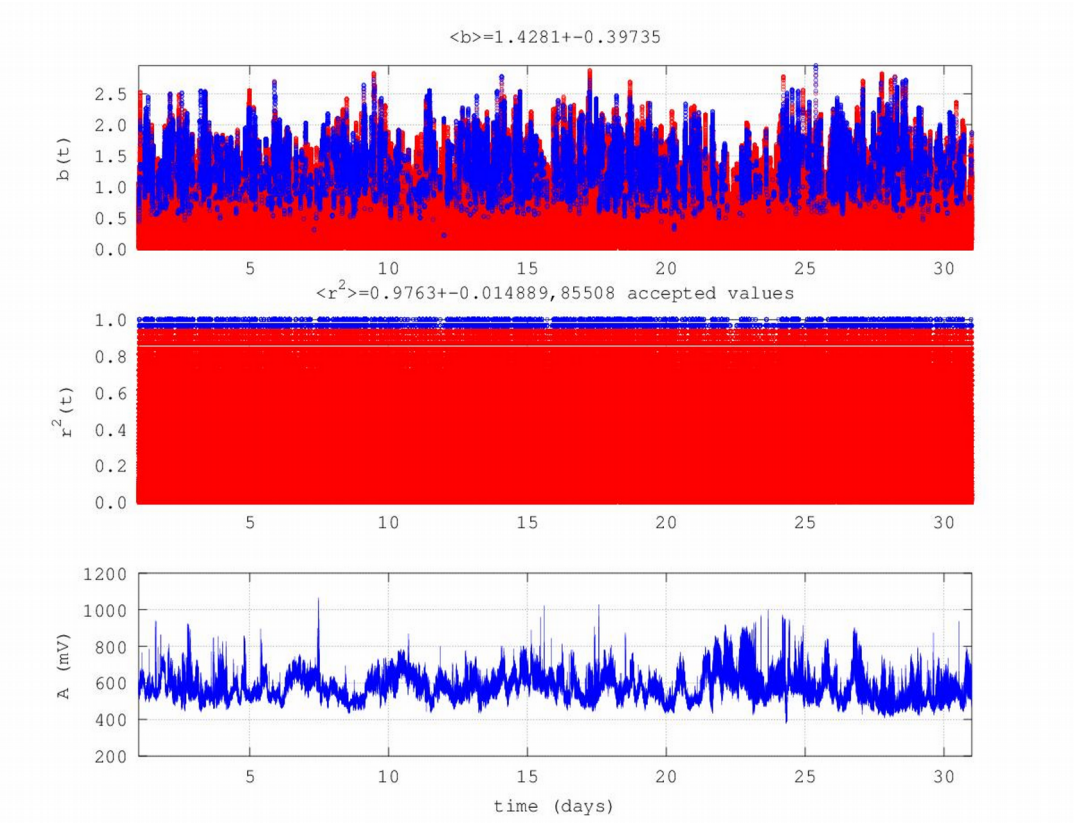

Figure 5.11: Time evolution of the power-law b exponent. Calculation through R/S analysis. EQ:11, **Table 3.2**, **Chapter 3**, Neapoli station, JDs 152-182, 2009, 41 MHz.

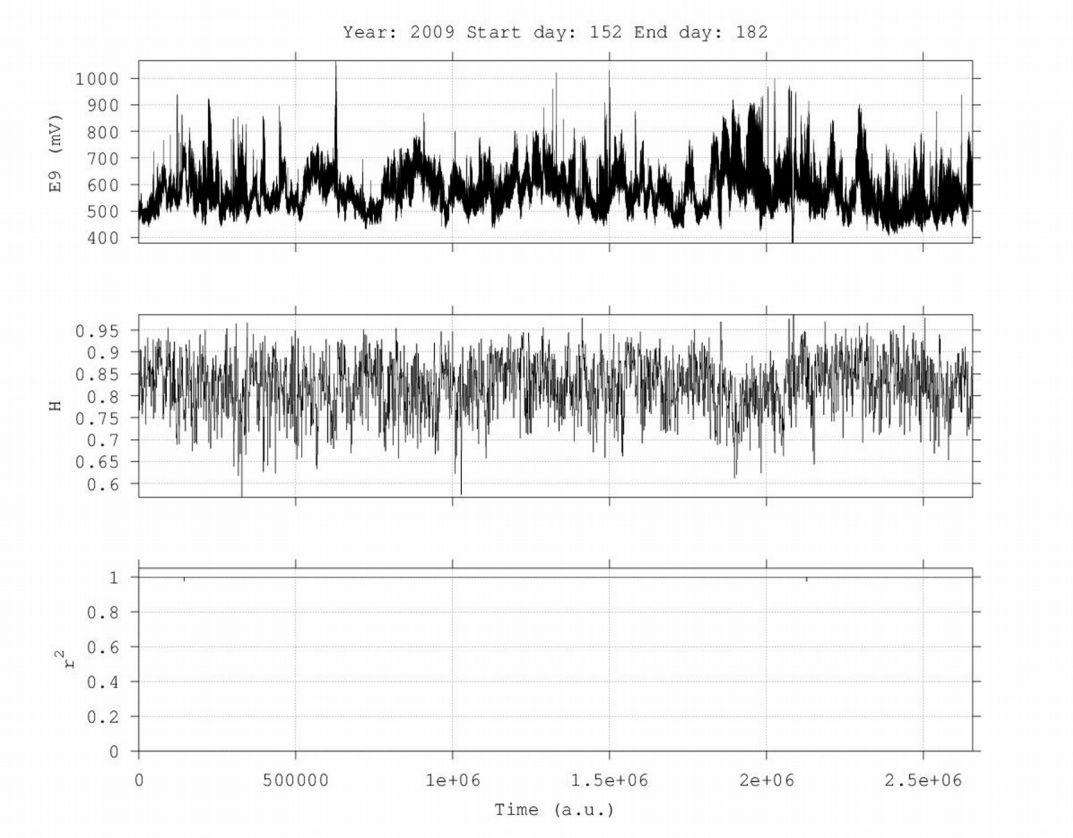

Figure 5.12: Time evolution of Hurst exponent. Calculation through sliding-window R/S analysis. EQ:11, **Table 3.2**, **Chapter 3**, Neapoli station, JDs 152-182, 2009, 41 MHz. Time in seconds (a.u.). Hurst analysis of the signal of **Figure 3.17**.

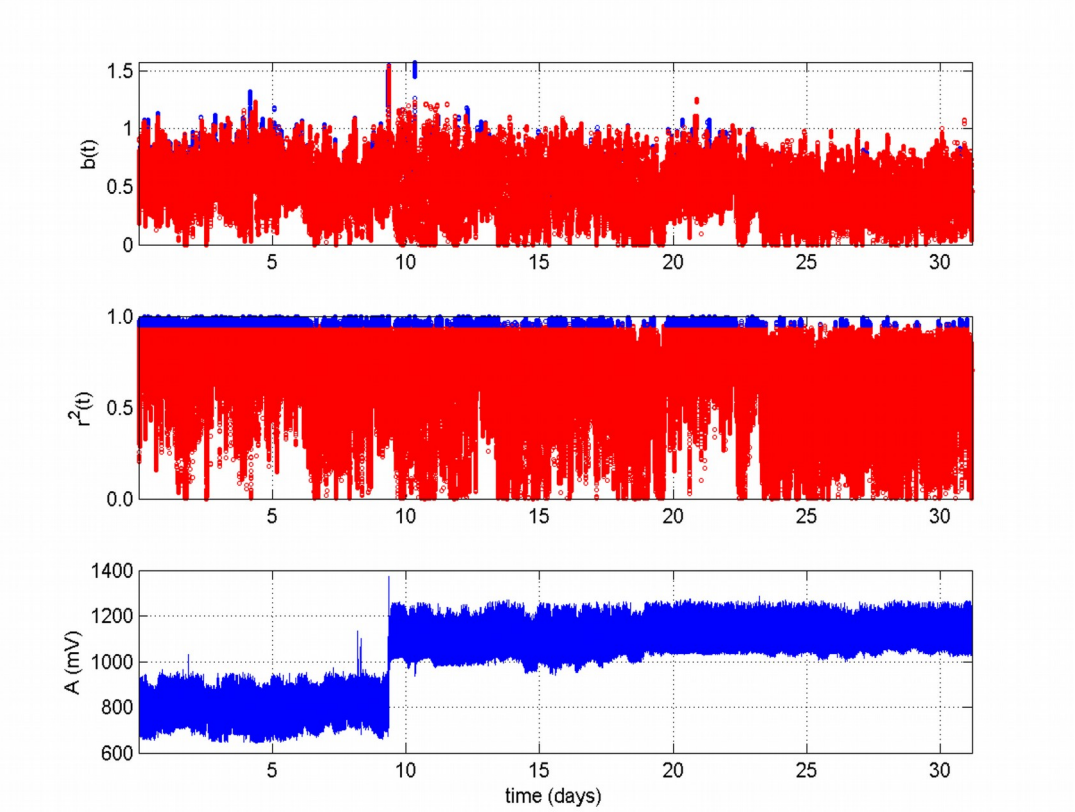

Figure 5.13: Time evolution of the power-law b exponent. Calculation through R/S analysis. EQ:29, **Table 3.2**, **Chapter 3**, Ioannina station, JDs 210-241, 2014, 41 MHz.

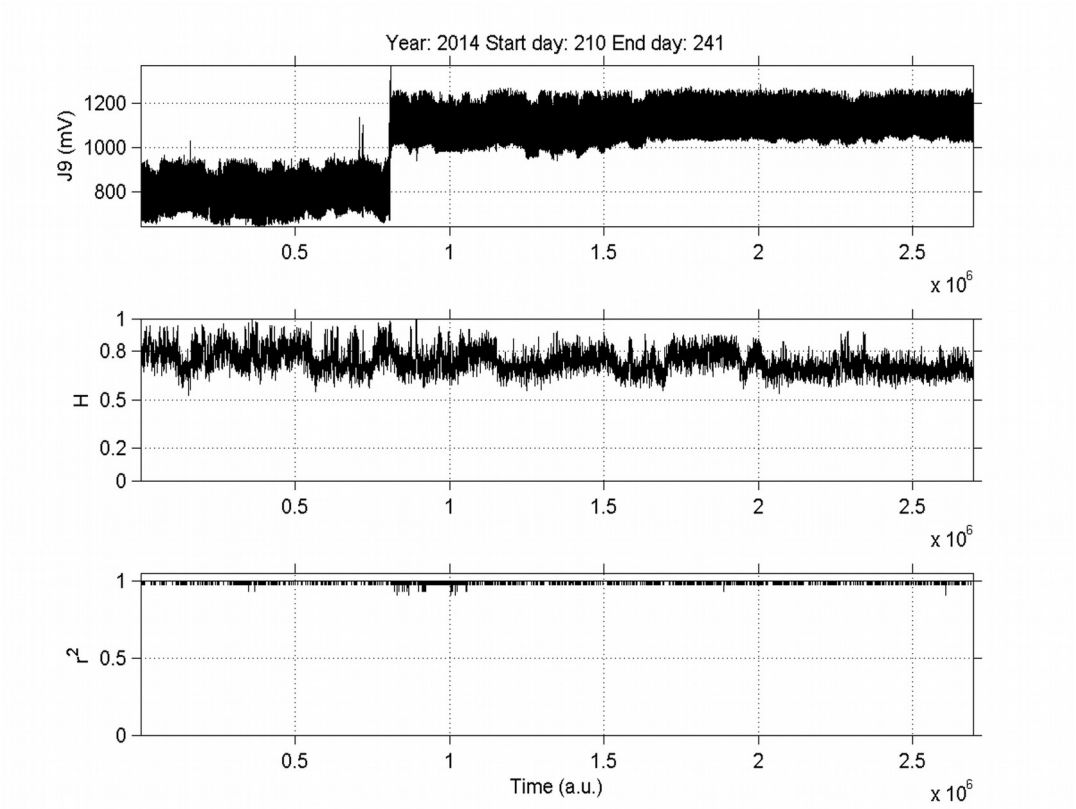

Figure 5.14: Time evolution of Hurst exponent. Calculation through sliding-window R/S analysis. EQ:29, **Table 3.2**, **Chapter 3**, Ioannina station, JDs 210-241, 2014, 41 MHz. Time in seconds (a.u.).

In reference to the **Figures 5.2-5.14** the following issues are of significance:

(a) Persistent Hurst exponents were calculated through the R/S analysis for the pre-earthquake MHz electromagnetic disturbances. Many H - exponents were in the range 0.7-0.9. Several exponents were above 0.9. This is characteristically shown in the Box and Whiskers plot of **Figure 5.10**. The whole issue is of

extreme importance and will be emphasised next.

(b) There were cases where the time-evolution of the Hurst exponent did not follow the one of the electromagnetic disturbances. Characteristic cases are shown in **Figures 5.5**, **5.7** and **5.8.** The latter figure (**5.8**) shows this behaviour more characteristically.

(c) In numerous cases, the detected MHz electromagnetic disturbances were associated with increase in the Hurst exponent. For example this is observed between $0.3\times10^{8}-0.5\times10^{8}\,s$ and $0.9\times10^{8}-1.0\times10^{8}\,s$ in **Figure 5.9**. Another characteristic case is shown in **Figure 5.6**. In this figure the Hurst exponents follow, more or less, the electromagnetic disturbances after $1.0\times10^{6}\,s$. The most characteristic case is shown in **Figure 5.4**.

(d) In most of the cases, the time profile of the Hurst exponent exhibits small bias. This is the example case of **Figure 5.8**. In other cases, the Hurst exponents presented noteworthy deviations. Such are the cases shown in **Figures 5.2**, **5.5** and **5.6**.

(e) The persistent behaviour of the Hurst exponent is identified, independent of the fractal behaviour of the signal (**Chapters 3** & **4**). This is characteristically shown in **Figures 5.12** and **5.14**. In **Figure 5.11** there are many successive ($r^{2}\geq0.95$) fBm ($1<b<3$) segments and the associated Hurst profile (**Figure 5.12**) is persistent. On the contrary, in **Figure 5.13** there are many not-

successive ($r^2<0.95$) segments and/or not-fBm ($b\notin(1-3)$) segments (see also **Figure 5.1**), whereas the associated Hurst profile (**Figure 5.14**) is again persistent. The issue is related to comment (a) above and is also of extreme importance. For this reason it will be emphasised as well.

(f) Some H -values were above 1. This contradicts to the theory (**section 3.2**, **Chapter 3**). To the opinion of the author, this is due to the statistical errors in estimations of the H -values. Indeed, in order to calculate the Hurst exponent, a least square fit is applied in the $\log(R)$ versus $\log(S)$ diagram (see also **section 5.2.1**). In the ± 99 % estimation of the corresponding slope, the H -values above 1 are mainly of statistical nature. The statistical errors were not presented in **Figures 5.2-5.14** for consistency.

The comments (a) and (f) contradict to some findings in the related literature regarding the MHz electromagnetic disturbances (see **Chapter 1** and e.g. Eftaxias, 2010; Eftaxias et al., 2008, 2009, 2010 and references in these publications). According to these publications, the MHz disturbances show anti-persistent behaviour in contrary to the kHz radiation which exhibits persistent fBm profiles (see for example Eftaxias et al., 2008 and references therein). The persistent behaviour of the kHz radiation has been interpreted, in these publications, as a footprint for the inevitable occurrence of an earthquake. The interpretations, however, were based, as mentioned, only on some kHz and MHz disturbances. Moreover, although the kHz radiation was associated to certain earthquakes (see **Chapter 1**), the same publications, as well as others (see also

Chapter 1), mention that there is no one-to one correspondence between earthquakes and anomalies. Most important however, is that the discussion of the Hurst exponent in these publications, was based mainly on the fractal-analysis of the signals and the aforementioned relations ($b=2\cdot H+1$ for the fBm class and $b=2\cdot H-1$ for the fGn class) which correlate H and b (see also **section 3.2**). Even in cases where two or three techniques were employed (see Eftaxias et al., 2009, 2010 and references therein), the reports did not provide indications on the segments of application of the techniques, nor the detailed manner of application. Indeed if one calculates Hurst exponents from the power-law b -exponents of the fractal-analysis method (through the above relations), then for certain segments, anti-persistent H -profiles are calculated. In the consensus of the above publications, a similar approach has been adopted previously in publications of the author (e.g. Nikolopoulos et al., 2012, 2014; Petraki, Nikolopoulos, Fotopoulos, Koulouras, et al., 2013 and references therein). However, very recent (2015) findings of the authors and colleagues (see Cantzos et al., 2015), indicated that the whole issue should be reconsidered. Indeed, the above publication reported very high percentage of reproduction of MHz signals of one-month duration through Support Vector Machine (SVM) classifiers, both in its fBm and fGn segments. To the author, this is another viewpoint of the certain fact shown here; both the fBm parts (e.g. **Figures 5.13** and **5.14**) and the fGn parts (e.g. **Figures 5.11** and **5.12**) are associated with persistent Hurst exponents through R/S analysis. These findings and the several outcomes reported so-far through the R/S analysis, indicate

that the MHz pre-earthquake precursors can exhibit as well persistent as anti-persistent behaviour. From another viewpoint, the deviations between the above publications and this research, could be probably because the relations $b=2\cdot H+1$ and $b=2\cdot H-1$ may finally not model well the actual situation. At first, these relations are based on pure mathematical basis (see **section 3.2** and references). When synthetic signals are used (**Figures 3.1** and **3.2**, **Chapter 3**), theory and interpretations are consistent; because the synthetic were produced from the above relations. In the actual situation of a pre-earthquake signals, there are many processes that act on various scales (see e.g. Eftaxias, 2010; Nikolopoulos et al., 2012, Smirnova, & Hayakawa, 2007) and for this reason, maybe, the relations $b=2\cdot H+1$ and $b=2\cdot H-1$ do not operate well and the reality deviates from theory. This viewpoint is supported in **Figures 5.15** and **5.16**, where the Hurst exponents of the two signals of **Figures 5.11-5.14** are presented, both through R/S analysis and as calculated from the corresponding b -values. It is characteristically shown that the corresponding H -values are quite different; those calculated from the power-law b -values are considerably lower. More specifically, **Figures 5.15** and **5.16** present parallel results for the first 2.7x10^6 s for the time-evolution of the Hurst exponent as derived by the R/S analysis and as calculated by the spectral fractal analysis for fBm segments, namely, by employing the relation $b=2\cdot H+1$ which is valid for the fBm class (see also **section 3.2**). As also outlined above, the Hurst exponents calculated from the fractal analysis method are quite lower

when compared to those derived by the R/S method. In addition, the Hurst exponents through the spectral fractal analysis exhibited high bias as the corresponding standard deviation of H is great. What is of great importance is that these facts were systematically observed in all the MHz signals of **Table 4.3**, **Chapter 4**. In relation, the following issue is of great significance; it was observed through several runs, that the H -values calculated by the outcomes of the fractal methods through the relations $b=2\cdot H+1$ and $b=2\cdot H-1$, corresponded to anti-persistent behaviour. This might also provide reasons why in previous publications of the author and others (e.g. Eftaxias et al., 2009, 2010; Nikolopoulos et al., 2012, 2014; Petraki, Nikolopoulos, Fotopoulos, Panagiotaras, Koulouras et al., 2013; Petraki, Nikolopoulos, Fotopoulos, Panagiotaras, Nomicos et al., 2013), mainly anti-persistent behaviour was reported for the MHz and radon pre-earthquake precursors. To the author, in the consensus of the above discussion, this was the effect of the sole use of fractal methods in the estimation of Hurst exponent. Complementary, in a recent publication of the author, persistent behaviour of the MHz radiation was also found and reported (Petraki et al., 2014). The latter issue has been extensively commented in **Chapter 3**.

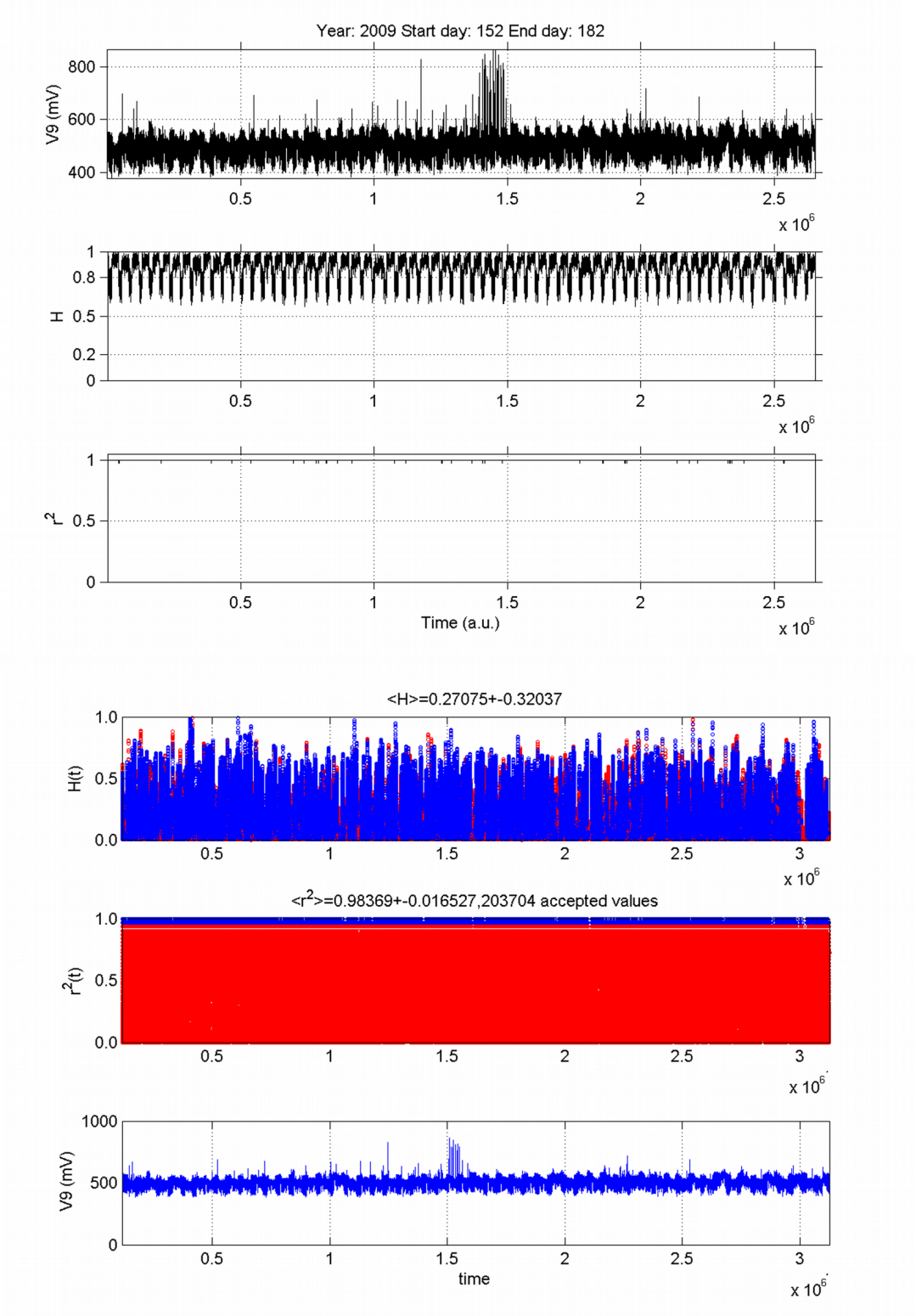

Figure 5.15: Time evolution of Hurst exponent for the same pre-earthquake signal (EQ:11, **Figure 3.17**, **Table 3.2**, **Chapter 3**, Vamos station, 41MHz) through R/S analysis (up figure-b/w) and fractal analysis for the fBm segments (down figure).

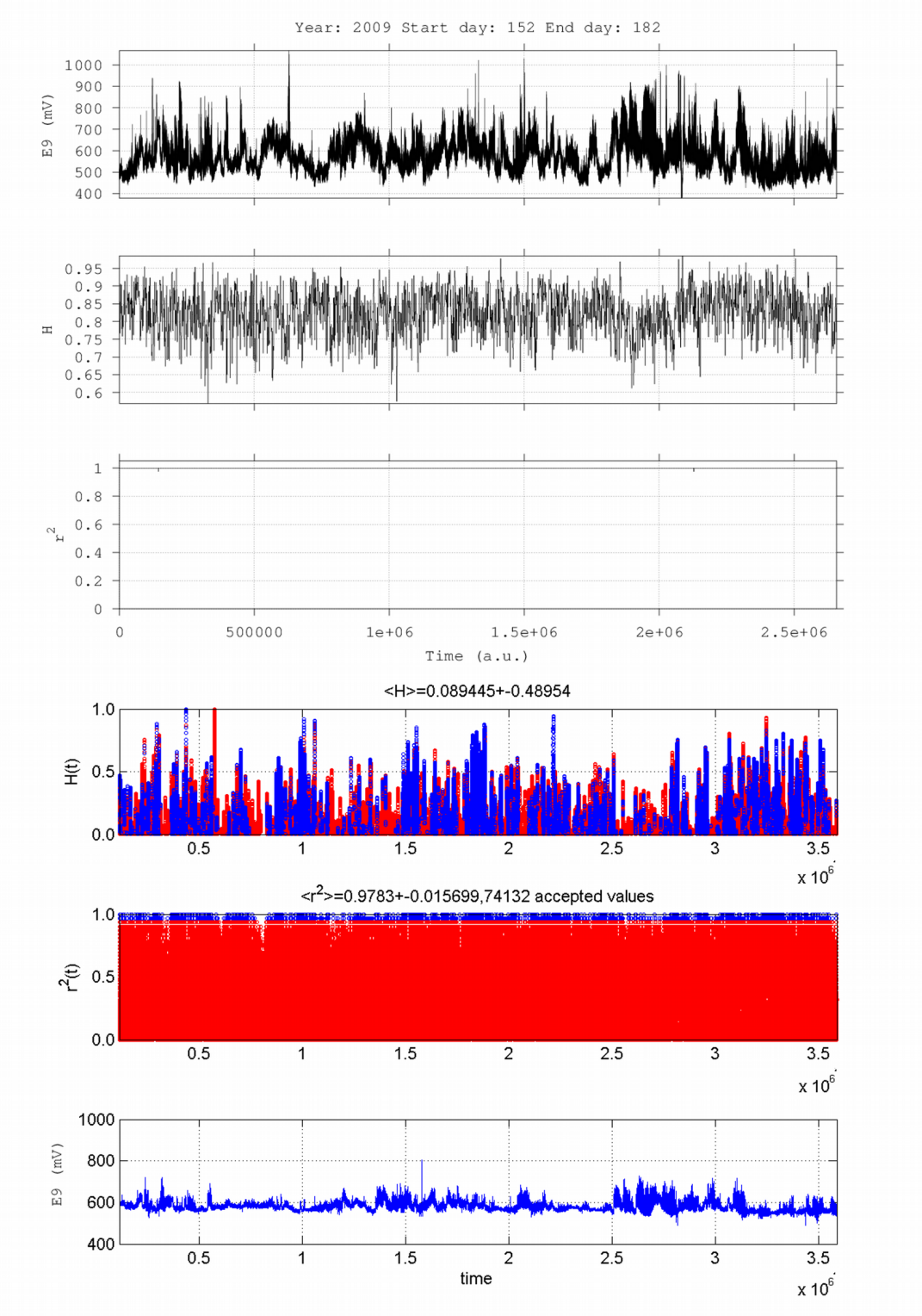

Figure 5.16: Time evolution of Hurst exponent for the same pre-earthquake signal (EQ:11 Neapoli station, JD 152-182, 2009, 41 MHz) through R/S analysis (up figure-b/w) and fractal analysis for the fBm segments (down figure).

From the example data of **Figures 5.15** and **5.16** it becomes evident that the R/S method provides a new insight. As mentioned, this has been supported also in a very recent publication of the author and colleagues (Nikolopoulos et al., 2015). What makes **Figures 5.15** and **5.16** very important, is that the Hurst exponents of these figures were calculated in the *same segments* both through the fractal analysis and through the R/S method. What reinforces the new viewpoint, is that the data from the R/S analysis correspond to a different mathematical basis (the one of R/S), which, most importantly, is considered as the gold-standard for the calculation of the Hurst exponent. The insight of these new aspects is also supported by the example data of **Figures 5.17** and **5.18.** These figures (**Figure 5.17** and **Figure 5.18**) present a significant new (2015) pronounced; the fBm segments of pre-earthquake MHz signals, present significantly higher Hurst exponents compared to the ones of the fGn segments. What is very important is that this behaviour was systematically addressed. This issue was also outlined in the above-mentioned recent publication of Cantzos et al. (2015).

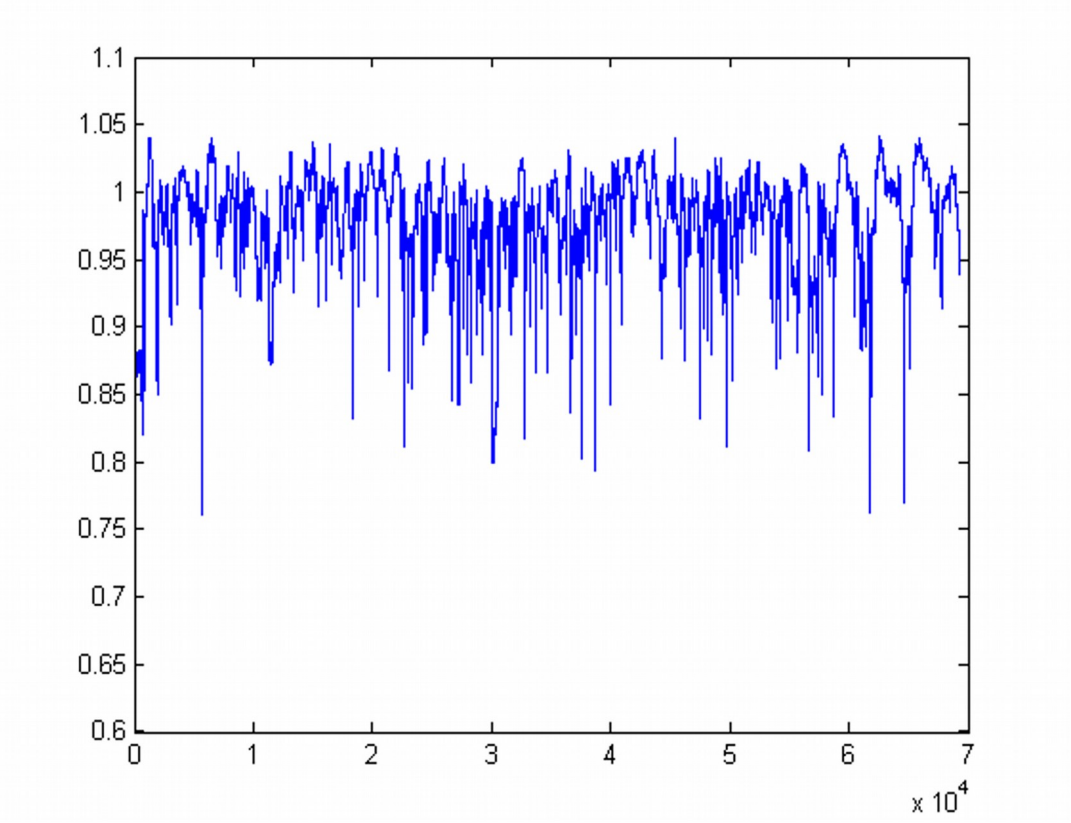

Figure 5.17: Time evolution of Hurst exponent. EQ:18, **Table 3.2**, **Chapter 3**, Neapoli station, JDs 76-105, 2015, 41 MHz.

Successive (blue, $r^2 \geq 0.95$) fBm ($1<b<3$) segments

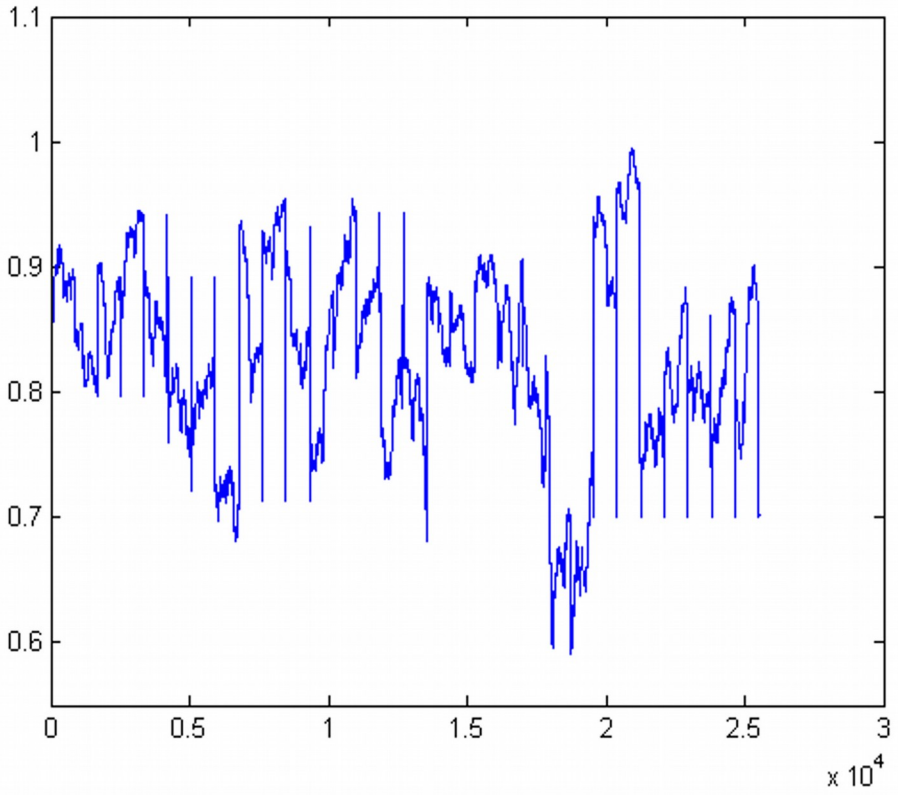

Figure 5.18: Time evolution of Hurst exponent. EQ:18, **Table 3.2**, **Chapter 3**, Neapoli station, JDs 76-105, 2015, 41 MHz.

Segments not-fBm ($-1<b<1$) and/or segments not-successive (red)

According to the data of **Figures 5.17** and **5.18**, the discussion of Cantzos et al (2015) and the systematics of the data of this research, it can be supported that **t**he R/S analysis is a very powerful method to trace significant *pre-earthquake patterns* hidden in pre-seismic time-series, *as increase in H-values of precursory successive (* $r^2 \geq 0.95$ *) fBm (* $1<b<3$ *) segments.* This has been supported also in a very recent publication of the author and colleagues (Nikolopoulos et al., 2015). The corresponding characteristic data are shown in **Figures 5.19-5.21**. These figures present a radon signal collected with Baracol prior to the twin earthquakes of 2014 (EQ:36 and EQ:37 **Table 3.2**, **Chapter 3**). The differentiation in the Hurst evolution of the three next figures is the way through which the window is slid during the sliding-window R/S technique. **Figures 5.19** and **5.20** refer to sliding windows of step 1. As already mentioned, this produces fine analysis results, because each window almost superimposes the preceding one. To apply the lumping technique of **Figure 5.21**, instead of the continuous sliding of one-sample per segment, the signal was lumped at the whole size of the segment, viz. the sliding step was set equal to the segment size. It is noted that the segment-size in **Figures 5.19** and **5.21** is 128 and this corresponds to radon recordings of 1,920 min duration, i.e., approximately 32 h of segmented analysis. The double value of the window-size (256) in **Figure 5.20** corresponds roughly to 64 h of segmented R/S analysis. It is worth to mention, that lumping is considered advantageous by some researchers (e.g. Karamanos, 2001; Karamanos, & Nicolis, 1999; Karamanos et al., 2005).

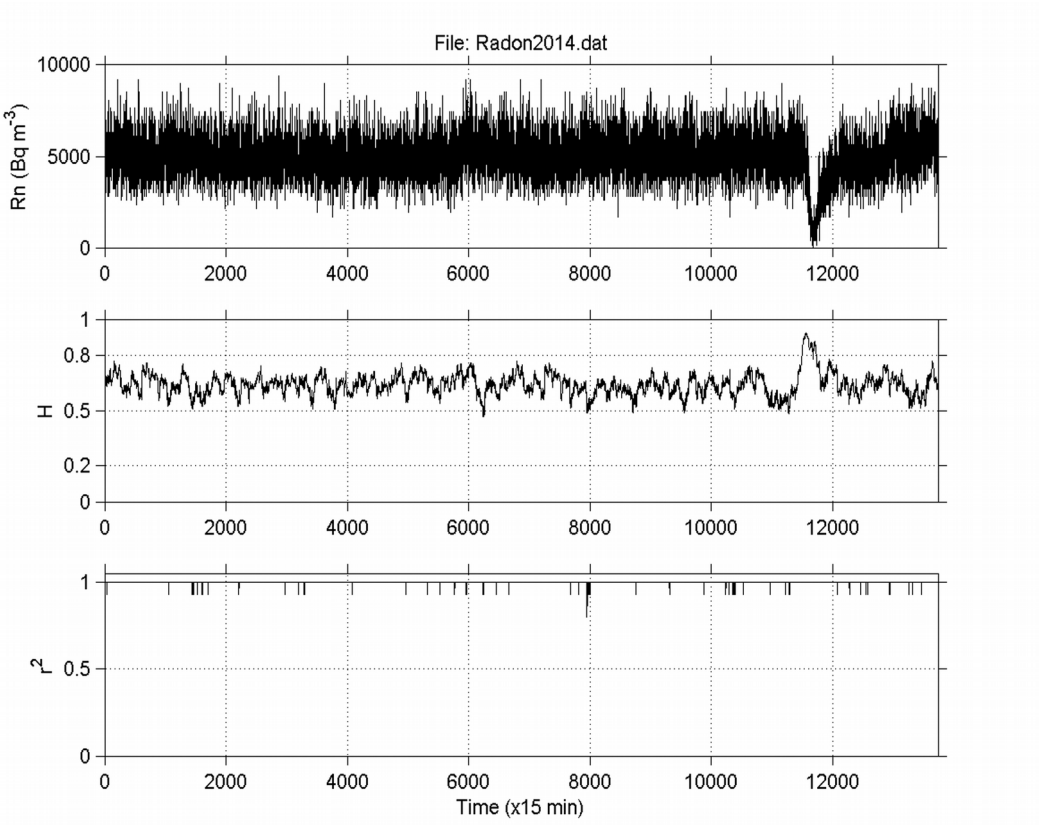

Figure 5.19: R/S analysis with the sliding window technique of window size of 128 samples. From top to bottom: (a) the radon signal of **Figure 4.15** (up); (b) the evolution of Hurst exponent calculated through R/S analysis; (c) evolution of the square of the associated Spearman's correlation coefficient.

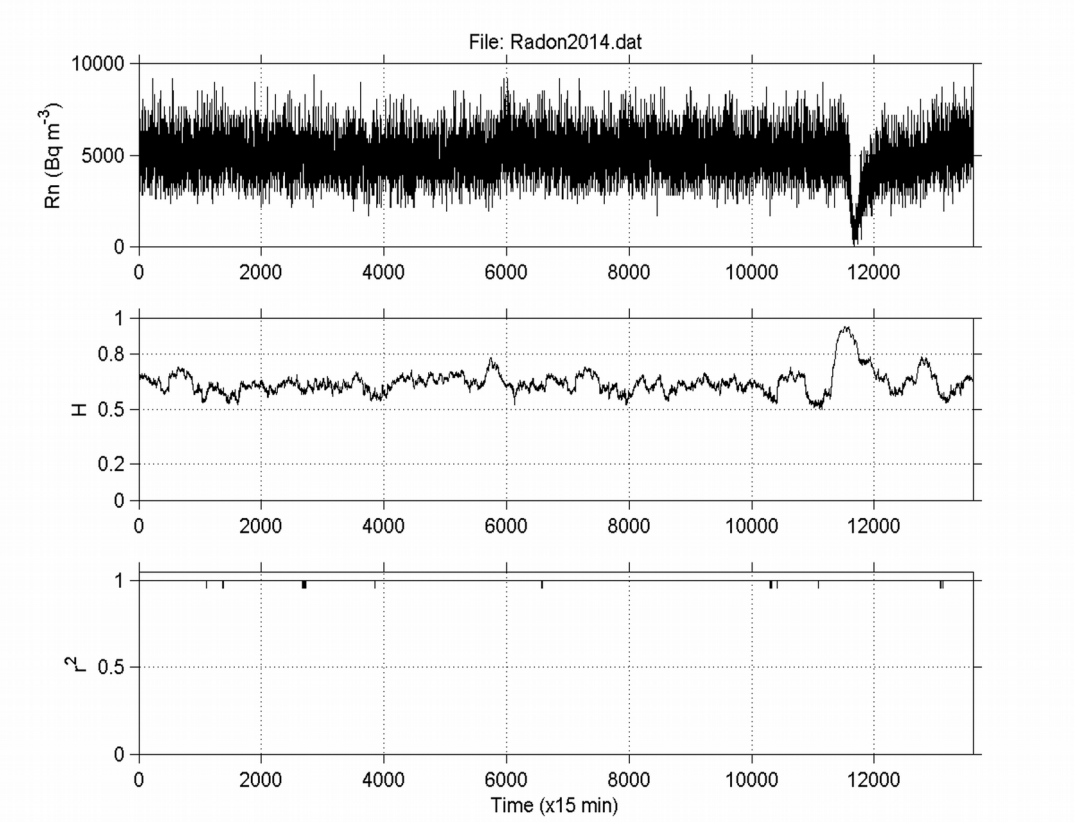

Figure 5.20: R/S analysis with the sliding window technique of window size of 256 samples. From top to bottom: (a) the radon signal of **Figure 4.15** (up); (b) the evolution of Hurst exponent calculated through R/S analysis; (c) evolution of the square of the associated Spearman's correlation coefficient.

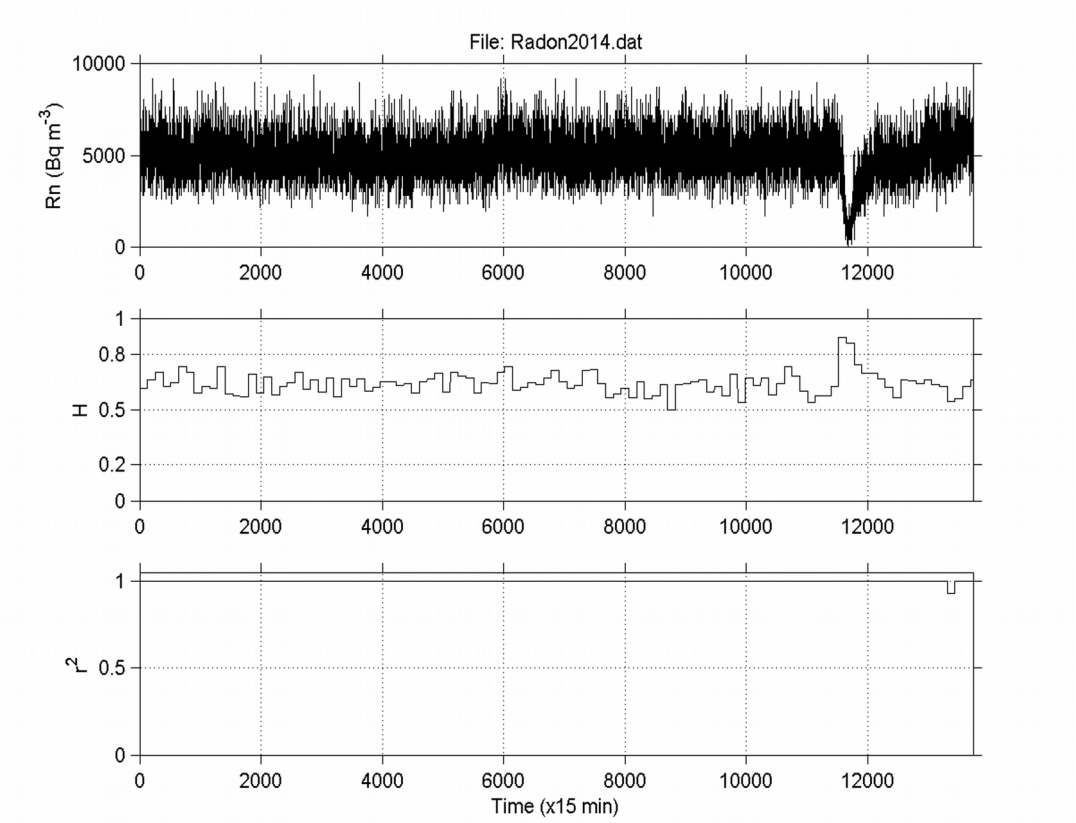

Figure 5.21: R/S analysis with lumping of window size of 128 samples. From top to bottom: (a) the radon signal of **Figure 4.15** (up); (b) the evolution of Hurst exponent calculated through R/S analysis; (c) evolution of the square of the associated Spearman's correlation coefficient.

Figures 5.19-5.21 reveal very important information about the time evolution of the Hurst exponent. It can be observed that all Hurst exponent values were in the range $0.5 < H < 1$. This means that the radon time-series had underlying memory associated with persistency. This implies that if the signal had a tendency to increase its values in a certain time period, it was most probable to continue increasing the values. In an alternative interpretation, if the signal decreased in a time period, it continued to decrease. Within the anomaly, the Hurst exponents increased above 0.8. This is indicative of very strong long memory. This has certain implications. The radon concentrations in a certain time period of long memory referred to their past values so as to define their present values and to define their future values. The very important finding of **Figures 5.19-5.21** is that all figures show a significant increase in the Hurst exponent during the visual anomaly (see also **Chapter 4** for the visual anomaly and the corresponding wavelet transform). This Hurst peaking within the anomaly implies that the anomaly-generating earth-system was not random. On the contrary, it was produced by fracture of cracks which propagated in the crust in a way that a certain crack of the past was a source of a present crack which was a source of a future crack. According to the asperity model presented in **Chapter 3**, the cracks of the past were organised with the cracks of the presence and the future, generating a backbone of self-organised asperities. This roadway, i.e., the asperities backbone provided a pathway for either radon sucking (continuous or abrupt decrease due to under pressure in the asperities) or radon emanation (continuous or abrupt increase due to over pressure in the asperities). Researchers have described this process under the so called DD model (dilatation and dilatancy) (**Chapter 4**). In this sense, the DD model could be descriptive of behavior of the Hurst exponent (**Figures 5.19-5.21**) only within the self-organisation phase of the

asperities. It is important to note that the aforementioned long-memory process was not quick since it lasted approximately 15 days. It is very important also that similar slow behaviour of anomalous concentration of radon in soil was also reported for Ileia, Greece prior to a very disastrous earthquake of 2008 in Ileia, Peloponnese (**Chapter 4**). It was also similar to a pre-earthquake anomaly of radon in soil detected in Lesvos Island, in 2008 (**Chapter 4**). It is important to mention here that the radon precursors have longer history, they are less dependent to noise and they are more convenient (see **Chapters 1** and **2**).

A very significant finding is that the Hurst exponents of **Figures 5.19-5.21** peaked well above 0.8 for the same time period as the radon anomaly. This parallel observation enhances the estimations. Another significant finding was that the Hurst peaking was observed both through the sliding window technique and through the lumping one. This fact indicates that the Hurst exponent increase during the anomalous concentration of radon in soil of **Figure 4.15** (up), was not an artifact of the sliding-window method. Further evidence can be provided by the DFA method. **Figures 5.22-5.24** present three characteristic DFA plots similar to those proposed in the literature (Peng et al., 1992, 1994, 1995, 1998) and are very useful so as to compare Hurst exponents (Eftaxias et al., 2009; Nikolopoulos et al., 2014, 2015; Petraki, Nikolopoulos, Fotopoulos, Panagiotaras, Koulouras et al., 2013). As mentioned, to apply the DFA method the experimental radon data were fitted to equation $F(n) \sim n^{\alpha}$. To identify existing long-lasting self-fluctuations in the experimental radon data, the outputs of the DFA method were plotted in $\log(F(n)) - \log(n)$ representation and fitted to linear trend-lines. It may

be recalled that the linear trend-line is not constant (independent of scale) and crossovers exist, i.e., its slope differs between the short and the long time scales. All generated DFA plots verified this and exhibited one crossover. The crossover can be observed in **Figures 5.22-5.24** as a change in the slope of the two trend-lines. It is important that the DFA plots prior and after the anomalous radon part were similar (**Figures 5.22** and **5.23**). The slopes of the short and long scales were analogous. On the contrary, the plots within the anomaly were mirror-like in comparison to those of the background. The characteristic plot of **Figure 5.24**, shows clearly that within the anomaly the long-scales have significantly higher slope of the linear trend-line. The following is very important: according to several DFA runs in segments within the anomaly it was found that the corresponding long-scale DFA slope was above 1.5, namely $1.5 < b < 1.8$. According to the literature (Eftaxias et al., 2009; Nikolopoulos et al., 2014, 2015; Peng et al., 1992, 1994, 1995, 1998; Petraki, Nikolopoulos, Fotopoulos, Panagiotaras, Koulouras et al., 2013), the DFA results within the radon anomaly show persistent long range correlations. This characteristic epoch of the radon signal is significantly different from the one of the radon background (**Figures 5.22** and **5.23**). This tendency was identified also in the DFA scatter plot of the signal of the Ileia (**Figure 5.25**) and in the one of Lesvos (**Figure 5.26**) (Nikolopoulos et al., 2014). Note that DFA is considered as very advantageous in short signals of high variations (Peng et al., 1992, 1994, 1995, 1998). It is also of importance that in the whole $F(n)-n$ range, the trend is linear in both parts of the $\log-\log$ transformation with high values of the square of the Spearman's correlation coefficient ($r^2 \geq 0.95$) in all cases.

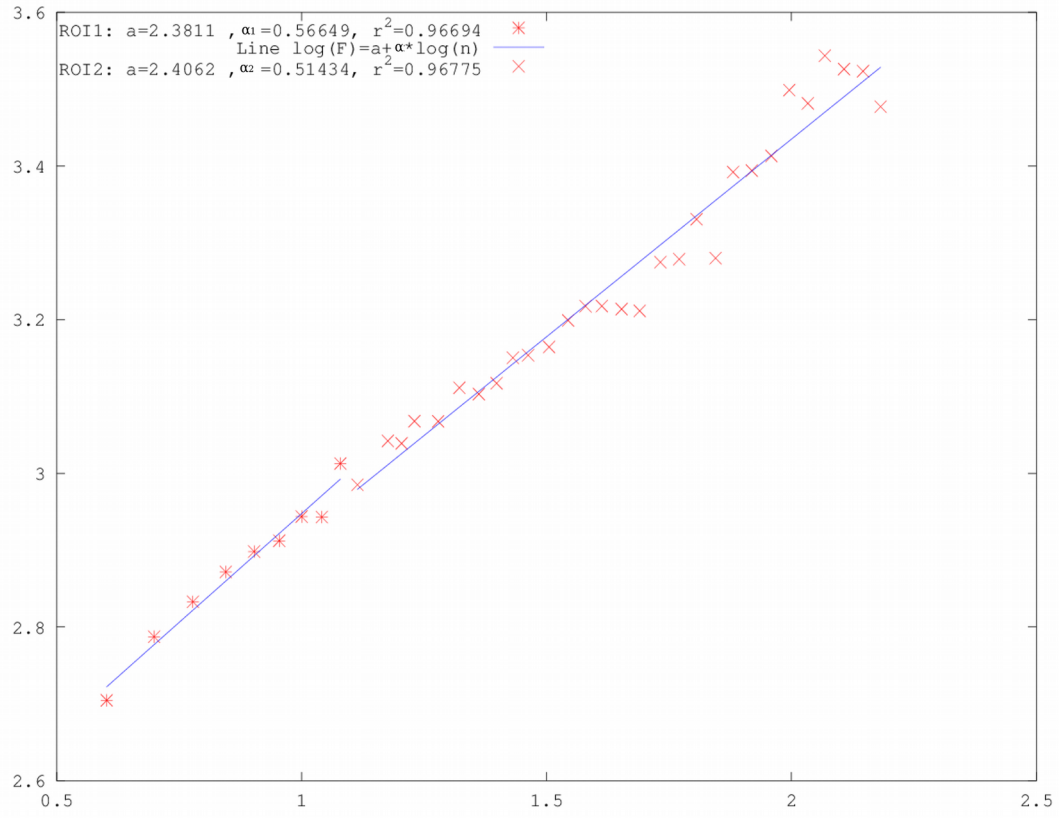

Figure 5.22: DFA plot of another background part of signal of **Figure 4.15** (up). Horizontal axis is $\log(n)$ and vertical axis is $\log(F(n))$ ($\log-\log$ representation of equation (5.15)). The legend provides the values α_1 and α_2 with corresponding Spearman's r^2 values.

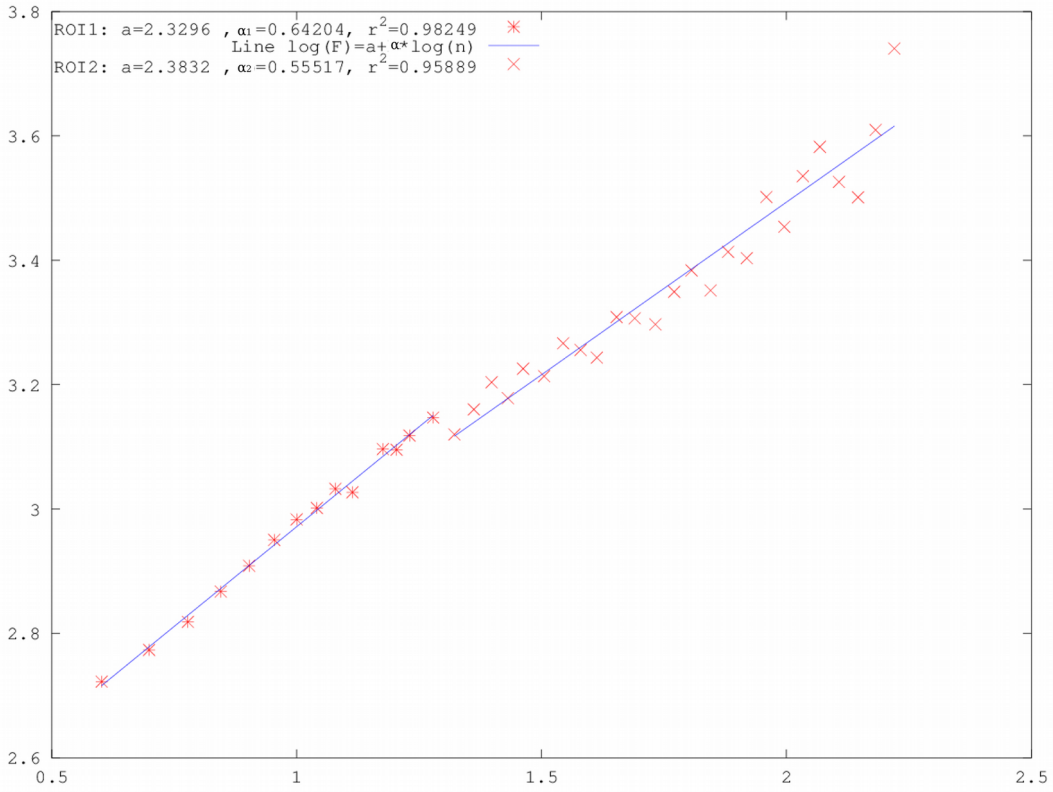

Figure 5.23: DFA plot of another background part of signal of **Figure 4.15** (up). Horizontal axis is $\log(n)$ and vertical axis is $\log(F(n))$ ($\log-\log$ representation of equation (5.15)). The legend provides the values α_1 and α_2 with corresponding Spearman's r^2 values.

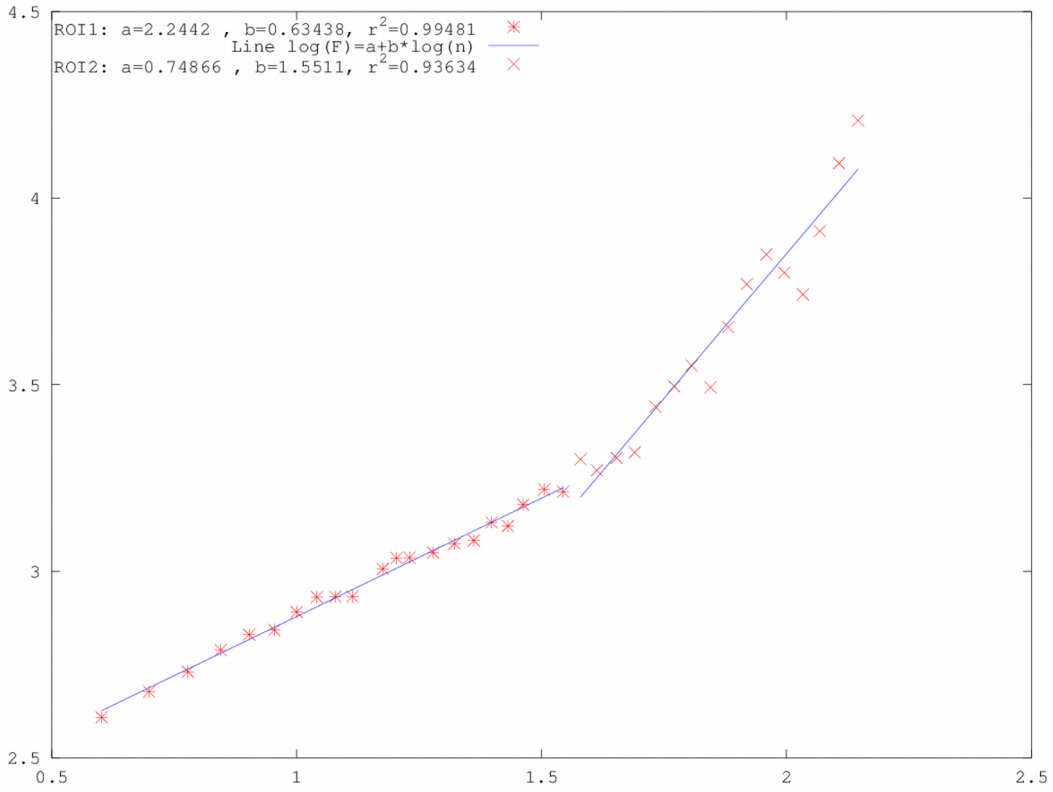

Figure 5.24: DFA plot of a part within the anomaly of signal of **Figure 4.15** (up). Horizontal axis is $\log(n)$ and vertical axis is $\log(F(n))$ ($\log-\log$ representation of equation (5.15)). The legend provides the values α_1 and α_2 with corresponding Spearman's r^2 values. Note the higher slope of the long scales (long-memory).

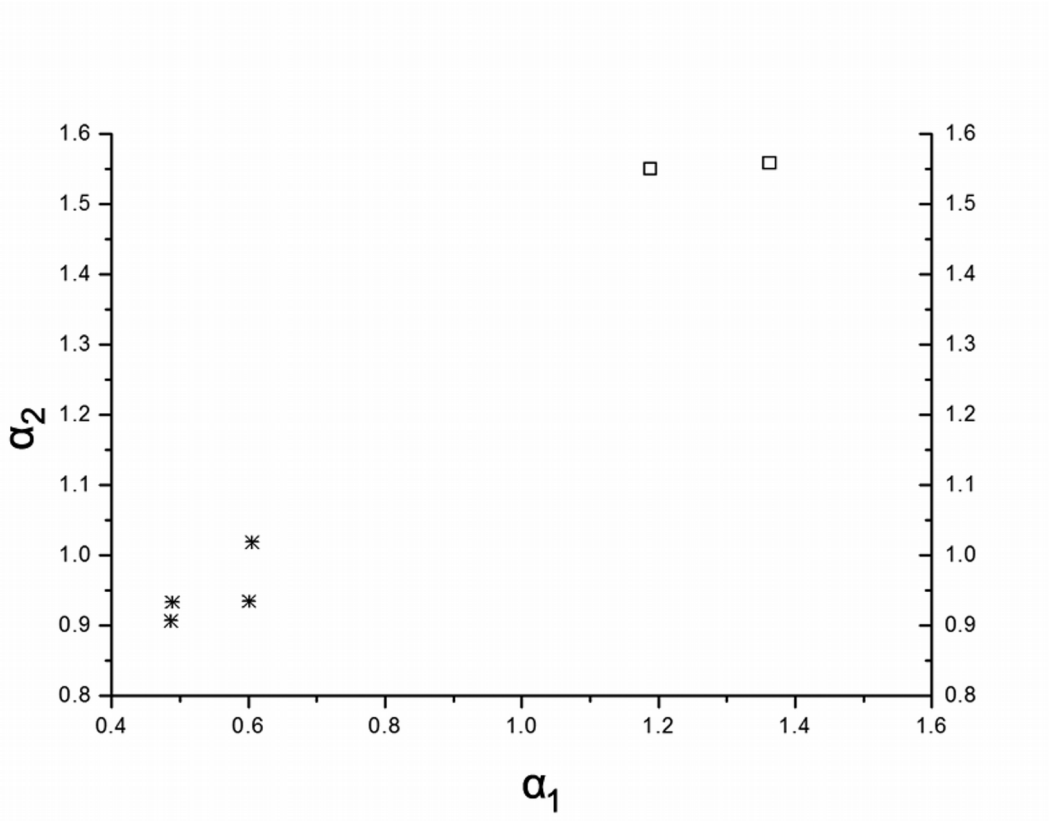

Figure 5.25: DFA scatter plot for the 2008 radon time-series of Ileia (**Figure 4.2(f)**, **Chapter 4**). α_1 is the DFA exponent for the small scales and α_2 is the exponent for the long scales.

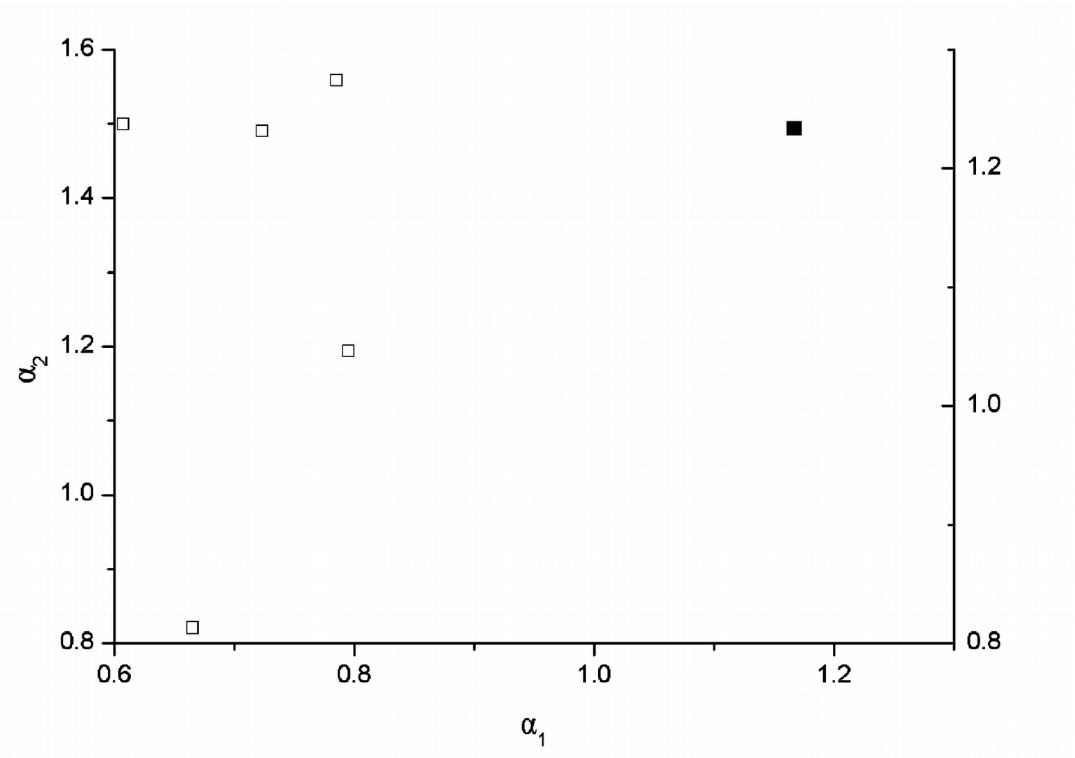

Figure 5.26: DFA scatter plot for the Lesvos radon time-series (**Figure 4.12**, **Chapter 4**). α_1 is the DFA exponent for the small scales and α_2 is the exponent for the long scales.

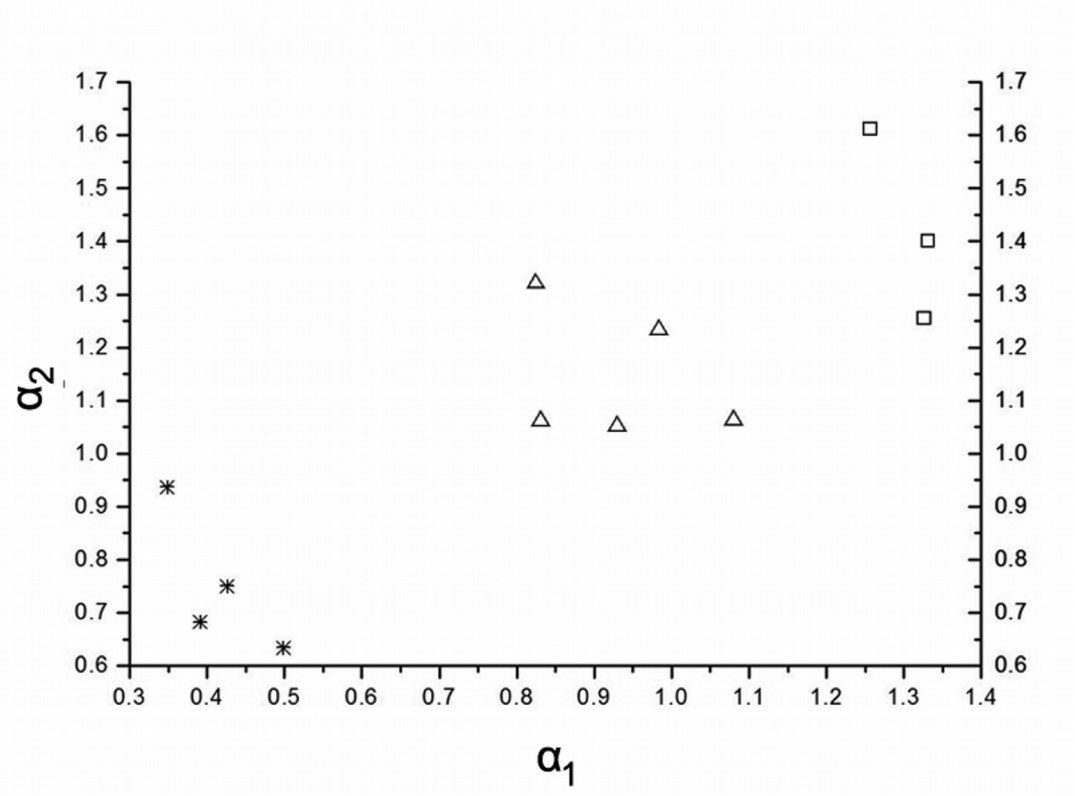

Figure 5.27: DFA scatter plot the electromagnetic data series of **Figures 3.29-3.32** (**Chapter 3**). α_1 is the DFA exponent for the small scales and α_2 is the exponent for the long scales.

As outlined above, **Figures 5.25** and **5.26**, present two characteristic DFA scatter plots for the cases of radon time-series of Ileia and Lesvos. **Figure 5.27**, presents a similar scatter plot for the electromagnetic time series of **Figures 3.29-3.32**. More specifically **Figure 5.25** refers to regions between the two 2008 radon spikes (**Figure 4.2(f)**, **Chapter 4**) and to regions away**.** The chosen signal area within the anomaly exhibited many accepted power-law beta-values (**Figure 4.8**, **Chapter 4**)**,** which were greater than 1.5 or 2, i.e., exhibited anti-persistent/persistent behaviour. **Figure 5.26** refers to the region within the anomaly of the Lesvos signal and to regions away (**Figure 4.12**, **Chapter 4**). The anomalous region of the Lesvos signal presented also many successive fBm segments with $b>1.5$ (**Figure 4.14**, **Chapter 4**). Note that some electromagnetic disturbances of the MHz range presented DFA plots with not one, but two crossovers (Petraki, Nikolopoulos, Fotopoulos, Panagiotaras, Koulouras et al., 2013) . From the **Figures 5.25** and **5.26**, it can be observed that the exponents a_1 and a_2 separate radon background from the high power-law b -values. The high power-law b -values are characterised by much larger combinations of a_1 and a_2 . More precisely, in the background the DFA exponents of the small scales (a_1) present values between 0.5 and 0.8, while in the region of the high power-law beta-value part, between 1.2 and 1.4. The aforementioned values of the DFA slopes shows that for the background, both a_1 and a_2 have values consistent with a fGn-model ($0<a<1$) (Eftaxias et al., 2009; Nikolopoulos et al., 2014, 2015; Peng et al., 1992, 1994, 1995,

1998; Petraki, Nikolopoulos, Fotopoulos, Panagiotaras, Koulouras et al., 2013). On the contrary, the region of the high power-law beta-values, presents the DFA exponents consistent with a fBm-model ($1<a<2$) (Eftaxias et al., 2009; Nikolopoulos et al., 2014, 2015; Peng et al., 1992, 1994, 1995, 1998; Petraki, Nikolopoulos, Fotopoulos, Panagiotaras, Koulouras et al., 2013). Especially in reference to **Figure 5.27**, the results showed three different areas. The first area, for electromagnetic noise, was accompanied by small slopes (for small scales: $0.35<a_1<0.5$ and for large scales: $0.7<a_2<0.9$). These DFA values are in close agreement to the corresponding values of the radon background. In addition, they are indicative of an underlying $1/f$ -noise which is consistent with the fGn-model (Eftaxias et al., 2009; Nikolopoulos et al., 2014, 2015; Peng et al., 1992, 1994, 1995, 1998; Petraki, Nikolopoulos, Fotopoulos, Panagiotaras, Koulouras et al., 2013). The interim area of electromagnetic DFA exponents (for small scales: $0.8<a_1<1.1$ and for large scales: $1.1<a_2<1.4$) was derived for signal areas during electromagnetic disturbances, however, considering only power-law beta-values below 1.5. These areas were close to the signal areas with high power-law beta-values. It is important to note, that this interim area was not identified in kHz signals under similar analysis (Eftaxias et al., 2010). The diversity between the scatter plots of radon and electromagnetic signals is probably due to the rather stable background of radon which is not observed, at the same range, in the electromagnetic signals of **Figures 3.29-3.32**. Note that due to the physical mechanisms of the detection of the electromagnetic disturbances (Nomicos, & Vallianatos, 1998), it is generally

quite difficult to identify in the MHz electromagnetic disturbances such a low-varying background as in radon. Areas with high power-law b -values showed DFA exponents between 1.25 and 1.6, fairly close to that of the fBm-model (Eftaxias et al., 2010; Peng et al., 1994).

To compare the estimation of the Hurst exponent through DFA the following logic was applied; H is related to the power-law exponent b by the formula $b=2\cdot H+1$ for the time-series model of fBm ($1<b<3$) and $b=2\cdot H-1$ for the time-series model of fGn ($-1<b<1$) . By employing the formula of $b=2\cdot\alpha-1$ which is valid both for the fBm and fGn models (Nikolopoulos et al., 2015), the relationship between Hurst and DFA exponents was derived: $H=\alpha-1$ for power-law b in the range $1<b<2$ and $H=\alpha$ for $0<b<1$. In this sense, as regards the **Figure 5.24**, the range $0.51<\alpha_1<0.70$ within the radon background (ROI-1), corresponds to Hurst exponents $0.51<H<0.70$ and the range $1.5<\alpha_2<1.8$ within the radon anomaly, to exponents in the range $0.5<H<0.80$. Despite that through this logic, DFA did not identified the peaking of Hurst exponents that was observed through the sliding-window R/S analysis, the DFA results are in agreement with those of the R/S

analysis. The latter is very significant because two independent techniques provide similar evidence regarding the long-memory of the system that generated the radon anomaly. Note again, that the discrepancies could be attributed to whether the relations $b=2\cdot H+1$ and $b=2\cdot H-1$ actually correspond to the reality.

If the above logic is applied in the data of **Figures 5.25** and **5.26**, the DFA slopes are consistent with values of $b\approx 1.3-1.4$ for the small time scales and $b\approx 1.8-2.1$ for the large time scales. Similarly, the background parts of **Figures 5.25** and **5.26**, are consistent with $-0.3<b<0.2$ for the small time scales and $0.7<b<1$ for the large time scales while the high power-law beta parts with $1.4<b<2.2$ for the small time scales and $1.5<b<2.2$ for the large time scales. This is in complete agreement with all the previous findings and indicate anti-persistency or/and persistency.

All these issues imply long-range spatial-temporal correlations, i.e., strong system memory during the high power-law b or the high DFA α parts. As aforementioned, each value correlates not only to its most recent value but also to its long-term history in a scale-invariant, fractal manner. The system refers to its history in order to define its future (non-Markovian behavior). This further suggests that the underlying dynamics are governed by positive feedback mechanisms and, hence, external influences tend to lead the system out of equilibrium. In this manner, the system acquires a self-regulating character and, to a great extent, the property of irreversibility, one of the important components of prediction reliability.

Despite that the **Figures 5.16-5.21** indicated that the Hurst exponents of the successive ($r^2 \geq 0.95$) fBm ($1<b<3$) segments are higher than those of the fGn segments and notwithstanding that the results of the DFA in these segments are in agreement with the ones of the R/S analysis, the relative estimations of the Hurst exponent may variate strongly. This is characteristically shown in **Figures 5.28** and **5.29.** At first, **Figure 5.28** presents the time evolution of the Hurst exponent of the radon time-series of the Lesvos signal (**Figure 4.12**, **Chapter 4**) according to wavelet spectral fractal analysis, for those parts that follow fBm-modelling. Missing values correspond to processes following persistent fGn-modelling. The plot is similar to the plots of **Figures 5.15** and **5.16**. The similarities in the data of **Figure 5.28** and those of **Figures 5.15** and **5.16**, verify the similarities already addressed in **Chapter 4** between radon and MHz electromagnetic disturbances. The sliding-window R/S analysis of this signal showed persistent Hurst exponents values in the range 0.7-1.0. However, when the R/S , R-L and Variogram techniques were applied to independent signal's segments, the estimations differed. In particular, **Figure 5.29** presents the Hurst exponents of the radon signal of Lesvos (**Figure 4.12**, **Chapter 4**) through lumping at completely independent segments. The median segments correspond to the area of the anomaly. It should be emphasised that fGn processes in Lesvos signal corresponded mainly to non-anomalous parts. This finding is in agreement with the findings of the 2008 radon time-series of Ileia (**Chapter 4**). Indeed, the stable part of the Ileia radon signal of 2008, as well as, of the radon background of 2010 and 2011 in Ileia, followed

also persistent fGn modelling. Some limited H -values in non-anomalous parts were consistent with anti-persistent fBm behaviour. However most importantly, the fBm H -values during the anomalous radon concentrations were significantly higher (P<0.001, ANOVA). It is significant also that these were also successive ($r^2 \geq 0.95$). The increase in H -values during radon anomalies was recognised also in the 2008 radon time-series (Petraki, Nikolopoulos, Fotopoulos, Panagiotaras, Nomicos et al., 2013). Most values in **Figures 5.28** and **5.29** were in the range $0<H<0.5$, i.e, they were anti-persistent. Some values were in the range $0.5<H<1$, i.e., they were persistent. It is very interesting that the Hurst exponents from the fractal methods (**Figures 5.28**) indicated also high Hurst exponents in contrary to the general tendency of the MHz electromagnetic radiation. It has to be emphasised though, that in **Figure 5.28** the increase in H is associated with an obvious anomaly. Of course the H estimations are biased by the uncertainties in radon concentration and this should be noted as well. In the non-anomalous radon parts, the relative uncertainties were below 1.5 %. The relative uncertainties within the spike was approximately 4 %. However, the low relative values of this source of bias do not contradict the significant differences in the H -values of the anomalous part.

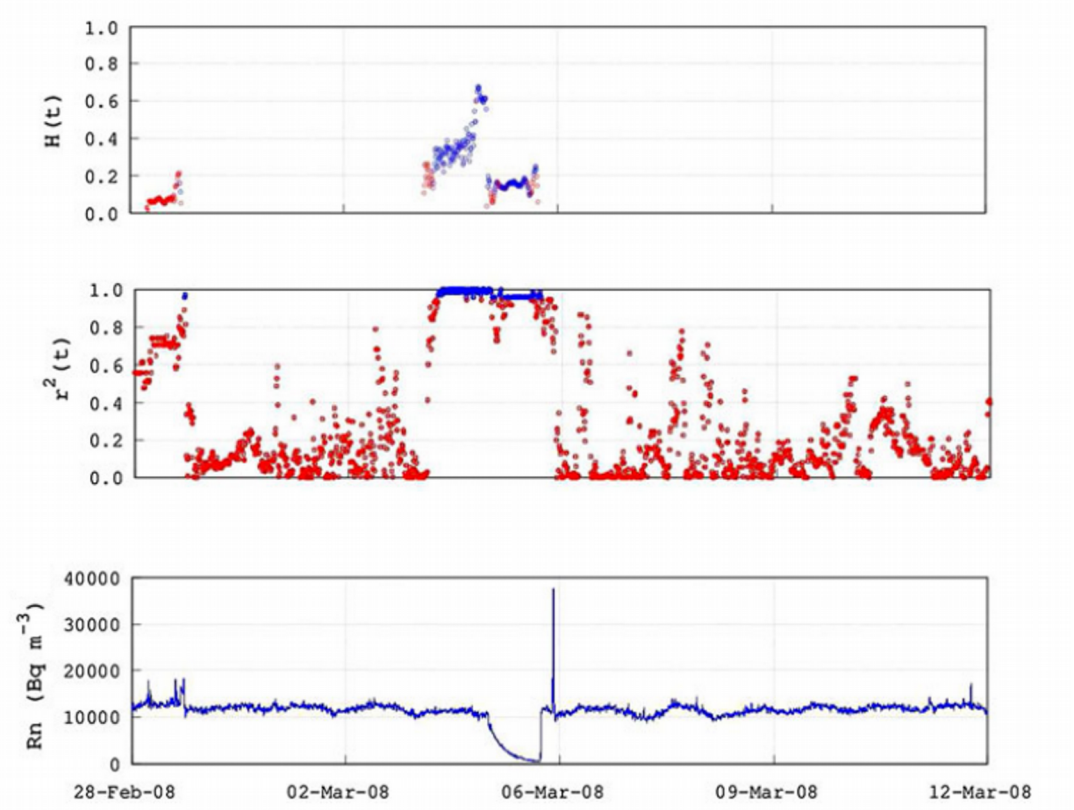

Figure 5.28: Hurst exponent of the Lesvos signal as calculated from the power-law b-values according to fBm modelling.

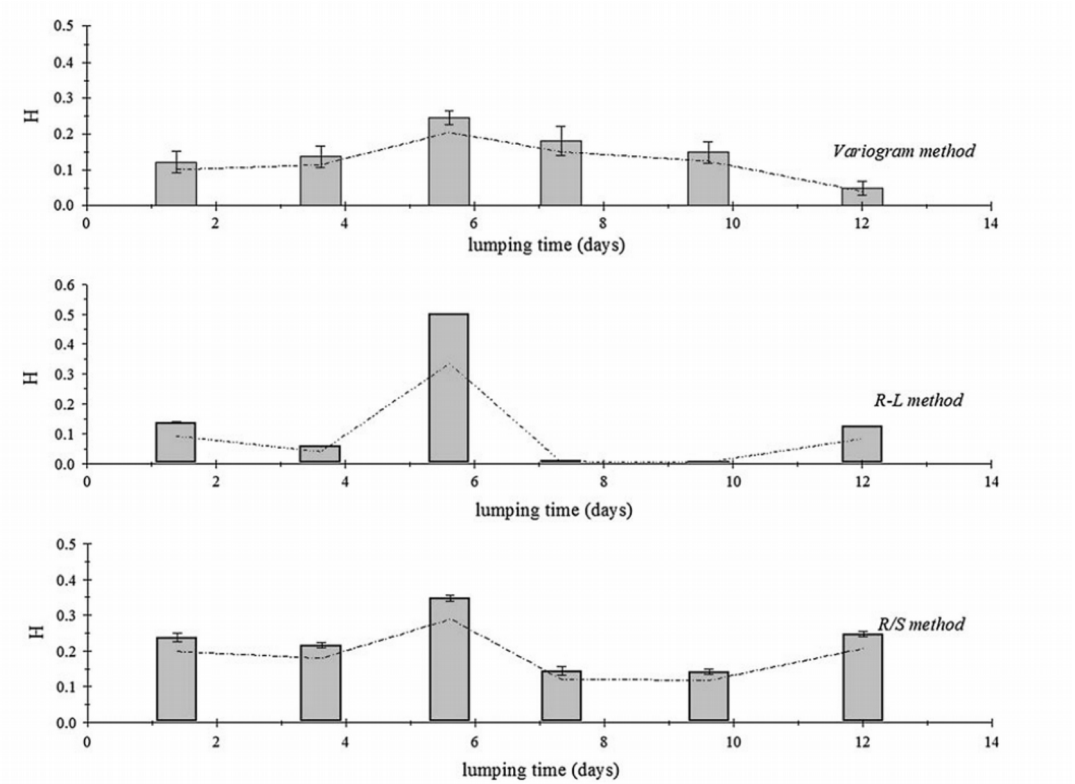

Figure 5.29: Time evolution of the Hurst exponent of the radon time series of Lesvos through lumping to completely independent segments according to R/S, R-L and Variogram methods.

Figure 5.29 presents the time evolution of the Hurst exponent, however through lumping via R/S, R-L and Variogram methods (Stratakos, & Sakellariou, 2006; Warwick, Stoker, & Meyer, 1982) in completely independent segments. For lumping, the signal was divided in six independent time windows. The time-length of each window was equal to that reported by Petraki, Nikolopoulos, Fotopoulos, Panagiotaras, Nomicos et al. (2013) for the time-evolution of H in Ileia. It is worth to note, that both in the Ileia and the Lesvos signal, this window-length was the optimum for revealing existing differentiations. As with wavelet spectral fractal analysis, the H-values of the anomalous parts were significantly higher (P<0.001, ANOVA) with all other techniques, namely R/S, R-L and Variogram. According to the R/S method, non-anomalous parts presented H-values with average (0.20 ± 0.05) and mean error 0.004. On the contrary, the anomalous parts presented $H = (0.347 \pm 0.008)$. It is important to note here, that this type of application of the R/S method provided anti-persistent Hurst exponents, in contrary to what the sliding window R/S technique provides. To the author, this issue is of extreme importance: indeed, to provide adequate estimations, one has to employ the various long-memory techniques in the same manner, otherwise significant discrepancies can be addressed. This issue has been outlined in the literature as well (e.g. Granero, Segovia, & Perez, 2008; Xie, Wan, & Zhu, 2011). Regarding the R-L method, this rendered to calculation

of lower H -values of (0.09 ± 0.07) and lower mean error, 0.0004, in the non-anomalous parts and quite higher values, $H = (0.5010 \pm 0.0006)$, in the anomalous part. The Variogram estimated mean Hurst exponent of $H = (0.13 \pm 0.05)$ in the non-anomalous part with mean error 0.08, while, values of $H = (0.25 \pm 0.02)$ in the anomaly. Note that the R-L method estimated H -values of low errors, whereas, the Variogram method calculated Hurst exponents of much higher errors. This is illustrated by the differentiations in the corresponding error bars of **Figure 5.29**, as well as, by the significant discrepancies of the average errors of each method in the non-anomalous parts. Completely similar behaviour was identified in the stable part of the 2008 signal of Ileia and in radon background of 2010 and 2011 (Petraki, Nikolopoulos, Fotopoulos, Panagiotaras, Nomicos et al., 2013). This fact is of extreme importance since it indicated the following fact: within a pre-earthquake anomaly the Hurst exponent is increased, and this is a pre-earthquake sign of some additive strength.

Another fact is important: the mean H -values of the radon anomaly, according to R-L method, refer to persistency. This, in relation with the remaining anti-persistent parts of the R-L method, indicates switching between persistency and anti-persistency. Similar switching, as aforementioned, was recognised also in **Figure 5.28** according to wavelet spectral fractal analysis. Through a different starting point, the same output is produced: switching between persistency and anti-persistency is addressed through the three methods employed in research for the estimation of H . Importantly, as

mentioned, this seems that can be recognised as a pre-earthquake footprint. It is important to note that other investigators (Granero et al., 2008; Kilcik et al., 2009; Kulatilake et al., 1998; Warwick et al., 1982) also reported differentiations in estimations of Hurst exponents through R/S , R-L and the Variogram methods. Among these, R-L, while providing slightly higher estimations, is considered as the best approximation (Warwick et al., 1982). The latter was also verified by the outcomes of **Figure 5.29**. Indeed, the R-L technique can be considered as best approximation since it was associated with much smaller errors, while simultaneously provided slightly higher estimations of H during the radon anomaly. Significant is that also the present analysis, provides new scientific evidence regarding chaotic long-memory behaviour of radon in soil prior to earthquakes. Noteworthy is also that, in respect to radon, Planinic, Radolic, & Lazanin (2001) and Planinic, Vukovic, & Radolic (2004) reported radon chaotic regimes through Hurst exponents. These papers provided value ranges of H from measurements of radon in soil and atmosphere. The reported exponents were similar to those of the non-anomalous parts of this paper. Important is also that, according to Kulatilake et al. (1998) the Variogram, spectral fractal and R-L methods are suitable for self-affine profiles. The fractal parameters calculated by each of these methods depend significantly on the input parameter values used in each method, as well as, on the stationary or non-stationary nature of the profile. The latter may also explain the differences observed in various H -estimating methods. Moreover, they provide reasons for differences within each method since the anomalous radon variations were consistent mainly with self-affine Brownian fractals

and include non-stationary window parts. Fractal dimensions followed completely opposite behaviour, since $D=2-H$. The fractal dimensions in the range $1.31<D<1.99$ correspond to wavelet spectral fractal analysis (**Figure 5.28**). The R/S method through lumping in independent segments, estimated values within $1.65<D<1.86$, while the corresponding range was $1.50<D<1.99$. D -value range from Variogram was $1.75<D<1.95$. All techniques revealed significantly lower average fractal dimensions (P< 0.001, ANOVA) in the radon anomaly compared to those of the other parts. Important is that significant differentiation in D has been recognised as ULF electromagnetic pattern of a SOC phase prior to earthquakes (Gotoh, Hayakawa, Smirnova, & Hattori, 2004; Smirnova & Hayakawa, 2007; Smirnova, Hayakawa, & Gotoh, 2004). Note that the increase in H is consistent with decrease in fractal dimension during the SOC phase of the preparation of earthquakes. The fractal dimensions of the non-anomalous parts were between 1.85 and 2.0. The above findings are consistent with weak system's memory. In other words this means that present non-anomalous radon values do not depend on past values and do not determine future trends. However, it should be stressed that completely opposite behaviour in evolution of D was recognised through several methods in pre-earthquake ULF disturbances, where the fractal dimensions prior to earthquakes increased (Gotoh, Hayakawa, Smirnova, & Hattori, 2004; Smirnova & Hayakawa,

2007; Smirnova, Hayakawa, & Gotoh, 2004) This behaviour was reported as peculiar and was discussed in view of a SOC pre-earthquake state.

5.4 Results based on the analysis of block entropy

Figure 5.30 illustrates the time evolution of the block entropies of the Ileia radon time-series of 2008, for block lengths n of 2 and 4 letters. The evolution for $n=3$ was intermediate and for this reason it is not presented here. The analysis was performed through lumping under the rule $n=N$, i.e., equal size of word blocks and lengths. The stable part of the 2008 signal, i.e., from approximately day 50 (Nikolopoulos et al., 2012) is characterised by significantly higher average values of Shannon entropy $H(n)$ ($p<0.001$, ANOVA). Similar high average values were found for the 2010 and 2011 radon signals. Since Shannon block entropy is the fundamental measure of randomness (Eftaxias et al., 2009), this finding means (Eftaxias et al., 2009; Karamanos et al., 2006) that the average amount of information necessary to predict a sub-sequence of length n is larger in background than in anomalies. Shannon block entropy per letter $h^{(n)}$ shows that the average uncertainty per letter (Eftaxias et al., 2009; Karamanos et al., 2006; Petraki, Nikolopoulos, Fotopoulos, Nomicos et al., 2013) of a block of size n (Eftaxias et al., 2009; Karamanos et al., 2006; Petraki, Nikolopoulos, Fotopoulos, Nomicos et al., 2013) is larger in the background than in bursts ($p<0.001$,

ANOVA on the averages). Conditional block entropy $h_{(n)}$ exhibits also significantly higher values ($p<0.001$, ANOVA) in radon background. This was also recognised in the 2010 and 2011 radon signals. The increase in $h_{(n)}$ means also increase in the uncertainty of predicting one step in the future provided the history of the present state and the previous $n-1$ states (Eftaxias et al., 2009; Petraki, Nikolopoulos, Fotopoulos, Nomicos et al., 2013). Significant decrease in $h_{(n)}$ is observed in the first 50 days of the signal for all the block sizes studied. This implies that during these 50 days, the average predictability of a state following a measured n -trajectory, is higher in radon bursts. This is reinforced by the findings of Eftaxias et al., (2009), according to which, any existing long-range memory decreases conditional entropy and improves the chance of prediction. The values of the Tsallis and normalised Tsallis entropy in **Figure 5.30** were estimated considering $q=1.80$ (Kalimeri et al., 2008). Tsallis entropy drops to lower values in the emerged radon anomalies in comparison to the background. This behaviour was identified in all block sizes. Similar high values of Tsallis and normalised Tsallis entropy were also detected in the background signals of 2010 and 2011. The Tsallis entropy drop during radon anomalies suggests that in radon background there are many kinds of patterns, while in the anomalies few (Eftaxias et al., 2009; Petraki, Nikolopoulos, Fotopoulos, Nomicos et al., 2013). This implies self-organisation. This finding in conjunction with the results of the long-memory methods implies that radon anomalies refer to a SOC state, characteristic of the preparation of earthquakes. It can be observed from **Figure 5.30** that all block entropies imply

comparable behaviour and clearly discriminate the anomalies from the background since low values are observed in the region of the anomalies and high values in the region of the background. It should be noted that, especially Tsallis entropy, is very sensitive in identifying possible effects of long-range interaction, long-time memories and multi-fractals (Eftaxias et al., 2009; Petraki, Nikolopoulos, Fotopoulos, Nomicos et al., 2013). The presented results thus indicate presence of long-range interactions and long-memory of the anomaly generating system. This long-range dependence is indicative of the prediction reliability of the system. In addition, **Figure 5.30** indicates also entropy differentiations with increase of letters. More specifically, Shannon block entropy increases approximately by half a unit for 2, 3 and 4 letters i.e. its range is $0.67 \leqslant H(n) \leqslant 1.38$ for 2 letters, $0.81 \leqslant H(n) \leqslant 2.07$ for 3 letters and $0.86 \leqslant H(n) \leqslant 2.73$ for 4 letters. The Shannon block entropy per letter $h^{(n)}$ and the conditional entropy $h_{(n)}$ are greater for 2 letters than for 3 letters while for 4 letters are almost stabilised. Tsallis entropy S_q and normalised Tsallis entropy $\hat{S}_q$ exhibit similar behaviour to Shannon block entropy $H(n)$ i.e. increase with number of letters. The range of Tsallis entropy S_q is $0.36 \leqslant S_q \leqslant 0.83$ for 2 letters, $0.43 \leqslant S_q \leqslant 1.01$ for 3 letters and $0.47 \leqslant S_q \leqslant 1.11$ for 4 letters. Furthermore, the

range of normalised Tsallis entropy is $0.50 \leqslant \hat{S}_q \leqslant 2.50$ for 2 letters, $0.65 \leqslant \hat{S}_q \leqslant 5.24$ for 3 letters and $0.75 \leqslant \hat{S}_q \leqslant 9.55$ for 4 letters. However, after a certain number of letters (7 letters) Shannon block entropy, Tsallis entropy S_q and normalised Tsallis entropy $\hat{S}_q$ were found to stabilise. All the above issues indicate the importance of symbolic dynamics in the study of pre-earthquake environmental signals since these techniques provide measures of complexity of signals (Eftaxias et al. 2009; Minadakis et al., 2012; Potirakis et al., 2012). For example, under similar analysis, reduction of complexity of the fracto-electromagnetic mechanism of the order of 30% or more has been observed during two electromagnetic bursts of a precursory earthquake signal which characterised high order of organization (Karamanos et al., 2005).

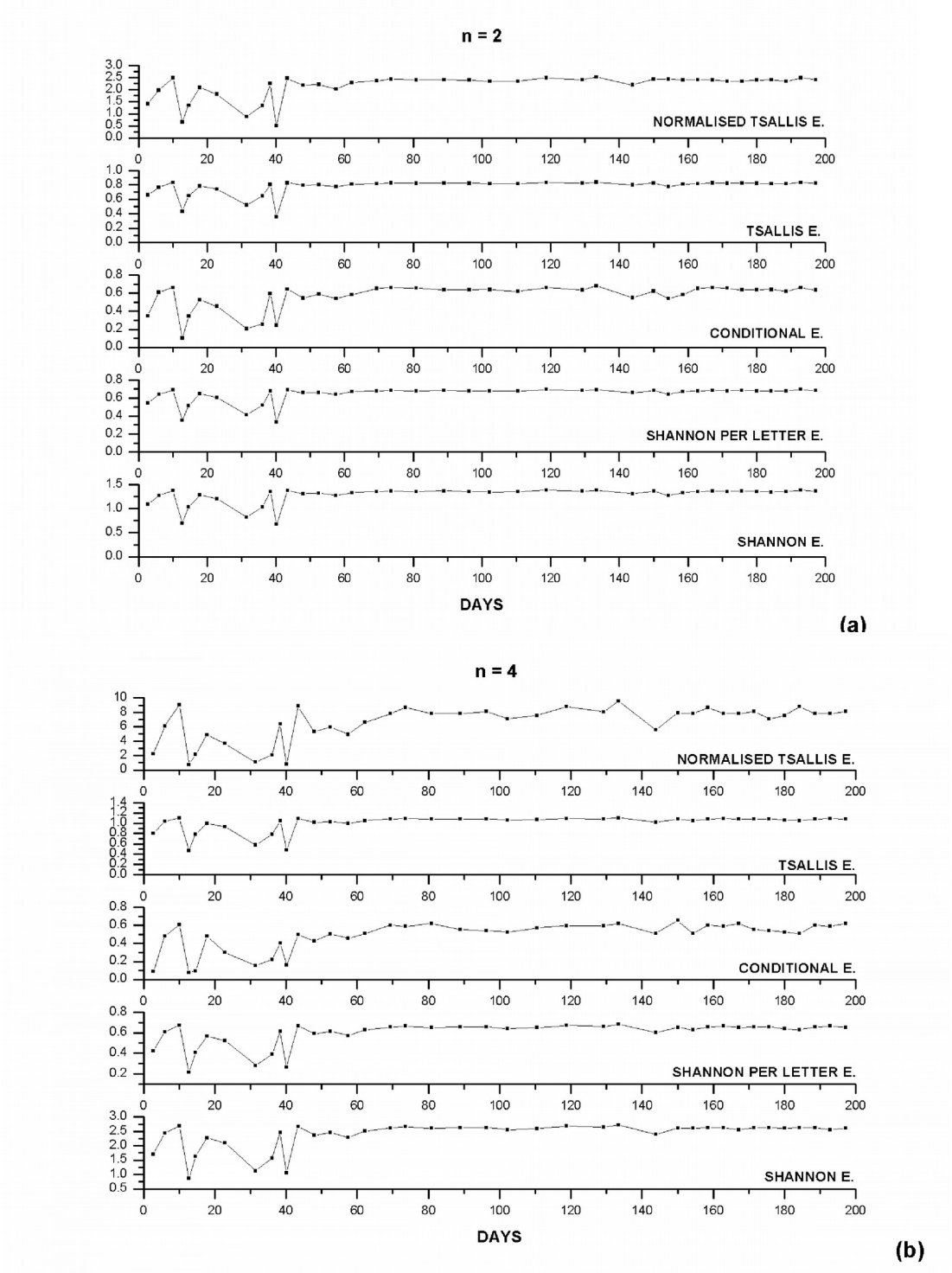

Figure 5.30: Block entropy analysis of the Ileia 2008 radon time-series through lumping and symbolic dynamics.

Entropy unit is $m^2 \cdot kg \cdot K^{-1} \cdot s^{-2} \left(x\, 1.3806488 \text{x} 10^{23} \right)$.

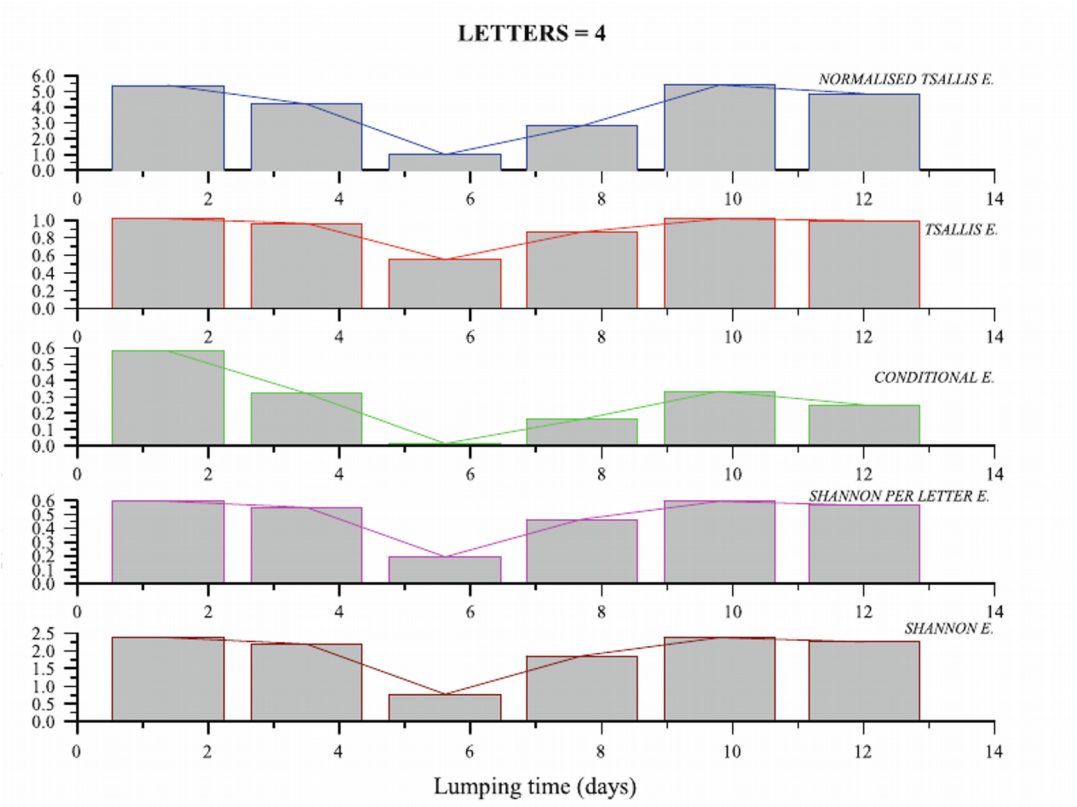

Figure 5.31: Block entropy analysis of the Lesvos 2008 radon time-series through lumping and symbolic dynamics.

Entropy unit is $m^2 \cdot kg \cdot K^{-1} \cdot s^{-2} \left(x 1.3806488 \text{x} 10^{23} \right)$.

Figure 5.31 illustrates the time evolution of the block entropies of the Lesvos 2008 signal for the intermediate block length of $n=4$. The entropy evolution for $n=3,5,6,7$, as well as, for $n>7$ was similar to those presented in **Figure 5.31**. It was observed that as block length increased, the absolute values of each entropic metric increased as well. The inter-entropy relation however remained unchanged. Important finding was that all entropy measures were led into saturation for $n>7$. Similar outcome was also observed in the Ileia radon signal. Note that the lumping segments were those of **Figure 5.28**. It is very important that the anomalous part of the Lesvos signal, presented significantly lower values (P<0.001, ANOVA) of all entropy measures. This significant finding suggests self-organisation of the underlying geological dynamics (Eftaxias et al, 2010; Eftaxias et al., 2009; Kalimeri et al., 2008; Karamanos, 2000, 2001; Karamanos et al., 2006; Minadakis et al., 2012; Petraki, Nikolopoulos, Fotopoulos, Panagiotaras, Koulouras, et al., 2013). More specifically, since Shannon block entropy is the fundamental measure of randomness (Eftaxias et al, 2010), the lower value observed in the radon anomaly, suggests that the average amount of information necessary to predict a sub-sequence of length n , is larger in non-anomalous parts than in the anomaly (Eftaxias et al, 2010; Karamanos et al., 2006). Decrease in Shannon (n) block entropy per letter h , implies that the average uncertainty per letter of a block of size n is larger in non-anomalous parts than in the radon anomaly (Eftaxias et al, 2010; Karamanos et al., 2006). Conditional block

entropy $h_{(n)}$ drop in the radon anomaly, means also increase in the uncertainty of predicting one step in future, provided the history of the present state and the previous $n-1$ states (Eftaxias et al, 2010; Karamanos et al., 2006). This further implies that the average predictability of a state following a measured n -trajectory, was higher in the radon anomaly. This is reinforced by the findings of other investigators (Eftaxias et al, 2010; Kalimeri et al., 2008; Karamanos et al., 2006) according to which, existing long-range memory, decreases conditional entropy and improves the chance of prediction. The values of the Tsallis and normalised Tsallis entropy in **Figure 5.31** were estimated considering $q=1.80$ (Kalimeri et al., 2008). Tsallis entropy drop into lower values in the emerged radon anomaly, suggests that in non-anomalous parts there are many kinds of patterns, while in the anomaly few (Kalimeri et al., 2008). It may be supported from the results of **Figure 5.31**, that all block entropy measures clearly discriminate the anomaly from the background. It should be emphasised that, especially Tsallis entropy, is very sensitive in identifying possible long-range interactions, long-memory and multi-fractals (Eftaxias et al., 2010; Kalimeri et al., 2008). The presented results, hence, indicate presence of long-range interactions and long-memory of the geo-environmental anomaly-generating system. This long-range dependence is indicative of the prediction reliability of the system. All above issues clearly present the importance of symbolic dynamics in the study of environmental signals.

5.5 Conclusions

From the data presented in **Chapter 5** in relation with the data presented in **Chapters 3** and **4**, it becomes evident that to identify pre-earthquake signs of enhanced significant value, the following steps should be followed (some already mentioned in **Chapters 3** and **4**):

(a) Employ fractal methods for identifying the fBm segments, because these are considered to be associated with long-memory dynamics. These methods can also screen the random fGn segments.

(b) After the first screening with (a), a second screening should be applied to identify the segments which are well away from randomness. According to the view of the author (as aforementioned) this is implemented for values of $b>1.5$. According to other investigators (e.g. Eftaxias et al., 2010), this is implemented for values of $b>2$.

(c) A third screening is the combined application of the R/S analysis, at the same segments as (a). If the high b segments are associated with increase in H-values, then the precursory value is enhanced.

(d) A fourth screening is the combined application of DFA. Since DFA is advantageous from all other methods, it could be employed also in independent segments. However, the application in the same segments is advantageous. If the areas of high b and H values ((b) & (c)) are associated with high DFA

a exponents, then the precursory value is even better.

(e) As a final screening, several entropy metrics can be calculated. If the areas identified in (a)-(e) are associated with significant drop of the entropy measures, then the quality of the precursor becomes significantly better.

In any case, even if the signal presents certain pre-earthquake patterns and even if (a)-(e) are simultaneously addressed, the inevitable occurrence of an earthquake could not yet be prognosed. The latter because as presented in **Chapters 1** and **2**, it is very difficult to associate either radon or electromagnetic disturbances to earthquake occurrences.

Chapter 6

Conclusions and Future Work

The first chapter of this research reviewed the electromagnetic precursors of general failure, detected prior to earthquakes internationally. The chapter analysed systematically the related scientific papers, some of which referred to great earthquakes of previous decades. In general, since the early eighties, the scientific community has concentrated on the precursory Radio Frequency (RF) signals of the Ultra-Low-Frequency (ULF) range. One of the great advances of this approach was the, so called, VAN (Varotsos-Alexopoulos-Nomicos) method with several successive prognoses up to now. From the late nineties, new approaches emerged with focus on the Low-Frequency (LF) and the High-Frequency (HF) electromagnetic RF precursors. Several investigators have claimed that certain reported pre-seismic electromagnetic signals were, indeed, precursory. A number of researchers have, additionally, claimed that the reported RF signals had direct links with certain earthquakes. Despite that the related research enumerates many papers in significant peer-reviewed scientific journals, it is still an open issue whether there exist definite rules to link certain pre-earthquake anomalies to specific seismic events, either if these are intense or mild. Most important seem to be whether there can be found hidden pre-seismic footprints in pre-earthquake RF electromagnetic time-series and, if so, which is the way to delineate these footprints. For this reason, despite the fairly abundant circumstantial evidence, the scientific community still debates the precursory value of the premonitory RF anomalies detected prior to earthquakes, while, on the other hand, the related research is continuously growing. Regarding signal analysis, it is worth noting that the vast

majority of the reported electromagnetic disturbances have been analysed visually, especially the ULF ones. It is only since the last decade, where advanced techniques have been introduced for the analysis of the precursory RF signals and this, still, on a restricted basis. Significantly, there seem to be the chaotic regimes based on the spectral analysis of spatio-temporal fractals, the evolution analysis of the Hurst exponent, the Detrended Fluctuation Analysis (DFA) and the analysis of Natural Time. All these techniques have been applied to the ULF precursors and more extensively to the KHz (LF) and the MHz (HF) pre-earthquake precursors. These techniques have been utilised because they can delineate the trends of long-memory of the earthquake generating system. The KHz and MHz RF precursors have been also analysed through several metrics of entropy, and this is indicative of self-organisation. Separately, or better when combined, the long memory analysis or the system's self-organisation, have provided significant findings regarding the earthquake generating system and the nodal evolution stages of earthquakes. Importantly, certain long-memory patterns and self-organisation trends have been proposed as well-established pre-earthquake traces. Since the investigation of RF precursors is an important ongoing investigation, this research contributed towards this direction. Significant approaches, some of which when combined, assist the delineation of the process of generation of earthquakes. Four of the recent peer-reviewed journal papers (2012-2015) with application of advanced techniques in electromagnetic disturbances of the MHz range were published as a result of the related contribution of this research.

The anomalous radon gas emissions have an equal long history in the science of earthquake prediction. The related papers have been reviewed in the second chapter of

this research. In general, several anomalous radon emissions have been observed prior to earthquakes and this has been recorded all over the world. The abnormal radon exhalation from the interior of the earth has been associated with earthquakes and is considered an important field of research. The abnormal pre-seismic radon disturbances have been detected in soil, atmosphere and water. The related literature started from the early seventies and is still in progress. Three are the proposed physical models which attempt to relate the observed radon disturbances with deformations occurring in the earth's crust prior to forthcoming earthquakes. While the models provide some physical explanations, there are many parameters that require further investigation. As with the electromagnetic precursors, the majority of the published pre-earthquake radon disturbances have been analysed visually. Advanced analysis is rare in the related literature. No more than nine papers have been published with application of advanced and state-of-the-art techniques. This research contributed, and this is very important, six of the nine recent peer-reviewed journal papers with advanced techniques that were published between 2012 and 2015. These papers analysed the time-evolution of the fractal dimension, the Hurst exponent, the power-law-beta fractal exponent, other long-memory exponents derived from DFA and several metrics of entropy. As aforementioned, such techniques have been employed in the analysis of the electromagnetic precursors of general failure. It is also very important to note that this research contributed two novel scientific peer-reviewed journal publications regarding the combined and unified confrontation of the pre-earthquake disturbances of both radon gas and electromagnetic emissions of the MHz range. Another novel contribution of this research was the multilevel analysis of a very significant active radon signal detected in a station in Peloponnese in Greece located only 29 km away from the

epicentre of the very destructive earthquake of Kato Achaia (Andravida) Greece of . Apart from the above, another significant related work was published from a team in India in 2012 by applying multi-fractal techniques in a three year radon signal. Such analysis have been also published since 2010 in the electromagnetic precursors as well. Either the visual analysis or the analysis of the various metrics of the long memory or the self-organisation of the earthquake generating system, provides significant outcomes regarding the earthquake prediction. However more research needs to be done to delineate the process of radon generation during earthquakes. This justifies the significance of this research.

The third chapter of this research reported the findings from the long-memory analysis based on fractals, regarding several pre-earthquake MHz electromagnetic time-series that were reported. According to the outcomes of the systematic time-evolution spectral analysis of fractals presented in **Chapter 3**, the following issues were addressed:

(1) More than a hundred pre-seismic MHz electromagnetic time-series have been analysed prior to thirty three significant earthquakes with $M_L \geq 5.0$ which occurred in Greece. This is the first time that such an extensive analysis is attempted prior to a significant number of earthquakes. Importantly, several of these MHz pre-seismic signals were of one-month duration.

(2) All the investigated signals exhibited characteristic epochs with fractal organisation in space and time. In some cases these epochs were continuous and on other cases scattered. Signals with no such epochs were associated with seismic quiet epochs. Scattered and continuous epochs were detected even in several one-month signals. The successive organisation was defined in terms of

successive (Spearman's $r^2 \geq 0.95$) segments of 1024 sample size each. The fractal organisation was identified in segments of greater size as well. For a unified approach, however, the segment size of 1024 was adopted in all the analysis of this research.

(3) Several successive ($r^2 \geq 0.95$) segments exhibited power-law b - values above 1.5. The majority of the successive fractal segments of electromagnetic RF disturbances were associated with anti-persistency ($1.5 < b < 2.0$). Numerous persistent ($2.0 < b < 3.0$) time-series RF parts were detected. Switching between persistency and anti-persistency was also found. Although several references suggested that the MHz electromagnetic precursors show only anti-persistent behaviour, the systematics of this research supports a different aspect. The electromagnetic MHz disturbances can be either anti-persistent or persistent. This was supported from the findings of **Chapter 5**. The most significant related finding which was the most valuable pre-earthquake pattern is the switching between persistency and anti-persistency.

(4) The Hellenic electromagnetic network showed sensitivity differentiations in the fractal behaviour due to locality. This was systematically addressed by all the investigated earthquakes of 2009. All the 2009 earthquakes with $M_L \geq 5.0$ were pre-signalized through interrupted or continuous fractal segments of long memory not necessarily by nearby stations. Only two earthquakes of 2009 were detected by two or more stations. The remaining stations did not give MHz signals with characteristic pre-earthquake fractal footprints. Cases were detected were the characteristic fractal epochs were identified in a rather far station and not in the near station. This was addressed in Vamos and Neapoli stations. This

research, did not attempt however to address this issue because the systematic approach needs investigation of much more significant earthquakes and related signals. Concluding *the presented fractal data*, although of great amount, *are still limited to identify the sensitivity dependencies* of the Hellenic network.

(5) Several significant pre-signalized earthquakes were associated with fractal warnings up to one month prior to each event. Some warnings evolved up to some hours prior to the earthquake. The remaining investigated MHz signals gave significant alarms usually 2-3 weeks and 1 week prior to the event. The latter was in agreement with the published behaviour of the MHz radiation, however from the study of only few earthquakes.

(6) The findings indicated self-organised critical state characteristic of the last stages of the investigated earthquakes.

(7) Various geological explanations were proposed mainly in the view of the asperity model. The persistent and the anti-persistent MHz anomalies were linked to the micro-cracking of the heterogeneous medium of the earth's crust which may have led the system's evolution towards global failure. This approach has been employed by other investigators as well.

(8) The thirty-three earthquakes studied which were associated with MHz electromagnetic disturbances of some days up to one-month duration prior to earthquakes of 2007, 2008, 2009, 2013, 2014 and 2015 with $M_L \geq 5.0$, indicated that the MHz electromagnetic disturbances can be used as reliable pre-seismic precursors of some scientific value.

(9) The precursory fractal epochs of noteworthy value are the ones associated with a successive ($r^2 \geq 0.95$) fBm class ($1 < b < 3$).

(10) Enhanced precursory fractal epochs are the successive fBm ones with *many successive* ($r^2 \geq 0.95$) *segments above 1.5* and better, *above 2.0.* These epochs indicate well-established long-memory dynamics well away from fGn randomness.

(11) The precursory value is enhanced more if *switching between persistency and anti-persistency is* also *identified*. This was supported by several publications of the author and colleagues.

(12) A s*udden and sharp increase in values of the spectral fractal exponent* b *is an enhanced potential pre-seismic pattern*, especially when *associated with a visual disturbance.*

(13) *The fractal analysis method can be employed as a first screening method for the identification of long-memory patterns hidden in pre-seismic time-series. It is also, from the results, a reliable method for identifying pre-earthquake patterns.*

Chapter 4 reported the findings from the long-memory analysis applied to significant signals of radon in soil derived between 2008 and 2015. The most significant signals were the (a) Ileia signal derived prior to the very destructive earthquake of Andravida, Greece, 2008 with M_L=*6.5*; (b) the concurrent 2008 Lesvos signal prior to a nearby earthquake; (c) two signals of 2015 prior to two twin earthquakes occurred in Chalkis, Greece. All these signals lasted several weeks and, importantly, were derived with active methods. It is very significant to recall that reports of active radon signals prior to very destructive earthquakes are rare in the literature. Especially the Ileia signal was of great importance because there were strong evidence that it may had linkage to the

strong earthquake of the 8th June of 2008 because the distance between the site of the detection of this anomaly and the epicentre of the earthquake was only 29 km, and this was extremely rare. The significance of these signals and their analysis was recognised in four peer-reviewed journal publications of the author and colleagues. Additionally, another signal was reported concurrent with the Ileia signal, however, derived through passive methods. The analysis of long-memory of the signals of **Chapter 4** was combined with similar investigation of several background parts to address the differences. In addition, since radon in soil is affected by environmental parameters, this research extended to the systematic study of environmental parameters in terms of (a) advanced multi-parameter statistical analysis with focus on outliers; (b) cross-correlation; (c) short time Fourier analysis; (d) analysis through the continuous wavelet transform. Importantly, this research was the first one to introduced this type of chaotic analysis to this extent and, due to this, it is considerably novel in this field of investigation. The findings from the long-memory analysis based on fractals of radon disturbances in the soil indicated a very significant issue: *the radon disturbances in the soil prior to earthquakes exhibit similar fractal behaviour as the MHz RF disturbances of general failure.* This issue was analysed in depth in three peer-reviewed journal publications. It also supported *the pre-seismic disturbances of radon in soil correspond to the same phase of preparation of an earthquake as the MHz ones* and that *usually the radon disturbances are expected to occur in a time lag of 2-3 months up to 1-3 weeks prior to an earthquake*, although the literature reports cases with disturbances less than a week and after the shock (post-earthquake activity). Summarising the most important findings, through the systematic chaotic analysis of four significant earthquakes in Greece, the following issues were supported:

(1) the disturbances of radon in soil can be used as reliable pre-seismic precursors of some scientific value.

(2) Almost all the investigated radon signals exhibited characteristic epochs with fractal organisation in space and time. As with the MHz radiation these epochs were those of a successive ($r^2 \geq 0.95$) fBm class ($1 < b < 3$).

(3) Enhanced precursory fractal epochs were also recognised with *successive* ($r^2 \geq 0.95$) *fBm segments above 1.5 (anti-persistency)* and in some times, *above 2.0 (persistency). Switching between persistency and anti-persistency* was identified and this was considered as those with *enhanced precursory value*.

(4) A s*udden and sharp increase in values of spectral fractal exponent* b *is an enhanced potential pre-seismic pattern*, especially when *associated with a visual disturbance.*

(5) *The radon precursors and the MHz electromagnetic correspond to the same pre-earthquake phase.*

(6) Geological explanations were proposed in view of the asperity model. Persistent & anti-persistent MHz anomalies were due to micro-cracking of the heterogeneous medium of the earth's crust which may have led the system's evolution towards global failure.

Chapter 5, finally presented the long-memory analysis of earthquake generation system in terms of Hurst exponent evolution, DFA and the system's self-organisation through block-entropy analysis. In specific, the main set of methods presented in **Chapter 5**, estimated the Hurst exponent directly or indirectly, whereas, the second set referred to the self-organisation of the system of earthquake generation through several

metrics of entropy. First the mathematical basis was given for both sets of methods. Then, the Hurst exponent analysis was employed through mainly the R/S technique. Detrended fluctuation analysis was also employed to some extend, mainly because it is a very robust method. Finally, the results from the entropic techniques were reported. Finalising, from the data presented in **Chapter 5** in relation with the data presented in **Chapters 3** and **4**, it was concluded that to identify pre-earthquake signs of enhanced significant value, the following steps should be followed:

(a) Employ fractal methods for identifying the fBm segments, because these are considered to be associated with long-memory dynamics. These methods can also screen the random fGn segments.

(b) After the first screening with (a), a second screening should be applied to identify the segments which are well away from randomness. According to the view of the author this is implemented for values of $b>1.5$. Other investigators suggest that this is implemented only for values of $b>2$.

(c) A third screening is the combined application of the R/S analysis, at the same segments as (a). If the high b segments are associated with increase in H - values, then the precursory value is enhanced.

(d) A fourth screening is the combined application of DFA. Since DFA is advantageous from all other methods, it could be employed also in independent segments. However, the application in the same segments is advantageous. If the areas of high b and H values ((b) & (c)) are associated with high DFA a exponents, then the precursory value is even better.

(e) As a final screening, several entropy metrics can be calculated. If the areas identified in (a)-(e) are associated with significant drop of the entropy

measures, then the quality of the precursor becomes significantly better.

The final conclusion of this research is that, more or less, *all techniques should be employed in sequential steps, albeit the power-law spectral fractal analysis is the first and most significant technique to trace long-memory patterns of* $1/f$ *processes as those of the processes of earthquakes*.

Appendix 1

Table A1: Earthquake precursory data: Earthquake data, type of electromagnetic precursor detected and related instrumentation, method of detection with precursory time and effective distance (ED) from the epicenter of the earthquake and literature data.

	Earthquake			**Disturbance**			**Detection**			
	Place	***Magnitude***	***Date(s)***	***Emission type***	***Frequency range***	***Instrumentation***	***Method(s)***	***Precursory time***	***ED***	***Reference***
Single events	Chile	10	22/05/1960	Radio	18 MHz	Radioastronomy receiver	Visual observation	b (6 days)	Worldwide	Warwick et al., 1982
	Hollister, California	5.2	28/11/1974	ULF magnetic		Array of 7 proton magnetometers	Visual observation	b(7week-several months)	11 km	Smith and Johnston, 1976
	Tangshan, China	7.8	28/07/1976	Resistivity			Visual observation	b(2-3 years)	<150 km	Zhao and Qian, 1994
	Tangshan, China	7.8	28/07/1976	Self potential, magnetotelluric			Visual observation	b(3 months)	<120 km	Zhao and Qian, 1994
	Sungpan–Pingwu,China	7.2	16/08/1976	Telluric currents			Visual observation	b(1month)	<200 km	Wallace and Teng, 1980
	Sungpan–Pingwu,China	6.8	22/08/1976	Telluric currents			Visual observation	b(1month)	<200 km	Wallace and Teng, 1980
	Sungpan–Pingwu,China	7.2	23/08/1976	Telluric currents			Visual observation	b(1month)	<200 km	Wallace and Teng, 1980
	Kyoto, Japan	7.0	31/03/1980	VLF electric	81 KHz	Electric antenna	Visual observation	b(1/2 h)	250 km	Gokhberg et al., 1982
	Tokyo, Japan	5.3	25/09/1980	VLF electric	81 KHz	Electric antenna	Visual observation	b(1h)	55 km	Gokhberg et al., 1982
	Tokyo, Japan	5.5	28/01/1981	VLF electric	81 KHz	Electric antenna	Visual observation	b(3/4h)	50 km	Gokhberg et al., 1982
	Kalamata, Greece	6.2	13/09/1986	Electric			Visual observation	b(3-5days)	200 km	Gershenzon and Gokhberg, 1993
	Spitak, Armenia	6.9 (M_s)	07/12/1988	ULF magnetic	0.01-1Hz	3-axis magnetometers	Visual observation & Statistical analysis	b(4h),a	128 km	Molchanov et al., 1992
	Spitak, Armenia	6.9 (M_s)	07/12/1988	ULF magnetic	0.005-1Hz		Visual observation & Statistical analysis	b(4h).a	120 km, 200 km	Kopytenko et al., 1993
	Loma Prieta, California	7.1 (M_s)	18/11/1989	ULF magnetic	0.01Hz		Visual observation & Statistical analysis	b(3h),a	7 km	Molchanov et al., 1992
	Loma Prieta, California	7.1 (M_s)	19/11/1989	ELF-VLF EM	0.01Hz-32KHz	Ground-based magnetometers	Visual observation	b(3h),d	52 km	Fraser-Smith et al., 1990
	Spitak, Armenia	6.9 (M_s)	23/01/89	ELF-VLF EM	140Hz,450 Hz 800Hz, 4500 Hz, 15000 Hz	COSMOS-1809 Satellite	Visual observation&Statistical Analysis&FFT	b(<3h)	Δlong < 6^0 Δlat 2^0-4^0 [12 from the 13 satelite orbits for f<450 Hz]	Serebryakova et al.,1992
	Upland, California	4.3	17/04/1990	ELF magnetic	3-4Hz	Vertical magnetic sensor	Statistical Analysis&PSD-FFT	b(1d)	160 km	Dea et al., 1993
	Western Iran	7.5	20/06/1990	Ionospheric(radiow ave)	0-8KHz,10-14KHz	INTERCOSMOS-19 satellite	Visual observation & Modelling	b(16d)	250 km-2000 km	Shalimov and Gokhberg, 1998

Earthquake			Disturbance			Detection			
Place	*Magnitude*	*Date(s)*	*Emission type*	*Frequency range*	*Instrumentation*	*Method(s)*	*Precursory time*	*ED*	*Reference*
Watsonville, California	4.3	23/03/1991	ELF magnetic	3.0–4.0 Hz	North–south magnetic sensor	Statistical Analysis&PSD-FFT	b (data averaged over 2 days)	600 km	Dea et al., 1993
Watsonville, California	4.3	23/03/1991	ELF magnetic	3.0–4.0 Hz	Vertical magnetic sensor	Statistical Analysis&PSD-FFT	b (data averaged over 2 days)	600 km	Dea et al., 1993
Coalinga, California	4.0	15/01/1992	ELF magnetic	3.0–4.0 Hz	Vertical magnetic sensor	Statistical Analysis&PSD-FFT	b (data averaged over 2 days)	400 km	Dea et al., 1993
Hokkaido, Japan	7.8	12/07/1993	foF_2 ionospheric			Visual observation & Statistical analysis	b (3 days)	290 km, 780 km, 1280 km	Ondoh, 1998
Guam	7.1 (M_s)	08/08/1993	ULF magnetic	0.02–0.05 Hz	3-axis ring–core-type fluxgatemagnetometer (NS, EW, Vertical)	Fractal analysis with PSD-FFT	b (1 month)	65 km	Hayakawa et al., 1996;Hayakawa et al., 1999; Smirnova and Hayakawa 2007
Guam	8.3 (M_{JMA})	08/08/1993	ULF magnetic	0.02–0.05 Hz	3-axis ring–core-type fluxgatemagnetometer (NS, EW, Vertical)	Multifractal Detrended Fluctuation Analysis	b (1 month)	65 km	Hayakawa et al., 2005
Hokkaido–Toho–Oki, Japan	8.1 (M_w)	04/10/1994	VLF electric		Borehole antenna	Visual observation	b (20 min)	>1000 km	Fujinawa and Takahashi, 1998
Hyogo-ken Nanbu (Kobe), Japan	7.2	17/01/1995	DC geopotential, ELF magnetic,VLF radio, MF–HF,VHF FM-wave	223 Hz, 1–20 KHz, 163 KHz, 77.1 MHz		Visual & statistical analysis	b (<7 days)	≥ 100 km	Enomoto et al., 1997
Hyogo-ken Nanbu (Kobe), Japan	7.2 (M_0)	17/01/1995	VLF radio	10.2 KHz	VLF Omega transmitter and receiver	Statistical Analysis (TT method) & Modelling	b (2 days)	70 km	Molchanov et al., 1998
Hyogo-ken Nanbu (Kobe), Japan	7.2	17/01/1995	Electric	22.2 MHz	Phase-switched interferometer with two horizontally-polarized antennas		b (1 h)	77 km	Maeda and Tokimasa, 1996
Kozani-Grevena, Greece	6.6 (M_w)	13/05/1995	Electric, magnetic				b (2 weeks)	70 m, 200 km	Bernard et al., 1997

Earthquake			Disturbance			Detection			
Place	*Magnitude*	*Date(s)*	*Emission type*	*Frequency range*	*Instrumentation*	*Method(s)*	*Precursory time*	*ED*	*Reference*
Kozani-Grevena, Greece	6.6 (M_w)	13/05/1995	VHF electromagnetic	E: 41 & 54 MHz M: 3 & 10 KHz	Electric dipole antennas, magnetic loop antennas	PSD-Wavelet Spestral Fractal analysis and Statistical methods.	b (20 h)	284 km	Kapiris et al., 2002
Kozani-Grevena, Greece	6.6 (M_w)	13/05/1995	VHF electromagnetic	E: 41 & 54 MHz M: 3 & 10 KHz	Electric dipole antennas, magnetic loop antennas	PSD-Wavelet Spestral Fractal analysis and Statistical methods.	b (20 h)	284 km	Kapiris et al., 2003
Kozani-Grevena, Greece	6.6 (M_w)	13/05/1995	VHF electromagnetic	E: 41 MHz	Electric dipole antennas, magnetic loop antennas	PSD-Wavelet Spestral Fractal analysis and Statistical methods.	b (20 h)	284 km	Kapiris et al. 2004.
Kozani-Grevena, Greece	6.6 (M_w)	13/05/1995	VHF electromagnetic	E: 41 & 54 MHz M: 3 & 10 KHz	Electric dipole antennas, magnetic loop antennas	Intermittent dynamics of critical fluctuations (IDCF)-model & Approximation of Power Spectral Density	b (20 h)	284 km	Contoyiannis et al., 2004
Kozani-Grevena, Greece	6.6 (M_w)	13/05/1995	SES	≤1 Hz	Electric dipole antennas, magnetic antennas	Visual and mathematical analysis	b (4 weeks)	70 km-80 km	Varotsos et al., 1999
Kozani-Grevena, Greece	6.8 (M_s)	13/05/1995	SES	≤1 Hz	Electric dipole antennas, magnetic antennas	Visual and mathematical analysis	b (24,25 days)	70 km-80 km	Varotsos et al., 2003
Kozani-Grevena, Greece	6.8 (M_s)	13/05/1995	SES	≤1 Hz	Electric dipole antennas, magnetic antennas	Visual and mathematical analysis	b (22 min-3min)	70 km-80 km	Varotsos et al., 2007

Earthquake			Disturbance			Detection			
Place	*Magnitude*	*Date(s)*	*Emission type*	*Frequency range*	*Instrumentation*	*Method(s)*	*Precursory time*	*ED*	*Reference*
Mid Niigata prefecture	6.8(M_{JMA})	16/08/2005	DC/ULF magnetic VHF/LF	0.02–0.05 Hz 40 KHz	3-axis ring–core-type fluxgatemagnetometer (NS, EW, Vertical) Discon-type antenna (from 25 MHz to 1300 MHz) with IC-RF75 VHF reciever	Signal analysis with FFT	b (17-21 days & 5-7 days)	<220 km, 55^0	Hayakawa et al., 2006
Miyagi-ken oki Japan	7.2 (M_w)	16/08/2005	VHF electromagnetic	49.5 MHz	Discon-type antenna (from 25 MHz to 1300 MHz) with IC-RF75 VHF reciever	(Spectral slope estimation, multi-fractal detrended fluctuation analysis & multi-fractal wavelet transform modulus maxima method.	b (2-3 weeks & few days-Kunimi station only)	90 km -140 km	Yonaiguchi et al., 2007
Akita-ken Nairiku-nanbu, Japan	5.9	11/08/1996	VHF electric	10 KHz- 1MHz	Vertical-dipole ground electrodes	Visual analysis and analysis of related parameters	b (6 days)	<100 km	Enomoto et al., 1997
Chiba-ken Toho-oki, Japan	6.6	11/09/1996	VHF electric	10 KHz- 1MHz	Vertical-dipole ground electrodes	Visual analysis and analysis of related parameters	b (3 days)	320 km, 430 km	Enomoto et al., 1997
Umbria–Marche, Italy	5.5	26/03/1998	LF radio	0.006 Hz	Radio wave vertical antenna		b (1.5 months)	818 km	Biagi et al., 2001
San Juan Bautista, California	5.1 (M_w)	12/08/1998	UHF magnetic	0.01–10 Hz	3-component magnetic field inductor coils	Statistical analysis and Power spectrum analysis (MA indices)	b (2 h)	3 km	Karakelian et al., 2002
Athens, Greece	5.9 (M_w)	07/09/1999	VLF electromagnetic	M: 3 & 10 KHz	Magnetic loop antennas	Delay Times Method, Approximate Entropy, Spectral Fractal Analysis	b (12-17 h)	247 km	Nikolopoulos et al., 2004
Athens, Greece	5.9 (M_w)	07/09/1999	VLF electromagnetic	M: 3 & 10 KHz	Magnetic loop antennas	Wavelet Power Spectrum analysis	b (12-17 h)	247 km	Kapiris et al. 2005

Earthquake			Disturbance			Detection			
Place	*Magnitude*	*Date(s)*	*Emission type*	*Frequency range*	*Instrumentation*	*Method(s)*	*Precursory time*	*ED*	*Reference*
Athens, Greece	5.9 (M_w)	07/09/1999	VLF electromagnetic	M: 3 & 10 KHz	Magnetic loop antennas	Symbolic Dynamics	b (12-17 h)	247 km	Kapiris et al. 2005
Athens, Greece	5.9 (M_w)	07/09/1999	VHF & VLF electromagnetic	E: 41 & 54 MHz M: 3 & 10 KHz	Electric dipole antennas, magnetic loop antennas	Wavelet Power Spectrum analysis	b (12-17 h)	247 km	Eftaxias et al., 2001 & Eftaxias et al., 2002
Athens, Greece	5.9 (M_w)	07/09/1999	VHF & VLF electromagnetic	M: 10 KHz	Electric dipole antennas, magnetic loop antennas	Block Entropy, Kolmogorov-Sinai Entropy, Conditional Entropy	b (12-17 h)	247 km	Karamanos et al., 2005
Athens, Greece	5.9 (M_w)	07/09/1999	VLF electromagnetic	M: 3 & 10 KHz	Magnetic loop antennas	Symbolic Dynamics	b (12-17 h)	247 km	Kapiris et al. 2005
Athens, Greece	5.9 (M_w)	07/09/1999	VHF & VLF electromagnetic	E:154 MHz M: 3 & 10 KHz	Electric dipole antennas, magnetic loop antennas	Intermittent dynamics of critical fluctuations (IDCF)-model & Approximation of Power Spectral Density	b (20 h)	247 km	Contoyiannis et al., 2004
Athens, Greece	5.9 (M_w)	07/09/1999	VHF & VLF electromagnetic	E: 135 MHz M:10 KHz	Electric dipole antennas, magnetic loop antennas	Intermittent dynamics of critical fluctuations (IDCF)-model & Hurst Analysis	b (>3 h)	247 km	Contoyiannis et al., 2005
Athens, Greece	5.9 (M_w)	07/09/1999	VHF & VLF electromagnetic	M: 10 KHz	Electric dipole antennas, magnetic loop antennas	Tsallis Entropy	b (12-17 h)	247 km	Kalimeri et al., 2008
Athens, Greece	5.9 (M_w)	07/09/1999	VHF & VLF electromagnetic	M: 10 KHz	Electric dipole antennas, magnetic loop antennas	Statistical Analysis	b (12-17 h)	247 km	Potirakis et al., 2011
Athens, Greece	5.9 (M_w)	07/09/1999	VHF & VLF electromagnetic	M: 10 KHz	Electric dipole antennas, magnetic loop antennas	Tsallis Entropy & Fisher Information (10 kHz)	b (12-17 h)	247 km	Potirakis et al., 2012
Athens, Greece	5.9 (M_w)	07/09/1999	VHF & VLF electromagnetic	M: 10 KHz	Electric dipole antennas, magnetic loop antennas	T-Entropy & R/S analysis & wavelet spectral fractal analysis	b (12-17 h)	247 km	Minadakis et al., 2012

	Earthquake			Disturbance			Detection			
	Place	*Magnitude*	*Date(s)*	*Emission type*	*Frequency range*	*Instrumentation*	*Method(s)*	*Precursory time*	*ED*	*Reference*
	Athens, Greece	5.9 (MW)	07/09/1999	VHF & VLF electromagnetic	10 KHz	Electric dipole antennas, magnetic loop antennas	Fisher Information, Approximate Entropy	b (<3h)	284 km	Potirakis et al., 2013
	Chi-Chi, Taiwan	7.6 (M_w)	20/09/1999	foF_2 ionospheric		IPS-42 ionosonde	Visual observation	b (3-4 days)	120 km	Chuo et al., 2002
	Chia-Yii, Taiwan	6.4 (M_w)	22/10/1999	foF_2 ionospheric		IPS-42 ionosonde	Visual observation	b (1-3 days)	179 km	Chuo et al., 2002
	L'Aquila, Italy	6.3	06/04/2009	VHF & VLF electromagnetic	E: 41 & 54 MHz M: 3 & 10 KHz	Electric dipole antennas, magnetic loop antennas	Block/ Kolmogorov/ Conditional approximate/Tsallis/normalised Tsallis entropy Entropy of the source, T-entropy, DFA,WPS, R/S,Hurst analysis	b(<3h)	816 km	Eftaxias et al. 2009, 2010.
Multiple Events	Greece (3 events)	6.0 [NW Crete] 5.0 [SE Crete] 5.0 [NE Samos]	21/11/1992 29/07/1995 07/05/1995	VHF electromagnetic	E: 41 & 54 MHz	Electric dipole antennas	Visual observation	b (1-3 days)	20-150 km	Ruzhin and Nomikos, 2005
	Greece (2 events)	6.6 (M) [Kozani-Grevena] 6.6 (M_w) [Athens]	13/05/1995 07/09/1999	ULF, VHF & VLF electromagnetic	SES 1Hz E: 41, 54 and 135 MHz M: 3 & 10 KHz	Electric dipole antennas, magnetic loop antennas	Wavelet Power Spectrum analysis, Symbolic Dynamics, T-Entropy, Approximate Entropy, normalised Tsallis Entropy	b (<3 h)	284km, 247 km	Eftaxias et al., 2007

Earthquake			Disturbance			Detection			
Place	*Magnitude*	*Date(s)*	*Emission type*	*Frequency range*	*Instrumentation*	*Method(s)*	*Precursory time*	*ED*	*Reference*
Greece (4 events)	6.6(M_W) [Kozani-Grevena] 5.9 (M_W) [Egio-Eratini] 6.6 (M_W) [Athens] 5.9 (M_W) [Lefkas]	13/05/1995 15/06/1995 07/09/1999 14/06/2003	VHF & VLF electromagnetic	E: 41 & 54 MHz M: 3 & 10 KHz	Electric dipole antennas, magnetic loop antennas	Wavelet Power Spectrum analysis, Symbolic Dynamics, T-Entropy, Approximate Entropy, normalised Tsallis Entropy,	b (12-17 h)	<300 km	Eftaxias et al., 2006
Japan (4 events) swarm earthquakes of depth~10km)	6.4 (M_{JMA}) [Izu-Peninsula] 6.1 (M_{JMA}) [Izu-Peninsula] 6.3 (M_{JMA}) [Izu-Peninsula] 6.0 (M_{JMA}) [Izu-Peninsula]	01/07/2000 09/07/2000 15/07/2000 18/08/2000	ULF geomagnetic	0.001-1 Hz	3-axis ring–core-type fluxgatemagnetometer (NS, EW, Vertical)	Fractal analysis with FFT, Higuchi and Bulgara-Klein methods	b (<1 month)	80 km-1160 km	Gotoh et al., 2004
Japan (5 events)	8.3 (M_{JMA}) [Guam] 6.4 (M_{JMA}) [Izu-Peninsula] 6.1 (M_{JMA}) [Izu-Peninsula] 6.3 (M_{JMA}) [Izu-Peninsula] 6.0 (M_{JMA}) [Izu-Peninsula]	08/08/1993 01/07/2000 09/07/2000 15/07/2000 18/08/2000	ULF geomagnetic	0.001-1 Hz	3-axis ring–core-type fluxgatemagnetometer (NS, EW, Vertical)	Fractal analysis with FFT, Fractal Dimension	b (<1 month)	80 km-1160 km	Smirnova et al., 2004

Earthquake				Disturbance			Detection			
Place	*Magnitude*	*Date(s)*	*Emission type*	*Frequency range*	*Instrumentation*	*Method(s)*	*Precursory time*	*ED*	*Reference*
Greece (2 events)	5.2 (M_L) & 5.8 (M_L)	18/01/2007 & 03/02/2007	SES	≤1 Hz	Electric dipole antennas & Magnetic antennas	Natural time analysis	b(22min),a(3min)	<150 km		Varotsos et al., 2007
Greece	Synthetic& 6.4 (M_w)	08/06/2008	SES	≤1 Hz	Electric dipole antennas & Magnetic antennas	Natural time analysis		<30 km		Varotsos et al., 2011
Japan	7.8 (M_{JMA}) [SW offshore Hokkaido] 8.2 (M_{JMA}) [E offshore Hokkaido] 7.6 (M_{JMA}) [far-offshore Hokkaido] 8.0 (M_{sMA}) [offshore Tokachi] 7.8 (M_{JMA}) [Near Chichi-jima] 9.0 (M_{sJMA}) [Tohoku]	07/12/1993 & 04/10/1994 & 28/12/1994 & 26/09/2003 & 22/10/2010 & 11/3/2011	SES	≤1 Hz	Electric dipole antennas& Magnetic antennas	Natural time analysis	b(1 month) [for Tohoku and remaining 6 major EQs with M_{JMA}≥7.6, depth <400 km]	ΔLat< 3^o Δlong< 3^o		Sarlis et al., 2013

Earthquake			Disturbance			Detection			
Place	*Magnitude*	*Date(s)*	*Emission type*	*Frequency range*	*Instrumentation*	*Method(s)*	*Precursory time*	*ED*	*Reference*
Sumatra, Indonesia	9.0 (M_w) [Sumatra-Andaman] 8.7 (M_w) [Sumatra-Nias]	26/12/2004 28/3/2005	ULF geomagnetic	1 Hz	3-axis ring–core-type fluxgatemagnetometer (NS, EW, Vertical)	Spectral density ratio analysis and transfer functions analysis based on wavelet transform method, fractal dimension.	b (<1.5 monhs)	<750 km	Saroso et al, 2009
Sumatra, Indonesia	9.3 8.7	26/12/2004 28/3/2005	Geomagnetic	1 Hz	CHAMP satellite vector magnetic antennas	Wavelet Power Spectrum analysis	b(few hours),a(2 hours)	700 km region	Balasis and Mandea, 2007
Worldwide (325 eq's)	> 5 (M_s)	1981 (Oct)-1983 (Dec)	ELF-VLF EM	140 Hz, 450Hz 800Hz, 4500Hz	ARCAD-3, AUREOL aboard	Statistical Analysis&Modelling	B(0-4h) [component B_z at 140Hz]	ΔLong< 20^0	Parrot, 1994
Japan (26 events)	5.0-6.6	1985-1990	VLF electric	82 KHz	Loop Antennas	Statistical Analysis	b(up to 2 days)	2 km-895 km	Yoshino et al., 1993
Greece (47 events)	3.4–6.8	1983	SES	≤1 Hz	Electric dipole antennas& Magnetic antennas	Visual observation	b	10 km-160 km	Varotsos and Alexopoulos 1984
Central Italy	3.0-4.3	1991–1994	LF radio waves	216 KHz	Electric field strength receivers	Visual analysis and analysis of related parameters	b (6–10 days)	<100 km	Bella et al., 1998
Crete, Greece (19 events)	≥5.0 (M_s)	1992-1995	VHF electromagnetic	3 and 10 KHz, 41 and 53 MHz	Electric dipole antennas, magnetic loop antennas	Visual observation	b(up to 6 days)	300-350 km	Valianatos and Nomikos, 1998
Crete, Greece (19 events)	≥5.0 (M_s)	1992-1995	VHF electromagnetic	41 and 53 MHz	Electric dipole antennas, magnetic loop antennas	Visual observation and Modelling	b(up to 6 days)	300-350 km	Ruzhin and Nomikos, 2004

The symbol b refers to disturbances detected prior to the earthquake(s) and the symbol a to those detected after the event(s). PSD refers to Power Spectral Density, FFT is the abbreviation of the Fast Fourier Transform and Greek delta (Δ) points to a difference in latitude or longitude. SES is the international abbreviation of the VAN method for the Seismic Electrical Signals

Appendix 2

Table 2. Earthquake precursory data: Earthquake data, size and duration of disturbance, precursory time, effective distance (ED) from the epicenter of the earthquake and literature data.

Earthquake					Disturbance		Detection			
Place		*Magnitude*	*Date(s)*		*δα (%)*	*Duration (days)*	*Precursory time (days)*	*ED (km)*	*Reference*
Single events									
USA									
Kettleman Hill	USA	5.6	8/4/85	+	100	Not reported	Not reported	300	Teng & Sun, 1986
Aladale, California	USA	3.7	June/1983	+	1200	3	15	13	Shapiro et al., 1985
France									
Ligurian Sea	France	3.9	1/5/86	+	100	5	3	56	Borchiellini et al., 1991
Japan									
Izu-Oshima	Japan	6.8	01/14/1978	+	7	230	Not reported	25	Wakita et al., 1988
Izu-Oshima	Japan	6.8	01/14/1978	−	8	7	Not reported	25	Wakita et al.: 1988
Izu-Oshima-kinkai	Japan	7.0	01/14/1978		Not reported	Not reported	Not reported	25	Majumdar, 2004
Kobe	Japan	7.2	01/17/1995		2 sd above the mean	Not reported	2 months	Not reported	Yasuoka et al., 2006
P.R. China									
Pohai Bay	PR China	7.4	6/18/1969	+	60	170	Not reported	170	Hauksson, 1981
Ningshin	PR China	4.3	5/8/71	+	200	40	Not reported	42	Hauksson, 1981
Hsingtang	PR China	4.9	6/6/74	+	290	16	Not reported	18	Hauksson, 1981
Haicheng	PR China	7.3	4/2/75	+	38	270	Not reported	50	Hauksson, 1981
Haicheng	PR China	7.3	4/2/75	+	17	50	Not reported	50	Hauksson, 1981
Haicheng	PR China	7.3	4/2/75	−	43	66	Not reported	140	Hauksson, 1981
Haicheng	PR China	7.3	4/2/75	+	20	8	Not reported	140	Hauksson, 1981
Haicheng	PR China	7.3	4/2/75		Not reported	Not reported	Not reported	26	Fleischer, 1981
Liaoyang	PR China	4.8	Not reported		Not reported	Not reported	Not reported	32	Fleischer, 1981
Tangshan	PR China	7.8	6/27/1976	+	15	970	Not reported	50	Hauksson, 1981
Tangshan	PR China	7.8	6/27/1976	+	50	15	Not reported	100	Hauksson, 1981

Earthquake				Disturbance			Detection		
Place		*Magnitude*	*Date(s)*		*δα (%)*	*Duration (days)*	*Precursory time (days)*	*ED (km)*	*Reference*
Tangshan	PR China	7.8	6/27/1976	−	40	1370	Not reported	130	Hauksson, 1981
Tangshan	PR China	7.8	6/27/1976	+	27	162	Not reported	130	Hauksson, 1981
Tangshan	PR China	7.8	6/27/1976		Not reported	Not reported	Not reported	1800	Fleischer, 1981
Chienan	PR China	6.0	3/7/1977	+	70	3	1	200	Teng, 1980
Sabteh	PR China	5.2	4/8/1972	+	55	12	Not reported	70	Teng, 1980
Takung	PR China	5.8	9/27/1972	+	34	12	Not reported	54	Teng, 1980
Luhuo	PR China	7.9	2/6/1973	+	120	9	Not reported	200	Wakita et al., 1988
Yiliang	PR China	5.2	4/22/1973	+	41	14	Not reported	340	Teng, 1980
Songpan	PR China	5.2	5/8/1973	+	40	14	Not reported	345	Hauksson, 1981
Mapien	PR China	5.5	6/29/1973	+	89	9	Not reported	200	Wakita et al., 1988
Lungling	PR China	7.5	5/29/1976	+	20	510	Not reported	20	Hauksson, 1981
Lungling	PR China	7.5	5/29/1976	+	15	425	Not reported	190	Hauksson, 1981
Lungling	PR China	7.5	5/29/1976	+	8	160	Not reported	210	Hauksson, 1981
Lungling	PR China	7.5	5/29/1976	+	12	130	Not reported	215	Hauksson, 1981
Lungling	PR China	7.5	5/29/1976	+	7	75	Not reported	360	Hauksson, 1981
Lungling	PR China	7.5	5/29/1976	+	20	290	Not reported	420	Hauksson, 1981
Lungling	PR China	7.5	5/29/1976	+	200	12	Not reported	450	Hauksson, 1981
Songpan-Pingwu	PR China	7.2	8/16/1976	+	29	480	Not reported	40	Hauksson, 1981
Songpan-Pingwu	PR China	7.2	8/16/1976	+	11	420	Not reported	100	Hauksson, 1981

Earthquake				Disturbance			Detection		
Place		*Magnitude*	*Date(s)*		*δα (%)*	*Duration (days)*	*Precursory time (days)*	*ED (km)*	*Reference*
Songpan-Pingwu	PR China	7.2	8/16/1976	+	70	1	Not reported	320	Teng, 1980
Songpan-Pingwu	PR China	7.2	8/16/1976	−	12	200	Not reported	320	Hauksson, 1981
Songpan-Pingwu	PR China	7.2	8/16/1976	+	90	48	Not reported	340	Hauksson, 1981
Songpan-Pingwu	PR China	7.2	8/16/1976	−	60	160	Not reported	340	Hauksson, 1981
Songpan-Pingwu	PR China	7.2	8/16/1976	+	55	160	Not reported	390	Hauksson, 1981
Songpan-Pingwu	PR China	7.2	8/16/1976	+	110	34	Not reported	560	Hauksson, 1981
Songpan	PR China	7.2	8/16/1976	+	100	1.5	10	350	Jiang & Li, 1981
Ex-USSR									
Taschkent	Ex-USSR	5.3	4/26/1966	+	20	400	Not reported	5	Hauksson, 1981
Taschkent	Ex-USSR	4.0	3/24/1967	+	100	11	Not reported	5	Hauksson, 1981
Taschkent	Ex-USSR	3.5	6/20/1967	+	23	3	Not reported	5	Hauksson, 1981
Taschkent	Ex-USSR	3.5	7/22/1967	+	20	3	Not reported	5	Hauksson, 1981
Taschkent	Ex-USSR	3.0	11/9/1967	+	23	8	Not reported	5	Hauksson, 1981
Taschkent	Ex-USSR	3.3	11/17/1967	+	23	7	Not reported	5	Hauksson, 1981
Taschkent	Ex-USSR	3.0	12/17/1967	+	23	4	Not reported	5	Hauksson, 1981
Uzbekistan	Ex-USSR	4.7	2/13/1973	+	47	5	Not reported	130	Hauksson, 1981
Markansu	Ex-USSR	7.3	8/11/1974	+	100	100	Not reported	530	Hauksson, 1981
Tien Shan	Ex-USSR	5.3	2/12/1975	+	10	110	Not reported	100	Hauksson, 1981

Earthquake				Disturbance			Detection		
Place		*Magnitude*	*Date(s)*		*δα (%)*	*Duration (days)*	*Precursory time (days)*	*ED (km)*	*Reference*
Gazli	Ex-USSR	7.3	5/17/1976	+	220	4	Not reported	470	Hauksson, 1981
Gazli	Ex-USSR	7.3	5/17/1976	+	25	90	Not reported	550	Hauksson, 1981
Not reporetd	Ex-USSR	7.0	Not reported		Not reported	Not reported	Not reported	700	Fleischer, 1981
Gazli	Ex-USSR	7.3	5/17/1976		Not reported	Not reported	Not reported	400	Fleischer, 1981
Isfarin-Batnen	Ex-USSR	6.6	1/31/1977	−	30	60	Not reported	190	Hauksson,1981; Fleischer, 1981
Isfarin-Batnen	Ex-USSR	6.6	1/31/1977	−	20	125	Not reported	200	Hauksson, 1981
Alma-Ata	Ex-USSR	7.1	3/24/1978	+	32	50	Not reported	65	Hauksson, 1981
Zaalai	Ex-USSR	6.7	11/1/1978	−	30	470	Not reported	270	Hauksson, 1981
Zaalai	Ex-USSR	6.7	11/1/1978	−	40	470	Not reported	300	Hauksson, 1981
Zaalai	Ex-USSR	6.7	11/1/1978	+	20	75	Not reported	150	Hauksson, 1981
Zaalai	Ex-USSR	6.7	11/1/1978	−	20	70	Not reported	150	Hauksson, 1981
Italy									
Irpinia	Italy	6.5	11/23/1980	+	25	150	150	220	Allegri et al., 1983
Irpinia	Italy	6.5	11/23/1980	+	170	180	180	200	Allegri et al., 1983
Mt Etna	Italy	3.5(Md)	11/3/2001		Not reported	4-5 days	6	650	Imme et al., 2005
India									
Uttarkashi	India	7	10/20/1991	+	200	7	15	450	Virk & Baljinder, 1994
Uttarkashi	India	7.0	10/20/1991	+	300	7	15	270	Virk & Baljinder, 1994
Uttarkashi	India	7.0	10/20/1991	+	180	7	3	330	Virk & Baljinder, 1994

Earthquake				Disturbance		Detection			
Place		*Magnitude*	*Date(s)*		*δα (%)*	*Duration (days)*	*Precursory time (days)*	*ED (km)*	*Reference*
Japan									
Fukushima	Japan	6.6	Jan 1987	−	2	0	0	260	Igarashi et al., 1990
Fukushima	Japan	6.7	Feb 1987	−	11	0	0	130	Igarashi et al., 1990
Fukushima	Japan	6.6	Apr 1987	−	9	0	0	110	Igarashi et al., 1990
Kobe	Japan	7.2	1/17/1995	+	99	Not reported	60	20	Yasuoka & Shinogi 1995
Kobe	Japan	7.2	1/17/1995	−	5	Not reported	Not reported	260	Ohno & Wakita, 1996
Taiwan									
Chengkung	Taiwan	6.8	10/12/03	−	57.8%	Not reported	65	20	Kuo et al., 2006
Antung	Taiwan	5.0(Mw)	Feb/2008		Not reported	Not reported	Not reported	Not reported	Kuo et al., 2009
Chengkung	Taiwan	6.8(Mw)	10/12/03		Not reported	Not reported	Not reported	55	Kuo et al., 2009
Taitung	Taiwan	6.1(Mw)	1/4/06		Not reported	Not reported	Not reported	55	Kuo et al., 2009
Philippines									
Mindoro	Philippines	7.1	11/14/1994	+	600	7	22	48	Richon et al., 2003
Uzbekistan									
Tashkent	Uzbekistan	Not reported	12/13/1980		Not reported	Not reported	Not reported	Not reported	Pulinets et al.,1997
Turkmenistan									
Ahkhabad	Turkmenistan	5.7	3/14/1983		Not reported	Not reported	Not reported	Not reported	Alekseev et al., 1995
Antarctica									
Scotia sea	Antarctica	7.5(Ms)	4/8/03		Not reported	Not reported	6	1176	Ilic et al., 2005
Algeria									
Boumerdes	Algeria	6.7(ML)	5/21/2003		Not reported	1-3days	2.0-7.0	1120	Cigolini et al., 2007

Earthquake				Disturbance		Detection		
Place		*Magnitude*	*Date(s)*	*δα (%)*	*Duration (days)*	*Precursory time (days)*	*ED (km)*	*Reference*
Greece								
Kato Achaia, Peloponnese	Greece	6.5(ML)	8/6/2008	Fractal analysis, statistical outlier s	3-5 days	2-3 months	20	Nikolopoulos et al., 2012
				RS analysis, RL, Variogram, Entropic techniques, Fractal dimension				Petraki et al., 2013
				DFA, fractal analysis, RS analysis				Petraki et al., 2013
				Fractal analysis, DFA, entropy analysis				Nikolopoulos et al., 2014
Mytilene, Lesvos Island	Greece	5.0(ML)		Fractal analysis, DFA, entropy analysis	3-5 days	2-3 months	80	Nikolopoulos et al., 2014
Multiple events								
Iceland								
Southern	Iceland	2.7	7/3/1978	+ 380	22	25	14	Hauksson & Goddard, 1981
Iceland	Iceland	3.4	8/28/1978	+ 60	17	30	5	Hauksson & Goddard, 1981
Seismic	Iceland	3,4	8/28/1978	+ 280	17	27	21	Hauksson & Goddard, 1981
Seismic	Iceland	4,3	11/19/1978	− 80	18	10	16	Hauksson & Goddard, 1981

Earthquake				Disturbance			Detection		
Place		*Magnitude*	*Date(s)*		*δα (%)*	*Duration (days)*	*Precursory time (days)*	*ED (km)*	*Reference*
Tjörnes Facture Zone	Iceland	4.1	12/15/1979	+	100	50	50	56	Hauksson & Goddard, 1981
USA									
South California	USA	2.9	9/24/1977	+	44	1	5	21	Shapiro et al., 1980
South California	USA	2.8	12/20/1977	+	40	10	24	12	Shapiro et al., 1980
Malibu	USA	4.6	1/1/1979		4 spikes	4 spikes	Not reported	54	Shapiro et al., 1980
Pasadena	USA	2.9	9/24/1977	+	25	14	5	21	Shapiro et al., 1980
Pasadena	USA	2.8	12/20/1977	+	72	3	Not reported	12	Shapiro et al., 1980
Malibu	USA	4.7	1/1/1979	+	225	9	Not reported	54	Shapiro et al., 1980
Imperial Valley	USA	6.6	10/15/1979	+	Not reported	2	Not reported	300	Fleischer, 1981
Raquette Lake	USA	3.9	Not reported		Not reported	10	7	14	Fleischer, 1981
Blue Mountain Lake	USA	1.5	Not reported	+	36	Not reported	Not reported	1	Fleischer, 1981
Pearblossom	USA	3.5	11/22/1976	−	50	Not reported	Not reported	25	Hauksson, 1981
Jocasse	USA	2.3	2/23/1977	+	62	31	Not reported	1	Hauksson, 1981
Malibu	USA	4.7	1/1/1979	+	310	42	Not reported	20	Hauksson, 1981
Big Bear	USA	5	6/28/1979	+	72	82	Not reported	85	Hauksson, 1981
Big Bear	USA	5	6/28/1979	+	400	12	Not reported	31	Hauksson, 1981
Imperial Valley	USA	6.6	10/15/1979	+	200	45	Not reported	335	Hauksson, 1981
Imperial Valley	USA	6.6	10/15/1979	+	72	116	60	310	Hauksson, 1981
Imperial Valley	USA	6.6	10/15/1979	+	64	95	2-7 months	265	Hauksson, 1981
Imperial Valley	USA	6.6	10/15/1979		Not reported	145	1 year	260	Hauksson, 1981

Earthquake				Disturbance			Detection		
Place		*Magnitude*	*Date(s)*		*δα (%)*	*Duration (days)*	*Precursory time (days)*	*ED (km)*	*Reference*
New Madrid Seismic Zone	USA	3.5	1/28/1983	+	60	2 months	Not reported	50	Steele, 1984
San Andreas fault	USA	4	12/15/1977		400	30	15	45	King, 1980
San Andreas fault	USA	4.2	8/29/1978	+	200	90	240	75	King, 1980
Kettleman Hills (California)	USA	5.6	4/8/85		Not reported	Not reported	2weeks	300	Teng & Sun, 1986
San Bernadino (California)	USA	5	1/10/85		Not reported	Not reported	6weeks	20 & 90	Teng & Sun, 1986
Equador									
Reventador	Equador	6.9	6/3/87		Not reported	Not reported	50	367	Flores Humantante et al. 1990
Reventador	Equador	6.9	6/3/87	+	230	Not reported	15-50	377	Flores Humantante et al. 1990
Reventador	Equador	6.9	6/3/87	+	400	Not reported	15-35	339	Flores Humantante et al. 1990
Reventador	Equador	6.9	6/3/87	+	100	Not reported	50	388	Flores Humantante et al. 1990
Reventador	Equador	6.9	6/3/87	+	100	Not reported	15-40	183	Flores Humantante et al. 1990
Reventador	Equador	6.9	6/3/87	+	300	Not reported	15-40	350	Flores Humantante et al. 1990
Japan									
Subducted zone	Japan	7.9	6/3/84		Not reported	2	9	1000	Igarashi & Wakita, 1990
Not reporetd	Japan	6.7	6/2/87		Not reported	4	3	130	Igarashi & Wakita, 1990
Taiwan									
Northern Taiwan	Taiwan	5.8	10/18/1980		Not reported	Not reported	19	39	Liu et al., 1985
Northern Taiwan	Taiwan	5.2	5/14/1981		Not reported	Not reported	11	23	Liu et al., 1985
Northern Taiwan	Taiwan	4.6	6/21/1981		Not reported	Not reported	15	14	Liu et al., 1985
Northern Taiwan	Taiwan	5.0	7/18/1981		Not reported	Not reported	4	37	Liu et al., 1985

Earthquake			Disturbance		Detection		
Place	*Magnitude*	*Date(s)*	*δα (%)*	*Duration (days)*	*Precursory time (days)*	*ED (km)*	*Reference*

	Uttarkashi	India	7.0(Ms)	10/20/1991	Not reported	Not reported	5	293	Walia et al., 2006
	Chamoli	India	6.5(Ms)	03/29/1999	Not reported	Not reported	Not reported	393	Walia et al., 2006
	Chamba	India	5.1(Ms)	03/24/1995	Not reported	Not reported	3	10	Walia et al., 2006
	Kharsali	India	4.9	07/23/2007	Not reported	Not reported	Few days	60	Choubey et al., 2009
Indonesia									
	Indonesia	Indonesia	9.1	12/26/2004	DFA	Not reported	Not reported	2275	Das et al., 2006
	West Sumatra	Indonesia	5.8	9/2/05	DFA	Not reported	Not reported	2120	Das et al., 2006
	North Sumatra	Indonesia	5.1	6/1/05	DFA	Not reported	Not reported	2070	Das et al., 2006
Turkey									
	Western Turkey	Turkey	3	4/6/07	Not reported	Not reported	Not reported	Not reported	Sac et al., 2011
	Western Turkey	Turkey	4.2	11/11/07	Not reported	Not reported	Not reported	Not reported	Sac et al., 2011
Greece									
	Chalkida,Evia Island	Greece	5.2(ML)	11/17/14	Hurst Analysis, DFA, RS analysis	15 days	1-3 weeks	80	Nikolopoulos et al., 2015
Seismic periods									
India	North-West Himalayas (25 events)	India	2.1-6.8	1992-1999	Not reported	Not reported	Not reported	53-393	Walia et al., 2003
	Kangra Valley & Hindu Kush area (6 events)	India	3.2-5.7	3/13/1984-12/26/2004	6 spikes	Not reported	Not reported	150-500	Ramola et al., 2008
	Kangra Valley & Hindu Kush area (7 events)	India	Not reported	March/1984-July/1987	7 spikes	Not reported	Not reported	Not reported	Virk, 1994
	Tehri Garhwal, Himalaya (21 events)	India	1.5-3.7	1/01/2005-12/30/2005	Not reported	Not reported	Not reported	16-250	Ramola et al., 2008
	Tehri Garhwal, Himalaya (4 events)	India	2.6-4.6	1/02/2006-Oct/1988	Not reported	Not reported	Not reported	16-250	Ramola et al., 2008
	Hindu Kush area (26 events)	India	4.2-6.4	5/12/2006-Dec/1991	9 spikes	Not reported	Not reported	400-500	Virk, 1994
	North-West Himalayas (9 events)	India	2.2-5.0	March/2007-June/2008	+ 2.6-72.8	Not reported	2-13days	19-196	Kumar et al. 2009
	North-West Himalayas (3 events)	India	2.2-5.0	Dec/2006-Sept/2007	+ 49-61	Not reported	4-13days	97-201	Singh et al., 2010
	North-West Himalayas (6 events)	India	2.2-5.0	Dec/2006-Dec/2007	+ 18.2-47.3	Not reported	3-14days	22-339	Singh et al., 2010
	Not reporetd	India	Not reported	Nov/2005-Nov/2008	Not reported	Not reported	Not reported	Not reported	Gosh et al., 2012
Japan									
	Earthquakes nearby the Fukushima Prefecture (16 events)	Japan	6.0-6.7	Jan/1984-July/1988	Not reported	Not reported	Few days	100-130 & 400	Wakita et al., 1988
	Place	**Earthquake**	***Magnitude***	***Date(s)***	**Disturbance** ***δα (%)***	***Duration (days)***	**Detection** ***Precursory time (days)***	***ED (km)***	***Reference***

Earthquake				Disturbance		Detection		
Place		*Magnitude*	*Date(s)*	*δα (%)*	*Duration (days)*	*Precursory time (days)*	*ED (km)*	*Reference*
Not reporetd (10 events)	Croatia	2.7-4.9	6/02/2005-5/26/2007	Not reported	Not reported	Not reported	4.0-295.0	Miklavcic et al., 2008
Slovenia								
Not reporetd (13 events)	Slovenia	0,7-3.2 (ML)	1999-2001	Not reported	Not reported	2.0-33.0	Re/Rd from 0.4 to 2.0	Gregoric et al., 2005;Zmazek et al., 2005; Zmazek et al., 2006
Taiwan								
Taiwan (30 events)	Taiwan	4.5-6.6 (ML)	03/01/2003-06/30/2004	16 peaks	0.2-12	1.3-20.0	4.9-174.2	Yang et al., 2005
Taiwan (37 events)	Taiwan	3.7-6.7 (ML)	11/01/2000-05/11/2003	Not reported	Not reported	1.12-13.00	1.5-257.5	Chyi et al., 2005
Taiwan (20 events)	Taiwan	3.7-6.2 (ML)	3/15/2005-8/12/2006	Not reported	Not reported	1.6-13.9	7.6-145.8	Fu et al., 2008
Hsincheng fault (38 events)	Taiwan	3.0-7.0	1/01/2006-7/14/2008	29 anomalies	Not reported	Not reported	Not reported	Walia et al., 2009
Hsinhua fault (28 events)	Taiwan	3.0-7.0	1/01/2006-7/14/2008	28 anomalies	Not reported	Not reported	Not reported	Walia et al., 2009
United Kingdom								
English Channel (1 event), Dudley (3 events), Manchester (11 events)	U.K.	1.2-5.0	08/26/2002-10/29/2002	Not reported	6-9-h spikes	Not reported	90.1-250.2	Crockett et al., 2006
Spain								
Tenerife Island	Spain	Greater than 2.5	From April 2004-2005	Not reported	Not reported	Several months	Not reported	Perez et al., 2007

Earthquake				Disturbance		Detection		
Place		*Magnitude*	*Date(s)*	*δα (%)*	*Duration (days)*	*Precursory time (days)*	*ED (km)*	*Reference*
Turkey								
Denizli Basin	Turkey	3.3-4.8	5/04/2000-12/11/2000	Not reported	Not reported	Not reported	3.0 – 23.0	Erees et al., 2007
Iceland								
South Iceland	Iceland	6.5(Mw)2 events & several magnitude 5+ events	June/2000	Not reported	Not reported	40-144	90.0	Einarsson et al., 2008
Turkey								
East Anatolian Fault (59 events)	Turkey	2.5-5.5	6/22/2004-6/27/2005	Not reported	Not reported	Not reported	Not reported	Baykara et al., 2009
Afyonkarahisar province	Turkey	2.6-3.9	Sep/2009-Sep/2010	Not reported	Not reported	Not reported	Not reported	Yalim et al., 2012
Iran								
Jooshan (SE of Iran)	Iran	2.6-5.4	Jan/2012-Feb/2012	Not reported	Not reported	3-6days	3.9-163.8	Namvaran & Negarestami, 2012
Romania								
Vrancea seismic area (Carpathians) (266 events)	Romania	2.0-4.9	Nov/2012-Nov/2011	Not reported	Not reported	2weeks-1month	Not reported	Zoran et al., 2012

List of references

Aggarwal, P., Sykes, R., Simpson, W., & Richards, G. (1975). Spatial and temporal variations in ts/tp and in P wave residuals at Blue Mountain Lake, New York: Application to earthquake prediction. *Journal of Geophysical Research 80*:718-732.
http://dx.doi.org/10.1029/JB080i005p00718

Alekseev, V.A., Alekseeva, N.G., & Jchankulievt, J. (1995). On relation between fluxes of metals in waters and radon in Turkmenistan region of seismic activity. *Radiation Measurements 25*(1-4): 637-639.
http://dx.doi.org/10.1016/1350-4487(95)00207-U

Allegri, L., Bella, F., Della Monica, G., Ermini, A., Improta, S., Sgrigna, V., Biagi, P.F. (1983). Radon and tilt anomalies detected before the Irpinia (south Italy) earthquake of November 23, 1980 at great distances from the epicenter. *Geophysical Research Letters 10*(4):269–272.
http://dx.doi.org/10.1029/GL010i004p00269

Al-Tamimi, M.H., & Abumura, K.M. (2001). Radon anomalies along faults in North of Jordan. *Radiation Measurements 34*(1-6):397-400.
http://dx.doi.org/10.1016/S1350-4487(01)00193-7

Anderson, O.L., & Grew, P.C. (1977). Stress corrosion theory of crack propagation with applications to geophysics. *Reviews of Geophysics 15*(1): 77–84.
http://dx.doi.org/10.1029/RG015i001p00077

Armitage, P., and Berry, G. *Statistical methods in medical research.* ISBN 0-632-03695-8, Blackwell Science L.td., Oxford, 1996.

Balasis, G., Daglis, I., Papadimitriou, C,, Kalimeri, M., Anastasiadis, A., & Eftaxias, K. (2008). Dynamical complexity in Dst time series using non-extensive Tsallis entropy. *Geophysical Research Letters 35*(14): L14102 (1-6). http://dx.doi.org/10.1029/2008GL03474

Balasis, G., Daglis, I.A., Papadimitriou, C., Kalimeri, M., Anastasiadis, A., & Eftaxias, K. (2009). Investigating dynamical complexity in the magnetosphere using various entropy measures. *Journal of Geophysical Research* 114:A00D06. http://dx.doi.org/10.1029/2008JA014035

Balasis, G., & Mandea, M. (2007). Can electromagnetic disturbances related to the recent great earthquakes be detected by satellite magnetometers? *Tectonophysics 431*(1-4): 173–195. http://dx.doi.org/10.1016/j.tecto.2006.05.038

Barman, C., Chaudhuri, H., Ghose, D., Deb, A., & Sinha, B. (2014). Multifractal Detrended Fluctuation Analysis of Seismic Induced Radon-222 Time Series. *Journal of Earthquake Science and Engineering 1*, 59-79.

Baykara, O., İnceöz, M., Doğru, M., Aksoy, E., & Külahcı, F. (2009). Soil radon monitoring and anomalies in East Anatolian Fault System (Turkey). *Journal of Psychoanalytical and Nuclear Chemistry 279*(1):159–164. http://dx.doi.org/10.1007/s10967-007-7211-2

Bella, F., Biagi, P.F., Caputo, M., Cozzi, E., Della Monica, G., Ermini, A., Plastino, W., & Sgrigna, V. (1998). Field strength variations of LF radio waves prior to earthquakes in central Italy. *Physics of the Earth and Planetary Interiors, 105*(3-4):279–286. http://dx.doi.org/10.1016/S0031-9201(97)00097-6

Bernard, P., Pinettes, P., Hatzidimitriou, P.M., Scordilis, E.M., Veis, G., & Milas, P. (1997). From precursors to prediction: a few recent cases from Greece. *Geophysical Journal International 131*(3):467-477. http://dx.doi.org/10.1111/j.1365-246X.1997.tb06590.x

Bevington, P. R. *Data Reduction and Error Analysis for the Physical Sciences,* McGraw-Hill, New York, 1969.

Biagi, P.F., Ermini, A., & Kingsley, S.P. (2001). Disturbances in LF Radio Signals and the Umbria-Marche (Italy) Seismic Sequence in 1997-1998. *Physics and Chemistry of the Earth (C) 26*(l0-12):755-759. http://dx.doi.org/10.1016/S1464-1917(01)95021-4

Borchiellini, S., Bernat, M., & Campredon, R. (1991). Ground variation of radon 222 for location of hidden structural features: example of the south of France (Alpes Maritimes). *Pure and Applied Geophysics 135*(4)*:625–638.* http://dx.doi.org/10.1007/BF01772411

Buldyrev, S.,Goldberger, A., Havlin, S., Manligna, R., Matsa, M., Peng, C., Simons, M., & Stanley, H. (1995). Long-range correlations properties of coding and noncoding DNA sequences: GenBank analysis. *Physical Review E, Statistical physics, plasmas, fluids, and related interdisciplinary topics 51*(5): 5084-5091. http://dx.doi.org/10.1103/PhysRevE.51.5084

Cantzos, D., Nikolopoulos, D., Petraki, E., Nomicos, C., Yannakopoulos, P.H., & Kottou, S. (2015). Identifying Long-Memory Trends in Pre-Seismic MHz Disturbances through Support Vector Machines. *Journal of Earth Science & Climatic Change 6*(3):1-9. http://dx.doi.org/10.4172/2157-7617.1000263

Chen, C., Thomas, D.M., & Green, R.E. (1995). Modelling of radon transport in unsaturated soil. *Journal of Geophysical Research-Solid Earth 100*(B8):15517–15525.
http://dx.doi.org/10.1029/95JB01290

Chen, Z., Ivanov, P., Hu, K., & Stanley, H. (2002). Effect of non-stationarities on detrended fluctuation analysis. *Physical Review E 65*(4): 041107/1-041107/15.
http://dx.doi.org/10.1103/PhysRevE.65.041107

Chen, C.C., Wang, W.C., Chang, Y.F., Wu, Y.M. & Lee, Y.H. (2006). A correlation between the b-value and the fractal dimension from the aftershock sequence of the 1999 Chi-Chi, Taiwan, earthquake. *Geophysical Journal International 167*(3): 1215–1219.
http://dx.doi.org/10.1111/j.1365-246X.2006.03230.x

Choubey, V.M., Kumar, N., & Arora, B.R. (2009). Precursory signatures in the radon and geohydrological borehole data for M4.9 Kharsali earthquake of Garhwal Himalaya. *Science of the Total environment 407*(22):5877-5883.
http://dx.doi.org/10.1016/j.scitotenv.2009.08.010

Chuo, Y.J., Liu, J.Y., Pulinets, S.A., & Chen, Y.I. (2002).The ionospheric perturbations prior to the Chi-Chi and Chia-Yi earthquakes. *Journal of Geodynamics 33*(4-5): 509–517.
http://dx.doi.org/10.1016/S0264-3707(02)00011-X

Chyi, L., Quick, T., Yang, T., & Chen, C. (2005). Soil gas radon spectra and earth-quakes. *Terrestrial Atmospheric and Oceanic Sciences 6*(4): 763-774.

Chyi, L.L., Quick, T.J., Yang, T.F., & Chen, C.H. (2010). The experimental investigation of soil gas radon migration mechanisms and its implication in earthquake forecast. *Geofluids 10*(4):556-563. http://dx.doi.org/10.1111/j.1468-8123.2010.00308.x

Chyi, L.L., Quick, T.J., Yang, T.F., & Chen, C.H. (2011). The origin and detection of spike-like anomalies in soil gas radon time series. *Geochemical Journal 45*(6):431-438. http://dx.doi.org/10.2343/geochemj.1.0145

Cicerone, R., Ebel, J., & Britton, J. (2009). A systematic compilation of earthquake precursors. *Tectonophysics 476*(3-4): 371-396. http://dx.doi.org/10.1016/j.tecto.2009.06.008

Cigolini, C., Laiolo, M., & Coppola, D. (2007). Earthquake–volcano interactions detected from radon degassing at Stromboli (Italy). *Earth Planet Science Letters 257*(3-4):511–525. http://dx.doi.org/10.1016/j.epsl.2007.03.022

Clements, W. E. (1974). *The effect of atmospheric pressure variation on the transport of ^{222}Rn from the soil to the atmosphere* (Ph.D dissertation). New Mexico, Institute of Mining and Technology:Soccorro.

Contoyiannis, Y.F., Diakonos, F.K., Kapiris, P.G., Peratzakis, A.S., & Eftaxias, K.A. (2004). Intermittent dynamics of critical pre-seismic electromagnetic fluctuations. *Physics and Chemistry of the Earth 29*(4-9):397-408. http://dx.doi.org/10.1016/j.pce.2003.11.012

Contoyiannis, Y.F., & Eftaxias, K. (2008). Tsallis and Levy statistics in the preparation of an earthquake. *Nonlinear Processes in Geophysics 15*(3):379–388.

http://dx.doi.org/10.5194/npg-15-379-2008

Contoyiannis, Y., Kapiris, P., & Eftaxias, K. (2005). Monitoring of a preseismic phase from its electromagnetic precursors. *Physical Review E 71*(6):066123. http://dx.doi.org/10.1103/PhysRevE.71.066123

Crockett, R.G.M., Gillmore, G.K., Phillips, P.S., Denman, A.R., & Groves-Kirkby, C.J. (2006). Radon anomalies preceding earthquakes which occurred in the UK, in summer and autumn 2002. *Science of the Total Environment 364*(1-3):138– 148. http://dx.doi.org/10.1016/j.scitotenv.2005.08.003

D'Addio, G., Accardo, A., Fornasa, E., Cesarelli, M. & De Felice, A. (2013). Fractal Behaviour of Heart Rate Variability Reflects Abnormal Respiration Patterns in OSAS Patients. *Computing in Cardiology (CinC), 2013 40*:445-448.

Das, N.K., Choudhury, H., Bhandari, R.K., Ghose, D., Sen, P., & Sinha, B. (2006). Continuous monitoring of ^{222}Rn and its progeny at a remote station for seismic hazard surveillance. *Radiation Measurements 41*(5):634–637. http://dx.doi.org/10.1016/j.radmeas.2009.11.039.

Dattatreya, G. (2005). *Hurst Parameter Estimation from Noisy Observations of Data Traffic Traces*. Paper presented at the 4th WSEAS International Conference on Electronics, Control and Signal Processing, Miami, Florida, USA, 17-19 November, 193–198.

Dea, J.Y., Hansen, P.M., & Boerner, W.M. (1993). Long-term EMF background noise measurements, the existence of window regions and applications to earthquake precursor emission studies. *Physics of the Earth and Planetary Interiors 77*(1-2):109-125. http://dx.doi.org/10.1016/0031-9201(93)90037-A

Devore, J. (2011). *Probability and Statistics for Engineering and the Sciences.* Duxbury Press; 8th edition.

Dieker, T. (2004). *Simulation of fractional Brownian motion* (Thesis dissertation). Amsterdam:University of Twente, Department of Mathematical Sciences.

Dobrovolsky, I.P., Zubkov, S.I., & Miachkin, V.I. (1979). Estimation of the Size of Earthquake Preparation Zones. *Pure and Applied Geophysics 117*(5):1025-1044. http://dx.doi.org/10.1007/BF00876083

Donner, R.V., Potirakis, S.M., Barbosa, S.M., Matos, J.A.O., Pereira, A.J.S.C., &. Neves, L.J.P.F (2015). Intrinsic vs. spurious long-range memory in high-frequency records of environmental radioactivity. *The European Physical Journal Special Topics May 2015 224*(4): 741-762. http://dx.doi.org/10.1140/epjst/e2015-02404-1

Draganov, A.B., Inan, U.S., & Taranenko, Yu N. (1991). ULF magnetic signatures at the Earth's surface due to ground water flow: a possible precursor to earthquakes. *Geophysical Research Letters 18*(6):1127–1130. http://dx.doi.org/10.1029/91GL01000

Einarsson, P., Theodorsson, P., Hjartardottir, A.R,, & Guojonsson, G.I. (2008). Radon changes associated with the earthquake sequence in June 2000 in the South Iceland seismic zone. *Pure Applied and Geophysics 165*(1):63–74. http://dx.doi.org/10.1007/s00024-007-0292-6

Eftaxias, K. (2010). Footprints of non-extensive Tsallis statistics, self-affinity and universality in the preparation of the L'Aquila earthquake hidden in a pre-seismic EM emission. *Physica A 389*(1):133-140.

http://dx.doi.org/10.1016/j.physa.2009.08.034

Eftaxias, K., Athanasopoulou, L., Balasis, G., Kalimeri, M., Nikolopoulos, S., Contoyiannis, Y., Kopanas, J., Antonopoulos, G., & Nomicos, C. (2009). Unfolding the procedure of characterizing recorded ultra low frequency, kHz and MHz electromagnetic anomalies prior to the L'Aquila earthquake as pre-seismic ones – Part 1. *Natural Hazards and Earth System Sciences 9*(6):1953-1971. http://dx.doi.org/10.5194/nhess-9-1953-2009

Eftaxias, K., Balasis, G., Contoyiannis, Y., Papadimitriou, C., Kalimeri, M., Athanasopoulou, L., Nikolopoulos, S., Kopanas, J., Antonopoulos, G., & Nomicos, C. (2010). Unfolding the procedure of characterizing recorded ultra low frequency, kHZ and MHz electromagnetic anomalies prior to the L'Aquila earthquake as pre-seismic ones - Part 2. *Natural Hazards and Earth System Sciences 10*(2):275–294. http://dx.doi.org/10.5194/nhess-10-275-2010

Eftaxias, K., Contoyiannis, Y., Balasis, G., Karamanos, K., Kopanas, J., Antonopoulos, G., Koulouras, G., & Nomicos, C. (2008). Evidence of fractional-Brownian-motion-type asperity model for earthquake generation in candidate pre-seismic electromagnetic emissions. *Natural Hazards and Earth System Sciences 8*(4):657-669. http://dx.doi.org/10.5194/nhess-8-657-2008

Eftaxias, K., Kapiris, P., Balasis, G., Peratzakis, A., Karamanos, K., Kopanas, I., Antonopoulos, G., & Nomicos, C. (2006). Unified approach to catastrophic events: from the normal state to geological or biological shock in terms of spectral fractal and nonlinear analysis. *Natural Hazards and Earth System*

Sciences 6:205-228.
http://dx.doi.org/10.5194/nhess-6-205-2006

Eftaxias, K., Kapiris, P., Dologlou, E., Kopanas, J., Bogris, N., Kopanas, I., Antonopoulos, G., Peratzakis A., & Hadjiconis V. (2002). EM anomalies before the Kozani earthquake: a study of their behavior through laboratory experiments. *Geophysical Research Letters 29*(8):69-1–69-4.
http://dx.doi.org/10.1029/2001GL013786

Eftaxias, K., Kapiris, P., Polygiannakis, J., Bogris, N., Kopanas, J., Antonopoulos, G., Peratzakis, A., & Hadjicontis, V. (2001). Signature of pending earthquake from electromagnetic anomalies. *Geophysical Research Letters 29*(17):3321–3324.
http://dx.doi.org/10.1029/2001GL013124

Eftaxias, K., Panin, V., Deryugin, Y. (2007). Evolution-EM signals before earthquakes in terms of meso-mechanics and complexity. *Tectonophysics, 431*(1-4): 273–300.
http://dx.doi.org/10.1016/j.tecto.2006.05.041

Enescu, B.D., Enescu, D., & Constantin, A.P. (1999). The use of electromagnetic data for short-term prediction of Vrancea (Romania) earthquakes: Preliminary data. *Earth Planets Space 51*(10):1099–1117.
http://dx.doi.org/10.1186/BF03351584

Enomoto, Y., Tsutsumi, A., Fujinawa, Y., Kasahara, M., & Hashimoto, H. (1997). Candidate precursors: pulse-like geoelectric signals possibly related to recent seismic activity in Japan. *Geophysical Journal International 131*(3): 485-494.
http://dx.doi.org/10.1111/j.1365-246X.1997.tb06592.x

Erees, F., Aytas, S., Sac, M., Yener, G., & Salk, M. (2007). Radon concentrations in thermal waters related to seismic events along faults in the Denizli Basin,Western

Turkey. *Radiation Measurements 42*(1): 80-86. http://dx.doi.org/10.1016/j.radmeas.2006.06.003

Feder, J. (1988). *Fractals*. New York: Plenum. http://dx.doi.org/10.1007/978-1-4899-2124-6

Finkelstein, M., Eppelbaum, L.V., & Price, C. (2006). Analysis of temperature influences on the amplitude-frequency characteristics of Rn gas concentration. *Journal of Environmental Radioactivity 86*(2): 251–70. http://dx.doi.org/10.1016/j.jenvrad.2005.09.004

Fitterman, D.V. (1978). Electrokinetic and magnetic anomalies associated with dilatant regions in a layered Earth. *Journal of Geophysical Research 83*(B12):5923–5928. http://dx.doi.org/10.1029/JB083iB12p05923

Fitterman, D.V. (1979). Theory of electrokinetic–magnetic anomalies in a faulted half-space. *Journal of Geophysical Research 84*(B11)*:*6031–6040. http://dx.doi.org/10.1029/JB084iB11p06031

Fleischer, R.L. (1981). Dislocation model for radon response to distant earthquakes. *Geophysical Research Letters 8*(5):477–480. http://dx.doi.org/10.1029/GL008i005p00477

Fleischer, R.L., & Mogro-Campero, A. (1985). Association of subsurface radon changes in Alaska and the north-eastern United States with earthquakes. *Geochimica Cosmochimica Acta 49*(4)*:* 1061–1071. http://dx.doi.org/10.1016/0016-7037(85)90319-9

Flores Humanante, B., Giroletti, E., Idrova, J., Monnin, M., Pasinetti, R., & Seidel, J.L. (1990). Radon signals related to seismic activity in Ecuador, March 1987. *Pure and Applied Geophysics 132*(3):505–520.

http://dx.doi.org/10.1007/BF00876926

Fraser-Smith, A. C., Bernardi, A., McGill, P.R., Ladd, M.E., Helliwell, R.A., & Viilard, O.G. (1990). Low-frequency magnetic field measurements near the epicenter of the Ms 7.1 Loma Prieta earthquake. *Geophysical Research Letters 17*(9):1465-1468.

http://dx.doi.org/10.1029/GL017i009p01465

Francesco, S.D., Tommasone, F.P., Cuoco, E., Verrengia, G., Tedesco, D. (2010). Radon hazard in shallow ground-waters: amplification and long term variability induced by rainfall. *Science of the Total Environment 408*(4): 779–789.

http://dx.doi.org/ 10.1016/j.scitotenv.2009.11.024

Fu, C.C., Yang, T.F., Du, J., Walia, V., Chen, Y.G., Liu, T.K., & Chen, C.H. (2008). Variations of helium and radon concentrations in soil gases from an active fault zone in Southern Taiwan. *Radiation Measurements 43*(1):S348–S352.

http://dx.doi.org/10.1016/j.radmeas.2008.03.035

Fujiwara, H., Kamogawa, M., Ikeda, M., Liu, J.Y., Sakata, H., Chen, Y.I., Ofuruton, H., Muramatsu, S., Chuo, Y.J., & Ohtsuki, Y.H. (2004). Atmospheric anomalies observed during earthquake occurrences. *Geophysical Research Letters 31*(17): L17110.

http://dx.doi.org/10.1029/2004GL019865

Fujinawa, Y., & Takahashi, K. (1998). Electromagnetic radiations associated with major earthquakes. *Physics of the Earth and Planetary Interiors 105*(3-4):249-259.

http://dx.doi.org/10.1016/S0031-9201(97)00117-9

Genitron, V., 1997. Alpha Guard PQ2000/MC50, Multiparameter Radon Monitor. Genitron Instruments, Frankfurt.

Gershenzon, N., & Gokhberg, M. (1993). On the origin of electrotelluric disturbances prior to an earthquake in Kalamata, Greece. *Tectonophysics 224*(1-3):169-174. http://dx.doi.org/10.1016/0040-1951(93)90069-V

Ghosh, D., Deb, A., Dutta, S., & Sengupta, R. (2012). Multifractality of radon concentration variation in earthquake related signal. *Fractals 20*(01): 33-39. http://dx.doi.org/10.1016/j.jappgeo.2009.06.001

Ghosh, D., Deb, A., & Sengupta, R. (2009). Anomalous radon emission as precursor of earthquake. *Journal of Applied Geophysics 69*(2):67-81. http://dx.doi.org/10.1016/j.jappgeo.2009.06.001

Gilmore, M., Yu, C., Rhodes, T., & Peebles, W. (2002). Investigation of rescaled range analysis, the Hurst exponent, and long-time correlations in plasma turbulence. *Physics of Plasmas 9*(4): 1312-1317. http://dx.doi.org/10.1063/1.1459707

Gokhberg, M.B., Morgounov, V.A., Yoshino, T. & Tomizawa, I. (1982). Experimental Measurement of Electromagnetic Emissions Possibly Related to Earthquakes in Japan. *Journal of Geophysical Research 87*(B9):7824-7828. http://dx.doi.org/10.1029/JB087iB09p07824

Gotoh, K., Hayakawa, M., Smirnova, N., & Hattori, K. (2004). Fractal analysis of seismogenic ULF emissions. *Physics and Chemistry of the Earth 29* (4-9):419–424. http://dx.doi.org/10.1016/j.pce.2003.11.013

Grammakov, A.G. (1936). On the influence of some factors in the spreading of radioactive emanations under natural conditions. *Zeitschrift für Geofizik 6:*123–148.

Granero, M.S., Segovia, J.T., & Perez, J.G. (2008). Some comments on Hurst exponent and the long memory processes on capital markets. *Physica A 387*(22), 5543–5551. http://dx.doi.org/10.1016/j.physa.2008.05.053.

Gregoric, A., Zmazek, B. & Vaupotic, J. (2008). Radon Concentration in Thermal Water as an Indicator of Seismic Activity. *Collegium Antropologicum 32* (S2):95-98.

Hadjicontis, V., Mavromatou, C., & Eftaxias, K. (2002). Preseismic earth's field anomalies recorded at Lesvos station, north-eastern Aegean. *Acta Geophysica Polonica 50*(2):151-158.

Hauksson, E. (1981). Radon content of groundwater as an earthquake precursor: evaluation of worldwide data and physical basis. *Journal of Geophysical Research 86*(B10):9397–9410. http://dx.doi.org/10.1029/JB086iB10p09397.

Hauksson, E., & Goddard, J.G. (1981). Radon earthquake precursor studies in Iceland. *Journal of Geophysical Research 86*(B8):7037–7054. http://dx.doi.org/10.1029/JB086iB08p07037

Hayakawa, M., & Hobara, Y. (2010). Current status of seismo-electromagnetics for short-term earthquake prediction. *Geomatics, Natural Hazards and Risk 1*(2):115-155. http://dx.doi.org/10.1080/19475705.2010.486933

Hayakawa, M., & Ito, T. (1999). Fractal analysis of ULF geomagnetic data associated with the Guam earthquake on August 8, 1993. *Geophysical Research Letters 26*(18): 2797-2800. http://dx.doi.org/10.1029/1999GL005367

Hayakawa, M., Ida, Y., & Gotoh, K. (2005). Multifractal analysis for the ULF geomagnetic data during the Guam earthquake. *Electromagnetic Compatibility and Electromagnetic Ecology, 2005. IEEE 6th International Symposium on 21-24 June 2005:*239 – 243.
http://dx.doi.org/10.1109/EMCECO.2005.1513113

Hayakawa, M., Kawate, R., Molchanov, O.A., & Yumoto, K. (1996). Results of ultra-low-frequency magnetic field measurements during the Guam earthquake of 8 August 1993.*Geophysical Research Letters 23*(3):241-244.
http://dx.doi.org/10.1029/95GL02863

Hayakawa, M., Ohta, K., Maekawa, S., Yamauchi, T., Ida, Y., Gotoh, T., Yonaiguchi, N., Sasaki, H., & Nakamura, T. (2006). Electromagnetic precursors to the 2004 Mid Niigata Prefecture earthquake. *Physics and Chemistry of the Earth 31*(4-9):351-364.
http://dx.doi.org/10.1016/j.pce.2006.02.023

Hu, K., Ivanov, P., Chen, Z., Carpena, P., & Stanley, H. (2001). Effect of trends on detrended fluctuation analysis. *Physical Review E 64* (1): O11114/1-O11114/19.
http://dx.doi.org/10.1103/PhysRevE.64.011114

Hurst, H. (1951). Long Term Storage Capacity of Reservoirs. *Transactions of the American Society of Civil Engineers 116*:770-799.

Hurst, H., Black, R., & Simaiki, Y. (1965). Long-term storage: an experimental study. London:Constable.

Igarashi, G., & Wakita, H. (1990). Groundwater radon anomalies associated with earthquakes. *Tectonophysics 180*(2-4):237–254.
http://dx.doi.org/10.1016/0040-1951(90)90311-U

Igarashi, G., Wakita, H., & Notsu, K. (1990). Groundwater observations at KSM site in northeast Japan: a most sensitive site to earthquake occurrence. *Tohoku Geophysical Journal 33*(2):163–175.

Ilic, R., Rusov, V.D, Pavlovych, V.N., Vaschenko, V.M., Hanzic, L., & Bondarchuk, Y.A. (2005). Radon in Antarctica. *Radiation Measurements 40*(2-4):415–422. http://dx.doi.org/10.1016/j.radmeas.2005.03.022

Imme´, G., Delf, S.L., Nigro, S.L., Morelli, D., & Patane´, G. (2005). Gas radon emission related to geodynamic activity on Mt. Etna *Annals of Geophysics 48*(1): 65-71.
http://dx.doi.org/10.4401/ag-3180

Jaime, B., Facchini, U., Giroletti, E., & Magnoni, S. (1995). Low dimensional chaos is present in radon time variations. *Journal of Environmental Radioactivity 28*(1):73-89.
http://dx.doi.org/10.1016/0265-931X(94)00044-W

Jouniaux, L., & Pozzi, J.P. (1995). Streaming potential and permeability of saturated sand-stones under triaxial stress: - consequences for electrotelluric anomalies prior to earthquakes. *Journal of Geophysical Research 100*(B6):10197-10209.
http://dx.doi.org/10.1029/95JB00069

Kalimeri, M., Papadimitriou, C., Balasis, G., & Eftaxias, K. (2008). Dynamical complexity detection in pre-seismic emissions using non-additive Tsallis entropy. *Physica A 387*(5-6):1161-1172.
http://dx.doi.org/10.1016/j.physa.2007.10.053

Kapiris, P., Balasis, G., Kopanas, J., Antonopoulos, G., Peratzakis, A., & Eftaxias, K. (2004). Scaling Similarities of Multiple Fracturing of Solid Materials. *Nonlinear*

*Processes in Geophysics 11:*137–151.

Kapiris, P.G., Eftaxias, K.A., & Chelidze, T.L. (2004). Electromagnetic Signature of Prefracture Criticality in Heterogeneous Media. *Physical Review Letters 92*(6): 065702-1/065702-4.

http://dx.doi.org/10.1103/PhysRevLett.92.065702

Kapiris, P.G., Eftaxias, K.A., Nomikos, K.D., Polygiannakis, J., Dologlou, E., Balasis, G.T., Bogris, N.G., Peratzakis, A.S., & Hadjicontis, V.E. (2003). Evolving towards a critical point: A possible electromagnetic way in which the critical regime is reached as the rupture approaches. *Nonlinear Processes in Geophysics 10*(6):511–524.

http://dx.doi.org/10.5194/npg-10-511-2003

Kapiris, P., Nomicos, K., Antonopoulos, G., Polygiannakis, J., Karamanos, K., Kopanas, J., Zissos, A., Peratzakis, A., & Eftaxias, K. (2005). Distinguished seismological and electromagnetic features of the impending global failure: Did the 7/9/1999 M5.9 Athens earthquake come with a warning? *Earth Planets Space 57*(3): 215–230.

http://dx.doi.org/10.1186/BF03351818

Kapiris, P., Polygiannakis, J., Peratzakis, A., Nomicos, K., & Eftaxias, K. (2002).VHF-electromagnetic evidence of the underlying pre-seismic critical stage. *Earth Planets Space 54*(12):e1237–e1246.

http://dx.doi.org/10.1186/BF03352452

Karakelian, D., Klemperer, S.L., Fraser-Smith, A.C., & Thompson, G.A. (2002). Ultra-low frequency electromagnetic measurements associated with the 1998 Mw 5.1 San Juan Bautista, California earthquake and implications for mechanisms of

electromagnetic earthquake precursors. *Tectonophysics 359*(1-2):65– 79. http://dx.doi.org/10.1016/S0040-1951(02)00439-0

Karamanos, K. (2001). Entropy analysis of substitutive sequences revisited. *Journal of Physics A: Mathematical and General 34*(43): 9231-9241. http://dx.doi.org/10.1088/0305-4470/34/43/309

Karamanos, K., Dakopoulos, D., Aloupis, K., Peratzakis, A., Athanasopoulou, L., Nikolopoulos, S., Kapiris, P., & Eftaxias, K. (2006). Preseismic electromagnetic signals in terms of complexity. *Physical Review E 74*(1)*:* 016104/1-016104/21. http://dx.doi.org/10.1103/PhysRevE.74.016104

Karamanos, K., & Nicolis, G. (1999). Symbolic dynamics and entropy analysis of Feigenbaum limit sets. *Chaos, Solitons and Fractals 10*(7):1135-1150. http://dx.doi.org/10.1016/S0960-0779(98)00095-2

Karamanos, K., Peratzakis, A., Kapiris, P., Nikolopoulos, S., Kopanas, J., & Eftaxias, K. (2005). Extracting preseismic electromagnetic signatures in terms of symbolic dynamics. *Nonlinear Processes in Geophysics 12*(6): 835–848. http://dx.doi.org/10.5194/npg-12-835-2005

Keilis-Borok, V. (2002). Earthquake Prediction: State-of-the-Art and Emerging Possibilities. *Annual Review of Earth and Planetary Sciences 30*:1–33. http://dx.doi.org/10.1146/annurev.earth.30.100301.083856

Keilis-Borok, V.I., & Soloviev, A.A. (2003). *Nonlinear Dynamics of the Lithosphere and Earthquake Prediction*. Heidelberg:Springer. http://dx.doi.org/10.1007/978-3-662-05298-3

Khan, P.A., Tripathi, S.C., Mansoori, A.A., Bhawre, P., Purohit, P.K., & Gwal, A.K. (2011). Scientific efforts in the direction of successful earthquake prediction.

International Journal of Geomatics and Geosciences 1(4): 669-677.

Khayrat, A.H., Oliver, M.A., & Durrani, S.A. (2001). The effect of soil particle size on soil radon concentration. *Radiation Measurements* 34(1-6):365–371. http://dx.doi.org/10.1016/S1350-4487(01)00187-1

Kilcik, A., Anderson, C., Rozelot, J., Ye, H., Sugihara, G., & Ozguc, A. (2009). Non linear prediction of solar cycle 24. *The Astrophysical Journal 693:* 1173–1177. http://dx.doi.org/10.1088/0004-637X/693/2/1173

King, C.Y. (1978). Radon Emanation on San Andreas Fault. *Nature 271*(5645): 516–519. http://dx.doi.org/10.1038/271516a0

King, C.Y. (1980). Episodic radon changes in Subsurface soil gas along active faults and possible relation to earthquakes. *Journal of Geophysical Research 85*(B6): 3065-3078. http://dx.doi.org/10.1029/JB085iB06p03065

King, C.Y. (1985). Impulsive radon emanation on a creeping segment of the San Andreas fault, California. *Pure and Applied Geophysics 122* (2-4):340-352. http://dx.doi.org/10.1007/BF00874603

Kinsney, W. (2007). A Unified Approach To Fractal Dimensions. *International Journal of Cognitive Informatics and Natural Intelligence 1*(4)*:* 26-46. http://dx.doi.org/10.4018/jcini.2007100103

Kopytenko, Yu A., Matiashviali, T.G., Voronov, P.M., Kopytenko, E.A., & Molchanov, O.A. (1993). Detection of ultra-low-frequency emissions connected with the Spitak earthquake and its aftershock activity, based on geomagnetic pulsations data at Dusheti and Vardzia observatories. *Physics of the Earth and Planetary Interiors*

77(1-2): 85-95.
http://dx.doi.org/10.1016/0031-9201(93)90035-8

Koulouras, G., Kontakos, K., Stavrakas, I., Stonham, J., & Nomicos, K. (2005). Embedded Compact Flash. *IEEE Circuits & Devices Magazine 21*(4): 27-34.
http://dx.doi.org/10.1109/MCD.2005.1492715

Kulatilake, P.H.S.W., Um, J., Pan, G. (1998). Requirements for accurate quantification of self-affine roughness using the variogram method. *International Journal of Solids and Structures, 35*(31–32): 4167-4189.
http://dx.doi.org/10.1016/S0020-7683 (97)00308-9

Kuo, T., Lin, C., Fan, K., Chang, G., Lewis, C., Han, Y., Wu, Y., Chen, W., & Tsai, C. (2009). Radon anomalies precursory to the 2003 M_w=6.8 Chengkung and 2006 M_w= 6.1 Taitung earthquakes in Taiwan. *Radiation Measurements 44*(3):295-299.
http://dx.doi.org/10.1016/j.radmeas.2009.03.020

Lay, T., Williams, Q., & Garnero, E.J. (1998). The core-mantle boundary layer and deep Earth dynamic. *Nature 392:* 461–468.
http://dx.doi.org/ 10.1038/33083

Li, X., Polygiannakis, J., Kapiris, P., Peratzakis, A., Eftaxias, K., & Yao, X. (2005). Fractal spectral analysis of pre-epileptic seizures in terms of criticality. *Journal of Neural Engineering 2*(2):11-6.

Liu, J.Y., Chen, Y.I., Pulinets, S.A., Tsai, Y.B., & Chuo, Y.J. (2000). Seismo-ionospheric signatures prior to M>6.0 Taiwan earthquakes. *Geophysical Research Letters 27*(19):3113-3116.
http://dx.doi.org/10.1029/2000GL011395

Liu, K.K., Yui, T.F., Yeh, Y.H., Tsai, Y.B., & Teng, T.L. (1985). Variations of radon con-

tent in ground waters and possible correlation with seismic activities in northern Taiwan. *Pure and Applied Geophysics 122*(2-4):231–244. http://dx.doi.org/10.1007/BF00874596

Lomnitz, C. (1994). *Fundamentals of Earthquake Prediction.* New York:John Wiley & Sons.

Lopez, T., Martınez-Gonzalez, C., Manjarrez, J., Plascencia, N., & Balankin, A. (2009). Fractal Analysis of EEG Signals in the Brain of Epileptic Rats, with and without Biocompatible Implanted Neuroreservoirs. *Applied Mechanics and Materials 15:* 127-136. http://dx.doi.org/10.4028/www.scientific.net/AMM.15.127

Louizi, A., Nikolopoulos, D., Koukouliou, V., & Kehagia, K. (2003). Study of a Greek area with enhanced indoor radon concentrations. *Radiation Protection Dosimetry 106*(3): 219–26.

Maeda, K., & Tokimasa, N. (1996). Decametric radiation at the time of the Hyogo-ken Nanbu earthquake near Kobe in 1995. *Geophysical Research Letters 23*(18):2433-2436. http://dx.doi.org/10.1029/96GL02307

Majumdar, K. (2004). A study of fluctuation in radon concentration behaviour as an earthquake precursor. *Current Science 86*(9)*: 1288-1292.*

Mandelbrot, B. B. and Van Ness, J. W. (1968). Fractional Brownian motions, fractional noises and applications. *SIAM Review 10*(4):422–437. http://dx.doi.org/10.1137/1010093

Martinelli, G., (1991). Isotopic and Geochemical Precursors of Earthquakes and Volcanic Eruptions. *Proceedings of an Advisory Group meeting, Vienna, 9-12*

September 1991, p.48.

Mazur, D., Janik, M., Loskiewicz, P., Olko, P., & Swankon, J. (1999). Measurements of radon concentration in soil gas by CR-39 detectors. *Radiation Measurements 31*(1-6): 295–300. http://dx.doi.org/10.1016/S1350-4487(99)00135-3

Mendenhall, W., and Sincich, T. *Statistics for engineering and the sciences,* ISBN 0-02-380581-1, Prentice-Hall, New Jersey, USA, 1995.

Miklavcic´, I., Radolic´, V., Vukovic´, B., Poje, M., Varga, M., Stanic´, D., & Planinic, J. (2004). Radon anomaly in soil gas as an earthquake precursor. *Applied Radiation and Isotopes 66*(10):1459–1466. http://dx.doi.org/10.1016/j.apradiso.2008.03.002

Minadakis, G., Potirakis, S., Nomicos, C., & Eftaxias, K. (2012). Linking electromagnetic precursors with earthquake dynamics: An approach based on non-extensive fragment and self-affine asperity models. *Physica A 391*(6):2232–2244. http://dx.doi.org/10.1016/j.physa.2011.11.049

Mizutani, H., & Ishido, T. (1976). A new interpretation of magnetic field variation associated with the Matsushiro earthquakes. *Journal of Geomagnetism and Geoelectricity 28*(2):179-188. http://dx.doi.org/10.5636/jgg.28.179

Mogro-Campero, A., & Fleischer, R. (1979). *Search for long-distance migration of subsurface radon.* Washington:US Department of Energy.

Molchanov, O.A. (2011). Underlying mechanism of precursory activity from analysis of upward earthquake migration. *Natural Hazards and Earth Systems Sciences*

11:135–143.
http://dx.doi.org/10.5194/nhess-11-135-2011

Molchanov, O.A., Hayakawa, M., Oudoh, T., & Kawai, E. (1998). Precursory effects in the sub ionospheric VLF signals for the Kobe earthquake. *Physics of the Earth and Planetary Interiors 105*(3-4): 239-248.
http://dx.doi.org/10.1016/S0031-9201(97)00095-2

Moore, G.W. (1964). Magnetic disturbances preceding the 1964 Alaska Earthquake. *Nature 203*:508-509.
http://dx.doi.org/10.1038/203508b0

Morelli, D., Martino, S.D., Imme´, G., Delfa, S.L., Nigro, S.L., & Patane´, G. (2006). Evidence of soil radon as tracer of magma uprising in Mt. Etna. *Radiation Measurements 41*(6): 721-725.
http://dx.doi.org/10.1016/j.radmeas.2006.04.026

Morgounov, V. (2001). Relaxation creep model of impending earthquake. *Annals of Geophysics 44*(2): 369-381.
http://dx.doi.org/10.4401/ag-3603

Namvaran, M., & Negarestani, A. (2012). Measuring the radon concentration and investigating the mechanism of decline prior to earthquake. (Jooshan, SE of Iran). *Journal of Radioanalytical and Nuclear Chemistry 298*(1):1-8.
doi:http://dx.doi.org/10.1007/s10967-012-2162-7

Nazaroff, W., & Nero, A. (1988). *Radon and its decay products in indoor air.* New York:Wiley.

NCRP (National Council on Radiation Protection and Measurements). (1988). Measurements in Radon and Radon Daughters in Air. *NCRP Report 97, Bethesda MD:*

Author.

Negarestani, A., Namvaran, M., Shahpasandzadeh, M., Fatemi, S.J., Alavi, S.A., Hashemi, S.M.,& Mokhtari, M.(2014). Design and investigation of a continuous radon monitoring network for earthquake precursory process in Great Tehran. *Journal of Radioanalytical and Nuclear Chemistry 300*(2): 757-767. http://dx.doi.org/10.1007/s10967-014-3020-6

Nicolis, G., & Gaspard, P. (1994).Toward a probabilistic approach to complex systems. *Chaos, Solitons and Fractals 4*(1):41-57. http://dx.doi.org/10.1016/0960-0779(94)90016-7

Nikolopoulos, S., Kapiris, P., Karamanos, K., & Eftaxias, K. (2004). A unified approach of catastrophic events. *Natural Hazards and Earth System Sciences 4*(5-6)*:*615–631. http://dx.doi.org/10.5194/nhess-4-615-2004

Nikolopoulos, D. & Louizi, A. (2008). Study of indoor radon and radon in drinking water in Greece and Cyprus: implications to exposure and dose. *Radiation Measurements 43*(7):1305-1314. http://dx.doi.org/10.1016/j.radmeas.2008.03.043

Nikolopoulos, D., Louizi, A., Koukouliou, V., Serefoglou, A., Georgiou, E., Ntalles, K., & Proukakis, C. (2002). Radon Survey in Greece-Risk Assessment. *Journal of Environmental Radioactivity 63*(2): 173–176. http://dx.doi.org/10.1016/S0265-931X(02)00026-7

Nikolopoulos, D., Louizi, A., Petropoulos, N., Simopoulos, S., & Proukakis, C. (1999). Experimental study of the response of cup-type radon dosimeters. *Radiation Protection Dosimetry 83*(3):263-266.

http://dx.doi.org/10.1093/oxfordjournals.rpd.a032681

Nikolopoulos, D., Petraki, E., Marousaki, A., Potirakis, S., Koulouras, G., Nomicos, C., Panagiotaras, D., Stonham, J., & Louizi, A. (2012). Environmental monitoring of radon in soil during a very seismically active period occurred in South West Greece. *Journal of Environmental Monitoring 14*(2):564-578. http://dx.doi.org/10.1039/c1em10387c

Nikolopoulos, D., Petraki, E., Nomicos, C., Koulouras, G., Kottou, S., & Yannakopoulos, P.H. (2015). Long-Memory Trends in Disturbances of Radon in Soil Prior M_L=5.1 Earthquakes of 17 November 2014 Greece. *Journal of Earth Science & Climatic Change 6*(244):1-11. http://dx.doi.org/10.4172/2157-7617.1000244

Nikolopoulos, D., Petraki, E., Vogiannis, E., Chaldeos, Y., Giannakopoulos, P., Kottou, S., Nomicos, C., & Stonham, J. (2014). Traces of self-organisation and long-range memory in variations of environmental radon in soil: Comparative results from monitoring in Lesvos Island and Ileia (Greece). *Journal of Radioanalytical and Nuclear Chemistry 299*(1):203-219. http://dx.doi.org/10.1007/s10967-013-2764-8

Nomicos, K., & Vallianatos, F. (1998). Electromagnetic variations associated with the seismicity of the frontal Hellenic arc. *Geologica Carpathica. 49*(1):57-60.

Ohno, M., & Wakita, H. (1996). Coseismic radon changes of the 1995 Hyogo-ken Nanbu earthquake. *Journal of Physics and Earth 44*(4):391–395.

Ondoh, T. (1998). Ionospheric disturbances associated with great earthquake of Hokkaido southwest coast, Japan of July 12, 1993. *Physics of the Earth and Planetary Interiors 105*(3-4):261-269.

http://dx.doi.org/10.1016/S0031-9201(97)00118-0

Papadimitriou, C., Kalimeri, M., & Eftaxias, K. (2008). Nonextensivity and universality in the earthquake preparation process. *Physical Review E 77*(3):036101-1–036101-14.

http://dx.doi.org/10.1103/PhysRevE.77.036101

Parrot, M. (1994). Statistical study of ELFNLF emissions recorded by a low-altitude satellite during seismic events. *Journal of Geophysical Research 99*(A12)*:*23339-23347.

http://dx.doi.org/10.1029/94JA02072

Peng, C., Buldyrev, S., Goldberger, A., Havlin, S., Sciortino, F., Simons, M.,& Stanley, H. (1992). Long-Range correlations in nucleotide sequences. *Letters to Nature 356*(6365): 168-170.

http://dx.doi.org/10.1038/356168a0

Peng, C., Buldyrev, S., Simons, M., Havlin, S., Stanley, H., & Goldberger, A. (1994). Mosaic organization of DNA nucleotides. *Physical Review E 49*(2): 1685-1689.

http://dx.doi.org/10.1103/PhysRevE.49.1685

Peng, C., Hausdor, J., Havlin, S., Mietus, J., Stanley, H., & Goldberger, A. (1998). Multiple-time scales analysis of physiological time series under neural control. *Physica A 249*(1-4): 491-500.

http://dx.doi.org/10.1016/S0378-4371(97)00508-6

Peng, C., Havlin. S., Stanley. H., & Goldberger. A. (1995).Quantification of scaling exponents and crossover phenomena in non-stationary heartbeat time series. *Chaos 5*(1): 82-87.

http://dx.doi.org/10.1063/1.166141

Peng, C., Mietus, J., Havlin, S., Stanley, H., & Goldberger, A. (1993). Long Range Anti-correlations and Non-Gaussian Behavior of the Heartbeat. *Physical Review Letters 70*(9): 1343-1346. http://dx.doi.org/10.1103/PhysRevLett.70.1343

Pereda, E., Gamundi, A., Rial, R., & Gonzalez, J. (1998). Non-linear behaviour of human EEG: fractal exponent versus correlation dimension in awake and sleep stages. *Neuroscience Letters 250*(2):91-4. http://dx.doi.org/10.1016/S0304-3940(98)00435-2

Perez, N. M., Hernadez, P. A., Padron, E. L., Melian,G., Marrero, R., Padilla,G., Barrancos, J., & Nolasco, D. (2007). Precursory Subsurface ^{222}Rn and ^{220}Rn Degassing Signatures of the 2004 Seismic Crisis at Tenerife, Canary Islands. *Pure and Applied Geophysics 164*(12): 2431–2448. http://dx.doi.org/10.1007/s00024-007-0280-x

Petraki, E., Nikolopoulos, D., Chaldeos, Y., Coulouras, G., Nomicos, C., Yannakopoulos, P., Kottou, S., & Stonham, J. (2014). Fractal evolution of MHz electromagnetic signals prior to earthquakes: results collected in Greece during 2009. *Geomatics, Natural Hazards and Risk (in press).* http://dx.doi.org/10.1080/19475705.2014.945496

Petraki, E., Nikolopoulos, D., Fotopoulos, A., Panagiotaras, D., Koulouras, G., Zisos, A., Nomicos, C., Louizi, A., & Stonham, J. (2013). Self-organised critical features in soil radon and MHz electromagnetic disturbances: Results from environmental monitoring in Greece. *Applied Radiation and Isotopes 72*:39–53. http://dx.doi.org/10.1016/j.apradiso.2012.09.005

Petraki, E., Nikolopoulos, D., Fotopoulos, A., Panagiotaras, D., Nomicos, C., Yan-

nakopoulos, P., Kottou, S., Zisos, A., Louizi, A., & Stonham, J. (2013). Long-range memory patterns in variations of environmental radon in soil. *Analytical Methods 5*(16):4010-4020. http://dx.doi.org/10.1039/c3ay26486f

Petraki, E., Nikolopoulos, D., Nomicos, C., Stonham, J., Cantzos, D., Yannakopoulos, P., & Kottou S. (2015). Electromagnetic Pre-earthquake Precursors: Mechanisms, Data and Models-A Review. *Journal of Earth Science & Climatic Change 6*(244): 1-11. http://dx.doi.org/10.4172/2157-7617.1000250

Petraki, E., Nikolopoulos, D., Panagiotaras, D., Cantzos, D., Yannakopoulos, P., Nomicos, C., & Stonham, J. (2015). Radon-222: A potential short-term earthquake precursor. *Earth Science & Climatic Change* (in press).

Pinault, J.L., & Baubron, J.C. (1996). Signal processing of soil gas radon, atmospheric pressure, moisture, and soil temperature data: A new approach for radon concentration modelling. *Journal of Geophysical Researh-Sol.EA 101*(2):3157–3171. http://dx.doi.org/10.1029/95JB03121

Pinault J.L., & Baubron, J.C. (1997). Signal processing of diurnal and semidiurnal variations in radon and atmospheric pressure: A new tool for accurate in situ measurement of soil gas velocity, pressure gradient, and tortuosity. *Journal of Geophysical Researh-Sol.EA 102*(B8): 18101–18120. http://dx.doi.org/10.1029/97JB00971

Planinic´, J., Radolic´, V., & Lazanin, Z. (2001). Temporal variations of radon in soil related to earthquakes. *Applied Radiation and Isotopes* 55(2):267-272. http://dx.doi.org/10.1016/S0969-8043(00)00387-0

Planinic´, J., Vukovic´, B., & Radolic´, V. (2004). Radon time variations and deterministic chaos. *Journal of Environmental Radioactivity 75*(1):35-45. http://dx.doi.org/10.1016/j.jenvrad.2003.10.007

Potirakis, S., Minadakis, G., & Eftaxias, K. (2012).Analysis of electromagnetic preseismic emissions using Fisher information and Tsallis entropy. *Physica A 391*(1-2): 300-306. http://dx.doi.org/10.1016/j.physa.2011.08.003

Potirakis, S.M., Minadakis, G., & Eftaxias, K. (2013). Relation between seismicity and pre-earthquake electromagnetic emissions in terms of energy, information and entropy content. *Natural Hazards and Earth System Sciences 12*(4):1179-1183. http://dx.doi.org/10.5194/nhess-12-1179-2012

Potirakis, S.M., Minadakis, G., Nomicos, C., & Eftaxias, K. (2011). A multidisciplinary analysis for traces of the last state of earthquake generation in preseismic electromagnetic emissions. *Natural Hazards and Earth System Science 11*(10):2859–2879. http://dx.doi.org/10.5194/nhess-11-2859-2011

Pulinets, S.A., Alekseev, V.A., Legenka, A.D., & Kbegai, V.V. (1997). Radon and metallic aerosols emanation before strong earthquakes and their role in atmosphere and ionosphere modification. *Advance Space Research 20*(11): 2173-2176. http://dx.doi.org/10.1016/S0273-1177(97)00666-2

Radolic, V., Vukovic, B., Stanic, D. & Planinic, J. (2005). Radon chaotic regime in the atmosphere and soil. *Fizika A 14*(1):195–206.

Ramola, R.C., Prasad, Y., Prasad, G., Kumar, S., & Choubey V.M. (2008). Soil-gas

radon as seismotectonic indicator in Garhwal Himalaya. *Applied Radiation and Isotopes 66*(10):1523– 1530.
http://dx.doi.org/10.1016/ j.apradiso.2008. 04.006

Ramola, R.C., Singh, M., Sandhu, A.S., Singh, S., & Virk, H.S. (1990). The use of radon as an earthquake precursor. *Nuclear Geophysics 4*(2): 275–287.

Reddy, D.V., Sukhija, B.S., Nagabhushanam, P., & Kumar, D. (2004). A clear case of radon anomaly associated with a microearthquake event in a stable continental region. *Geophysical Research Letters 31*: L10609.
http://dx.doi.org/10.102912004GLOI9971

Rehman, S., & Siddiqi, A. (2009). Wavelet based Hurst exponent and fractal dimensional analysis of Saudi climatic dynamics. *Chaos, Solitons & Fractals 39*(4): 1081-1090.
http://dx.doi.org/10.1016/j.chaos.2007.08.063

Richon, P., Bernard, P., Labed, V., Sabroux, J.C., Beneïto, A., Lucius, Abbad, S. & Robe, M.C. (2007). Results of monitoring 222-Rn in soil gas of the Gulf of Corinth region, Greece. *Radiation Measurements 42*(1): 87-93.
http://dx.doi.org/10.1016/j.radmeas.2006.06.013

Richon, P., Sabroux, J.C., Halbwachs, M., Vandemeulebrouck, J., Poussielgue, N,, Tabbagh, J., & Punongbayan, R. (2003). Radon anomaly in the soil of Taal volcano, the Philippines: a likely precursor of the M7.1 Mindoro earthquake (1994). *Geophysical Research Letters 30*(9):1481(34-1 – 34-4).
http://dx.doi.org/10.1029/2003gl016902

Rikitake, T. (1987). Earthquake precursors in Japan: precursor time and detectability. *Tectonophysics 136*(3-4): 265-282.

http://dx.doi.org/10.1016/0040-1951(87)90029-1

Roumelioti, Z., Benetatos, C., & Kiratzi, A. (2009). The 14 February 2008 earthquake (M6.7) sequence offshore south Peloponnese (Greece): source models of the three strongest events. *Tectonophysics 471* (3–4): 272–284. http://dx.doi.org/ 10.1016/j.tecto.2009.02.028

Ruzhin, Y., & Nomicos, C. (2005). Radio VHF precursors of earthquakes. *Natural Hazards 40*(3):573-583. http://dx.doi.org/10.1007/s11069-006-9021-1

Sac, M.M., Harmansah, C., Camgoz, B., & Sozbilir, H. (2011). Radon Monitoring as the Earthquake precursor in Fault Line in Western Turkey. *Ecology 20*(79):93-98. http://dx.doi.org/10.5053/ekoloji.2011.7912

Sarlis, N., Skordas, E., & Varotsos, P. (2010). Effect of significant data loss on identifying electric signals that precede rupture estimated by detrended fluctuation analysis in natural time. *Chaos 20*(033111):1-20. http://dx.doi.org/10.1063/1.3479402

Sarlis, N., Skordas, E., Varotsos, P., Nagao, T., Kamogawa, M., Tanaka, H., & Uyedae, S. (2013). Minimum of the order parameter fluctuations of seismicity before major earthquakes in Japan. *PNAS 110*(34): 13734–13738. http://dx.doi.org/10.1073/pnas.1312740110

Saroso, S., Hattori, K., Ishikawa, H., Ida, Y., Shirogane, R., Hayakawa, M., Yumoto, K., Shiokawa, K., & Nishihashi, M. (2009). ULF geomagnetic anomalous changes possibly associated with 2004–2005 Sumatra earthquakes. *Physics and Chemistry of the Earth 34*(6-7):343-349. http://dx.doi.org/10.1016/j.pce.2008.10.065

Sasai, Y. (1991). Tectonomagnetic modeling on the basis of the linear piezomagnetic effect. *Bulletin of the Earthquake Research Institute The University of Tokyo 66*:585–722.

Scholz, C.H., Sykes, L.R., & Agarwal, Y.P., (1973). Earthquake prediction: A physical basis. *Science 181*(4102)*:* 803–10. http://dx.doi.org/10.1126/science.181.4102.803

Shapiro, M.H., Melvin, J.D., Tombrello, T.A., & Whitcomb, J.H. (1980). Automated radon monitoring at a hard-rock site in the southern California Transverse Ranges. *Journal of Geophysical Research 85*(B6):3058–3064. http://dx.doi.org/10.1029/JB085iB06p03058

Shapiro, M.H., Rice, A., Mendenhall, M.H., Melvin, J.D. & Tombrello, T.A. (1985). Recognition of environmentally caused variations in radon time series. *Pure and Applied Geophysics 122*(2-4):309–326. http://dx.doi.org/10.1007/BF00874601

Shrivastava, A. (2014). Are pre-seismic ULF electromagnetic emissions considered as a reliable diagnostics for earthquake prediction? *Current Science 107*(4): 596-600.

Singh, M., Ramola, R., Singh, B., Singh, S., & Virk, H. (1991). Subsurface soil gas radon changes associated with earthquakes. *Nuclear Tracks and Radiation Measurements 19*(1-4): 417-420. http://dx.doi.org/10.1016/1359-0189(91)90229-B

Singh, M., Kumar, R.K., Jain, R., and Chatrath, P. (1999). Radon in ground water related to seismic events. *Radiation Measurements 30*(4): 465–9. http://dx.doi.org/10.1016/S1350-4487(99)00049-9

Singh, S., Kumar, A., Singh, B.B., Mahajan, S., Kumar, V., & Dhar, S. (2010) . Radon

Monitoring in Soil Gas and Ground Water for Earthquake Prediction Studies in North West Himalayas, India. *Terrestrial, Atmospheric and Oceanic Sciences 21*(4): 685-695. http://dx.doi.org/10.3319/TAO.2009.07.17.01(TT)

Smirnova, N.A., & Hayakawa, M. (2007). Fractal characteristics of the ground-observed ULF emissions in relation to geomagnetic and seismic activities. *Journal of Atmospheric and Solar-Terrestrial Physics 69*(15):1833-1841. http://dx.doi.org/10.1016/j.jastp.2007.08.001

Smirnova, N., Hayakawa, M., & Gotoh (2004). Precursory behavior of fractal characteristics of the ULF electromagnetic fields in seismic active zones before strong earthquakes. *Physics and Chemistry of the Earth 29*(4-9):445-451. http://dx.doi.org/10.1016/j.pce.2003.11.016

Smith, B., & Johnston, M. (1976). A tectonomagnetic effect observed before a magnitude 5.2 earthquake near Hollister, California. *Journal of Geophysical Research* 81(20):3556-3560. http://dx.doi.org/10.1029/JB081i020p03556

Spiegel, M.R., *Schaum's Outline of Theory and Problems of probability and statistics.* ISBN 0-07-060220-4, McGraw-Hill, New York, 1975.

Stavrakas, I., Clarke, M., Koulouras, G., Stavrakakis, G., & Nomicos,C. (2007). Study of directivity effect on electromagnetic emissions in the HF band as earthquake precursors: Preliminary results on field observations. *Tectonophysics 431*(1-4):263–271. http://dx.doi.org/10.1016/j.tecto.2006.05.037

Steele, S.R. (1984). Anomalous radon emanation at local and regional distances preced-

ing earthquakes in the New Madrid Seismic Zone and adjacent areas of the central Mid-Continent of North America 1981–1984. *Pure and Applied Geophysics 122*(2-4):353–368.

http://dx.doi.org/10.1007/BF00874604

Steinitz, G., Martın, M.C., Gazit-Yaari, N., Quesada, M.L., Nuez, J., Casillas, R., Malika, U., & Begin, Z.B. (2006). Multi-day radon signals with a radioactive decay limb—Occurrence and geophysical significance. *Applied Radiation and Isotopes 64*(4): 520–524.

http://dx.doi.org/10.1016/j.apradiso.2005.10.004

Steinitz, G., Piatibratova, O., & Barbosa, S.M. (2007). Radon signals in the Elat Granite pluton , Southern Arava, Israel. *Report GSI/18/06, Geological Survey of Israel, Jerusalem.*

Stratakos, J., & Sakellariou, M. (2006). An Evaluation of Methods for the Estimation of the Fractal Dimension of Rock Surfaces. *Technical Chron. Science Journal*, I, No 1–2.

Surkov, V., Uyeda, S., Tanaka, H., & Hayakawa, M. (2002). Fractal properties of medium and seismoelectric phenomena. *Journal of Geodynamics 33*(4-5):477-487.

http://dx.doi.org/10.1016/S0264-3707(02)00009-1

Tansi, C., Tallarico, A., Iovine, G., Gallo, M.F., & Falcone, G. (2005). Interpretation of radon anomalies in seismotectonic and tectonic-gravitational settings: the south-eastern Crati graben (Northern Calabria, Italy). *Tectonophysics 396*(3-4): 181-193.

http://dx.doi.org/10.1016/j.tecto.2004.11.008

Talwani, P., Moore, W.S., & Chiang, J. (1980). Radon anomalies and microearthquakes at Lake Jocassess, South Carolina. *Journal of Geophysical Research 85*(B6): 3079–88. http://dx.doi.org/10.1029/JB085iB06p03079

Telesca, L., & Lasaponara, R. (2006). Vegetational patterns in burned and unburned areas investigated by using the detrended fluctuation analysis. *Physica A 368*(2): 531–535. http://dx.doi.org/10.1016/j.physa.2005.12.006

Teng, T.L. (1980). Some recent studies on groundwater radon content as an earthquake precursor. *Journal of Geophysical Research 85*(B6):3089–3099. http://dx.doi.org/10.1029/JB085iB06p03089

Teng, T.L., & Sun, L.F. (1986). Research on groundwater radon as a fluid phase precursor to earthquakes. *Journal of Geophysical Research 91*(B12):12305-12313. http://dx.doi.org/10.1029/JB091iB12p12305

Thomas, D. (1988). Geochemical precursors to seismic activity. *Pure and Applied Geophysics 126*(2):241–266. http://dx.doi.org/10.1007/BF00878998

Toutain, J.P., & Baubron, J.C. (1999). Gas geochemistry and seismotectonics: a review. *Tectonophysics 304*(1-2): 1–27. http://dx.doi.org/doi:10.1016/S0040-1951(98)00295-9

UNSCEAR (United Nations Scientific Committee on the Effects of Atomic Radiation). (2008). *Sources and effects of ionizing radiation.* New York:Author.

Uyeda, S. (2000). In defense of VAN's earthquake predictions. *EOS, Transactions*

American Geophysical Union 81(1): 3–6.

Uyeda, S., Nagao, T., & Kamogawa, M. (2009). Short-term earthquake prediction: current status of seismo-electromagnetics. *Tectonophysics 470*(3-4):205–213. http://dx.doi.org/10.1016/j.tecto.2008.07.019

Vallianatos, F., & Nomikos, K. (1998). Seismogenic Radio-emissions as Earthquake Precursors in Greece. *Physics and Chemistry of the Earth 23*(9-10):953-957. http://dx.doi.org/10.1016/S0079-1946(98)00126-8

Varotsos, P.A. (2006). Recent Seismic Electric Signals (SES) activities in Greece. *Acta Geophysica 54*(2):158-164. http://dx.doi.org/10.2478/s11600-006-0019-6

Varotsos, P., & Alexopoulos, K. (1984a). Physical properties of the variations of the electric field of the earth preceding earthquakes, I. *Tectonophysics 110*(1-2):73-98. http://dx.doi.org/10.1016/0040-1951(84)90059-3

Varotsos, P., & Alexopoulos, K. (1984b). Physical properties of the variations of the elec electric field of the earth preceding earthquakes, II, determination of epicenter and magnitude. *Tectonophysics 110*(1-2):99-125. http://dx.doi.org/10.1016/0040-1951(84)90060-X

Varotsos, P., Alexopoulos, K., & Lazaridou, M. (1993). Latest aspects of earthquake prediction in Greece based on Seismic Electric Signals II. *Tectonophysics 224*(1-3):1-37. http://dx.doi.org/10.1016/0040-1951(93)90055-O

Varotsos, P., Alexopoulos, K., Nomicos, K., & Lazaridou, M. (1986). Earthquake prediction and electric signals. *Nature 322*:120.

http://dx.doi.org/10.1038/322120a0

Varotsos, P., & Lazaridou M. (1991). Latest aspects of earthquake prediction in Greece based on Seismic Electric Signals. *Tectonophysics 188*(3-4)*:*321−347. http://dx.doi.org/10.1016/0040-1951(91)90462-2

Varotsos, P., Sarlis, N., Eftaxias, K., Lazaridou, M., Bogris, N., Makris, J., Abdulla, A., & Kapiris, P. (1999). Prediction of the 6.6 Grevena-Kozani Earthquake of May 13, 1995. *Physics and Chemistry of the Earth 24*(2):115-121. http://dx.doi.org/10.1016/S1464-1895(99)00006-X

Varotsos, P., Sarlis, N., Lazaridou, M., & Bogris, N. (1996). Statistical evaluation of earthquake prediction results. Comments on the success rate and alarm rate. *Acta Geophysica Polonica 44*(4): 329-347.

Varotsos, P.A., Sarlis, N.V., & Skordas, E.S. (2003). Electric Fields that "Arrive" before the Time Derivative of the Magnetic Field prior to Major Earthquakes. *Physical Review Letters 91*(14): 148501-1/148501-4. http://dx.doi.org/10.1103/PhysRevLett.91.148501

Varotsos, P.A., Sarlis, N.V., & Skordas, E.S. (2009). Detrended fluctuation analysis of the magnetic and electric field variations that precede rupture. *Chaos 19:* 023114. http://dx.doi.org/10.1063/1.3130931

Varotsos, P., Sarlis, N., & Skordas, E. (2011). Scale-specific order parameter fluctuations of seismicity in natural time before main shocks. *Europhysics Letters 96*(5): 59002-p1/59002-p6. http://dx.doi.org/10.1209/0295-5075/96/59002

Varotsos, P., Sarlis, N., & Skordas, E. (2012). Scale-specific order parameter fluctuations of seismicity before mainshocks: Natural time and Detrended

Fluctuation Analysis. *EPL 99*(59001):1-6. http://dx.doi.org/10.1209/0295-5075/99/59001

Varotsos, P.A., Sarlis, N.V., Skordas, E.S., & Lazaridou, M.S. (2007). Electric pulses some minutes before earthquake occurrences. *Applied Physics Letters 90*(6): 064104-1/064104-3. http://dx.doi.org/10.1063/1.2450779

Virk, H.S. (1996). Radon studies for earthquake prediction. *Himalayan Geology 17:91–103.*

Virk, H.S., & Baljinder, S. (1994). Radon recording of Uttarkashi earthquake. *Geophysical Research Letters 21*(8):737–740. http://dx.doi.org/10.1029/94GL00310

Virk, H.S., Walia, V., & Kumar, N. (2001). Helium/radon precursory anomalies of Chamoli earthquake, Garhwal Himalaya, India. *Journal of Geodynamics 31*(2):201–210. http://dx.doi.org/10.1016/S0264-3707(00)00022-3

Vogiannis, E., & Nikolopoulos, D. (2008). Modelling of radon concentration peaks in thermal spas: Application to Polichnitos and Eftalou spas (Lesvos Island—Greece). *Science of the Total Environment 405*(1): 36-44. http://dx.doi.org/10.1016/j.scitotenv.2008.06.029

Vogiannis, E., & Nikolopoulos, D. (2015). Radon sources and associated risk in terms of exposure and dose. *Frontiers in Public Health, Environmental Health 2*(207):1-10. http://dx.doi.org/10.3389/fpubh.2014.00207

Wakita, H., Nakamura, Y., & Sano, Y. (1988). Short-term and intermediate-term geo-

chemical precursors. *Pure and Applied Geophysics 126(2-4)*:267–278. http://dx.doi.org/10.1007/BF00878999

Walia, V., Virk, H.S., Bajwaa, B.S., & Sharmac, N. (2003). Relationships between radon anomalies and seismic parameters in N-W Himalaya, India. *Radiation Measurements 36*(1):393 – 396. http://dx.doi.org/10.1016/S1350-4487(03)00158-6

Walia, V., Yang, T., Hong, W., Lin, S., Fu, C., Wen, K., & Chen C. (2009). Geochemical variation of soil–gas composition for fault trace and earthquake precursory studies along the Hsincheng fault in NW Taiwan. *Applied Radiation and Isotopes 67*(10): 1855-1863. http://dx.doi.org/10.1016/j.apradiso.2009.07.004

Wallace, R., & Teng, T. (1980). Prediction of the Sungpan-Pingwu earthquakes, 1976. *Bulletin of the Seismological Society of America 70*: 1199-1223.

Warwick, J., Stoker, C., & Meyer, T. (1982). Radio Emission Associated With Rock Fracture: Possible Application to the Great Chilean Earthquake of May 22, 1960. *Journal of Geophysical Research 87*(B4):2851-2859. http://dx.doi.org/10.1029/jB087iB04p02851

Whitehead, N.E., Barry, B.J., Ditchburn, R.G., Morris, C.J., & Stewart, M.K. (2007). Systematics of radon at the Wairakei geothermal region, New Zealand. *Journal of Environmental Radioactivity 92*(1): 16-29. http://dx.doi.org/10.1016/j.jenvrad.2006.09.003

Wornell, G. (1995). *Signal Processing with Fractals. A wavelet-based approach.* Indianapolis, United States of America: BooksCraft, Inc.

Xie, D., Wan, L & Zhu Y. (2014). The Effectiveness Evaluation of Two Kinds of Fractal

Sequences on Detrended Fluctuation Analysis. *Mathematical Computation* 3(2): 58-62.

Yalım, H.A., Sandıkcıog, A., Ertugrul, O., & Yıldız, A. (2012). Determination of the relationship between radon anomalies and earthquakes in well waters on the Aksehir-Simav Fault System in Afyonkarahisar province, Turkey. *Journal of Environmental Radioactivity 110*:7-12. http://dx.doi.org/10.1016/j.jenvrad.2012.01.015

Yannakoloulos, P.H. (2012). *Digital Communications*. Athens, Greece: Sinchroni Ekdotiki E.P.E.

Yasuoka, Y., Igarashi, G., Ishikawa, T., Tokonami, S., & Shinogi, M. (2006). Evidence of precursor phenomena in the Kobe earthquake obtained from atmospheric radon concentration. *Applied Geochemistry 21*(6): 1064-1072. http://dx.doi.org/10.1016/j.apgeochem.2006.02.019

Yasuoka, Y., & Shinogi, M. (1995). Anomaly in atmospheric radon concentration: a possible precursor of the 1995 Kobe, Japan, earthquake. *Health Physics 72*(5):759-761.

Yépez, E., Angulo-Brown, F., Peralta, J.A., Pavía , C.G., & González-Santos, G. (1995). Electric field patterns as seismic precursors. *Geophysical Research Letters 22*(22): 3087-3090. http://dx.doi.org/10.1029/95GL03072

Yonaiguchi, N., Ida, Y., Hayakawa, M., & Masuda, S. (2007). Fractal analysis for VHF electromagnetic noises and the identification of preseismic signature of an earthquake. *Journal of Atmospheric and Solar-Terrestrial Physics 69*(15):1825-1832. http://dx.doi.org/10.1016/j.jastp.2007.08.002

Yoshino, T., Tomizawa, I., & Sugimoto, T. (1992). Results of statistical analysis of low-frequency seismogenic EM emissions as precursors to earthquakes and volcanic eruptions. *Physics of the Earth and Planetary Interiors 77* (1-2):21-31. http://dx.doi.org/10.1016/0031-9201(93)90031-4

Zafrir, H., Steinitz, G., Malik, U., Haquin, G., & Gazit-Yaari, N. (2009). Response of Radon in a seismic calibration explosion, Israel. *Radiation Measurements 44*(2): 193-198. http://dx.doi.org/10.1016/j.radmeas.2009.01.002

Zhao,Y., & Qian, F. (1994). Geoelectric precursors to strong earthquakes in China. *Tectonophysics 233*(1-2):99-113. http://dx.doi.org/10.1016/0040-1951(94)90223-2

Zmazek, B., Todorovski, L.,Zivcic , M., Dzeroski, S., Vaupotic, J., & Kobala, I. (2006). Radon in a thermal spring: Identification of anomalies related to seismic activity. *Applied Radiation and Isotopes 64*(6):725–734. http://dx.doi.org/10.1016/j.apradiso.2005.12.016

Zmazek, B., Zivcic, M., Todorovski, L., Dzeroski, S., Vaupotic, J., & Kobal, I. (2005). Radon in soil gas: how to identify anomalies caused by earthquakes. *Applied Geochemistry 20*(6):1106–1119. http://dx.doi.org/10.1016/j.apgeochem.2005.01.014

Zoran, M., Savastru, R., Savastru, D., Chitaru, C., Baschir, L., & Tautan, M. (2012). Monitoring of radon anomalies in South-Eastern part of Romania for earthquake surveillance. *Journal of Radioanalytical and Nuclear Chemistry 293*(3):769-781. http://dx.doi.org/10.1007/s10967-012-1780-4